2007

Middle to late Holocene sea-level change in Western Denmark : a diatom-based study

Szkornik, Katie

COPYRIGHT STATEMENT

MIDDLE TO LATE HOLOCENE SEA-LEVEL CHANGE IN WESTERN DENMARK: A DIATOM-BASED STUDY

by

Katie Szkornik

A thesis submitted to the University of Plymouth in partial fulfilment for the degree of

DOCTOR OF PHILOSOPHY

School of Geography
Faculty of Social Science and Business

April 2007

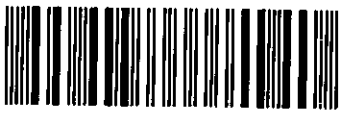

Abstract

Middle to late Holocene sea-level change in western Denmark: a diatom-based study

Katie Szkornik

Modern diatom assemblages and associated environmental variables were collected from six transects across the salt-marsh surface in the Ho Bugt embayment in western Denmark. The relationship between diatom assemblages and environmental variables (elevation, pH, salinity, loss on ignition, grain size) was explored using ordination techniques to assess the potential use of diatoms as sea-level indicators. Results for the two data sets analysed in ordinations indicate that elevation exerts a strong, independent and statistically significant influence on modern diatom distrbutions in the Ho Bugt embayment. Diatom-based transfer functions were subsequently developed to reconstruct changes in palaeomarsh-surface elevation based on the relationship between diatoms and elevation in the modern training set. Maximum likelihood (ML), weighted averaging (WA) and weighted-averaging partial least squares (WA-PLS) transfer functions were developed from 97 surface samples and 151 taxa. The WA-PLS transfer function were found to perform best ($RMSEP_{jack}$ = 0.12 m, r^2 = 0.93 and max $bias_{jack}$ = 0.11 m) and was subsequently applied to interpret the diatom assemblages in a series of fossil cores and reconstruct palaeomarsh-surface elevations. The statistical reliability of these reconstructions was assessed via the use of 'goodness of fit' and 'analogue' statistics. Combination of these palaeomarsh-surface records with reliable age-depth models has enabled the relative sea-level history of the Ho Bugt embayment to be reconstructed. Relative sea-level curves for the Ho Bugt embayment document around 7 m of rise in the last 7000 cal. yr BP. Four stages in the evolution of the Ho Bugt salt marshes can be recognised: basal peat formation from 7000 – 2000 cal. yr BP, salt-marsh formation from 2000 – 1200 cal. yr BP, a fresh water phase from 1200 – 350 cal. yr BP and renewed salt-marsh deposition from 350 cal. yr BP to the present. Geophysical modelling suggests that the dominant control on relative sea-level change in the Ho Bugt embayment during the last 5000 cal. yr BP is glacial isostatic adjustment, following decay of the Fennoscandian Ice Sheet. The Ho Bugt relative sea-level data are best matched by a glacial isostatic adjustment model that includes a zero eustatic function for the last 5000 cal. yr BP.

AUTHOR'S DECLARATION

At no time during the registration for the degree of Doctor of Philosophy has the author been registered for any other University award without prior agreement of the Graduate Committee. This study was financed with the aid of a studentship from the Natural Environment Research Council (NER/S/A/2003/11314). During the programme of study work was presented at regular international conferences and seminars. Courses and consultations relevant to the study were pursued, and a study visit was made to the NERC Radiocarbon Laboratory, East Kilbride. In addition to the presentations detailed below, two departmental seminars were given during the course of study.

Publications:

Gehrels, W.R., **Szkornik, K.,** Bartholdy, J., Kirby, J.R., Bradley, S.L., Heinemeier, J., Pedersen, J.B.T. and Marshall, W.A., 2006. Late Holocene sea-level changes and isostasy in western Denmark. *Quaternary Research,* 66 (2): 288-302. (Appendix 1).

Szkornik, K., Gehrels, W.R. and Kirby, J., 2006. Salt-marsh diatom distributions in Ho Bugt (western Denmark) and the development of a transfer function for reconstructing Holocene sea-level changes. *Marine Geology*, 235 (1-4): 137-150. (Appendix 2).

Szkornik, K., 2004. Holocene deposits in the northern part of Ho Bugt. In: J. Bartholdy, C. Christiansen, J.B.T. Pedersen and N. Vinther (Eds.). Fieldtrip guide B1, sediments and morphodynamics along the Danish West coast from Skagen to the Wadden Sea. 6th International Conference on Tidal Sedimentology, Copenhagen, Denmark. Institute of Geography, University of Copenhagen: 78pp. (Appendix 3).

Conference presentations (oral or poster presentation indicated):

Szkornik, K., Kirby, J. and Gehrels, W.R., 2004. Middle to late Holocene sea-level changes in Denmark: A diatom based study. *Tidalites 2004, 6th International Conference on Tidal Sedimentology, Copenhagen, Denmark. August 2nd – 5th 2004.* Oral presentation.

Szkornik, K., Kirby, J. and Gehrels, W.R., 2004. Middle to late Holocene sea-level changes in Denmark: A diatom based study. *The Quaternary Research Association 3rd International Postgraduate Symposium, royal Belgium Institute of Natural Sciences, Belgium Geological Survey, Brussels, Belgium. September 14th – 17th 2004.* Oral presentation.

Szkornik, K., Kirby, J. and Gehrels, W.R., 2005. The use of salt-marsh diatoms as sea-level indicators in Ho Bugt, western Denmark. *"Late Quaternary Coastal Changes: Sea Level, Sediment Forcing and anthropogenic Impacts". INQUA and IGCP-496 Joint Meeting, Dunkerque, France. 28th June – 2nd July 2005.* Oral presentation.

Gehrels, W.R., **Szkornik, K.,** Kirby, J., Bradley, S., Milne, G., Bartholdy, J., Pedersen, J.B.T., Heinemeier, J. and Marshall, W.A., 2005. Salt-marsh stratigraphy and late Holocene sea-level changes in Ho Bugt, western Denmark: Implications for the 'regional eustatic' history of the North Sea. *"Late Quaternary Coastal Changes: Sea Level, Sediment Forcing and anthropogenic Impacts". INQUA and IGCP-496 Joint Meeting, Dunkerque, France. 28th June – 2nd July 2005.* Oral presentation by W.R. Gehrels.

Szkornik, K., Gehrels, W.R., Kirby, J., Bartholdy, J., Pedersen, J.B.T. and Marshall, W.A., 2005. Salt-marsh stratigraphy of Ho Bugt, western Denmark and the implications for Holocene sea-level reconstructions. *Quaternary Research Association 4th International Postgraduate Symposium, School of Geography, University of Plymouth, UK. August 31st – September 2nd 2005.* Oral presentation.

Szkornik, K., Gehrels, W.R., Murray, A., 2006. Little Ice Age sand invasion of the Ho Bugt salt marshes in Western Denmark during low relative sea level. *HOLIVAR Open Science Meeting, University College London, June 12th – 15th 2006.* Poster presentation.

Szkornik, K., Gehrels, W.R., Kirby, J., Kent, M. and Charman, D., 2006. Using diatom-based transfer function to reconstruct Holocene sea-level changes: Highlighting the need for caution in model selection and in interpreting results. *"Quaternary Land-Ocean Interaction: Natural and Human Forcings on Coastal Evolution". IGCP 495 Meeting, Balneário Camboriú, Santa Catarina, Brazil. September 17th – 22nd 2006.* Oral presentation.

Szkornik, K., Gehrels, W.R. and Murray, A., 2006. Little Ice Age sand invasion of the Ho Bugt salt marshes in Western Denmark during low relative sea level. *"Quaternary Land-Ocean Interaction: Natural and Human Forcings on Coastal Evolution". IGCP 495 Meeting, Balneário Camboriú, Santa Catarina, Brazil. September 17th – 22nd 2006.* Poster presentation.

Szkornik, K., Gehrels, W.R. and Charman, D., 2006. The use of diatoms as sea-level indicators in Ho Bugt, western Denmark. *British Diatomists' Meeting 2006, Malham Tarn Field Studies Centre, North Yorkshire, UK. 27th – 29th October 2006.* Poster presentation.

Additional conferences attended:

11th International Scientific Wadden Sea Symposium, Esbjerg, Denmark. April 4th–8th 2005.

Additional courses attended:

March 2004 **Numerical and statistical analysis of biological data.** Run by Prof. H.J. B. Birks and Dr. G. Simpson. NERC short course, Environmental Change Research Centre, University College, London. Attendance funded by NERC.

June 2004 **Diatom analysis.** Run by Prof. R. Battarbee, Dr. V.J. Jones and others. NERC short course, Environmental Change Research Centre, University College, London. Attendance funded by NERC.

Further funding obtained:

£11,700 NERC AMS ^{14}C dating allocation number 1117.1005 "The glacio-eustatic contribution to global sea-level rise in the late Holocene." (Principal investigator W.R. Gehrels).

Word count of main body of thesis:

68, 150 (including figure captions, tables and table captions)

Signed..L Dullmuller.....

Date...24th April 2007.....

Acknowledgements

Firstly I would like to express my thanks to my supervisors, Roland Gehrels and Dan Charman for their continuous encouragement and guidance throughout the duration of this thesis. I have learnt a great deal from them both during the last three years and this thesis would not have been possible without the support that they have provided me with. I am also grateful to Jesper Bartholdy and Jørn Pedersen (University of Copenhagen) for their fruitful discussions and input into this thesis, to Jason Kirby (Liverpool, John Moore's), Sue Dawson (St Andrews) and Helen Roe (Queen's, Belfast), for providing advice on diatom taxonomy and identification of difficult diatom taxa, and to Glen Milne and Sarah Bradley (Durham) for providing geophysical model predictions. A number of colleagues in the School of Geography, University of Plymouth (UoP), have provided advice at various stages of this thesis. In particular I would like to thank Martin Kent, for stimulating discussion on statistics, and Wil Marshall for his advice on lead-210 and radiocarbon dating. I would also like to express my thanks to Antony Long (Durham) for fruitful discussion during several IGCP meetings.

I am extremely grateful to Roland, Wil, Jesper, Jørn, Steffen Svinth, and UoP students Emma-Jayne Hopla and Kristian White for their assistance in the field. I would like to thank Jesper and Christian Christiansen (University of Copenhagen) for allowing us to use the facilities at the Skallingen laboratory during our field trips and for their hospitality during my time in Denmark. I am grateful to the many landowners around Ho Bugt who provided us with access to their land. I would like to thank Asgar Lauridsen and Ole Knudsen (Danish Forest and Nature Agency) for granting us permission to sample the salt marshes on Langli Island, and for providing us with accommodation and transport during our stay.

In the laboratory, Andy Elmes, Ann Kelly, Kevin Solman, Richard Hartley, Ben Meredith and Debbie Bauckham have provided a great deal of assistance. I would like to thank them for their efficiency in preparing equipment for my fieldtrips and for their continuous support throughout my time spent in the lab. I am especially grateful to Ann for ensuring that I completed my lab work in one piece! Jamie Quinn, Tim Absalom and Brain Rogers offered valuable advice on cartography related issues and have provided invaluable assistance in preparing figures for publication. Thanks to Naomi Swales and Julie Thompson for administrative support.

This PhD was funded by a NERC studentship (NER/S/A/2003/11314) for which I am grateful. Radiocarbon dates presented in this thesis were funded by the European Commission under the Fifth Framework (EVK2-2000-00563) as part of the HOLSMEER Project, and by NERC Radiocarbon Laboratory Steering Committee dating allocation number 1117.1005. OSL dates were provided through collaboration with Andrew Murray (University of Aarhus, Denmark). Data from the HOLSMEER Project provided the initial stimulus for this thesis and I am grateful for the exploratory work carried out by the HOLSMEER Partners. These data form an integral part of this thesis, and where presented they are clearly indicated.

On a more personal note I would like to thank Becky, Liz, Jodie, Lou and Jessie for their friendship during my time in Plymouth. I would also like to thank the many staff and postgrads, both past and present, at the UoP whose support has been extremely valuable throughout the duration of this thesis. I would especially like to express my thanks to Matt, whose support, encouragement and advice have been unfailing. Matt has kept me going during my numerous ups and downs and has always believed that I would get there in the end. Last, but by no means least, I would like to say a special thank you to Mum and Dad for 27 years of selfless support – I hope I have made you proud.

Contents

List of Figures

List of Tables

Chapter 1

Introduction

This study presents the development and application of a diatom-based transfer function for reconstructing changes in relative sea level in the Ho Bugt embayment in western Denmark (Section 3.1). It establishes a series of local water-level curves which span the last 5,000 years and reconstructs the millennial-scale sea-level history of the Ho Bugt embayment. In doing so, this thesis generates data that can provide valuable constraints on model parameters in glacio- hydro- isostatic models (Lambeck, 1995, Shennan et al., 2000a). Although many of the statistical methods employed in this study are well established in the fields of biogeography, oceanography and palaeolimnology, the statistical methodology adopted by the sea-level community in transfer function development is less well defined. This is especially true with regard to data screening and the use of ordination techniques to investigate relationships in the modern environment. The use of such techniques in this study therefore provides a potentially new and original contribution to Holocene sea-level research.

1.1 Quaternary sea-level change

Fluctuations in sea level throughout the Earth's history have been of interest since the first geological observations began during the later part of the 19th century. These observations were associated with the development of glacial theory (Agassiz, 1837 cited in Charlesworth, 1966) and the recognition of links between glacier expansion and contraction (Maclauren, 1841 cited in Lowe and Walker, 1997). Maclauren reasoned that during times of glacier expansion, sea levels would fall as water became locked up in ice sheets, and following ice melt, sea levels would rise as this water returned to the ocean basins. Glacio-isostatic theory arose from the work of the Scottish geologist Jamieson who was the first to make links between raised shoreline evidence and glacial theory. Jamieson concluded that crustal depression resulted from the weight of the ice sheets on land and once the weight was removed, rebound would occur (Jamieson, 1865 cited in Charlesworth, 1966). Following Jamieson's work postglacial (Holocene) sea-level changes have been recognised to be primarily the result of a combination of two processes, glacio-eustasy and glacio-isostasy.

- Glacio-eustasy is the oscillation in sea level that directly results from the expansion and contraction of the ice sheets and glaciers ('eustatic changes').
- Glacio-isostasy is the deformation of the Earth's crust caused by the weight of ice on the land ('isostatic changes').

In a number of locations, particularly in areas close to the margins of the former ice sheets, eustatic and isostatic processes operate together and result in *relative* sea-level changes.

1.2 Post-glacial sea-level change

With the development of radiocarbon (^{14}C) dating, a world-wide interest into the phenomenon of changing sea levels was established (Fairbridge, 1961). The assumption was that because the oceans of the world were interconnected, changes in sea level would be synchronous worldwide (Kidson, 1982). Thus the search for a worldwide eustatic sea-level curve was initiated. The early 1960s saw the division of the sea-level community into two major schools of thought following the publication of two benchmark papers. The first of these, produced by Fairbridge (1961), argued for a postglacial sea-level rise that was sporadic and included both transgressive and regressive phases. Support for these arguments was provided by the investigations of Mörner (1969a, 1969b) in the Kattegat region (Figure 1.1a) and Tooley (1974) in north western England. A second paper produced by Shepard (1963), argued that post-glacial sea-level rise was continuous, occurring at a steadily rising rate. His work was supported by Jelgersma (1961), providing evidence from the Netherlands and Kidson and Heyworth (1973), providing evidence from the Bristol Channel, UK. Sea-level research at this time saw a broad division into either the Fairbridge or Shepard schools of thought.

In the late 1970s the study of sea-level change saw new stimulus with the implementation of International Geological Correlation Programme (IGCP) Project 61 in 1979, which sought to establish a single curve of sea-level movements for the Earth (Tooley, 1982). However, in the mid 1980s it became apparent that the influence of local factors, primarily vertical crustal movements (Tooley, 1982), and global factors, such as an unstable geoid (Mörner, 1976), would make construction of a single eustatic sea-level curve impossible. The two original schools of thought became united as the sea-level community sought the development of a uniform methodology and interdisciplinary approach (Tooley, 1982, Shennan et al., 1983). The primary objective of a new IGCP project (IGCP Project 200)

was to identify and quantify the processes that operate to control sea-level change, through the production of local and regional sea-level curves (Tooley, 1982, 1985). Since this time sea-level research has focussed on the construction of such local and regional sea-level curves, as is the intention of this thesis, to understand better the spatial and temporal variability of sea-level change on a global scale.

1.3 Recent advances in sea-level research

Microfossil-based transfer functions have been widely used in sea-level studies to reconstruct changes in relative sea level since the late 1990s (e.g., Gehrels, 2000; Hamilton and Shennan, 2005a, 2005b). The development of such a methodology has been a major theme in sea-level research in recent years, highlighted at international meetings of the International Geological Correlation Programme (IGCP) Project 495 working group ("Quaternary Land-Ocean Interactions: Driving mechanisms and Coastal Responses"[1]). One of the major aims of IGCP Project 495 has been to develop quantitative, high resolution records of relative sea-level change that can be compared with other local, regional and global records of environmental change. Microfossil-based transfer functions provide one way in which to achieve this aim.

Despite the increasing popularity of the use of transfer functions in sea-level research, the statistical methodology adopted by the sea-level community differs to that employed by many biogeographers, oceanographers and palaeolimnologists, particularly with regards to data screening and the use of ordination techniques in training set development. A particular focus of this thesis has been to integrate statistical aspects from the palaeolimnological community, where diatom-based transfer functions have been used for sometime. In addition, many sea-level studies which use transfer functions focus solely on interpreting the statistical output generated by such models. A second major focus of this thesis has been to highlight the need for an integrated approach using the combined results of microfossil-based, lithological and biostratigraphical investigations to provide a more complete picture. The use of statistical methods provides one way of generating a result but they do not necessarily provide the full answer.

[1] http://www.geography.dur.ac.uk/research/IGCP_495/Project_Outline/index.html

1.4 The importance of Denmark's location for Holocene sea-level studies

North West Europe is an important location for the study of Holocene relative sea-level change (Mörner, 1976, 1979; Shennan, 1987). With an excellent geological record of crustal response to glacial loading and unloading, it remains an important region for testing glacio- hydro- isostatic models (Lambeck et al., 1998a). Denmark itself occupies a particularly interesting location at the margins of the former Fennoscandian Ice Sheet. Danish coastlines show evidence of emergence to the north and submergence to the south (Gehrels et al., 2006a) (Figure 1.1). This setting is important for constraining the melting history of the Fennoscandian Ice Sheet (Lambeck et al., 1998b, Shennan et al., 2000b) and for studying associated crustal movements (Shennan, 1987).

Despite the importance of Denmark's location, sea-level and coastal changes in the region are poorly understood, particularly those along the Danish North Sea coast. This is especially true of changes in the late Holocene. The Danish North Sea coast remains one of the longest stretches of coastline around the North Sea basin with comparatively few middle and late Holocene sea-level data (Shennan, 1987). This is somewhat surprising given the importance of Denmark's location. Certain areas of Denmark lie close to the hinge line between the uplifting and subsiding coasts (Figure 1.1a). This means that, potentially, very little land movement has occurred in these areas in the past millennia and the late Holocene relative sea-level history from this region therefore has the potential to reflect primarily glacio-eustatic controlled sea-level change. Several studies have contributed to understanding sea-level change in Denmark and these are reviewed in Chapter 2. The more recent work of Clemmensen et al (2001a), at Skagen Odde in the north of Denmark (Figure 1.1) has provided a much needed update to sea-level research in the region but reliable data still remain sparse.

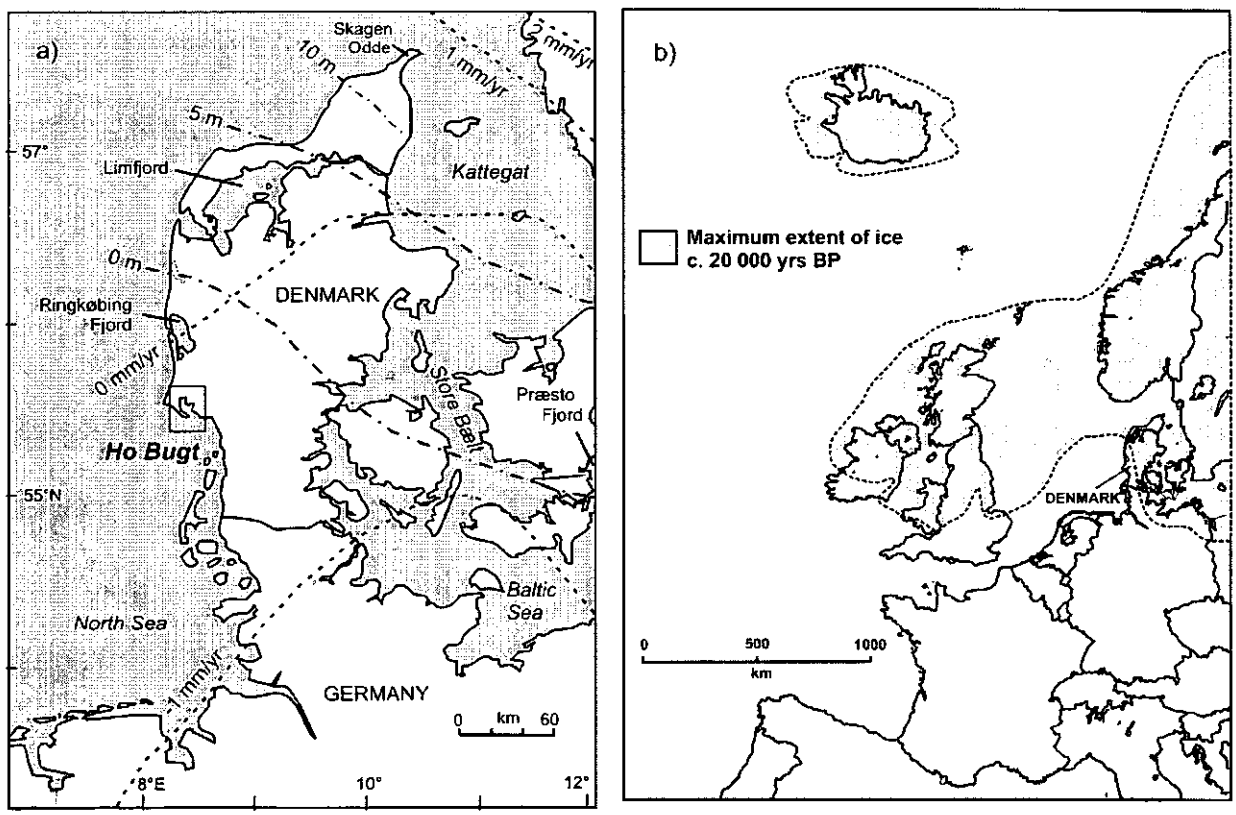

Figure 1.1. a) Danish coastlines in relation to contours of elevation of Holocene marine deposits (m) from Krog (1979a) and contours of contemporary crustal motion in mm/yr measured by Global Positioning Satellite (GPS) (www.ecgs.lu/pdf/jlg89/JLG89_3_Scherneck.pdf). The location of Ho Bugt, the study site of this thesis (further detailed in Chapter 3) and places mentioned in text are indicated. b) Location of Denmark in relation to former Fennoscandian and British Ice Sheets at the height of the last glaciation c. 18 000 cal. yrs BP (Adapted from Sejrup et al., 2000).

1.5 Thesis Aims

The overall aim of this thesis is to reconstruct the relative sea-level history of the Ho Bugt embayment for the last 7000 years, primarily using diatoms as sea-level indicators by:

- Documenting the modern diatom assemblages and their controlling environmental variables across the salt marshes in the Ho Bugt embayment
- Recording the detailed stratigraphy of the Ho Bugt embayment to gain an understanding of the major lithostratigraphical and environmental changes occurring
- Establishing the dominant control on diatom assemblages in this embayment through the use of several ordination techniques
- Developing a diatom-based transfer function for reconstructing changes in palaeomarsh-surface elevation
- Applying this transfer function to a series of fossil cores to interpret changes in palaeomarsh-surface history and assessing the reliability of these reconstructions
- Combining these palaeomarsh-surface records with age depth-models to produce a series of local water-level curves and comparing these curves with the local tide-gauge record
- Documenting the millennial-scale relative sea-level history of the Ho Bugt embayment through reconstruction of samples from a number of different cores
- Comparing this transfer-function predicted relative sea-level curve with those established using a qualitative interpretation of lithology
- Comparing the sea-level curves established in this study with predictions based on a series of glacial isostatic adjustment models, to explore the controls on relative sea-level change in the Ho Bugt embayment.

The above aims are achieved through the use of field sampling, the analysis of modern and fossil material and the subsequent application of statistical techniques. In achieving the aims of this investigation, an attempt has been made to harmonise the statistical methodology used to explore modern training sets and to develop diatom-based transfer functions for sea-level reconstruction by incorporating methodological aspects from several communities. In addition, the need for an integrated approach using the results of statistical, lithological and biostratigraphical investigations to provide a more complete picture has been acknowledged throughout.

1.6 Thesis structure

The first part of this thesis (Chapter 2) provides a background and context for the current study. Existing knowledge of past sea-level change in Denmark and the nearby German North Sea coast is reviewed and the significance of relative sea-level records, particularly for providing constraints on geophysical models, is discussed. The two main approaches to sea-level reconstruction (lithology-based techniques and quantitative techniques) are introduced, with a particular focus on the development of microfossil-based transfer functions. Some background information on the microfossil group chosen for this study, diatoms, and the reasons behind this choice are outlined. Particular focus is given to the use of diatoms as sea-level indicators.

Chapter 3 introduces the study area of Ho Bugt and describes the field and laboratory-based methods used throughout this investigation. A detailed methodology of the statistical methods incorporated into this study is given, with a particular focus on the use of data screening techniques and ordination methods. Chapter 4 presents the results from the investigation of the modern salt-marsh environment in Ho Bugt. Results of the analysis of a number of environmental variables are presented alongside modern diatom data. The vertical zonation of diatom taxa with respect to elevation is tested via the use of unconstrained cluster analysis and the relationship between diatom taxa and environmental variables is explored through the use of several ordination techniques.

Chapters 5 and 6 present results from the litho- and biostratigraphical investigations of the Ho Bugt embayment. The lithostratigraphy of the embayment is presented alongside detailed sedimentological characteristics of a master core sequence. Chronological control is provided by radiocarbon (^{14}C), optically stimulated luminescence (OSL), Lead-210 (^{210}Pb), Cesium-137 (^{137}Cs) and Americium-241 (^{241}Am) ages. High resolution diatom records are presented from two core sections. Low resolution diatom analyses of several core sections provide an overview of the main biostratigraphical changes in the Ho Bugt salt marshes.

Chapter 7 details the development of a series of diatom-based transfer functions for inferring changes in palaeomarsh-surface elevation. The use of Maximum Likelihood (ML), Weighted-Averaging (WA) and Weighted-Averaging Partial Least Squares (WA-PLS) regression models, alongside the Modern Analogue Technique (MAT), is explored.

The reliability of these reconstructions is assessed with the use of 'goodness of fit' and 'analogue' statistics. In Chapter 8 diatom assemblages in a series of fossil cores are calibrated using the transfer function to reconstruct changes in palaeomarsh-surface elevation. The development of age-depth models using ^{14}C, OSL, ^{210}Pb, ^{137}Cs and ^{241}Am ages is illustrated. These models are then used in combination with the transfer-function predicted palaeomarsh-surface elevations to reconstruct changes in local water levels.

In Chapter 9, the millennial-scale sea-level history of the Ho Bugt embayment is reconstructed. This record is compared with a record reconstructed using a qualitative lithology-based technique. Local water-level curves established in this study are placed in the context of litho- and biostratigraphical results to explore the evolution of the Ho Bugt embayment. The dominant process controlling relative sea-level change in the Ho Bugt embayment is examined through comparison of the relative sea-level data with predictions from a series of geophysical models. Chapter 10 presents the conclusions of this study and makes recommendations for future work.

1.7 Presentation of radiocarbon dates

All ^{14}C dates in this thesis are presented in calibrated radiocarbon years before present (cal. yr BP) unless otherwise stated. OSL, ^{210}Pb and ^{137}Cs ages are converted to a 1950 datum to ensure consistency with the ^{14}C ages (i.e. the ^{137}Cs peak at 1986 is shown as -36 yr BP).

Chapter 2

Background and Context

This chapter reviews existing sea-level research along the Danish North Sea coast and the nearby German North Sea coast and outlines the significance of relative sea-level records for providing constraints on geophysical models. The two main approaches (lithology-based approaches and quantitative reconstructions) to relative sea-level reconstructions are reviewed, with a particular focus on the development of microfossil-based transfer functions. Differences between the statistical methodology behind transfer function development in sea-level studies and that employed in palaeolimnology are highlighted. The use of diatoms in relative sea-level studies is discussed, with a particular focus on their value as sea-level indicators.

2.1 Sea-level change in Denmark

2.1.1 Eemian shorelines

Southwestern Denmark lies beyond the limits of the last glaciation (c. 75, 000 – 10,000 yr BP) and has not been covered by ice during the last 100,000 years (Konradi et al., 2005). During the last interglacial period, the Eemian (128 – 116 kyr BP), the southern North Sea was a shallow marine area with numerous embayments and fjords (Gripp, 1964; Konradi 1976; Kosack and Lange 1985; Strief, 1990; Temmler, 1995; Konradi et al., 2005). Although it was previously thought that there was no connection across the Jutland peninsula between the Baltic and the North Sea during the Eemian (Petersen, 1985), more recent research has speculated that a connection may have existed (Schulz et al., 2001; Konradi et al., 2005).

2.1.2 The early Holocene rise in relative sea level

The whole Danish coastline experienced a dramatic rise in sea level during the early to middle Holocene, primarily considered to be the result of eustatic rise (Jelgersma, 1979). The Danish North Sea coast was no exception. Krog (1960, 1973) was one of the first researchers to document this rapid rise in sea level for the Store Bælt region (Figure 1.1) on the basis of pollen analysis and ^{14}C dating. Krog's curve (Figure 2.1) documents a transgression of approximately 25 m between 8000 – 6500 cal. yr BP. It is thought that this transgression resulted in the coastline of Denmark attaining somewhere close to the present day extent (Krog, 1979b). Krog acknowledges the 'tentative' nature of his curve, in

particular the steepness of the eustatic rise, commenting on the lack of fixed points and the fact that is it based upon evidence from above present day sea level.

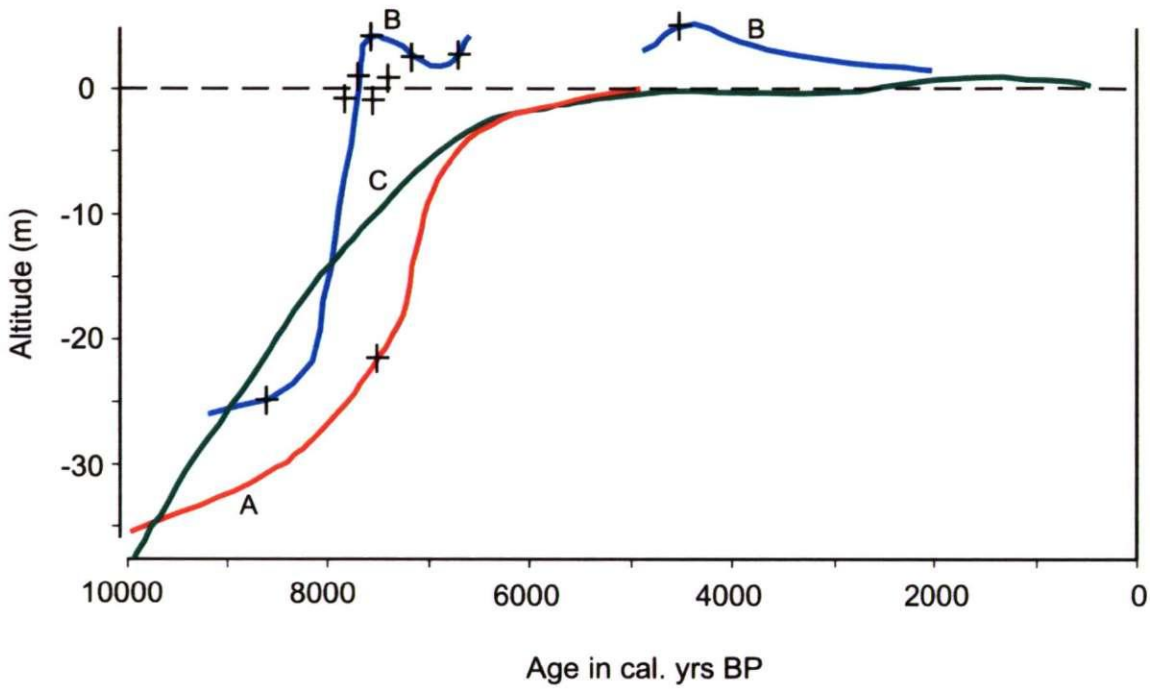

Figure 2.1. Published sea-level curves for Denmark. A) Krog (1960, 1973) for the Store Bælt, B) Petersen (1981) and Petersen and Rasmussen (1995) for the Limfjord and C) Mikkelsen (1949) for Præsto Fjord. Curves are redrawn and revised from Pirazzoli (1991). Locations are illustrated in Figure 1.1 and are discussed in text. Where possible data points are included, but these are often not presented by the authors.

Petersen's (1981) research in the Skagerak – Limfjord region, Northern Jutland, built upon Krog's earlier work. From a borehole at Vust, north of the Limfjord (Figure 1.1), Petersen (1981) reconstructed the whole course of the early Holocene transgression and provided a rate for the eustatic sea-level rise. Based mainly upon radiocarbon dating of marine molluscan fauna, he traced the transgression from -25 m at c.9000 – 8000 cal. yr BP to +3 m above present day sea level at 7000 cal. yr BP. The resulting sea-level curve documents some 28 m of sea-level rise in around 880 years (Figure 2.1). Revisions made to these figures following developments in U/Th age determination (Bard et al., 1993) and radiocarbon calibration (Stuvier and Reimer, 1993) resulted in an even steeper rate of rise of 28 m in 850 years (3.3 cm/yr) (Petersen and Rasmussen, 1995). These results correspond well with Mörner's (1976) eustatic sea-level curve for the region (Figure 2.3). Petersen's work has been widely cited, in part because it offers some of the most recent data on sea-level changes in Denmark. However, the steepness of the eustatic rise seems

questionable, particularly when considering the lack of data points to support this section of the curve (Shennan, 1987).

2.1.3 Middle to late Holocene relative sea-level changes

For the Danish Kattegat and Baltic coasts (Figure 1.1), evidence of sea-level changes for the period following the dramatic rise in sea level is well documented. Extensive work by Iversen (1937), Troels-Smith (1937, 1942) and Jessen (1937) along these coastlines document a sequence of minor fluctuations in sea level known as the Littorina Transgressions. Additional supporting studies were also carried out at Blekinge and Baresebäck, in southern Sweden (Berglund, 1971 and Digerfeldt 1974, respectively). Later work by Mikkelsen (1949) at Præsto Fjord (Figure 1.1) did not provide support for the notion of regressive phases separated by transgressive phases, but did demonstrate some changes in salinity based on diatom evidence. Mikkelsen's investigations form some of the most extensive work undertaken within the Danish part of the Baltic and resulted in the construction of a shoreline displacement curve for Præsto Fjord (Figure 2.1). This curve illustrates an uninterrupted transgression from 10,000 – 7000 cal. yr BP, which slows around 6000 cal. yr BP, before a further rise around 2000 cal. yr BP of up to 1 m above present day sea levels (Mikkelsen, 1949; Krog, 1979b). For the Danish North Sea coast, corresponding evidence of sea-level changes during this time is sparse.

For the late Holocene (post 5000 yrs BP), the sea-level history of the region is poorly documented, and again evidence from the Danish North Sea coast is sparse (Clemmensen et al., 2001). The sea-level curves produced by Mikkelsen (1949) and Krog (1960, 1973) show some evidence to suggest above present sea level c. 2000 – 1500 cal. yr BP but the latter parts of these curves are poorly defined (Figure 2.1). Several authors provide evidence to suggest that sea level has fluctuated during the most recent part of the Holocene. Bartholdy and Pejrup (1994) suggest that between 5700 – 2900 cal. yr BP sea-level attained at least three highstands, of which at least one exceeded present day sea level. Their arguments are however based on the assumption that the curve for eustatic sea-level rise (Figure 2.3), produced by Mörner (1976), is correct. This point is discussed further in Section 2.1.4. In a more recent study, Clemmensen et al (2001) use small-scale fluctuations in peat elevation along the Skagen Odde spit system in northern Denmark, to document a series of sea-level highstands (Figure 2.2). Highstands are identified at 5450, 4700 and 2450 cal. yr BP, with accompanying lowstands at 5200, 4100 and 1650 cal. yr

BP. The total maximum eustatic sea-level change for the period under study is estimated to be c. 4.5 m, depending on which isostatic model is used (Clemmensen et al., 2001).

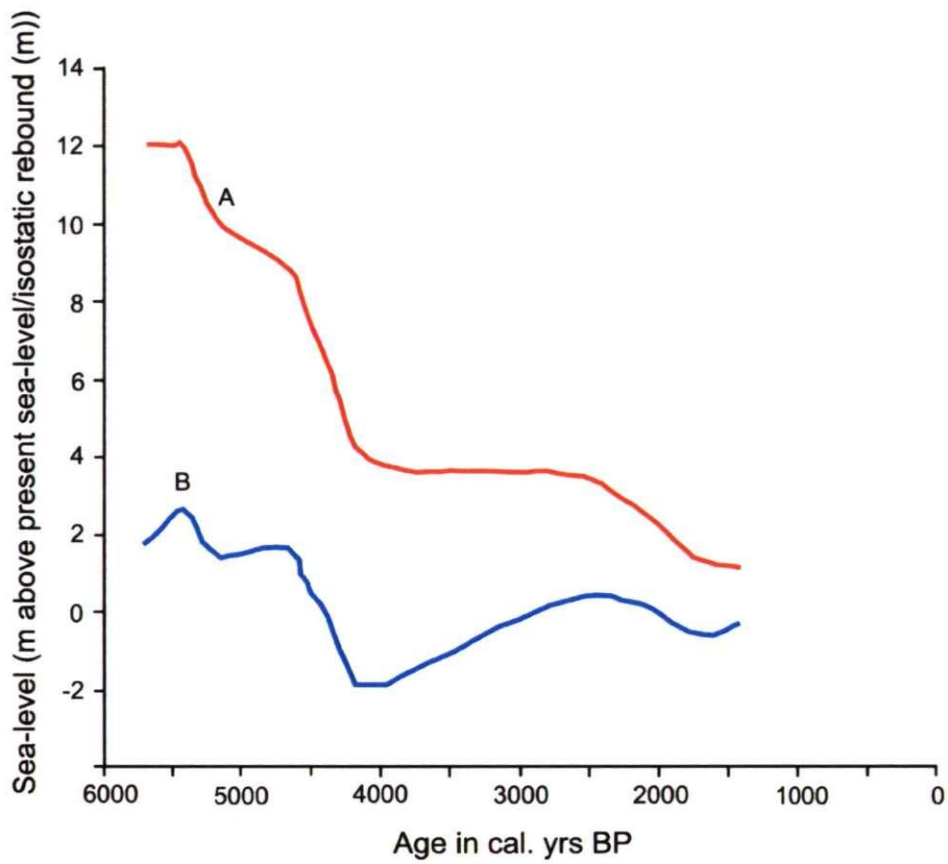

Figure 2.2. Sea-level variation at Kanderstederne, Skagen Odde. A) Relative sea level. B) Relative sea level minus land uplift. Adapted from Clemmensen et al. (2001).

2.1.4 Relative sea-level change along the southern Danish North Sea Coast

As early as the 1920s Mertz (1924) shows the hinge line between the uplifting and subsiding coastlines intersecting the Danish North Sea coast north of the Ringköbing Fjord (Figure 1.1), based on the presence of Holocene marine deposits on land (Krog 1979a). It is generally believed that those localities situated close to this hinge line have been isostatically stable during the Holocene (Bartholdy and Perjup, 1994). Recent research, some of which forms part of this thesis, suggests that this may not be the case (Gehrels et al., 2006a) (Section 9.7). There have been numerous speculations in the literature about higher-than-present sea levels during the middle and late Holocene along the southern Danish North Sea coast. One such area is the coastline between Blåvands Huk and the Ringköbing Fjord (Figures 1.1 and 2.3).

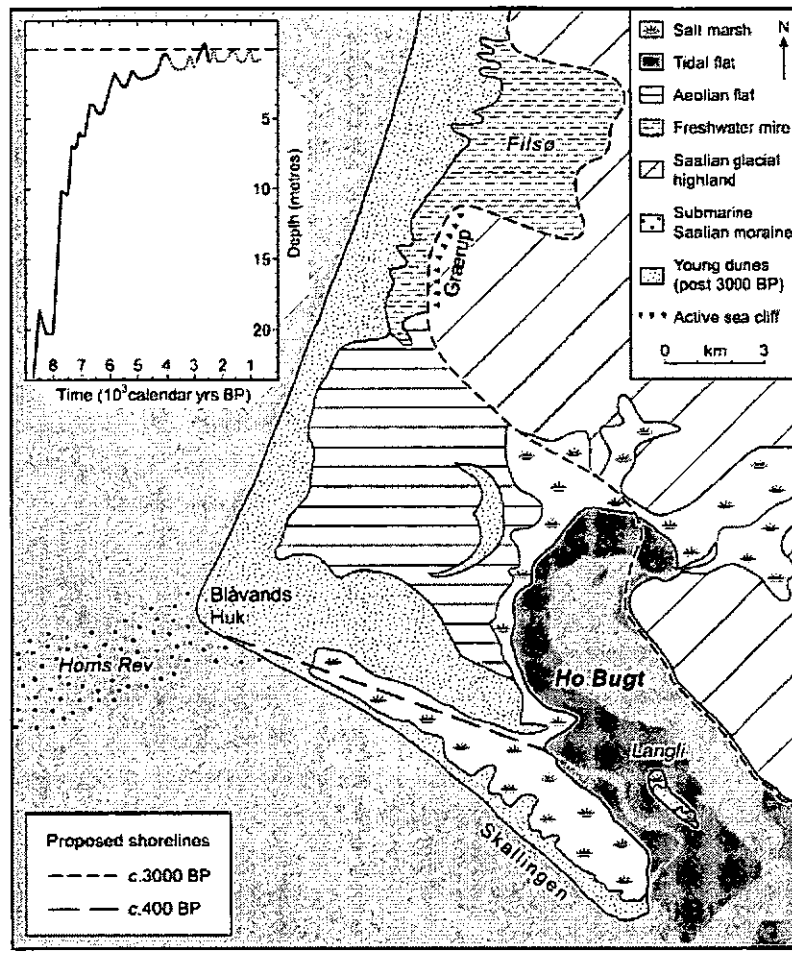

Figure 2.3. Geomorphological map of the Ho Bugt area based on Aagaard et al. (1995) and Clemmensen et al. (1996) and taken from Gehrels et al. (2006a). The Kattegat sea-level curve of Mörner (1976) is shown as an insert. The late Holocene highstand in the Mörner curve has been used to support the findings of Aagaard et al. (1995) and Davis et al. (1997, 2001) for higher than present sea level c. 3000 cal. yrs BP (see text).

Jessen (1920) was the first author to highlight the anomalous heights of Holocene beach ridges north of Blåvands Huk of up to 4.7 m above Danish National Datum (DNN). Working in the same area, Jonassen (1957) suggested that the inland marine cliff at Grærup, to the east of the dune ridges marks a Holocene sea-level position +5 m above present. These observations were supported by two important findings. Firstly, Petersen (1994) found the marine mollusc *Donax vittatus* at an elevation of approximately –7 m DNN and dated to 2620 ± 75 yrs BP (AAR-1480). Petersen (1994) used this shell as evidence to suggest that the cliff line was active approximately 2500 – 3000 ^{14}C years BP. *Donax vittatus* molluscs are indicative of a high energy environment and this finding led some authors to suggest that the shoreline at this time was that of the maximum Holocene transgression (e.g., Mörner, 1976; Aagaard et al., 1995). Second, Clemmensen et al. (1996) identified 'marine deposits' close to the Grærup cliff at a level of + 1.5 m DNN using

ground penetrating radar, and also documented the height of the nearby gravel barriers to 4 - 4.5 m DNN. These two separate findings have led to the speculation that sea level in west Denmark was at least 1.5 m above present c. 2500 – 3000 cal. yr BP (Aagaard et al., 1995; Davis et al., 1997; 2001). The authors use Mörner's widely cited Kattegat sea-level curve to support their arguments, which shows a sea-level highstand between 2500 and 3000 cal. yr BP (Figure 2.3 insert).

Originally produced as the outcome of a PhD study in 1969 (Mörner, 1969a, 1969b) and revised in 1976 (Mörner, 1976), the Kattegat sea-level curve has been argued to represent the regional eustatic sea-level history for the entire North Sea basin (Shennan, 1987). Mörner (1979) argued that during the Holocene the entire North Sea acted uniformly to global- scale geoidal changes and proposed the concept of 'regional eustasy'. The 2500 – 3000 cal yr BP highstand is an important feature of the Kattegat sea-level curve (Mörner, 1969a; 1969b; 1976) and if correct represents the highest position reached by the sea during the Holocene.

2.1.5 Evidence from the German North Sea coast

Unlike Denmark, the German North Sea region (Figure 2.4) has been the subject of several comprehensive studies to reconstruct Holocene relative sea-level change (e.g., Behre et al., 1979; Ludwig et al., 1981; Freund and Streif, 2000; Freund et al., 2004; Behre 2004). Recent studies along this coastline provide some of the best evidence concerning middle to late Holocene sea-level changes and are highly relevant to this study. It is possible that relative sea-level changes observed along the German North Sea coast can also be identified in records from southwestern Denmark.

Relative sea-level change was first studied in the German North Sea region by Schütte (1933, 1939) who examined coastal subsidence and uplift in relation to time in the Jade-Weser region (Figure 2.4). Evidence for the early Holocene rapid rise in sea level is first provided by Behre and Menke (1969) in the form of a well-dated peat on the southern Dogger Bank (Behre and Menke, 1969; Behre et al., 1979). This transgression has been traced to a sea level of –46 m c. 9500 ^{14}C yrs BP (Behre et al., 1979), approximately 500 yrs earlier than documented by Krog (1979a, 1979b) in Denmark. Other data on the rise in sea level during the early Holocene is provided by Menke's (1976) relative mean high

water curve from the Eider-Miele region (Figure 2.5) and the curve produced by Ludwig et al. (1979, 1981) for the southern North Sea (Figure 2.5).

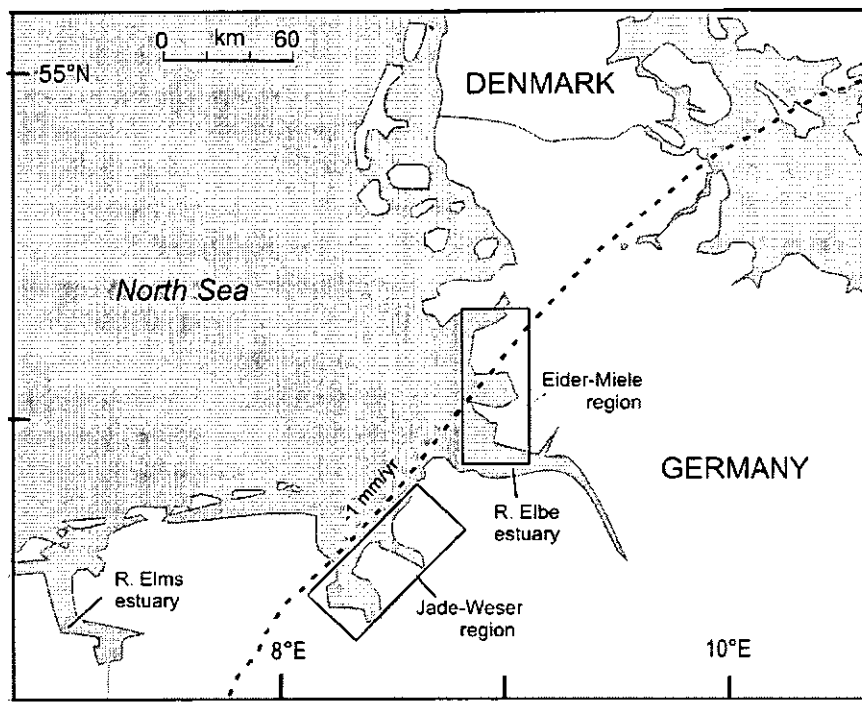

Figure 2.4. German North Sea coast showing location of places mentioned in text.

The record from the German part of the North Sea for the middle to late Holocene period is far more comprehensive than the one in Denmark. Müller (1962) proposed two curves, based on fifty-seven ^{14}C dates, documenting mean high water changes along the southern North Sea coast of Germany (Pirazzoli, 1991) (Figure 2.5). Both curves show small amplitude fluctuations in mean high water throughout the middle and late Holocene. If these changes represent true eustatic fluctuations, it is highly likely that these fluctuations were propagated along the North Sea coast of Denmark. More recently Streif (2004) has interpreted the regressive overlap of peat layers on tidal flat sedimentation as an indication of temporary reversals of sea level from c. 7300 cal. yr BP onwards. Evidence for these peat layers is found throughout the coastal lowlands between the Ems and Elbe estuaries (Streif 2004). Behre (2004) presents a sea-level curve of mean high water for the most recent part of the Holocene for Lower Saxony (Figure 2.6). Intercalated peat layers at c. 5000, 4400, 3500 and 3000 cal. yr BP are argued to correspond with large-scale regressions of the North Sea (Behre, 2004). Behre's curve has however been heavily criticised by colleagues from the Netherlands and Belgium (e.g., Bateman, 2006) because it draws together several types of evidence from multiple basins but does not correct for the differences in tidal range.

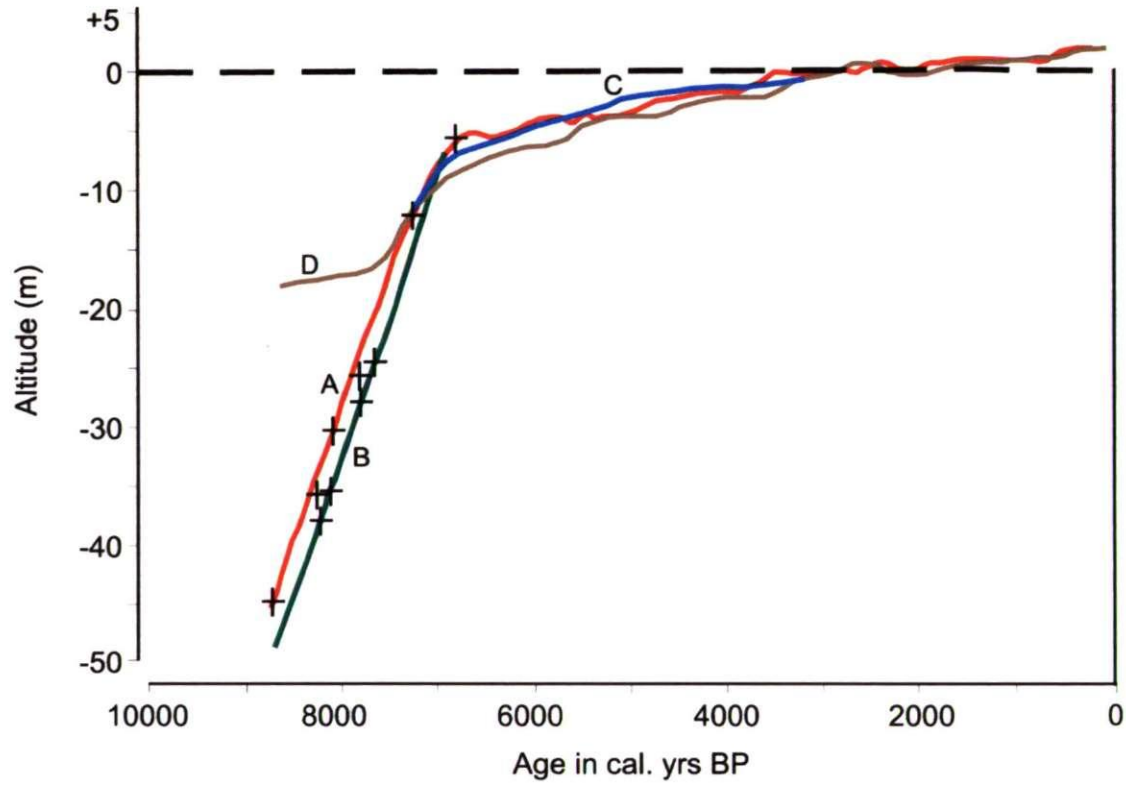

Figure 2.5. Published sea-level curves for the German North Sea coast. A) Menke (1976) for the Eider-Miele region, B) Ludwig et al. (1979, 1981) for the southern North Sea, C) and D) Müller (1962) for the German North Sea region. Curves are redrawn and modified from Pirazzoli (1991). Locations are illustrated in Figure 2.4 and are discussed in text. Where possible data points are included, but these are often not presented by the authors.

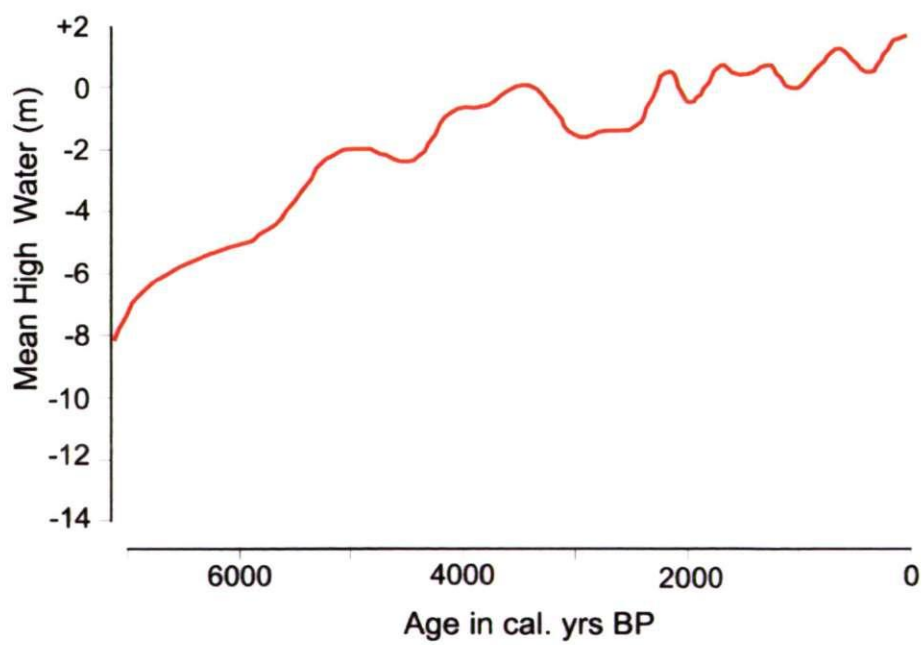

Figure 2.6. Sea-level curve of mean high water for the most recent part of the Holocene for Lower Saxony, Germany (Behre, 2004).

2.2 Significance of relative sea-level records

Records of Holocene sea level show both temporal and spatial variation around the globe as result of the interplay between several key processes operating at the global, regional and local scale (Lambeck, 1990). These processes occur as a direct result of the melting of the Pleistocene ice sheets and include the response of the Earth's crust to redistributed surface loading, volumetric changes to the ocean caused by ice melt and the tectonic movement of shorelines independent of any glacio- hydro- isostatic origin (Lambeck, 1990). Peltier (1994) argues that relative sea-level data provide one of the best available records of these processes, and of the surface loading component in particular. Observations of relative sea-level changes can therefore provide valuable constraints on model parameters in glacio- hydro- isostatic models (Lambeck, 1995, Shennan et al., 2000a). Comparison of sea-level observations with model predictions has enabled estimates of ice thickness and the extent of ice margins to be established (Lambeck, 1995, 1996; Milne et al., 2002). Although GPS observations of crustal motion have become an important tool for constraining glacial isostatic adjustment (GIA) models (e.g., Milne et al., 2001, 2006), relative sea-level observations remain important because they cover longer time-scales. A combination of both GPS and sea-level observations are therefore important for constraining and testing the latest generation of 3-D geophysical models, which take into account lateral Earth structure changes (e.g., Latychev et al., 2005a, 2005b, 2005c; Whitehorse et al., 2006), and recently refined GIA models such as ICE-5G (Peltier, 2004).

2.3 Sea-level reconstruction techniques

Much of the work reviewed in the previous section has increasingly employed a methodology that allows high resolution sea-level changes to be reconstructed. Reconstructions that can obtain precisions of only a few cm are becoming increasingly important when considering the low magnitude changes in sea level that have occurred during the last 2000 - 3000 yrs (Varekamp, 1992). The techniques employed in these reconstructions can be divided into two main categories: 1) lithology-based techniques and 2) quantitative techniques.

2.3.1 Lithology-based approaches

Prior to the integration of quantitative techniques within sea-level research, the community relied heavily on lithology-based reconstructions. Methodologies described by Shennan (1982, 1986a, 1986b) and developed within the context of IGCP Projects 61 and 200

(Preuss, 1979; van de Plassche, 1986) relied on the analysis of stratigraphic boundaries between freshwater and marine facies. Although increasingly quantitative techniques are being employed in sea-level research, a thorough understanding of the lithostratigraphy should form the framework of any sea-level study. For example, the most recent work on sea-level changes along the German North Sea coast is based on high-resolution interpretation of lithological changes (e.g., Streif, 2004; Behre, 2004). In this study, diatom-inferred quantitative relative sea-level histories are compared with those produced using a qualitative interpretation of litho- and biostratigraphic units in fossil cores.

2.3.2 Quantitative techniques

In 1971, Imbrie and Kipp provided the first quantitative estimate of environmental change using foraminifera in ocean cores to reconstruct sea-surface temperature and salinity. Since this time, quantitative techniques have been extensively developed within biogeography, oceanography, palaeolimnology, and more recently, within Holocene sea-level studies. By developing and applying transfer functions (Birks, 1995), quantitative techniques aim to increase the accuracy of reconstructions by establishing a better understanding of the present day relationship between biological indicators (e.g., foraminifera, diatoms, testate amoebae) and environmental variables. Examples of the many environmental variables which have been reconstructed using such quantitative techniques include: sea-surface temperature and salinity (Imbrie and Kipp, 1971), salinity and water-level fluctuations (Fritz, 1990), salinity and climate (Fritz et al., 1991), climate and summer temperatures (Korhola and Weckström, 2000), pH (Davis and Anderson, 1985; Birks et al., 1990a; Battarbee et al., 2005; Larsen et al., 2006), lake-water chemistry (Birks et al., 1990b; Gasse et al., 1995; Korsman and Birks, 1996; Davis et al., 2002), chlorophyll and nutrient enrichment (Jones and Juggins, 1995; Bennion et al., 1996; Burgess, 2004).

Principles of transfer functions

The primary aim of any quantitative reconstruction is to express the value of an environmental parameter (e.g., pH, temperature, elevation) as a function of the biological data (e.g., diatoms, foraminifera, pollen) (Birks, 1995). Transfer functions are biological response functions, which model biology as a function of the environment (Juggins, *pers. comm.*). The methodology used in developing transfer functions and providing quantitative estimates of environmental variables can be summarised in four main stages (adapted from Birks, 1995; 1998):

1. Collection of a modern training set comprising both biological and environmental data
2. Analysis of these data to relate species assemblages to the environmental variable of interest, usually using ordination techniques
3. Modelling of these relationships using regression analysis to develop a transfer function
4. Application of this transfer function to a fossil core to reconstruct environmental variables based on species assemblages and infer past environmental conditions.

The models used to analyse relationships in the modern training set (ordination methods), and regression models used to subsequently develop transfer functions, fall into two main categories, linear-based and unimodal-based techniques (Birks, 1995). Ordination methods commonly employed in such studies include the linear-based methods of Principal Components Analysis (PCA: Orlóci, 1966)) and Redundancy Analysis (RDA: van den Wollenberg, 1977) and the unimodal-based methods of Detrended Correspondence Analysis (DCA: Hill, 1979) and Canonical Correspondence Analysis (CCA: ter Braak, 1986). A full discussion of these techniques is given in Lepš and Šmilauer (2003) and Jongman et al., (1995). The ordination methods employed in this study are further discussed in Chapters 3 and 4. Regression models used to develop transfer functions include the linear-based method of Partial Least-Squares (PLS: Wold et al., 1984) and the unimodal-based methods of Maximum Likelihood (ML), Weighted Averaging (WA; ter Braak, 1987b) and Weighted-Averaging Partial Least Squares (WA-PLS; ter Braak and Juggins, 1993). The Modern Analogue Technique (MAT; Prell, 1985) is additionally used in transfer function development, but does not assume an underlying response model.

Regression models employed in this study include ML, WA, WA-PLS and MAT. ML regression is based on the concept that the relationship between the abundance of a taxon (y) and an environmental variable (x) can be estimated by fitting a response model which comprises systematic and random error components (Birks, 1995) (Figure 2.7a). These curves are fitted to all taxa in the modern training set using unimodal regression. Species composition and likely abundances at a given value of x are determined by the curves for all taxa (Birks, 1995). These models can then be used to calculate the probability that a certain value of x would occur given a certain species assemblage (Birks, 1995). The ML estimate is where the value of x gives the highest probability (Birks, 1995). It has been argued that ML regression and calibration provide a robust approach to environmental

reconstruction and can perform as well or even better than WA-based methods (Birks, 1995, 2001).

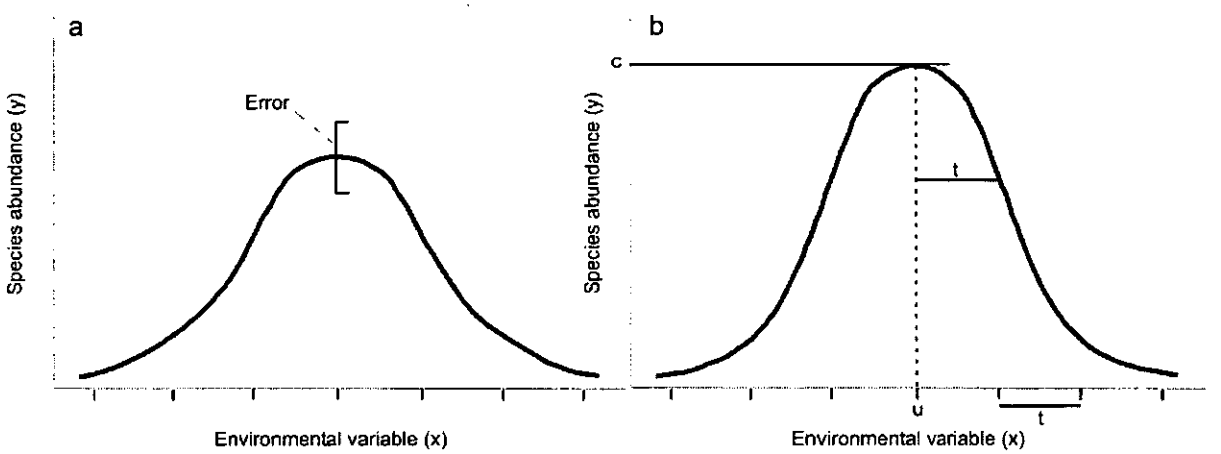

Figure 2.7. Unimodal species response models a) Systematic response model used in maximum likelihood regression showing relationship between species abundance (y) and an environmental variable (x), and b) Gaussian unimodal relationship between species abundance (y) and an environmental variable (x). u = species optimum, t = species tolerance and c = maximum abundance. Modified from ter Braak (1987c).

WA is based on the assumption that species respond unimodally to environmental gradients. Along an environmental gradient, a taxon's optimum occurs at the point where it is most abundant. An estimate of a taxon's optimum can be calculated by taking an average of all the x values where the taxon occurs, weighted by the relative abundance of the taxon at each site (ter Braak and van Dam, 1989, Birks, 1995). The optimum for each taxon is therefore a 'weighted-average' (ter Braak, 1987b). In calibration, an estimate of the unknown variable is a weighted average of the x optima of all species present. The species-environmental relationship behind weighted averaging approaches is shown in Figure 2.7b.

WA methods have been shown to suffer from several problems. Firstly, they tend only to perform well when the entire environmental range of each species in the modern training set is sampled and they are sensitive to the distribution of sample sites in the training set (ter Braak and Looman, 1986). Secondly, WA considers each environmental variable separately and ignores any residual correlations in the data set that may be the result of environmental variables not included in the WA (ter Braak and Juggins, 1993). As an improvement to WA, ter Braak and Juggins (1993) developed WA-PLS. WA-PLS regression utilises residual correlations in the species data to improve the fit between species assemblages and the environmental variable of interest (ter Braak and Juggins, 1993).

The MAT method is also explored in this study. MAT uses a dissimilarity measure to compare species assemblages in a fossil samples with species assemblages in the modern training set (Birks, 1995). The value of the environmental variable for that fossil sample is inferred from the modern sample with which it is most similar (Birks, 1995). For MAT to be successful, it requires an extensive modern training set that covers the likely range of species and environmental variables in the past. Unreliable reconstructions can result if a large number of 'no analogue' species are present in the fossil data (Birks, 1998). This is where a species is present in fossil data but absence from the modern training set. Such requirements often limit the applicability of the MAT technique (Birks, 1995). Nevertheless, MAT has been argued to provide a relatively simple and robust method, which can reconstruct one or more environmental variable simultaneously (Birks, 1998). In this study MAT is additionally used to assess the reliability of the environmental reconstructions. This is further discussed in Chapter 8.

Quantitative techniques in sea-level studies

Quantitative techniques have been used in Holocene sea-level studies since the late 1990s to reconstruct changes in relative sea level. Examples of such studies include: Gehrels (2000), Hamilton and Shennan (2005a, 2005b), Horton and Edwards (2005) Boomer and Horton (2006) and Edwards and Horton (2000, 2006). The transfer function methodology is now widely adopted in sea-level research. However, two significant problems are apparent. Firstly, although numerous studies have focussed on the development of modern training sets to reconstruct changes in relative sea level (stage 1, 2 and 3 above); far fewer studies actually demonstrate such reconstructions. This is especially true for diatom-based reconstructions. This is a similar situation to that identified in palaeolimnology by Birks in the late 1990s (Birks, 1998). Secondly, the statistical methodology adopted by the sea-level community differs to that employed by many biogeographers, oceanographers and palaeolimnologists, particularly with regards to data screening and the use of ordination techniques in training set development. A major aim of this study is to harmonise the statistical methodology used to explore modern training sets and to develop diatom-based transfer functions for sea-level reconstruction, by incorporating methodological aspects from several communities. A particular focus of this thesis has been to integrate statistical aspects from the palaeolimnological community, where diatom-based transfer functions have been extensively used.

Recent advances in quantitative techniques

Some of the most recent advances in quantitative reconstruction techniques include Artificial Neural Networks (ANNs; Malmgren et al., 2001) and Bayesian approaches. Whereas the majority of calibration models (e.g., PLS, WA, WA-PLS) assume either a linear or unimodal underlying response model, ANNs are able to incorporate and model taxa with very different ecological responses (Birks, 1998). Such an approach is highly valuable because in reality species may show a skewed or sigmoid response to the environmental variable of interest (Birks, 1998). The application of ANN techniques to environmental reconstruction is a fairly recent advance and only a limited number of studies in the fields of palaeolimnology (e.g., Racca et al., 2001; Koster et al., 2004) and oceanography (e.g., Kucera et al., 2005; Malmgren et al., 2001; Barrows and Juggins, 2005) have attempted to use such a method. Bayesian approaches are based on prior information and probability (Birks, 1998). Several very recent studies highlight the potential of Bayesian statistics for environmental reconstructions (e.g., Brooks, 2006; Erasto and Holmstrom, 2006; Haslett et al., 2006).

2.4 Diatoms

Diatoms are microscopic unicellular algae (Battarbee et al., 2001), found in lakes, ponds, estuaries, salt marshes and in the sea. They live in environments dominated by water and natural light (Palmer and Abbott, 1986). Diatoms are used extensively in palaeoenvironmental reconstructions because they are considered excellent indicators of past environmental change (Mackay et al., 2003). In sea-level studies, benthic diatoms are of greatest importance, and they are found in association with various biological and geological substrates (Palmer and Abbott, 1986). Within the coastal environment diatoms are sensitive to a range of environmental variables including salinity (Palmer and Abbott, 1986), substrate (Whiting and McIntire, 1985), and tidal inundation (Nelson and Kashima, 1993). Diatoms occur in large numbers in both contemporary and fossil environments and the majority of taxa have a widespread geographical distribution, making them highly suitable for use in quantitative studies (Gasse et al., 1995).

2.4.1 The importance of diatoms for sea-level research

Diatoms have been widely used in sea-level studies to infer past changes in relative sea-level (e.g., Palmer and Abbott, 1986; Nelson and Kashima, 1993; Shennan et al., 1996; Dawson and Smith, 1997; Zong, 1997, 1998). More recently the suitability of diatoms as sea-level indicators has been demonstrated by a number of studies on modern species-environment relationships using multivariate statistical approaches (e.g., Zong and Horton, 1999; Gehrels et al., 2001; Patterson et al., 2005). At present there are few examples of the use of diatoms to reconstruct, quatitatively, changes in relative sea-level (e.g., Shennan and Hamilton, 2005a, 2005b). Other microfossils commonly used as sea-level indicators include foraminifera (e.g., Gehrels, 1999; Horton, 1999; Gehrels 2000; Gehrels and Newman, 2004), and testate amoebae (Charman et al., 2002; Gehrels et al., 2001, 2006b). In this study diatoms are used in preference to any other sea-level indicator for the following reasons:

- Whilst foraminifera were found to be well preserved in the modern salt-marsh environment in this study site (Gehrels and Newman, 2004), preservation in fossil cores was poor and counts were generally very low (Gehrels et al., 2006a).

- Studies demonstrating the use of testate amoebae as sea-level indicators are at an early stage. Much additional work would be required to use such a microfossil group to reconstruct relative sea level. In addition, testate amoebae generally live around mean high water spring tides (MHWST) (Gehrels et al., 2001) and their distribution within the tidal frame was not considered large enough for them to be used independently in this study.

- Preliminary work on both the modern and fossil material in the Ho Bugt study site suggested that diatom preservation was very good in both the modern and core material (Gehrels et al., 2006a; Szkornik et al., 2006).

2.4.2 Influences on diatom distribution in the coastal zone

The use of diatom biostratigraphical techniques to reconstruct changes in relative sea level requires a strong understanding of contemporary diatom assemblages across the intertidal zone (Zong and Hoton, 1999). The use of diatoms in such studies is therefore often constrained by a poor understanding of the relationship between diatom assemblages and environmental variables (Zong, 1997; Zong and Horton, 1998). Although the general ecology of many coastal diatoms is well understood (Vos and De Wolf, 1993; Denys, 1994), understanding of their specific habitat preferences is limited, especially in areas where marine and terrestrial systems interact (Zong, 1997). Several studies have examined the influence of various environmental parameters on modern diatom distributions in the coastal zone. These are reviewed below.

Salinity

It has long been recognised that particular diatom taxa inhabit water of a particular salinity (Palmer and Abbott, 1986). A comprehensive review of the development of salinity classification schemes for diatoms based on salinity is provided by Juggins (1992). In this study the halobian system of classification is used, originally developed by Kolbe in 1927 and further refined by Hustedt (1953, 1957). The halobian scheme of Hustdet (1953, 1957) is summarised in Table 2.1, taken from Juggins (1992). For the purposes of this study, only the division within the oligohalobous group is identified. Sub-divisions within the mesohalobous group are classified together. The Hustedt scheme is used in preference to the classification scheme proposed by van der Werff and Huls (1957 – 1964), which divides species into marine, brackish and freshwater taxa, to provide consistency with other recent diatom-based sea-level studies (e.g., Zong and Horton, 1998; Hamilton and Shennan, 2005a, 2005b).

1. Polyhalobian: > 30 g l^{-1}
2. Mesohalobian
    a) Euryhaline mesohalobous: 0.2 – 30 g l^{-1}
    b) A-mesohalobous: lower brackish water > 10 g l^{-1}
    c) B-mesohalobous: upper brackish water 0.2 – 10 g l^{-1}
3. Oligohalobous
    a) Halophilous: optimum in slightly brackish water
    b) Indifferent: optimum in freshwater but tolerant of slightly brackish water
4. Halophobous: exclusively freshwater

Table 2.1. Halobian scheme of Hustedt (1953, 1957), reproduced from Juggins (1992).

Substrate

Several studies have demonstrated the role of substrate in controlling contemporary diatom distributions (e.g., Chapman, 1941; Whiting and McIntire, 1985; Trites et al., 2005). At Netarts Bay, Oregon, USA, Whiting and McIntire (1985) showed that diatom taxa formed a continuum with species abundance correlating with mean grain size. Other studies have demonstrated the association between the type of sediment and life form (e.g., Nelson and Kashima, 1993; Zong, 1997; Zong and Horton, 1998, 1999). High frequencies of epipelic diatoms are associated with fine grained silts and clays whilst episammic diatoms are associated with a sandy substrate (Zong, 1997; Zong and Horton, 1999; Sawai, 2001).

Elevation

Some of the most recent research in the intertidal zone has examined the relationship between diatoms and elevation. Nelson and Kashima (1993), Hemphill-Haley (1995), Shennan et al. (1995, 1996), Zong (1997), Zong and Horton (1998, 1999) and Gehrels et al. (2001), have demonstrated that diatom distributions are strongly related to elevation above mean sea level. Tidal inundation and associated hydrology and salinity control diatom distributions, but the level of tidal inundation is controlled by elevation (Gehrels, 2000). Correlations between diatom distributions and elevation are therefore often apparent. These observations strongly support the concept of a vertical zonation of diatom species with respect to the tidal frame (Nelson and Kashima, 1993). Such studies have been fundamental in the development of microfossil-based transfer functions which seek to establish the history of sea-level changes from fossil cores.

Hydrology

An additional environmental variable which may have an influence on diatom distributions across the intertidal zone is hydrology. The relationship between diatom species and physical parameters such as water depth, soil moisture and length of submergence has been explored in several lake-based studies (e.g. Gaiser et al., 1998, 2001). Such studies have direct application within the salt-marsh environment, where water levels vary greatly over short temporal scales. With the exception of the study by Gehrels et al. (2001) who relate diatom species to the degree of tidal flooding, the influence of these physical parameters on diatom distributions are rarely acknowledged in sea-level based investigations.

As with salinity and substrate, described above, classification schemes have also been developed based on taxon-specific responses to soil moisture and drought (e.g. Petersen, 1935; Lund, 1946). In this study it is likely that 'eu-terrestrial' or 'facultative' taxa (Petersen, 1935; Florin, 1970) such as *Hantzschia amphioxys* and *Pinnularia borealis*, may be found at high elevations. Here, the salt marshes are only flooded during the very highest tides and diatom species need to be capable of surviving periods of drought and desiccation (Patrick and Reimer, 1966; Gaiser et al., 1998).

2.4.3 Taphonomic issues

Studies which involve the use of microfossils to interpret fossil sequences make the assumption that no post-depositional changes have occurred but such assumptions are often erroneous. Several key taphonomic processes can be identified which are known to affect diatom assemblages in coastal marshes. These include transportation (Vos and de Wolf, 1993), fragmentation (Sherrod et al., 1989, Nelson and Kashima, 1993), bioturbation (Nelson and Kashima 1993) and dissolution (Hemphill-Haley, 1995; Sherrod, 1999). Other processes such as sample preparation, chemical analysis, digenesis and compaction (Beyens and Denys, 1982) may be further problems to take into consideration.

Transportation

The transportation of diatom frustules from surrounding environments is one of the most significant problems in diatom-based palaeoecological studies (Sherrod, 1999). In particular, the distinction between autochthonous (locally produced) and allochthonous (transported) diatoms is of major importance (Vos and De Wolf, 1993). In low-energy environments such as lakes, the problem is generally considered insignificant (Vos and De Wolf, 1993). However, the issue becomes more significant in coastal environments where higher energy levels dominate (Brockmann, 1940). In some tidal areas, the allochthonous influx has been found to exceed the autochthonous population (e.g., Simonsen, 1969; Vos and de Wolf, 1988; Sherrod et al., 1989). Importantly, within a salt-marsh environment a species may be allochthonous in some environments but autochthonous in others. Beyens and Denys (1982) devised a system for determining the allochthonous component of *fossil* assemblages based on salinity dependence and life-form, although they do not distinguish individual taxa. Vos and De Wolf (1988; 1993) developed a classification scheme that divided coastal diatoms into broad ecological groups relating to specific environments. They proposed several criteria to assess whether diatoms are allochthonous or autochthonous. More recently, several authors (e.g., Sherrod, 1999; Sawai, 2001; Sawai et al., 2004) have attempted to 'separate out' the allochthonous and autochthonous components of diatom assemblages and have provided further criteria for assessment.

Fragmentation and dissolution

Selective fragmentation and dissolution of diatom frustules can greatly affect palaeoecological interpretation, particularly of fossil assemblages (Sherrod et a., 1989; Nelson and Kashima, 1993). Delicate taxa may be broken during transport and digenesis and weaker, less silicified taxa such as *Gyrosigma* spp. are often depleted in an assemblage (Nelson and Kashima, 1993; Sherrod et al., 1989). Such processes also play an important role in enhancing the relative abundance of certain diatom taxa within an assemblage because they are more resilient to these processes (Sherrod, 1999). For example, *Parlia sulcata* is often dominant in coastal assemblages (Hemphill-Haley, 1995) but this is in part due to its greater resilience to breakage and dissolution (Sherrod et al., 1989). The fragmentation and dissolution of diatom valves has been extensively studied for lake environments (e.g., Battarbee et al., 2001; Ryves et al., 2005, 2006) but few corresponding examples are available for coastal environments (e.g., Hemphill-Haley, 1995).

2.5 Chapter summary

This chapter has reviewed existing sea-level research along the Danish North Sea coast and the nearby German North Sea coast. The importance of relative sea-level records, from the Danish North Sea coast in particular, for providing constraints on glacio- hydro- and isostatic models and has been discussed. The two main approaches to present day relative sea-level reconstructions have been outlined, with a particular focus on the development of microfossil-based transfer functions. The importance of diatoms in sea-level research and their potential use as sea-level indicators has been examined, and the reasoning behind their use in this study has been justified. The next chapter begins by further detailing the study site of Ho Bugt before going on to discuss the various field and laboratory-based methods used throughout this investigation.

Chapter 3

Methodology

This chapter outlines the various field and laboratory-based methods used throughout this investigation. The first part of this chapter details those techniques employed in the field, firstly in the investigation of the modern salt marsh environment and secondly, in the investigation of the palaeoenvironment. The second part of this chapter describes the laboratory methods employed in the processing and analysis of these samples. Details of the procedures used in diatom analysis, and the statistical techniques employed to examine these data are discussed in the last sections of this chapter. The statistical methods used in the development of a diatom-based transfer function are discussed separately in Chapter 7.

3.1 Study Site

This study is located in the tidal embayment of Ho Bugt in western Denmark (Figures 1.1 and 3.1). Ho Bugt is located in the northern most extreme of the Danish Wadden Sea, an intertidal area extending from the northern coast of the Netherlands, along northern Germany and into southern Denmark. The salt marshes within the Ho Bugt embayment form the largest section of undiked marsh land in the Danish Wadden Sea (Jepsen, 1996). Grazing and the use of fertilizers have been restricted in recent years under management by the Wadden Sea National Park authorities, resulting in an intertidal environment that can be considered relatively pristine, especially when compared to other marshes in the North Sea region. The embayment is micro-tidal, with a mean tidal range of ~1.5 m (Christiansen et al., 2004). Tidal levels in the Ho Bugt embayment are detailed in Table 3.1. During major storm surges, which on average occur once or twice a year, water levels may reach as high as 4 m above the Danish national vertical datum (DNN) (Bartholdy and Pejrup, 1994; Aagaard et al., 1995). The only significant freshwater discharge into Ho Bugt is via the Varde Å river in the northeast (Figure 3.1). Due to this freshwater supply, a gradient in salinity exists from the bay head (10 ‰) to the mouth of the Ho Bugt embayment (30 ‰) (Pejrup, 1986). To the north and east Ho Bugt is bounded by glacial moraine deposits of Saalian age (Aagaard et al., 1995). To the west the marshes are backed by an upland that consists of Holocene beach ridges covered by dunes. The Varde Å river valley contains salt-marsh deposits up to more than 10 km inland, underlain by glaciofluvial deposits of Weichselian age (Aagaard et al., 1995). The salt marshes in the Varde Å river valley receive fine grained material from a turbidity maximum in the northern part of Ho Bugt (Bartholdy, 1984; Bartholdy and Madsen, 1985; Bartholdy and Folving, 1986).

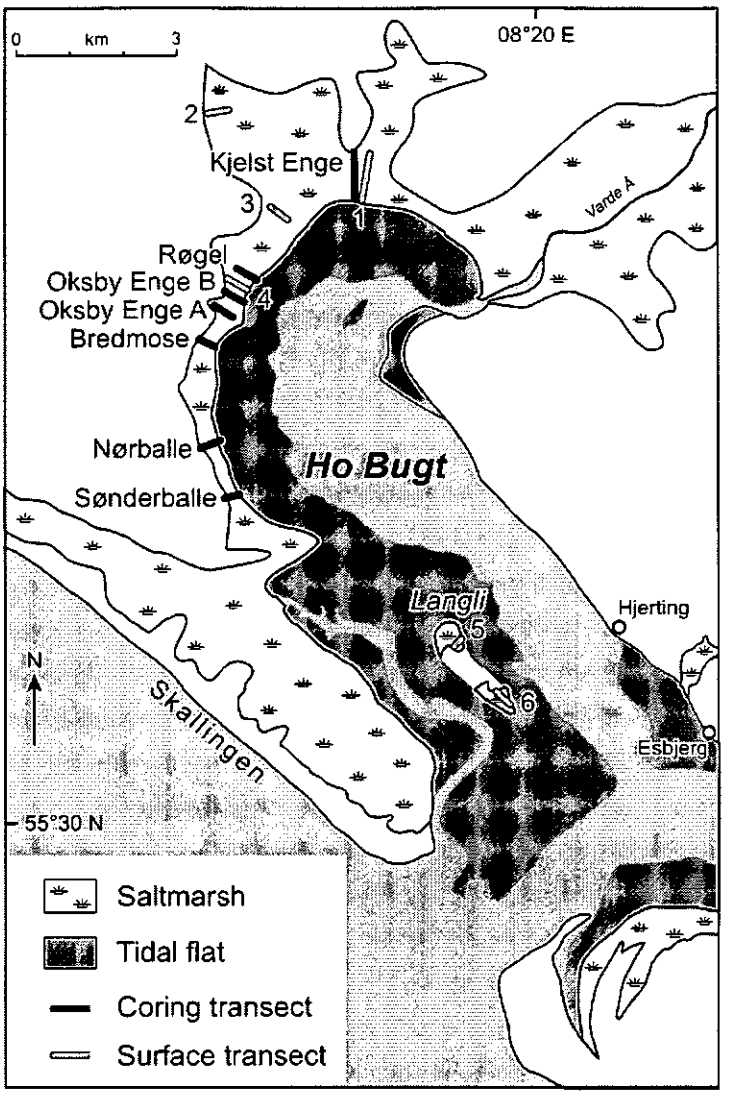

Figure 3.1. Ho Bugt location map showing modern and coring transects. Coring transects are labelled by name, modern transects are labelled by number. 1 = Kjelst Enge, 2 = Moservå, 3 = Storbæk, 4 = Oksby Enge, 5 = Langli North and 6 = Langli South.

Tidal Level	Height (m CD)	Height (m DNN)
Lowest Astronomical Tide (LAT)	-0.2	-0.89
Mean Low Water of Springs (MLWST)	0.0	-0.69
Mean Low Water of Neaps (MLWNT)	0.4	-0.29
Mean Sea Level (MSL)	0.9	0.21
Mean High Water of Neaps (MHWNT)	1.4	0.71
Mean High Water of Springs (MHWST)	1.8	1.11
Highest Astronomical Tide (HAT)	2.0	1.31

Table 3.1. Tidal levels at Esbjerg relative to Chart Datum (CD) and Danish national vertical datum (DNN). Data are from Admiralty Tide Tables (2004) and reproduced from Gehrels and Newman (2004).

3.2 Fieldwork

Fieldwork in Ho Bugt was carried out between May 2002 and April 2005. In May 2002, fieldwork was undertaken as part of the HOLSMEER Project (Scouse and others 2004). Data from the HOLSMEER Project are used in this study and where presented they are clearly indicated. Three separate field sessions were undertaken as part of this PhD: April – May 2004, July – August 2004 and in April 2005. In total, two and a half months were spent in the field. The methods and sampling strategies used in the field to investigate aspects of both the modern and palaeoenvironment are described below.

3.3 Surface transects

3.3.1 Site selection and rationale

Potential modern transect locations were identified during a preliminary reconnaissance survey of the Ho Bugt embayment. Transect locations were selected where:

1. A clear vegetation zonation was observed across the salt marsh

2. The transect would compliment existing transects, taken during the HOLSMEER Project, by extending the vertical range of samples and therefore the types of environment sampled

3. The salt marsh was reasonably accessible.

3.3.2 Sampling Design

A total of six modern transects were sampled from locations within Ho Bugt. These transects were taken across the salt marsh surface at Kjelst Enge, Moservå, Storbæk, Oksby Enge, Langli North and Langli South (Figure 3.1). The Kjelst Enge transect was sampled in May 2002 as part of the HOLSMEER Project. Along each transect a series of individual samples were taken from the salt-marsh surface at regular vertical (altitudinal) intervals. Where possible, the transect extended from the high salt marsh down to the tidal flat. At Moservå and Storbæk, transect length was constrained by the presence of the Storbæk drainage channel which bounds the seaward extent of these marshes. This channel proved impossible to cross and hence sampling was restricted in both these locations to the high and middle salt marshes. At Oksby Enge, the seaward extent of the marsh is bounded by an erosional cliff. Sampling here did not extend out onto the tidal flat due to the

presence of eroded blocks of salt-marsh sediment. The number of samples taken along each transect was dependent upon the transect length and the elevation change observed across the marsh surface. Where possible, sampling along each transect was conducted at similar stages in the tidal cycle. A summary of the six transects, detailing the transect length, number of samples, elevation range and range of environments sampled, is presented in Table 3.2.

Transect	Number of samples	Transect length (m)	Elevation range (m DNN)	Range of environments sampled	Date sampled
Kjelst Enge*	27	380	+0.7 to +1.9	High salt marsh – tidal flat	May 2002
Moservå	14	200	+1.9 to +2.7	Fresh water marsh – middle salt marsh	April 2004
Storbæk	13	40	+1.34 to +1.46	High salt marsh – middle salt marsh	May 2004
Oksby Enge	22	360	+1.25 to +2.2	High salt marsh – low salt marsh	July 2004
Langli North	31	130	+0.23 to +1.76	High salt marsh – tidal flat	July 2004
Langli South	33	440	+0.67 to +1.78	High salt marsh – tidal flat	July 2004

Table 3.2. Summary of the six modern transects sampled detailing the transect length, number of samples, elevation range and range of environments sampled. * Indicates the sampling was undertaken as part of the HOLSMEER Project.

3.3.3 Sampling methodology

At each individual sampling site, two surface samples were taken using a hand-held volume surface sampler (Figure 3.2). One sample of approximately 200 cm^2 was taken for diatom analysis whilst the other, of the same volume, was taken for further analysis of environmental variables. Both samples were transferred to plastic pots, the lids held securely in place using insulation tape to make the container airtight. Samples were stored in cool, dark conditions. Once back in the UK, they were refrigerated at 4°C until needed for sampling.

Figure 3.2 Hand-held sampler used to take the modern surface samples.

3.3.4 Surveying

To establish the surface elevation of each sample, samples were surveyed to a nearby geodetic benchmark using a Zeiss Elta S20 (Trimble 360) total station and linked to Danish national vertical datum (DNN). Three main benchmarks, established by the Danish Geological Survey, were used in this study; their details are given in Table 3.3. A fourth benchmark, on Langli Island, was established by colleagues in Copenhagen using differential GPS. Since some sampling sites were located some distance away from the nearest benchmark, a comprehensive network of temporary benchmarks was set up to facilitate the ease of surveying.

Benchmark number	Established by	Height (m DNN)	Easting	Northing	Description
BM 134-01-9051	Danish Geological Survey	8.322	451498	6163019	Bolt on East side of house
BM 134-01-9053	Danish Geological Survey	9.3	451318	6161039	Bolt on East side of house
BM 134-04-843	Danish Geological Survey	24.069	450681	6155858	Trig point on sand dune
640001	Differential GPS	12.08	456789	6152399	Trig point on sand dune

Table 3.3. Details of the main benchmarks used in this study, established by the Danish Geological Survey or by differential GPS.

3.3.5 Environmental variables

In order to characterise the morphological and sedimentary characteristics of the substrate a series of environmental variables were measured. At each sampling site a total of eight environmental variables were measured. Elevation, described above, pH and conductivity (salinity) were measured in the field at the Skallingen laboratory. The remaining environmental variables measured; particle size (sand, silt and clay fractions), loss on ignition (LOI) and calcium carbonate ($CaCO_3$) content, were measured in the laboratory at Plymouth and their methods are detailed in Section 3.5 below. For the Kjelst Enge transect, sampling was completed as part of the HOLSMEER Project and only elevation, pH and conductivity (salinity) were measured, all of which were conducted in the field. There was no remaining archived material from which to measure the additional environmental variables.

pH and conductivity were measured using approximately 10 g of soil, disaggregated in a 1:2.5 soil-water mix. pH was measured using a K&M7002 probe. Conductivity was recorded using a LF/WTW conductivity meter. Values were converted into salinity (sodium chloride (NaCl) equivalents), using a standard equation (Equations 3.1 & 3.2).

For conductivity range 0 to 2000 μScm^{-1}

Salinity (mgl^{-1} NaCl) = $0.5073\ (EC_{25}) - 10.7$ **Equation 3.1**

For conductivity range 5 to 50 $mScm^{-1}$

Salinity (gl^{-1} NaCl) = $0.0079\ (EC_{25})^2 + 0.2959\ (EC_{25}) + 0.8095$ **Equation 3.2**

Where EC_{25} = Electrical conductivity measured at 25 °C. Salinity values are expressed as NaCl equivalents in gl^{-1}.

3.4 Palaeoenvironments

3.4.1 Site selection and rationale

Potential coring locations were identified during a preliminary reconnaissance survey and on the basis of existing work completed under the HOLSMEER Project. Coring locations were selected with the following objectives in mind:

1. To gain a thorough understanding of the underlying stratigraphy of the Ho Bugt embayment

2. To provide sample cores for further laboratory analysis (Diatoms, macrofossils, sedimentology, geochemistry)

3. To complement and extend existing transects, cored as part of the HOLSMEER Project, and to core in areas of the embayment not yet investigated

4. To examine the temporal and spatial extent of the humified black layer identified by Dr Roland Gehrels and co-workers under the HOLSMEER Project in May 2002 (Gehrels et al., 2006a)

5. To obtain datable material from deeper basal peat samples.

3.4.2 Sampling design

A total of eight transects were cored at various locations within the Ho Bugt embayment. Coring transects were undertaken at Kjelst Enge, Røgel, Oksby Enge (two transects), Bredmose, Nørballe, Sønderballe and Langli Island (Figure 3.1). Seventy-six cores were collected in total, 37 as part of this PhD study and 39 as part of the HOLSMEER Project. In addition to the coring transects, a number of monolith sections were also obtained. Sites were chosen where the salt-marsh cliff was clearly exposed and where monolith samples would complement existing coring transects. Four cliff sections were sampled using monolith tins, at Oksby Enge (three sections), and at Sønderballe (one section).

3.4.3 Sampling methods

Initially, the coring interval along each transect was fairly large to gain an overview of the stratigraphy at each location. Additional cores were taken at a higher spatial resolution where interesting changes in the depth and nature of the stratigraphy were observed. All cores were taken using an Eijkelkamp hand-held corer (20 mm, 30 mm or 60 mm diameter barrels) and the lithostratigraphy was logged in the field. Coring extended until impenetrable sediments were reached. The cores that were subjected to laboratory analysis (diatoms, macrofossils, sedimentology, and geochemistry) were collected with a Russian peat sampler (50 mm diameter barrel). In some locations, it was impossible to penetrate the sediment using the Russian peat sampler and sample cores were taken using an Eijkelkamp corer.

Monolith samples were collected using stainless steel tins 0.6 x 0.10 x 0.08 m. The exposed cliff face was cut back, cleaned and made vertical, to avoid sampling of oxidised and weathered material and to minimise contamination. Monolith tins were held vertical whilst carefully being driven into the exposure. Tins were positioned so that some overlap between samples occurred (Figure 3.3). This was to ensure retrieval of a continuous, undisturbed stratigraphic section. Tins were removed from the cliff face by carefully digging away the surrounding material.

All cores and monolith sections were surveyed to a nearby geodetic benchmark using a Zeiss Elta S20 (Trimble 360) total station and linked to DNN. Samples were labelled with a location identifier, depth, number and year. Cores and monolith sections were wrapped in non-PVC cling-film and kept in cool, dark conditions. Once back in the UK, they were refrigerated at 4°C until needed for sampling. A summary of all borehole data collected is given in Table 3.4. The sampling design and methodology used along each individual coring transect is described below. Transects are described in a north – south direction.

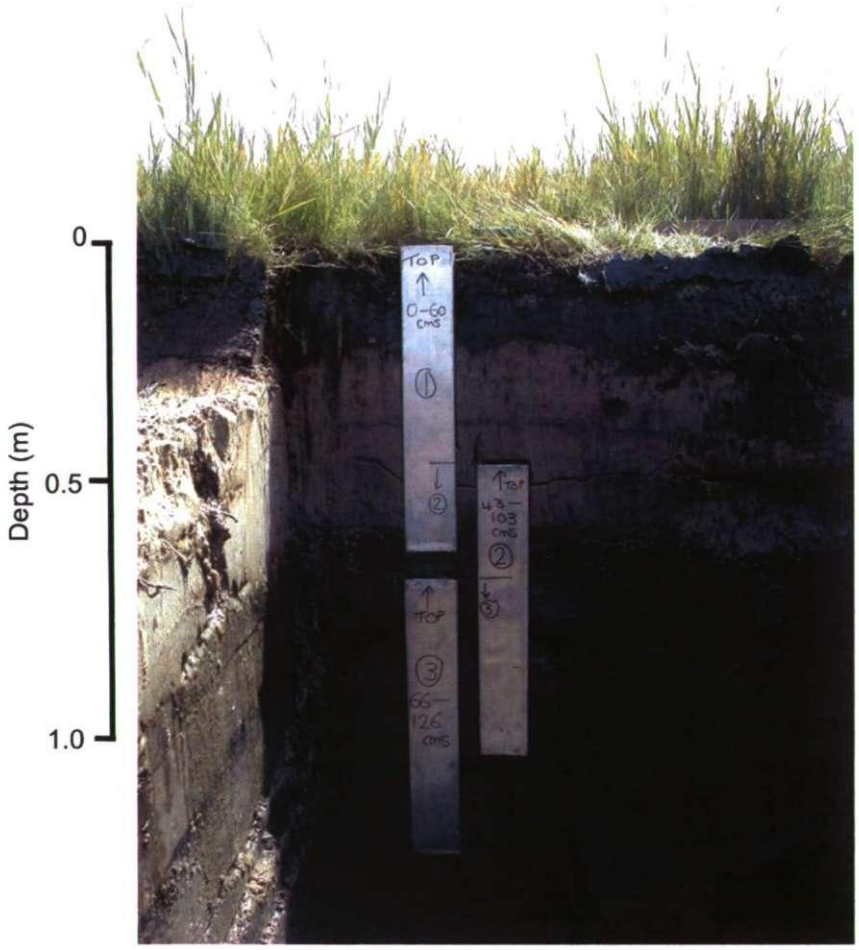

Figure 3.3. Sampling the salt-marsh exposure using monolith tins at Oksby Enge (Monolith OEB5)

Transect	Transect length (m)	No. of cores	Date sampled	Maximum depth cored (m)	Cores sampled
Kjelst Enge*	628	14	May 2002 July 2004	7.18	KE2 (2002) KE1, KE12, KE13 (2004)
Røgel	410	10	May 2004	2.54	RØ1
Oksby Enge A*	610	7	May 2002	4.50	Monolith OEA
Oksby Enge B	320	11	July 2004	2.15	Monoliths OEB5 and OEB
Bredmose*	450	15	May 2002	4.00	BR1, BR2, BR9, BR12
Nørballe*	125	4	May 2002	2.25	
Sønderballe	150	8	May 2004	3.29	Monolith SOA
Langli Island	60	7	July 2004	0.70	

Table 3.4. Summary of all borehole data collected. *Indicates that the transect was either cored or partly cored as part of the HOLSMEER Project. The sampling design and methodology used along each individual coring transect is described below.

Kjelst Enge

A transect of 11 cores was established in May 2002. Cores were taken at approximately 30 m intervals in order to sample the full extent of the salt marsh. An additional three cores were taken in July 2004 as part of this study. One previous core (KE1 from 2002) was extended in July 2004 to reach the deepest part of the basal peat (7.18 m). Cores KE1, KE12 and KE13 were selected for sampling, alongside core KE2 sampled in May 2002. These cores contained the deepest penetrable material sampled from the Ho Bugt marshes. All four cores contained extensive basal peat layers from which to obtain material for radiocarbon dating.

Røgel

A transect of 10 cores was established in May 2004. Cores were taken at 40 m intervals. One complete core section (RØ1) was selected for analysis and was sampled using a Russian peat sampler. Core RØ1 was selected for analysis for the following reasons:

1. The core was located where an interesting change in the nature of the black layer occurred, according to reconnaissance coring and preliminary field sketches

2. The core was located at a similar altitudinal position on the salt marsh to that of core KE2 (HOLSMEER master section) making it a suitable test of replicability.

Core RØ1 was taken in triplicate to ensure ample material was available for analysis (diatoms, macrofossils, sedimentology, and geochemistry). For each core, two holes approximately 0.5 m apart were used, and each 0.5 m section was extracted from them alternately. In the upper section of this transect an extensive sand layer is found. Neither the Eijkelkamp nor the Russian corer could penetrate this material. A small pit was therefore excavated on the surface of the salt marsh to enable the upper 0.5 m of sediment to be sampled using a monolith tin. The sand layer did not preserve well during sampling and the section 0.18 – 0.33 m depth in the monolith was poorly preserved.

Oksby Enge A

A transect of 7 cores was established in May 2002. Cores were taken at 20, 40 or 60 m intervals. In May 2004 monolith sections were taken from the cliff face at the seaward end of the Oksby Enge A transect. These monolith sections are hereafter referred to as OEA.

The exposed cliff face extended down to a depth of 0.70 m. To extend the depth of the sampled exposure, a small pit was dug next to the cliff face. Sampling then extended below the surface of the tidal flat, down to 1.65 m. At this depth, both the basal peat and the basal sand were exposed.

Oksby Enge B

A transect of 11 cores was established in July 2004. Cores were taken at 20 or 40 m intervals. Although a previous coring transect was established at Oksby Enge (*Oksby Enge A*) in May 2002, this second transect was taken in an ungrazed field (Lauridsen, local land owner, *pers. comm.*). This transect was considered more suitable for analysis, since there is less likelihood of the sediments having been affected by animal trampling.

In July 2004 monolith sections were taken from the cliff face at the seaward end of the Oksby Enge B transect. These monolith sections are hereafter referred to as OEB. Sampling extended down to a depth of 1.45 m. These sections, taken from an ungrazed field, provided a more reliable section for analysis than those taken in May 2004. In August 2004, monolith sections were taken from a small trench, excavated in collaboration with researchers at the Institute of Geography, University of Copenhagen, along the Oksby Enge B transect at core location OEB5. A 1.26 m monolith section was retrieved from this trench (Figure 3.3). These monolith sections are hereafter referred to as OEB5.

Bredmose

A transect of 15 cores was established in May 2002. Cores were taken at 10, 20 or 40 m intervals. Sample cores BR1, BR2 and BR12 were selected for analysis since they contained extensive basal peat units. These cores were sampled using a Russian peat sampler. Core BR9, at the seaward end of the transect, was sub-sampled and used for ^{210}Pb dating. Due to the presumed high sedimentation rate at this site, as determined by Pedersen (2004), this core was selected to enable a comparison of records with a core from Kjelst Enge, where the sedimentation rate was speculated to be lower.

Nørballe

A transect of 4 cores was established in May 2002. Cores were taken at 20 or 30 m intervals.

Sønderballe

A transect of 8 cores was established in May 2004. Cores were taken at 20 m intervals. This transect is the southernmost location in which the humified black layer is found. Reconnaissance coring of the marshes to the south of Sønderballe indicated that these salt marshes were much younger in age and were therefore not sampled as part of this study. In May 2004 monolith sections were taken from the cliff face at the seaward end of the Sønderballe transect. These samples were taken primarily as back up material and would have been used if problems arose in the analysis of other core and monolith sections.

Langli Island

A transect of 7 cores was cored in July 2004. Cores were taken at 10 m intervals due to the comparatively narrow extent of the salt marsh. The salt-marsh sediments on Langli were found to be very shallow and impenetrable sediments were reached after less than 1 m.

3.5 Laboratory-based methods.

Laboratory work was completed between April 2004 and April 2006. The following section describes the laboratory methods employed in the processing and analysis of samples collected in the field and sub-sampled in the laboratory. Details of the procedures used in diatom sampling, preparation and analysis are described separately in Section 3.7.

3.5.1 Environmental variables

In the laboratory, particle size (sand, silt and clay fractions), loss on ignition (LOI) and calcium carbonate content ($CaCO_3$) were measured from each of the modern samples. Only the top 1 cm of the sample was used in the analysis. Sedimentation rates in the Ho Bugt embayment, determined by ^{210}Pb dating, suggest that this depth of sediment represents approximately two years accumulation and can therefore be considered as modern (Pedersen, 2004). For particle size, it was necessary to use the top 2 cm of the sample since more material was needed. For each technique, the same methodology was also used in the processing of the core samples. The detailed methodologies are therefore described only once in the relevant sections below.

3.5.2 Lithology

In the laboratory, the stratigraphy of each core or monolith section was checked against that logged in the field. Before sampling, all cores and monolith sections were cleaned, by carefully scraping away the material at the exposed surface. All core sections were photographed to document the intact stratigraphy. In general, the material was well preserved and signs of oxidation and microbial decay were minimal.

3.5.3 Sedimentology

A number of sedimentological parameters were investigated in the laboratory, primarily from the master core section (core RØ1), in order to characterise the nature of the sediments. These included: bulk density, loss on ignition, carbonate content and grain size (sand, silt and clay fractions).

Bulk Density

Post-depositional compaction is a particular problem for most studies of sea-level change, where it can cause a vertical lowering of index points from their original elevation (Long et al., 2006). To evaluate in a qualitative way the degree to which sediments had been affected by compaction, dry bulk density was investigated for all core sections from which ^{14}C and ^{210}Pb dating material was obtained (Section 3.6).

For the Røgel master core section (core RØ1), core depth 0 – 0.18 m was sampled at 0.5 cm resolution, as these data were required as part of the ^{210}Pb dating methodology (Section 3.6.3). Core depth 0.33 – 1.6 m was sampled at 1 cm resolution, core depth 1.6 – 2.0 m at 2 cm resolution and core depth 2.0 – 2.25 m at 10 cm resolution. From this core the largest number of ^{14}C dates was obtained (Section 3.6.1) and so a comprehensive dry bulk density record is useful for assessing compaction. Monolith sections OEB5 and OEA were sampled initially at 4 cm resolution and then at 2 cm resolution. It was originally thought that the black layer was highly compacted. This layer was therefore sampled at 1 cm resolution in both these sections, in addition to the samples from the black layer in core RØ1, to test this hypothesis. Bredmose core BR9 was sampled for dry bulk density at 1 cm resolution in the upper 0.3 m, alongside sampling for diatoms to assess compaction in the upper part of this sequence where a ^{210}Pb record is established.

To establish dry bulk density, a sample of known volume was taken intact from the sediment. For all cores, a 1 cm wide slice was cut out of the core and placed flat on a piece of paper. A ruler was then used to cut a sample of 2 x 1 x 1 cm sub-sample. For the monolith sections, a scalpel was used to outline an area of approximately 1 x 3 cm. This was extracted from the monolith using a spatula. Once again, the sub-sample was placed flat on a piece of paper and a ruler was used to cut a 2 x 1 x 1 cm sub-sample. Where possible, larger samples were cut from each of the monoliths to increase the degree of accuracy obtained. The narrow width of most of the cores prevented larger samples from being taken. The sand layer, present in several of the monolith sections, presented a particular problem for sampling. The nature of the material meant that stratigraphic integrity was lost as soon as any attempt was made to cut out the sample. For these sections a 6.5 x 1 x 1 cm shape cutter was used. The slightly damp sand was held intact by the cutter and transferred directly to a sample pot.

All sub-samples were placed in an oven at 105°C and left to dry for at least 48 hours. This ensured that the sample was completely dry before weighing. Dry bulk density was then calculated using the following formula:

$$\text{Dry bulk density } g/cm^3 = \frac{\text{Dry weight (g)}}{\text{Volume } (cm^3)} \qquad \textbf{Equation 3.3}$$

Loss on Ignition

Loss on ignition (LOI) and calcium carbonate content ($CaCO_3$) were measured according to procedures described by Ball (1964) and Folk (1965). Samples for LOI and $CaCO_3$ were taken from all modern surface samples and the Røgel master core section. For the core, samples were taken at 1 cm resolution in the top 1 m of the core, at 2 cm resolution between core depths 1 and 1.6 m, at 4 cm resolution between core depths 1.6 and 2 m and at 8 cm resolution from core depth 2 m to the bottom of the core (2.25 m). $CaCO_3$ measurements were taken from core RØ1 to provide a useful record with which to compare with the diatom record. Samples with high $CaCO_3$ values indicate an inflow of minerogenic material, which is often associated with an increase in the abundance of transported diatom taxa (Kirby, *pers. comm.*). For each sub-sample, between 0.5 and 2 grams of oven-dried material was placed in a crucible, weighed and then burnt at 550°C for a minimum of four hours to establish the percentage of organic matter. After re-weighing, the samples were returned to the furnace and burnt at 950°C for a minimum of four hours to establish the percentage calcium carbonate content. The establishment of LOI and $CaCO_3$ for each of the surface samples followed the same methodology.

Particle Size

To characterise the sedimentary characteristics of the substrate, particle size analysis was completed on all modern surface samples and on the Røgel master core (core RØ1). For the core, this record provided information on the detailed sedimentary structure of the various lithological units. Sand, silt and clay fractions were identified by particle size analysis using a Malvern long-bed Mastersizer X, with wet sample unit MS17. Sub-samples of between 2 and 10 grams of wet sediment were placed in 200 ml Petri dishes and 20 ml of 6% hydrogen peroxide (H_2O_2) was added. The samples were then heated, using water baths, for between 4 and 6 hours until all organic material was removed. In most cases, the samples were very active and were left to react overnight before any heat was added. After heating, the samples were left to cool and settle before any remaining

H_2O_2 was removed using a pipette. Samples were transferred to 100 ml beakers and approximately 25 ml of water was added to re-suspend the sediment.

Using a magnetic stirrer, the samples were then well mixed. During mixing, four 4 ml sub-samples were taken using a pipette and placed in cuvettes. The sub-samples were held in polystyrene trays and placed in large plastic sampling bags to minimise evaporation. Each bag was clearly labelled with the transect name, sample labels and the date sampled. Samples were refrigerated at 4°C until needed for analysis.

Using the Malvern Mastersizer two sets of analysis were conducted for each sample; one using a 45μm lens to analyse material in the fine-grained range, and the other using a 100μm lens to analyse material in the coarse-grained range. For each sample, one of the four sub-samples taken was used for 45μm analysis and the other three were used for 100μm analysis. During the 45μm analysis, three replicates were run for each sample. For the 100μm analysis, five replicates were run for each sample. In addition to the replicates analysed, a quality control check was also run on every sample to determine the reliability of the results obtained. The same methodology was followed for all of the surface samples with some minor modifications. Some surface samples, such as those from Langli Island, contained visible shell material. The laser sizer is unable to analyse particles > 2 mm and so these samples were sieved through a 2 mm round hole sieve to remove this material. All shell material removed was placed in sample bags and labelled for future reference.

3.5.4 Black layer investigations

Several analyses were conducted on the Røgel master core section as an aid in determining the nature of the humified black layer. Similar black layers have been identified along the northeast German Baltic Sea coast (Lampe, 2005) and the types of analyses undertaken here aimed to try and replicate those results obtained from the Baltic. Total Organic Carbon (TOC), Total Inorganic Carbon (TOI), the amount of humic substances insoluble in sodium hydroxide (NaOH), Iron (Fe), Calcium (Ca), Magnesium (Mg) and Manganese (Mn) concentrations were analysed for the upper 0.72 m of the Røgel master core to compare with the Baltic records (Lampe, *unpublished data*). In addition, the black layer in the Røgel master section was analysed for microscopic charcoal.

Sub-sampling strategy and rationale

Initially, 40 sub-samples were taken from the top part of the Røgel master core for analyses. Core depth 0 – 0.24 m was sampled at 2 cm resolution and core depth 0.33 – 0.6 m was sampled at 1 cm resolution. The higher sampling resolution in the lower parts of the core section covers the black layer, which is the section of greatest interest in this instance. It was not possible to obtain samples between core depths 0.25 – 0.32 m as this part of the sand layer was not preserved intact. Preliminary results of TOC analysis suggested that TOC values were very high in the black layer and were still high at 0.6 m core depth. Sub-sampling at 1 cm resolution was then extended until TOC values returned to pre-black layer levels (c. 0.72 m).

All samples were dried in a drying cupboard at 40°C for at least 72 hours to ensure the samples were completely dry. Using an agate pestle and mortar, each sample was ground into a fine powder and passed through a 500 μm sieve. Approximately 3 grams of powdered and sieved sample was needed in order to complete all analyses. Only plastic sampling instruments were used in the preparation of samples and plastic gloves were worn to minimise the risk of contamination. Samples were stored in airtight plastic vials ready for analysis.

Total Organic Carbon

The amount of TOC was measured in addition to the conventional loss-on-ignition furnace technique for the upper 0.72 m of the Røgel master core. Measurement of TOC gives a potentially more accurate result than the LOI furnace technique. Samples were analysed for TOC using a Skalar Primacs Carbon Analyser. For each sample, one sub-sample was used to measure Total Carbon (TC) and a second sub-sample was used to measure Inorganic Carbon (IC). Before running any samples, one TC and one IC 'flush' sample was run to ensure the Carbon Analyser was properly calibrated. To measure TC, 10 – 20 mg of sample was placed in a ceramic receptacle, covered with quartz wool and positioned in the 'TC' Carbon Analyser port. The quartz wool ensured that the sample stayed in the receptacle even at the high combustion temperatures used. To measure IC, 80 mg of sample was placed in a boiling tube and two or three drops of distilled water was added. The sample was then positioned in the 'IC' Carbon Analyser port. TOC was then calculated as:

TOC = TC – IC **Equation 3.4**

Geochemistry

The concentration of Fe, Ca, Mg and Mn in the samples from the Røgel master core was established using acid digestion. For each sample, 1.00 g ± 0.005 g of dried and sieved soil was transferred into 100 ml borosilicate glass digestion tubes. Approximately 0.5 ml of distilled water was added to wet each sample. 7.0 ml of hydrochloric acid and 2.5 ml of nitric acid was then carefully added to each tube. The samples were then transferred to a heating block and allowed to reflux gently. Due to the high organic content of some samples, especially those from the black layer, the digests were heated for up to ten hours to a maximum temperature of 140° C.

Once cooled, approximately 20 ml of distilled water was added to each sample and the sample was carefully mixed using a rotary mixer. The extract was then filtered into a 50 ml volumetric, topped up with distilled water and transferred to a 50 ml polypropylene tube. Samples were refrigerated at 4°C until needed for analysis. Samples were analysed using an Atomic Absorption Spectrometer. For each element, three standards were first analysed. These standards were later used to construct the calibration curves needed to interpret the results (Figure 3.4). The standards were intermittently checked to ensure values remained consistent. Initial results for all elements suggested that the metal concentrations were very high and in many cases, above the range of the Spectrometer. All samples were then diluted again to give a 1 in 5000 dilution.

Samples were analysed for each element in turn and the resulting absorption value recorded. With the exception of Fe, each element was analysed using a single wavelength. Lower concentrations of Fe in some of the diluted black layer samples required a second analysis on a shorter wavelength, using a new set of standards. To convert absorption values to concentrations a series of calibration curves were constructed using the measured standard values. For each curve, a linear trend line was added and the equation of the line obtained. The calibration curve for Fe measured at 386 μm wavelength is shown in Figure 3.4 as an example.

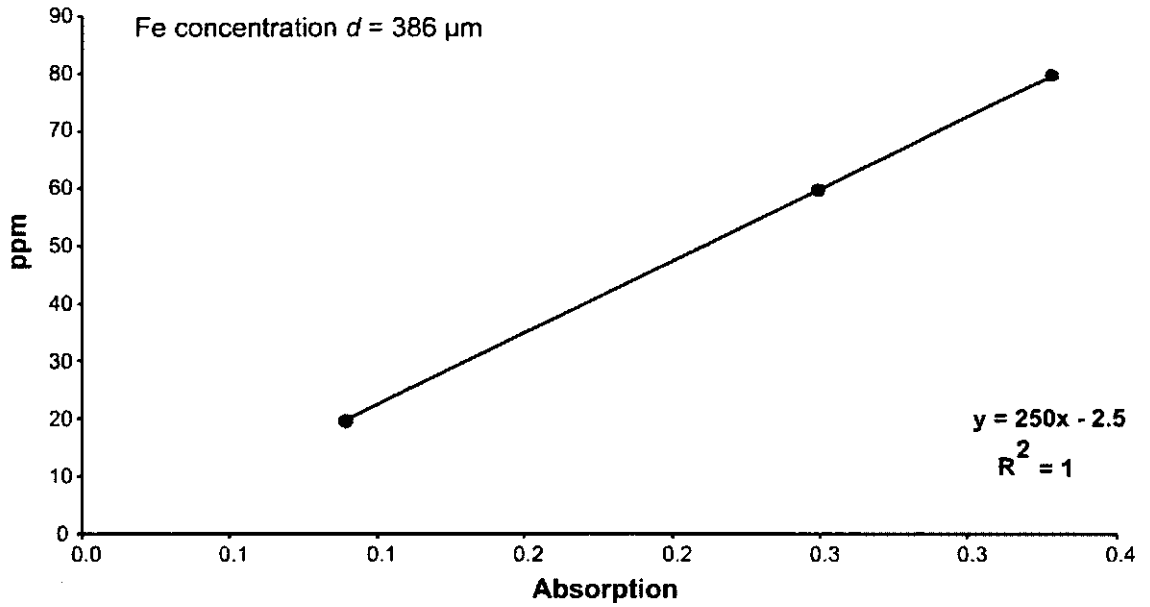

Figure 3.4. Calibration curve for Fe measured at 386 µm wavelength showing linear trend line and equation.

Measured absorption values were then converted to parts per million (ppm) using the linear regression equation. In this example;

$$y = 250x - 2.5 \qquad \textbf{Equation 3.5}$$

where y = Concentration in parts per million
x = Measured absorption value.

This process was repeated for each element. For Fe, two calibration curves were constructed since some samples were analysed on a different wavelength. In order to relate the values obtained to the initial weight of sample and dilution used, it was necessary to convert ppm values to the commonly expressed milligrams per kilogram (mg kg^{-1}) using the following formula;

$$\text{Metal concentration in mg kg}^{-1} = (a/b) \times c \qquad \textbf{Equation 3.6}$$

where a = Sample dilution used
b = Initial weight of sample
c = Metal concentration in ppm

Some concentrations were found to be very high and consequently results for Fe, Ca and Mg are expressed as grams per kilogram (g kg^{-1}). Results are presented in Section 5.2.3.

Humification

Decomposition was determined following the light transmission method detailed in Blackford and Chambers (1993). This method is the standard method used to determine the degree of decomposition in peaty soils. Although not altogether suitable when used on other sediment types, the method was applied here in an attempt to assess the degree of humification of the black layer following the methodology of Lampe (*unpublished data*).

The percentage light transmission was measured for each sample at a 550 nm wavelength using a Zeiss Specord M500 spectrophotometer and the programme Aspect Plus, version 1.31. The 550 μm wavelength was selected because it produces the greatest difference in observed readings of differently humified peats (Hazell, 2004). Each sample was analysed exactly 4 hours after the NaOH was added to obtain the maximum light transmission value (Blackford and Chambers, 1993). The samples were placed in turn in a clear glass cuvette and measured against a standard of distilled water. Three replicates were measured for each sample and the average calculated. Results are presented in Section 5.2.3.

Microscopic charcoal analysis

Samples were prepared for microscopic charcoal analysis following procedures detailed in Turner et al. (2006) and Turner (2007). Microscopic charcoal was extracted using heavy liquid separation (Lithium Hereopolytungstate; LST) (Turner et al., 2006; Turner, 2007). Although developed primarily for use on lake sediments, the method was applied here since this work was considered exploratory. To calculate charcoal concentration, the exotic marker *Lycopodium* was added to each sample during preparation (Stockmarr, 1971). Samples were analysed for microscopic charcoal at x 200 magnification using an Olympus BX50, high power microscope. Charcoal particles were counted until 250 *Lycopodium* spores were reached (Finsinger & Tinner, 2005; Turner, 2007). The identification of microscopic charcoal is a somewhat subjective process. Identification of charcoal particles in this study follows Turner et al. (2006). Absolute charcoal counts were converted to concentrations using TILIA (version 2.02) (Grimm, 2004). Results are presented as the concentration of charcoal particles per cm^3 of sediment analysed in Section 5.2.3.

3.6 Chronology

A combination of several radiometric dating techniques (AMS ^{14}C, ^{210}Pb, ^{137}Cs, and ^{241}Am, OSL) were used in this investigation to derive chronologies for the cores and monolith sections. Using a number of different dating methods makes it possible to construct reliable age-depth models (Section 8.7) and to link chronologies between different cores and stratigraphic sections. The methodology employed for each of the dating techniques used is discussed below.

3.6.1 AMS ^{14}C dating

Previous studies have shown the usefulness of AMS ^{14}C dating in sea-level studies (e.g., Gehrels, 1999; Gehrels et al., 1996, 2002; Törnquist et al., 1998). Targeting small, horizontally embedded plant fragments allows the precise dating of the former land surface and minimises the possibility that the samples are reworked. Cores and monolith sections were therefore meticulously dissected cm by cm to obtain datable material to meet the following objectives:

1. To establish a chronology for a master section from which a high resolution diatom record is established. The record will be used to test the replicability of the reconstruction of core KE2 (HOLSMEER master core section)

2. To date key stratigraphic units including the black layer and the sand layer

3. To provide additional (older) compaction free sea-level index points derived from basal peat.

For the core sections, each core was dissected cm by cm alongside sampling for diatoms, particle size and LOI. All monolith sections were sliced along their longest (height) axis. One section was retained for future use whilst the other section was meticulously dissected and examined for suitable dating material. To avoid *in-situ* roots and horizontal *Phragmites* rhizomes, only plant fragments that were clearly broken, detritral in nature, and away from the edges of the core or monolith were sampled. All datable material was carefully removed and washed with distilled water. The material was examined, when wet, under a low power microscope to check for contamination by vertical rootlets. Any visible rootlets were carefully removed with tweezers. The datable material was then dried at

40°C, weighed and stored in plastic, airtight vials at 4 °C to inhibit microbial decay. A complete inventory of all datable material found in the sediments is presented in Appendix 4.

A total of 26 samples were selected for analysis (Table 5.2), based on sample weights and the degree to which they met the above objectives, and were further prepared at the NERC Radiocarbon Laboratory, East Kilbride. A further 18 samples were previously analysed at the AMS ^{14}C Dating Laboratory, University of Århus, Denmark as part of the HOLSMEER Project (Table 5.1). A visit was made to the Radiocarbon Laboratory, East Kilbride (January 2006) to assist with the preparation of the samples. Samples were digested in 2M HCL at 80°C for 8 hours, washed with deionised water, dried and homogenised. The total carbon was recovered as carbon dioxide (CO_2) by heating with copper oxide (CuO) in a sealed quartz tube. CO_2 was then converted to graphite by iron/zinc (Fe/Zn) reduction. Samples were analysed at the Scottish Universities Environmental Research Centre (SUERC) AMS Facility for ^{14}C analyses. The ^{14}C ages were calibrated to calendar ages with CALIB version 5.0.2 (Stuvier et al., 2005), using the non-marine INTCAL04 calibration curve (Reimer et al., 2004). The age-depth models derived from these dates are presented in Section 8.7.

3.6.2 OSL dating

The presence of the buried sand unit, identified in many of the coring transects, provided an opportunity to sample material for OSL dating. Samples were taken in locations where the sand unit was clearly exposed and easily accessible. A total of four samples were taken for OSL dating in two locations, at Røgel and Oksby Enge. The location, core depth and stratigraphic context of these samples are summarized in Table 5.3. Three of these samples were taken in order to provide constraints on the age of the buried sand unit. The fourth sample, from the basal sand at Oksby Enge, was taken to provide an estimate of the age of this unit and to provide a maximum age for the overlying basal peat.

Two plastic tubes were driven horizontally into the exposure at each of the locations and depths specified (Figure 3.5). Samples were taken in duplicate to ensure enough material was available for processing. The depth of each sample was measured from the salt-marsh surface down to the centre of the tube. The tubes were removed by carefully digging away at the surrounding material. Both ends of each tube were sealed quickly with black duct tape to ensure as little light as possible entered the tube. The samples were labelled clearly with a location identifier, depth, date and the direction in which the tube was driven into the exposure. This last label was important for determining which end of the tube had received the greatest exposure to light. Samples were kept in cool, dark conditions to inhibit microbial decay. Once back in the UK, samples were refrigerated at 4°C until needed for analysis. Samples were prepared and analysed at the Nordic Laboratory for Luminescence Dating, Roskilde, Denmark. A detailed discussion of the preparation and analysis techniques used can be found in Murray and Olley (2002) and Madsen et al. (2005, 2006) and is not repeated here.

Figure 3.5. OSL sampling tubes in position in the cliff exposure at Oksby Enge (Sample number 4, Table 5.3).

3.6.3 Lead-210 dating

One of the most widely used methods to date recent sediments (0 - 150 years), is ^{210}Pb (Appleby, 2001). This technique is considered most reliable in environments with uniform sediment accumulation rates. However, several studies have successfully used ^{210}Pb dating on cores from salt marshes where non-uniform accumulation rates often prevail (e.g., Gehrels et al., 2002, 2005; Pedersen, 2004; Horton et al., 2006). The artificial radionuclides ^{137}Cs and ^{241}Am are often measured alongside ^{210}Pb. Cesium-137 is derived both from atmospheric nuclear weapons testing during 1953-63, and from the Chernobyl accident in 1986 (Appleby, 2001). Americium-241 is derived from atmospheric nuclear weapons testing during 1953-63 (Appleby, 2001). Measurement of these two artificial radionuclides often provides additional chronological control on sediment cores (Appleby, 2001).

^{210}Pb, ^{137}Cs and ^{241}Am age estimates were obtained from Røgel monolith to integrate with ^{14}C and OSL dates obtained from this same core (Sections 3.6.1 and 3.6.2). The upper 0.18 m of this section were carefully sliced at 0.5 cm resolution. Sampling did not extend below this depth due to the presence of the sand layer. Coarse-grained material such as sand is not considered suitable for use in ^{210}Pb dating due to the increased mobility of isotopes in these

sediments. The 0.5 cm sampling resolution was selected since only a relatively small section of sediment was to be analysed (0 – 0.18 m). It was important to have a large enough number of samples between these depths from which to construct a reliable decay curve of ^{210}Pb activity.

Each 0.5 cm slice was placed flat on a piece of paper and a sub-sample with a known area was removed for ^{210}Pb dating. The samples were then dried at 40 °C, weighed and ground into a coarse matrix. The dried samples were analysed for ^{210}Pb, Radium-226 (^{226}Ra), ^{137}Cs and ^{241}Am by direct gamma assay at the Liverpool University Environmental Radioactivity Laboratory, using Ortec HPGe GWL series well-type coaxial low background intrinsic germanium detectors (Appleby et al., 1986). Following three weeks storage in sealed containers to allow radioactive equilibration, ^{210}Pb was determined via its gamma emissions at 46.5 keV, and ^{226}Ra by the 295 keV and 352 keV γ-rays emitted by its daughter isotope, ^{214}Pb. ^{137}Cs and ^{241}Am were measured by their emissions at 662 keV and 59.5 keV respectively. The absolute efficiencies of the detectors were determined using calibrated sources and sediment samples of known activity. Corrections were made for the effect of self-absorption of low energy γ-rays within the sample (Appleby et al., 1992). The age-depth models derived from these chronologies are presented in Section 8.7.

3.7 Diatoms

The following section describes the techniques used in the sampling, preparation, counting and analysis of diatom samples from both modern and fossil samples. Statistical techniques employed to analyse the modern diatom and environmental data are discussed in Section 3.8.

3.7.1 Diatom Sampling

Before sampling, all samples, cores and monolith sections were checked for signs of oxidation and microbial decay. This was a particularly important check since microbial decay could greatly affect the diatom counts obtained. In general, the samples were well preserved and no signs of decay were noted. For the surface samples, the top 1 cm of each surface sample was used for diatom analysis and any surface vegetation was carefully scraped away using a knife. For the core samples, all cores were cleaned prior to any analysis being undertaken. Approximately 0.5 g of wet sediment was used for each diatom sample. Initial test preparations showed that this weight would result in optimal diatom concentrations. A second sub-sample of approximately 1g in weight was taken alongside each of the diatom samples from which to establish soil moisture and calculate the dry weight of sediment used. To analyse diatom assemblages in the palaeoenvironment, cores and monolith sections were sampled for diatoms to meet the following objectives:

1. To establish a high-resolution diatom record from one master core section to compare with the existing record from core KE2 (analysed for diatoms as part of the HOLSMEER Project)

2. To provide samples from the upper core sections of Bredmose and Røgel to correlate with ^{210}Pb dates

3. To provide water-level relationships (the 'indicative meaning') for horizons from which datable material was obtained

4. To establish the palaeoenvironmental conditions of the black layer.

Sub-sampling strategies and rationale

Initially, diatom samples were taken at 8 cm resolution from cores and monolith sections at Røgel (RØ1) and Oksby Enge (OEB5 and OEA) to gain an understanding of the diatom changes occurring over a fairly wide spatial scale. These three sections were selected for initial diatom analysis since they contained the most abundant material for radiocarbon dating (Section 3.6.1). They were therefore the most likely core sections from which to obtain a robust chronology to accompany the diatom changes. Following initial analyses, higher resolution sub-sampling was conducted on several core and monolith sections and is described and justified below.

Røgel

Røgel core RØ1 was selected as the master core section from which to obtain a high resolution diatom record. Although initially selected as the master section whilst in the field, core RØ1 was confirmed as a suitable master section after initial investigations and for the following reasons:

1. The skeleton diatom stratigraphy (8 cm resolution) showed interesting changes in the abundance and presence of several diatom taxa, especially in the upper 0.80 m of the core

2. Core RØ1 contained the most abundant material for radiocarbon dating from which a robust chronology could be constructed.

Diatom samples were taken at 1 cm resolution throughout the entire core section down to a depth of 2.22 m. Samples from the upper 0.5 m were taken from Røgel monolith. Between 0.19 and 0.33 m core depth, the sand unit was not well preserved. Pilot samples taken from the sand unit at this and at other locations, suggested that diatoms were not preserved and most samples were barren.

Bredmose

Core BR9 from the salt marsh at Bredmose was analysed for diatoms to meet two objectives:

1. To provide a high resolution diatom record from the upper core section to correlate with existing ^{210}Pb dates

2. To establish the palaeoenvironmental conditions of the black layer.

To meet the first objective, diatom samples were analysed at 1 cm resolution in the upper 0.30 m of the core. The black layer in this core is 3 cm thick and extends from 0.755-0.785 m core depth. To investigate the palaeoenvironmental conditions of the black layer and meet the second objective, samples were analysed at 1 cm resolution from 0.74 – 0.82 m core depth, and then at 2 cm resolution down to 0.88 m core depth. Three samples were analysed from the black layer itself, three from the clay unit below the black layer and two from the clay unit overlying the black layer. These samples served as early pilot samples for determining the nature of the black layer and assessing the potential for diatom preservation (Gehrels et al., 2006a).

Additional Diatom Samples

For depths from which radiocarbon dates were obtained (Table 5.2) additional samples were also taken for diatom analysis. The purpose of these samples was to establish the water-level relationship (the 'indicative meaning') of the sediment, using the modern diatom training set. The determination of the indicative meaning of each of these samples is discussed in Section 8.5.

3.7.2 Preparation of samples for diatom analysis

Diatom samples were prepared for microscope analysis according to a modification of standard procedures described by Palmer and Abbott (1986) and Battarbee et al. (2001). The method followed is outlined in Figure 3.6. Modifications to the standard method were made following initial experimental preparations. Some samples, particularly those from Moservå, were found to be highly reactive to hydrogen peroxide (H_2O_2). In these cases it was necessary to use 6% H_2O_2 rather than the 30% H_2O_2 as outlined in the standard method. The addition of deionised water in between stages resulted in a much 'cleaner' solution being produced. Once added, the deionised water was left to completely settle before being removed. The use of a centrifuge was avoided in processing to prevent further breakage of diatom valves. Early pilot samples suggested that this may be a problem for some core sections (Chapter 6).

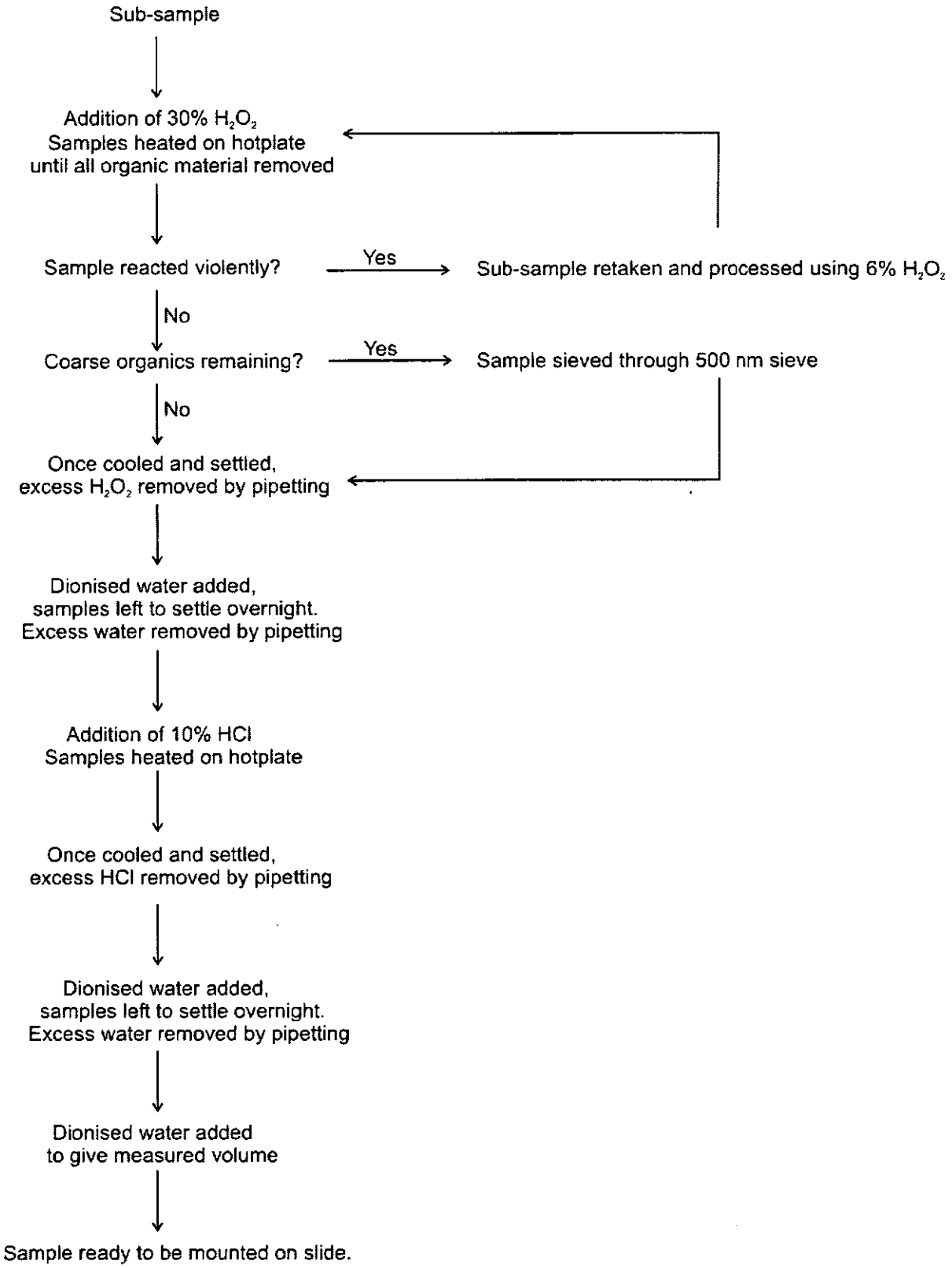

Figure 3.6. Summary of the stages used in the preparation of samples for diatom analysis. Method is adapted from standard procedures described by Palmer and Abbott (1986) and Battarbee et al. (2001).

Slide Preparation

A measured volume of each prepared diatom suspension was carefully dropped by pipette onto a clean cover slip. The remaining cover slip volume was made up with water. For each sample, two different concentration cover slips were made up; one at a relatively high concentration, and the other at a lower concentration, to minimise the need to make up additional slides. The samples were left to settle and allow the water to evaporate at room temperature. This method is preferable to evaporating the cover slips using heat, since it usually results in a more even spread of diatoms across the cover slip. To avoid dust contamination during settling, the cover slips were moved into a fume cupboard. When dry, the cover slips were mounted using Naphrax® resin. One drop of Naphrax® was placed at both ends of a slide and was heated at approximately 130°C for 15 minutes to drive off the toluene. The two cover slips were then inverted and placed onto the Naphrax® at each end of the slide. Once cool, each slide was checked to ensure that the cover slip did not move and labelled with a sample number, the cover slip concentrations and a date. All slides were then examined under the microscope to ensure that the concentration of diatom values on the cover slip was appropriate for counting.

3.7.3 Diatom identification and taxonomy

Diatoms were identified, where possible, to species and sub-species level under a light microscope using oil immersion at 1000x magnification and brightfield illumination. Both Olympus CH30 and Olympus BH2 models were used in counting. The image analysis system, AnalySIS®, was used to aid taxonomic work and images were taken via this system for future reference using a Leica DC100 camera attached to an Olympus BX-50 microscope. Additionally, an Olympus camera attached to the BH2 microscope was used to obtain 'still' black and white images of some diatom species. The primary identification references and floras consulted included: Van der Werff and Huls (1957), Round et al (1990), Krammer and Lange-Bertalot (1991a, 1991b, 1997a, 1997b) and Hartley (1996). Taxonomy follows Krammer and Lange-Bertalot (1991a, 1991b, 1997a, 1997b) as this was the primary flora consulted. The Automatic Diatom Identification and Classification (ADIAC) and the European Diatom Database (EDDI) websites were consulted as additional resources. Drs Nigel Cameron and Viv Jones (ECRC, UCL) assisted with taxonomy early on in the project. The diatom data from Kjelst Enge was analysed by Dr. Jason Kirby (John Moores, Liverpool). Several taxonomic sessions were organised with Dr Kirby to ensure identification, taxonomy and counting techniques (see below) were

comparable before these data were integrated with that produced by this study. Drs. Jason Kirby and Sue Dawson (St Andrews) assisted with identification of difficult diatom taxa. Salinity classifications follow the halobian scheme of Hustedt (1953; 1957). The Hustedt scheme is used here because of its relative simplicity and to ensure consistency with other recent diatom-based sea-level studies (e.g., Zong and Horton, 1998; Hamilton and Shennan, 2005).

3.7.4 Counting Techniques

The number of valves to be counted varies greatly with the type of analysis (Battarbee et al., 2001). To determine the appropriate number to count, the relationship between the number of taxa, the number of valves and the species number change was explored for several samples (following Battarbee, 1986). This experiment was conducted on samples from both the modern and palaeoenvironment to ensure an appropriate number of valves were counted. Whilst marked differences in the percentages between a count of 100 and 200 valves were noted, between 200 and 300 valves the percentages were found to level off. As a large number of high resolution samples were counted for this study, a relatively low count of 300 valves was considered sufficient to account for the variation in the diatom data. This number is commonly used in similar mudflat, salt marsh and coastal studies (e.g., Zong, 1997; Patterson et al., 2000; Gehrels et al., 2001; Sawai, 2001; Trites et al., 2005; Sawai et al., 2004).

A representative proportion of each cover slip was examined by counting individual fields of view along continuous traverses, ensuring equal edge and centre sections of the cover slip were examined. Each single valve was considered as one counting unit and complete frustules were counted as two (Battarbee et al., 2001). Diatom preservation was found to be highly variable with many broken valves present. A robust and consistent counting methodology was developed to deal with these broken fragments after several experimental counts. All fragments that included the centre part of the valve were counted as one. For taxa which do not possess recognisable centres (e.g., some *Nitzschia* species), fragments where at least 60% of the valve was present were also counted as one. All smaller fragments were ignored, although this was somewhat subjective. For example, the species *Campylodiscus echeneis* is usually only found in small fragments, and very rarely found as a whole valve, because of its size. For this species, and a few others, it was necessary to count fragments smaller than 60% of the total valve size otherwise some

important indicators would have been excluded from the counts. Any double or multiple counting of such species would also be replicated in the fossil counts. The counting methodology adopted was consistent with that employed by Dr. J. Kirby who counted the Kjelst Enge diatom samples.

No systematic distinction between allochthonous (transported) and autochthonous (*in-situ*) taxa are made during counting in this study. The distinction between locally produced and transported taxa poses a major problem in the use of diatoms in palaeoecological research, especially in the case of high energy coastal environments (Brockmann, 1940). Assumptions for this investigation initially followed those of Zong (1997), who argued that since a mixture of both allochthonous and autochthonous valves occurs in sediments that accumulated in the palaeoenvironment, their presence in modern samples can be considered less significant. However, in this study allochthonous taxa present several problems. These issues are further explored in Chapters 6, 7, 8 and 9.

3.7.5 Presentation of diatom data

Diatom data were graphically displayed using a combination of two computer packages: TILIA (version 2.0.2, Grimm, 2004), and C^2 (version 1.4.2, Juggins, 2003). Diatom counts are expressed as percentage relative abundance. Only taxa which had a maximum relative abundance of at least 3% or 5% are presented for each location to ease visual interpretation.

3.7.6 Diatom zonation

For both the modern (Chapter 4) and core material (Chapter 6), diatom assemblage zones were identified using incremental sum-of-squares cluster analysis (CONISS; Grimm, 1987) based on a square-root transformation of data (Edwards and Cavalli Sforza's chord distance). In the case of frequency data, such as that used in this investigation, this transformation increases the weights of rare variables relative to abundant ones (Grimm, 1987). Such a data transformation assists in stabilizing variances and is often applied to percentage data sets with a high number of variables (Prentice, 1980). Unconstrained cluster analysis was applied to the surface samples to establish diatom assemblage zones. Stratigraphically constrained cluster analysis was applied to the biostratigraphical data from the cores. In order to minimise the effects of rare taxa, the cluster analysis excluded all taxa where relative abundances are < 1%.

3.8 Statistical Analysis

The following section details the various statistical methods employed in the analysis of the modern diatom and environmental data.

3.8.1 Inclusion of samples

The following samples were excluded from the data set before any statistical analysis due to insufficient diatom counts: MO14, LN1, LN7, LN8, LN20, LS1, LS2, LS3, LS20, LS22, LS24 and LS26. Sample LN05 was also excluded before any statistical analysis since no particle size data was obtained for this sample (Section 4.2). Samples were excluded from both the diatom and environmental data. The twenty-seven samples from Kjelst Enge, where only three environmental variables were measured (elevation, pH and salinity), were included in the initial analysis (normality tests, Spearman's Rank) of environmental variables. Two data sets were analysed in the ordinations: the first data set (hereafter referred to as DataSetA), excluded the Kjelst Enge samples and contained six environmental variables measured from five transects (elevation, pH, salinity, LOI, $CaCO_3$, sand, silt, clay). The Kjelst Enge samples were excluded from this data set as only three environmental variables were measured along this transect and the analysis could not be performed on variables with absent values The second data set (hereafter referred to as DataSetB), contained samples from all six transects (127 samples) but only three environmental variables (elevation, pH and salinity). The samples and environmental variables included in each of these data sets are summarised in Table 4.2.

3.8.2 Inclusion of species

Previous studies have shown that rare species need to be removed from a data set before any analysis is carried out (Patterson and Fishbein, 1989; Fishbein and Patterson, 1993; Patterson et al., 2005). In coastal environments, species with relative abundances of < 1% are likely to be allochthonous (transported) taxa and are not often used in interpretation (Nelson and Kashima, 1993). Commonly, coastal type studies often employ a 3 or 5% cut-off (Roe, *pers. comm.*). However, early experimentation with a 2, 3 and 5% cut-off level in this study resulted in a significant loss of biological information and an increased number of fossil taxa with no modern analogue. For these reasons a 1% cut-off level was employed. Individual samples which contain rare taxa (i.e. where a species may only be present in one sample) can also significantly distort the analysis (Hill, 1979). Diatom taxa

were therefore included in ordinations if a) their relative abundance was ≥ 1%, and b) the species was present in more than one sample.

3.8.3 Correlations between environmental variables

Within any large data set, environmental variables commonly show a high degree of inter-correlation with one another resulting in redundancy in the data set (Birks, 1995). Prior to the implementation of any ordination techniques, the degree of intercorrelation between environmental variables was assessed using a correlation coefficient. A Pearson product-moment correlation coefficient matrix is commonly employed when exploring environmental data and developing diatom training sets (e.g., Hall and Smol, 1992; Jones et al., 1993; Ng and Sin, 2003; Trites et al., 2005). However, a prerequisite of this test is that the environmental data are normally distributed (Kent and Coker, 1992).

Tests for normality were conducted on all eight environmental variables measured in MINITAB® Release 14, using the Anderson-Darling normality test. In this test, the *null* hypothesis (H_0) states that the data follow a normal distribution. Where *p*-values were less than a rejection level of 0.05 (95% confidence), the null hypothesis was rejected and the data were assumed not to be normally distributed. Normality tests for elevation, pH and salinity included the samples from Kjelst Enge.

The majority of environmental variables tested did not show a normal distribution (Table 4.3). Several attempts were made to obtain normal distributions by transforming the variables, but most still did not obtain normality (Table 4.3). For this reason correlation coefficients in this study were calculated using a Spearman's Rank correlation coefficient, which does not require data to be normally distributed, instead of the more commonly used Pearson's correlation coefficient. Spearman's Rank correlation coefficients were subsequently calculated between pairs of environmental variables using MINITAB®. A scatter plot matrix showing relationships between environmental variables was constructed to enable visual interpretation of the relationships. The results are presented in Section 4.5.2.

3.8.4 Ordinations

Ordination techniques provide an objective way in which to examine species and environmental data. They aim to identify variability in the biological composition of samples and to visualise this variability in the form of a diagram (an ordination diagram) (Lepš and Šmilauer, 2003). With the addition of environmental variables, constrained ordination can be used to identify the variability in biological composition that is explained by these variables (Lepš and Šmilauer, 2003). The ordination techniques employed in this study included: Principal Components Analysis (PCA), Detrended Correspondence Analysis (DCA), Canonical Correspondence Analysis (CCA) and Detrended Canonical Correspondence Analysis (DCCA). In all ordinations, Monte Carlo permutation tests were run using restricted permutations (499 permutations under a restricted model), to account for the spatial structure that results from sampling along line transects (J. Birks, *pers comm*). All ordinations were performed using the computer programme CANOCO version 4.51 (ter Braak and Šmilauer, 2003). Ordination diagrams were plotted using CANODRAW version 4.1 (Šmilauer, 1999 - 2003).

Data Screening

Any large ecological data set is likely to contain redundant environmental information, anomalous samples and environmental variables which do not exert an independent influence on diatom distributions (Birks et al., 1990a). Before implementation of the final ordinations, several preliminary ordinations were performed to identify and subsequently eliminate these data. In this study the data screening process consisted of three stages:

a) PCA was used to highlight and subsequently eliminate samples with extreme environmental characteristics
b) DCA were used to identify anomalous or 'outlier' samples with unusual species assemblages.
c) CCA was used to identify redundancies in environmental information and to eliminate environmental variables which did not exert an independent influence on diatom distributions.

The above data screening process follows the methodology commonly employed in palaeolimnology studies (e.g., Birks et al., 1990a; Hall and Smol, 1992; Jones and Juggins, 1994; Ng and King, 1999; Burgess, 2004). As yet there are few examples of such a

thorough screening process being used when developing training sets in the coastal environment, particularly when developing models to reconstruct relative sea-level change. Some notable exceptions include the work of Ng and Sin (2003) and Charman et al. (2002), where several aspects of this screening process were implemented. A thorough screening process is important because outlier samples and redundant environmental information can significantly distort the species-environment relationships.

Principal Components Analysis (PCA)

PCA is an indirect (unconstrained) gradient technique and was used in this study to summarise environmental information and to highlight samples with extreme environmental characteristics. Whilst PCA is no longer recommended as an ordination technique with which to examine the variation in species data, it is still widely used as a method to synthesise environmental information (Kent and Coker, 1992). Standardised PCA was performed on a correlation matrix, obtained by centering and standardisation of the environmental data. The results of PCA and the subsequent removal of outlier samples based on these results are presented in Section 4.5.3.

Detrended Correspondence Analysis (DCA)

Detrended Correspondence Analysis (DCA) (Hill, 1979) is an indirect (unconstrained) gradient technique, and was used in this study to reveal major patterns in the diatom species data, to highlight anomalous or 'outlier' samples and to determine whether linear or unimodal methods were suitable for further exploration of the modern training set. DCA aims to overcome problems such as the 'arch' or 'horseshoe' effect (Kendall, 1971; Gauch et al., 1977), and the distortion of ordination axis (Hill and Gauch, 1980), associated with earlier methods. DCA is generally considered an improvement on other indirect ordination techniques such as CA, although it is not without criticism (e.g., Dargie, 1986; Wartenberg et al., 1987).

DCA was performed using detrending by segments with no species transformation. Rare taxa were down weighted in proportion to their frequency (Hill and Gauch, 1980). Detrending by segments, considered as inappropriate by some authors (e.g., Wartenberg et al., 1987; Knox, 1989) was used here in preference to detrending by polynomials since no environmental variables were present in the analysis. The results of DCA can be used to indicate whether linear or unimodal methods of direct gradient analysis are suitable for

exploration of the species-environment relationships within the data set. Where gradient lengths are short, < 3 standard deviations (SD), linear models are usually used. Where gradient are long (> 4 SD), unimodal methods are usually more appropriate (Lepš and Šmilauer, 2003). In this study, gradient lengths of > 3 SD have been taken to indicate the suitability of unimodal direct gradient analysis techniques. The results of DCA and the subsequent removal of outlier samples based on these results is presented and detailed in Section 4.5.3.

Canonical Correspondence Analysis (CCA)

DCA axis one gradient lengths of 3.342 and 3.065 SD for the two data sets analysed (Tables 4.7 and 4.16) indicated that most species responses can be approximated with a unimodal model. The unimodal ordination method of CCA was therefore chosen to explore the species-environment relationships within the two data sets. CCA (ter Braak, 1985; 1986; 1987b) is a direct (constrained) gradient analysis technique which is used to analyse the variability in species composition that can be explained by the measured environmental variables (Lepš and Šmilauer, 2003). CCA was performed with a focus on inter-species distances and Hills' scaling. Hills' scaling was chosen in preference to biplot scaling because of the longer gradient lengths established by the DCA (Jongman et al., 2002; Lepš and Šmilauer, 2003; ter Braak and Šmilauer, 2002). In this study CCA was initially applied to the data sets as a screening exercise to i) remove outlier samples with environmental variables which had extreme influence or 'leverage'(Montgomery and Peck, 1982) ii) to identify and exclude environmental variables which did not exert an independent influence on diatom distributions and iii) to eliminate any redundancies in environmental information.

An initial CCA was run on both of the full data sets. Outlying samples, identified through PCA and DCA, were excluded from the CCA ordinations. Samples with environmental variables with extreme influence or 'leverage' (Montgomery and Peck, 1982) were detected based on the results of this initial CCA. Any sample with > 5x the average influence in the CCA was considered to be outlying (Birks et al., 1990a, 1990b). Following the initial CCA, the screening process to remove environmental variables consisted of the following stages:

1. Constrained CCAs

A series of constrained CCAs were run to identify and subsequently exclude any environmental variable which did not exert an independent and statistically significant influence on diatom distributions (ter Braak and Šmilauer, 2002). Constrained CCAs were run for each environmental variable in turn. Variables with high eigenvalue ratios between axes 1 and 2 (λ_1/λ_2), were considered more important in explaining the variance in the species data. Variables were removed from subsequent analyses if they showed no independent influence over diatom distributions ($p > 0.05$).

2. Intercorrelation between environmental variables

Intercorrelations between environmental variables were initially identified from a Spearman's Rank correlation matrix (Table 4.4). Examination of the inter-set correlations between the variables and the ordination axes, and the information gained from the Spearman's Rank correlations, was used to identify a subset group of variables to be tested in a partially constrained CCA. Highly intercorrelated variables, which also showed high correlation with axis one, were selected in this subgroup.

3. Preliminary CCA with automatic forward selection

A preliminary CCA was run using automatic forward selection to determine which of the environmental variables in the group (identified through step two above), was most important for explaining the amount of variance in the diatom data. This environmental variable was then used in step four as a representative of that group of correlated environmental variables.

4. Partially constrained CCAs

A series of partially constrained CCAs was run to determine if other environmental variables in the intercorrelated correlated group exerted an independent influence on diatom distributions. The environmental variable identified in step three was used as the sole environmental variable in a partially constrained CCA. Correlated environmental variables were then entered in turn as sole covariables. The significance of the first canonical axis was tested ($p = < 0.05$, with 499 permutations under a reduced model, restricted for spatial structure (Birks, *pers. comm.*)). Any covariable not exerting an independent influence of diatom distributions was subsequently removed from the analysis.

5. Examination of variance inflation factors (VIFs)

As a final screening measure, VIFs were examined from the results of the final CCA. High VIFs are an indication of multicollinerarity among environmental variables (ter Braak and Šmilauer, 2002). VIFs with a value > 20 indicate that the environmental variable is nearly perfectly correlated with other environmental variables and should be removed from the analysis (ter Braak and Šmilauer, 2002). Variables with VIFs < 20 were deemed to have stable canonical coefficients and merited interpretation (ter Braak, 1986).

6. CCA with manual forward selection

Following the data screening process, a final CCA was run using manual forward selection to identify a final subset of variables that explained a statistically significant amount of variation in the diatom data. The statistical significance of each variable was tested in turn. Variables that were statistically significant ($p < 0.05$), were added to the model in turn.

7. Variance Partitioning

The relative strengths of the major gradients in the final CCA were explored using a series of partial CCAs (Borcard et al., 1992). Partial CCAs were used to determine the proportion of explained variance that was attributed to each of the remaining environmental variables. The use of partial CCAs also allowed determination of the amount of covariance between remaining variables. Variables explaining high, independent and significant proportions of variance in the diatom data were deemed suitable variables from which to develop diatom-based transfer functions.

Detrended Canonical Correspondence Analysis (DCCA)

Following a through exploration of the modern environmental and species data, DCCA (ter Braak, 1986, 1987b), was used to determine which type of models, linear or unimodal, were most suitable to use in subsequent transfer function development. The methodology used is discussed in detail in Section 7.5.

3.9 Chapter Summary

This chapter has detailed the various methods used throughout this investigation in the collection, processing and subsequent analysis of material and samples. The next section of this thesis presents the results of these investigations, firstly from the modern salt-marsh environment (Chapter 4), and secondly from the palaeoenvironment (Chapters 5 and 6).

Chapter 4

Modern salt-marsh environments

Having detailed the methodology used throughout this study in the previous chapter, this chapter presents results from the analysis of modern diatom assemblages and associated environmental variables. The chapter begins with a description of the topography and vegetation of the salt marsh at each of the six transects locations investigated. Results of the analysis of a number of environmental variables are presented alongside modern diatom data from each transect location. The vertical zonation of diatom species with respect to the tidal frame is tested via the use of unconstrained cluster analysis. In the second part of this chapter, the relationship between diatom species and environmental variables is explored through the use of several ordination techniques.

4.1 Modern salt-marsh environments

A total of six modern transects were investigated across the salt-marsh surface from locations within Ho Bugt as detailed in Chapter 3 (Figure 3.1). A description of the marsh surface topography and vegetation zonation at each transect location is given below. Transects are described in a north – south direction. Examples of the vegetation types identified along each transect are shown in Figure 4.1. Marsh surface topography, vegetation zonation and tidal levels are illustrated in Figures 4.2 – 4.4.

Kjelst Enge (Figure 4.2*a*)

At Kjelst Enge, the topography of the marsh is flat and varies between +0.7 and +1.9 m DNN. A levee-like feature is found where the high marsh reaches its seaward extent. Seaward of the 'levee' the low marsh slopes steeply down to the tidal flat. The high salt marsh is dominated by the vascular plants *Agrostis stolonifera, Festuca rubra, Armeria maritima* and *Cochlearia officinalis*. *Salicornia* spp. and *Spergularia* spp. are found in the low marsh. Stands of *Carex* spp. occur in the low marsh as a result of freshwater drainage from a nearby channel.

Moservå (Figure 4.2*b*)

At Moservå, the marsh surface lies between +1.9 m and +2.7 m DNN. The landward extent of the marsh is marked by transition to scrubland. The marsh is bounded at the seaward extent by the *Storbæk* drainage channel. The marsh surface slopes gently down towards the drainage channel. The marsh is dominated by the common reed, *Phragmites australis*.

High marsh grasses such as *Agrostis stolonifera* and *Festuca rubra* are found mixed with *Phragmites australis* along the entire Moservå transect, except its uppermost part.

Storbæk (Figure 4.3*a*)

The marsh surface at Storbæk lies between +1.34 and +1.46 m DNN. At the landward extent, the salt marsh is bounded by a steep rising gradient, linked to the Holocene dune ridges which lie immediately to the west. The seaward extent of the marsh is again bounded by the Storbæk drainage channel. At high elevations the marsh is dominated by a large expanse of *Phragmites australis*. At slightly lower elevations, where more moisture is present, *Juncus gerardi* and *Juncus effusus* are found. Grasses such as *Agrostis stolonifera* and *Festuca rubra* dominate the seaward extent of the marsh.

Oksby Enge (Figure 4.3*d*)

At Oksby Enge, the marsh surface lies between +2.2 and +1.25 m DNN. At the landward margin, the marsh is bounded by scrubland. At the seaward extent, the marsh borders onto the tidal flat and the transition is marked by a single erosional cliff. Species such as the thistle, *Cirsium palustre* are found in the scrubland at the landward extent of the marsh. *Phragmites australis* is common at slightly lower elevations. Towards the seaward extent of the marsh, several grasses are dominant including *Agrostis stolonifera* and *Festuca rubra*. Patches of *Juncus gerardi* are found at lower elevations.

Langli North (Figure 4.4*a*)

At the northern end of Langli Island, the marsh surface lies between +0.23 and +1.76 m DNN. Marsh surface topography is fairly flat, although the gradient steepens with transition from the middle to low marsh. On the low marsh, *Spartina x towsendii* and *Spartina anglica* (Pedersen, 1974; Bartholdy et al., 2004) is the dominant vegetation type alongside occurrences of *Salicornia perennis* and *Puccinellia maritima*. The middle marsh is characterised by species such as *Limonium vulgare, Plantago maritima* and *Artemisia maritima*. At the landward extent of the marsh, increasing occurrences of *Halimione portulacoides* are found. Here the salt marsh is bounded by a line of sand dunes.

Langli South (Figure 4.4*b*)

The marsh surface at the southern end of Langli Island lies between +0.67 and +1.78 m DNN. The marsh surface is again relatively flat. However, the topography is complicated by the presence of several major creeks which run in an approximate east – west direction. Vegetation zones are very similar to those found on the north of the island and here also, the marsh is bounded at the landward extent by a sand dune ridge.

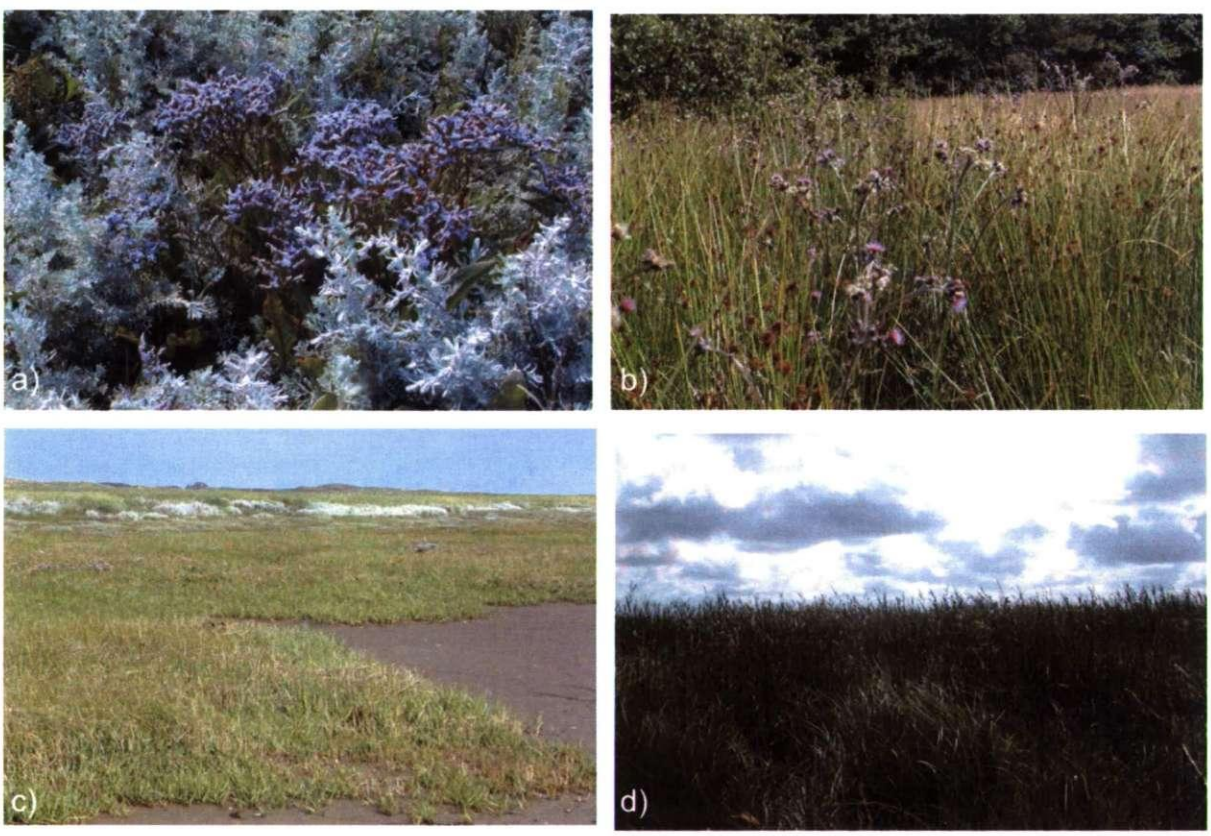

Figure 4.1. Examples of the types of salt-marsh vegetation identified along transects within the Ho Bugt embayment, a) *Artemisia maritima* and *Limonium vulgare,* Langli North, b) *Cirsium palustre,* Oksby Enge, c) *Spartina towsendii,* Langli South and d) *Phragmites australis*, Oksby Enge.

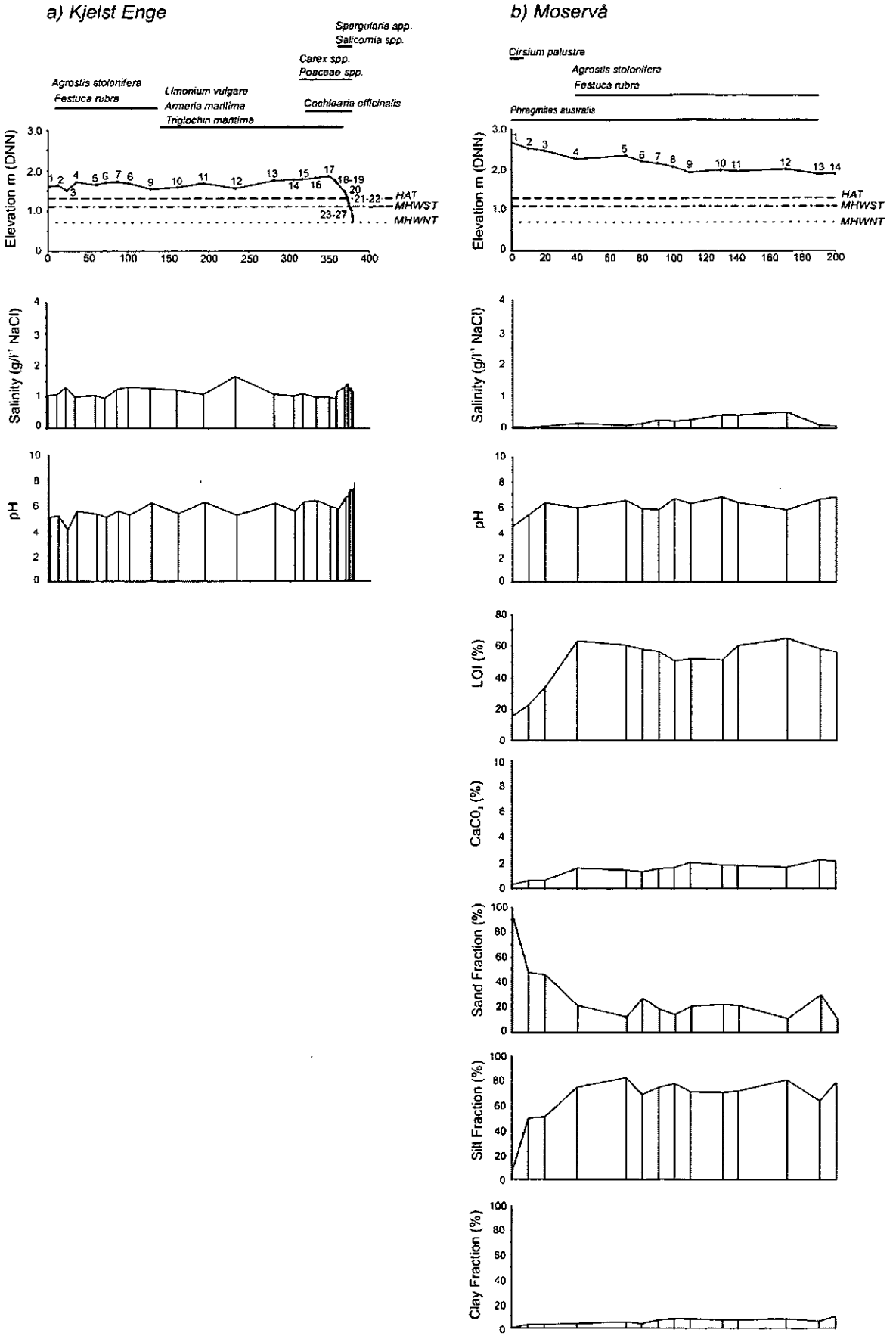

Figure 4.2. Environmental variables measured along transect at a) Kjelst Enge and b) Moservå, alongside topography, tide levels and vegetation zones. Sampling locations are indicated.

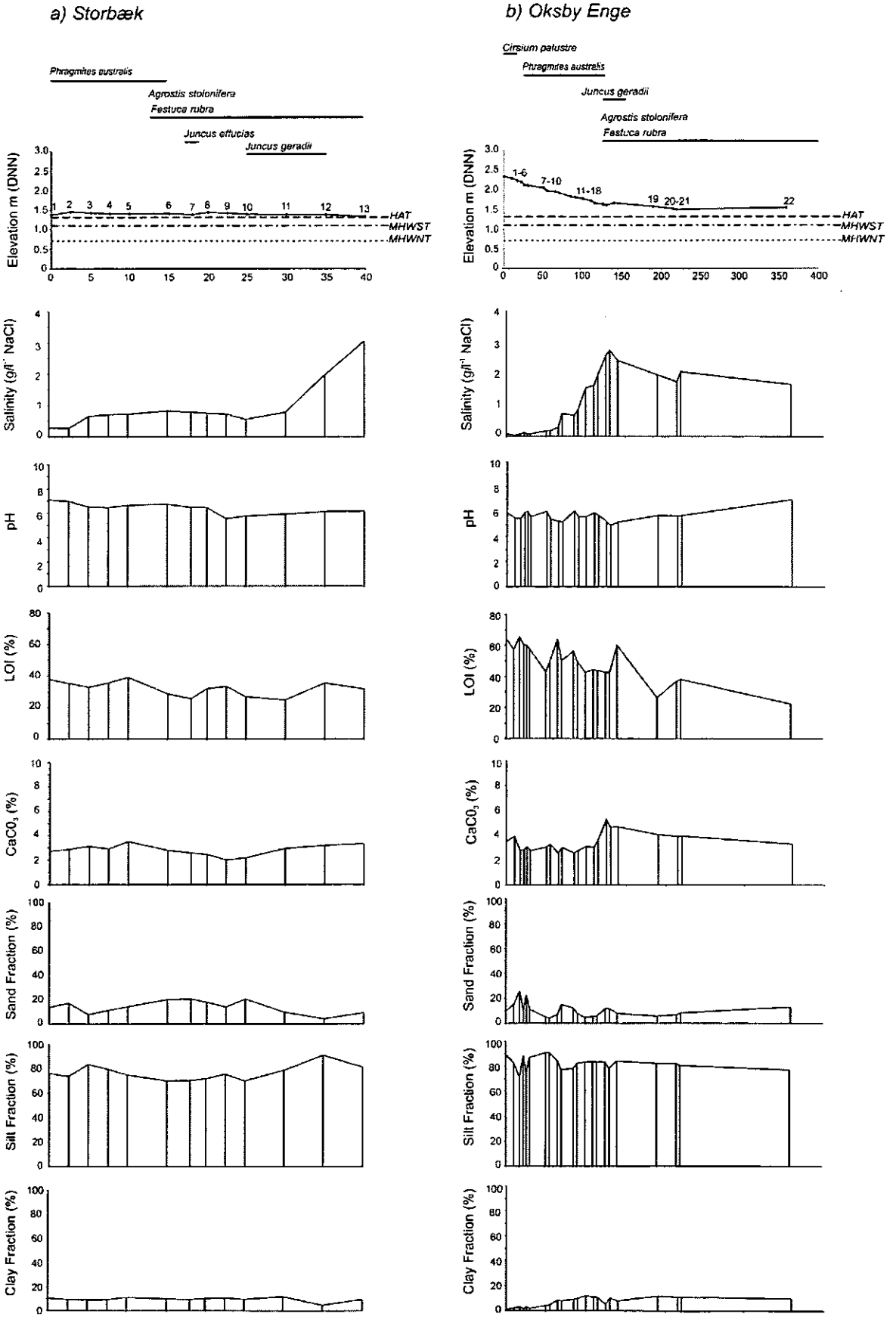

Figure 4.3. Environmental variables measured along transect at a) Storbæk and b) Oksby Enge, alongside topography, tide levels and vegetation zones. Sampling locations are indicated.

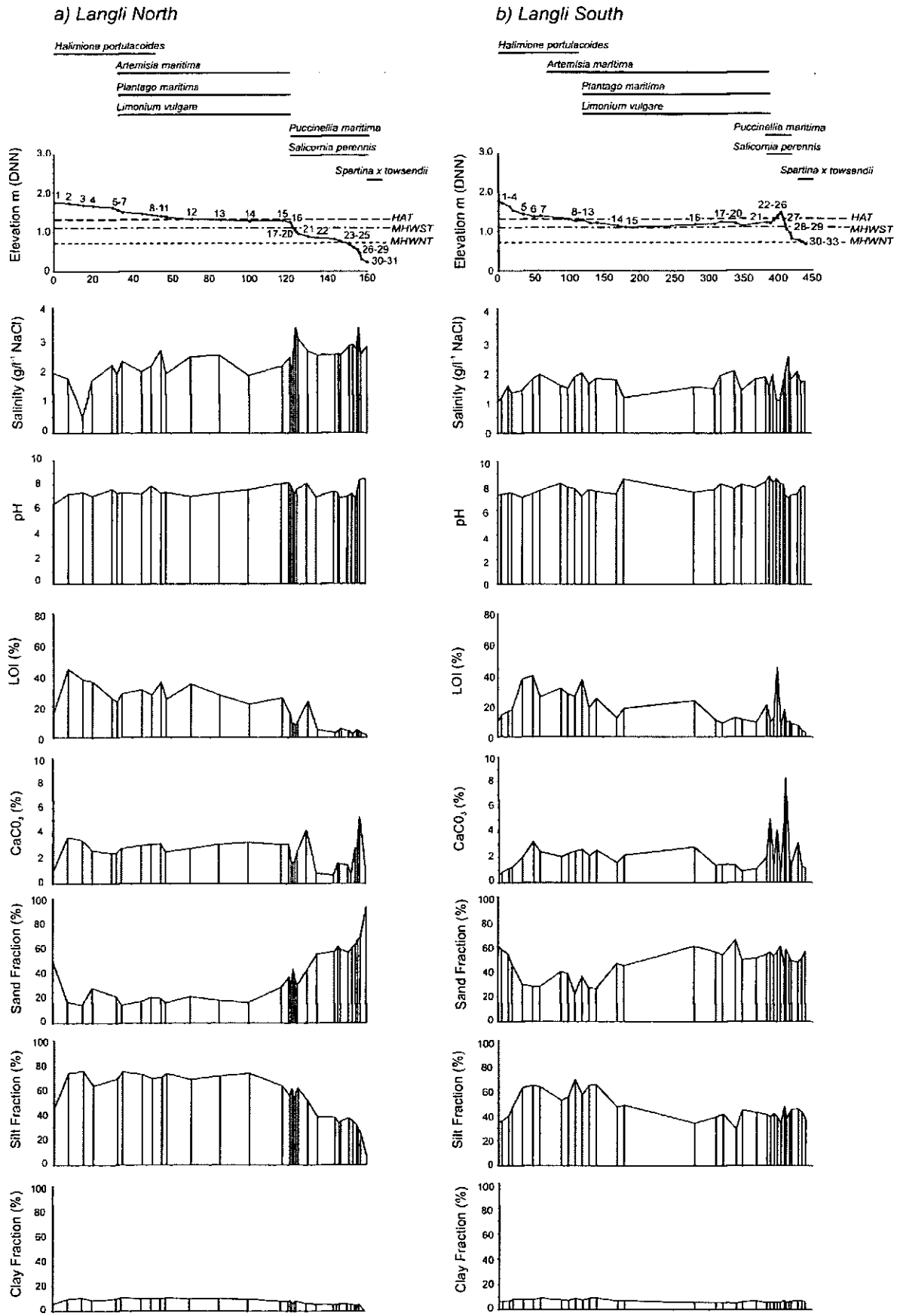

Figure 4.4. Environmental variables measured along transect at a) Langli North and b) Langli South, alongside topography, tide levels and vegetation zones. Sampling locations are indicated.

4.2 Environmental variables

A total of six environmental variables were investigated along each of the modern transects sampled: elevation, pH, salinity (conductivity), LOI, $CaCO_3$ and grain size (sand, silt and clay fractions). For the Kjelst Enge transect, which was sampled as part of the HOLSMEER Project, only elevation, pH and salinity were measured. All variables were successfully measured from all samples, at each of the transect locations unless otherwise stated. Results are described below and illustrated in Figures 4.2 – 4.4. Transects are described in a north – south direction.

Kjelst Enge (Figure 4.2*a*)

Along the Kjelst Enge transect, salinity ranges from 0.93 – 1.64 g/l^{-1}. Salinity is variable across the marsh with the highest salinity values found in the middle marsh. Towards the seaward extent of the transect, salinity values are slightly lower. Values here are affected by the *Storbæk* drainage channel, which drains water from the higher marshes out into the Ho Bugt embayment. The pH ranges from 4.09 – 7.85 and is variable across the transect. Highest pH values are found at the very seaward end of the transect.

Moservå (Figure 4.2*b*)

Salinity is very low across the marsh at Moservå, ranging from 0.02 – 0.51 g/l^{-1} but increases towards the seaward extent of the transect. The pH ranges from 4.5 – 6.8 and is found to be highly variable across the transect. The pH is lowest in samples from the *Phragmites* marsh and increases in the seaward direction. The percentage of organic matter (LOI) in the surface samples at Moservå varies from 15 - 65%. Lowest LOI values are found in samples from the *Phragmites* water marsh with values increasing in the seaward direction. The percentage of calcium carbonate ($CaCO_3$) found in the surface samples, measured as a percentage of the original material, varies from 0.3 – 2 %. Lowest values are found in the high marsh. Grain size (sand, silt and clay fractions) varies greatly across the Moservå transect. The surface sample which borders the scrubland environment is characterised by a high sand content (> 95%) and low silt and clay fractions. With movement seaward, the sand fraction decreases greatly and silt and clay fractions increase. The high marsh samples are characterised by high silt fractions (> 65%).

Storbæk (Figure 4.3*a*)

Salinity across the Storbæk transect ranges from 0.3 – 3.1 g/l^{-1}. Salinity is higher at the seaward extent of the transect. The pH ranges from 5.5 – 7.1. In general, values are lowest in samples from the high marsh and increase in the seaward direction. LOI is variable across the Storbæk transect with values ranging between 25 and 39%. $CaCO_3$ varies from 2. – 3.4 % and is also highly variable across the transect. Grain size analysis shows the surface sediments at Storbæk to be predominantly composed of silts. The silt fraction accounts for at least 70% of the minerogenic matter in all surface samples. Sand content is variable across the transect and the clay fraction is low in all samples (< 12%).

Oksby Enge (Figure 4.3*b*)

At Oksby Enge salinity ranges from 0.04 – 2.8 g/l^{-1}. In general, salinity values are higher towards the seaward extent of the transect. The highest salinity values are found in the middle marsh. The pH ranges from 4.9 – 7.0. Values fluctuate across the transect but are highest in the most seaward of the samples. LOI varies from 22 – 66%. Highest LOI values are found in the *Phragmites* marsh and the high salt marsh, with values decreasing in the seaward direction. $CaCO_3$ varies from 3 – 5%. The lowest $CaCO_3$ values are found in samples from the fresh water and high salt marshes. Grain size analysis shows that the surface sediments at Oksby Enge are predominantly composed of silts. Here, as is the case at Storbæk, the silt fraction accounts for at least 70% of the minerogenic matter in all surface samples.

Langli North (Figure 4.4*a*)

At Langli North salinity ranges from 0.5 – 3 g/l^{-1}. Salinity is variable across the transect with the highest values found towards the seaward end. The pH ranges from 6 – 8.5. The highest values are found in the low marsh and values decrease towards the high marsh. LOI varies from 1.2 – 44%. Highest LOI values are found in samples from the high marsh and lowest LOI values (c. 4%) are found in samples from the low marsh and tidal flat. $CaCO_3$ varies from 0.7 – 5.3%. Values fluctuate greatly across the salt-marsh surface. Grain size at Langli North is highly variable across the transect. At the seaward extent of the transect, where samples border onto the tidal flat, surface sediments are composed predominantly of sand (> 60% sand fraction). Samples from the high marsh, which border onto the sand dune ridge, also have a high sand fraction. In the high and middle salt marshes, samples are mainly composed of silt. Here, the silt fraction accounts for greater

than 70% of the minerogenic material in the surface samples. No particle size data is available for sample LN05. The quality control check on this sample suggested that the result was not reliable and so this sample has been excluded from the results and all subsequent analysis.

Langli South (Figure 4.4*b*)

Salinity at Langli South ranges from 1 – 2.5 g/l^{-1}. Salinity is variable across the transect but values tend to be higher towards the most seaward end. pH is fairly consistent across the transect, ranging from 7.0 – 8.8%. LOI varies from 3 to 45% and is highly variable along the transect. The percentage $CaCO_3$ varies from 0.6 – 8.4%. In general, the highest $CaCO_3$ values are found on the low salt marsh and the tidal flat. Grain size at Langli South is highly variable across the transect. Samples from the tidal flat are dominated by high sand fractions (> 50% sand fraction), with relatively low silt and clay fractions. High fractions of sand (> 45 %) are also found in samples from the high salt marsh, which borders onto the sand dune ridge. Samples from the middle marsh are dominated by high silt fractions (> 60%).

Kjelst Enge	Moservå	Storbaek	Oksby Enge	Langli North	Langli South	
Environment not present	*Cirsium palustre* *Phragmites australis* 2.1 m DNN	Environment not present	*Cirsium palustre* *Phragmites australis* 1.9 m DNN	Environment not present	Environment not present	**Fresh water marsh**
Agrostis stolonifera *Festuca rubra* *Limonium vulgare* *Armeria maritima* *Triglochin maritima* 1.3 m DNN	*Phragmites australis* *Agrostis stolonifera* *Festuca rubra*	*Phragmites australis* *Agrostis stolonifera* *Juncus effelfusus* *Juncus gerardi* 1.5 m DNN	*Agrostis stolonifera* *Festuca rubra* *Juncus gerardi*	*Halimione portulacoides* *Artemisia maritima* *Plantago maritima* *Limonium vulgare* 1.4 m DNN	*Halimione portulacoides* *Artemisia maritima* *Plantago maritima* *Limonium vulgare* 1.5 m DNN	**High salt marsh**
Salicornia spp. *Spergularia spp.* *Carex spp.*	Not sampled	Not sampled	Not sampled	*Puccinellia maritima* *Salicornia perennis* *Spartina x townsendii* 0.6 m DNN	*Puccinellia maritima* *Salicornia perennis* *Spartina x townsendii* 0.75 m DNN	**Low salt marsh**
Vegetation absent	Not sampled	Not sampled	Not sampled	Vegetation absent	Vegetation absent	**Tidal flat**

Table 4.1. Marsh zones at each of the six transects investigated, defined by vegetation type. The elevation of the transition between tidal flat, low salt marsh, high salt marsh and fresh water marsh along each of the transects is indicated where applicable. These 'salt-marsh zones' are referred to throughout the remainder of this thesis. See text for an explanation of marsh zones 'not sampled' at each transect location.

4.3 Modern Diatom Assemblages

Modern diatom data from the six transects investigated are plotted with respect to elevation and presented in Figures 4.5 – 4.16. The results of unconstrained incremental sum-of-squares cluster analysis (CONISS; Grimm, 1987) are shown for each of the six transect locations (Figures 4.5 – 4.16) and resulting diatom assemblage zones are illustrated using box plots. (Figures 4.5 – 4.16). Transects are described in a north – south direction. The location of each transect is illustrated in Figure 3.1.

Kjelst Enge

Modern diatom data from the salt marsh at Kjelst Enge are presented in Figure 4.5. Samples were analysed by Dr. J. Kirby as part of the HOLSMEER Project. A total of 95 diatom taxa were identified across the salt marsh at Kjelst Enge, of which 62 taxa were found with relative abundances ≥ 1%. All 27 surface samples analysed returned full counts of between 250 and 300 diatom valves. In general, valve preservation was very good across the majority of the transect.

The salt marsh at Kjelst Enge is dominated mainly by polyhalobous and mesohalobous taxa such as *Achnanthes delicatula*, *Diploneis didyma* and *Delphineis surirella,* indicative of a brackish to marine environment. Several of these taxa are also allochthonous (transported) and their occurrence in relatively high abundances, especially at higher elevations may complicate the diatom signal. The oligohalobous – halophile taxon, *Navicula cincta* – type is also found in high abundances across this transect. Relatively few fresh water taxa, represented by the oligohalobous – indifferent group, are identified. At lowest elevations there is an increase in the abundance of species within this group. *Navicula rhynchocephala* is found with a relative abundance of >15% in the two samples with the lowest elevation. This is somewhat surprising and the occurrence of this taxon at such low elevations may be linked to the proximity of these samples to the nearby Storbæk drainage channel. This channel drains fresh water from the higher salt marshes out into the Ho Bugt embayment.

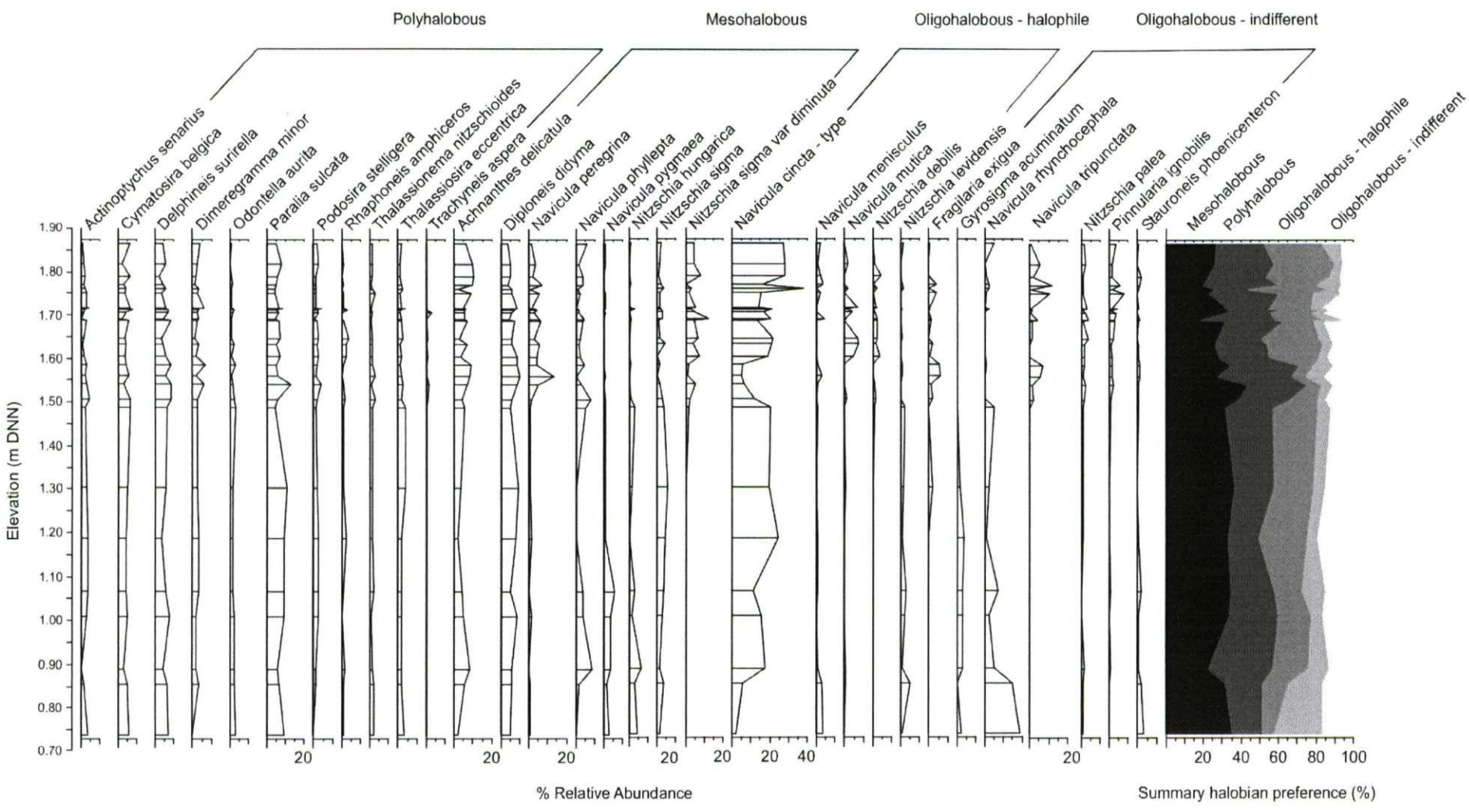

Figure 4.5. Modern diatom data from the salt-marsh at Kjelst Enge (analysist J.R. Kirby). Only species with > 3% relative abundance are shown. Summary halobian preference only includes species with at least 3% relative abundance.

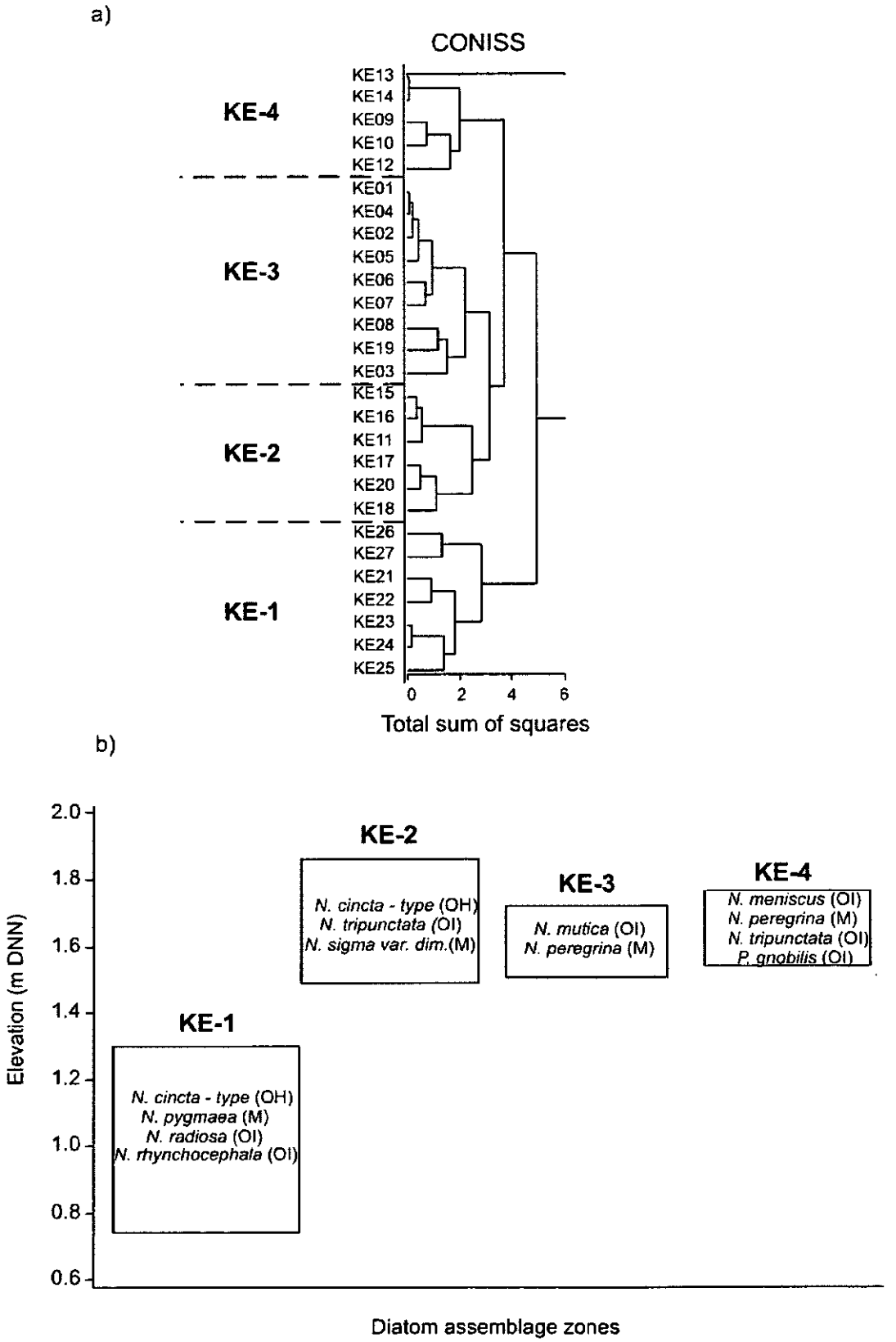

Figure 4.6. a) Results of unconstrained cluster analysis on the Kjelst Enge diatom data. Cluster analysis excludes all taxa where relative abundances are < 1%. b) Elevation range and dominant taxa of diatom assemblage zones, identified from unconstrained cluster analysis. Halobian preferences of these taxa are indicated. P = polyhalobous, M = mesohalobous, OH = oligohalobous – halophile, OI = oligohalobous – indifferent, H = halophobous.

Unconstrained cluster analysis divides the modern samples into four diatom assemblage zones (Figure 4.6a). The elevation range and dominant taxa in each zone are presented in Figure 4.6b. The diatom assemblages across the salt marsh at Kjelst Enge show some evidence of a vertical zonation. However, samples in zones two, three and four have very similar elevation ranges and no clear vertical zonation is apparent within these samples. This is most probably due to the presence of high abundances of allochthonous taxa in all of these samples. The zonation is also likely to be affected by the presence of the oligohalobous – indifferent taxon, *Navicula rhynchocephala*, in the lower marsh samples. It is clear from this analysis that the diatoms in the samples from Kjelst Enge do not demonstrate a vertical zonation. This transect in particular is highlighted for further analysis (Section 4.5.3) and the possible exclusion of at least some of these samples from the final training set.

Moservå

Modern diatom data from the salt marsh at Moservå are presented in Figure 4.7. A total of 142 diatom taxa were identified across the salt marsh, of which 71 taxa were found with a relative abundance ≥ 1%. Two species remain unidentified, Species G1 and Species X1, both of which occur with a maximum relative abundance of 1.1%. Unidentified diatom taxa, with relative abundances ≥ 1%, are described in Appendix 5. Of the 14 surface samples analysed, 13 of them returned full counts of 300 valves. Sample MO14 reacted violently to H_2O_2 treatment and proved difficult to process. No data is available for this sample and it has therefore been excluded from the results and subsequent analysis. In general, valve preservation was very good across the whole transect, although diatom concentrations were low and highly concentrated slides were needed to obtain full counts.

The salt marsh at Moservå is dominated by taxa in the oligohalobous – indifferent group, indicative of a fresh water environment. Taxa such as *Nitzschia terrestris, Hantzschia amphioxys* and several species of *Pinnularia* are abundant across this transect. At lower elevations there is an increasing abundance of taxa within the oligohalobous – halophile, mesohalobous and polyhalobous groups, indicative of a more brackish water environment. Taxa such as *Navicula mutica, Nitzschia debilis and Navicula cincta* – type are found in increasing abundances towards lower elevations. The abundance of polyhalobous and mesohalobous species remains very low overall, but increasing abundances of species such as *Cymatosira belgica* and *Diploneis didyma* are found in samples with the lowest elevations.

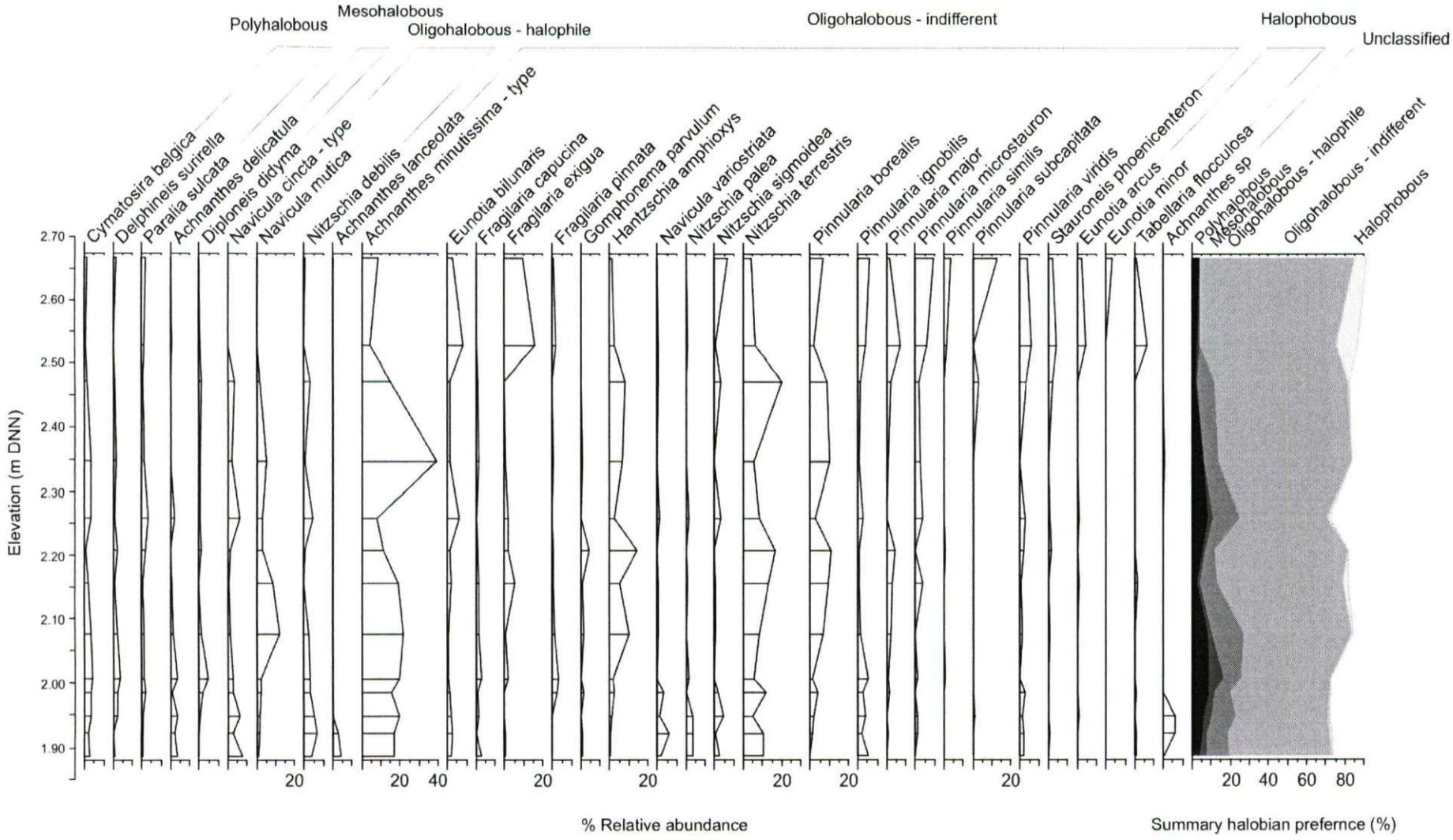

Figure 4.7. Modern diatom data from the salt-marsh surface at Moservå. Only species > 3% relative abundance are shown. Summary halobian preferences only include species with at least 3% relative abundance.

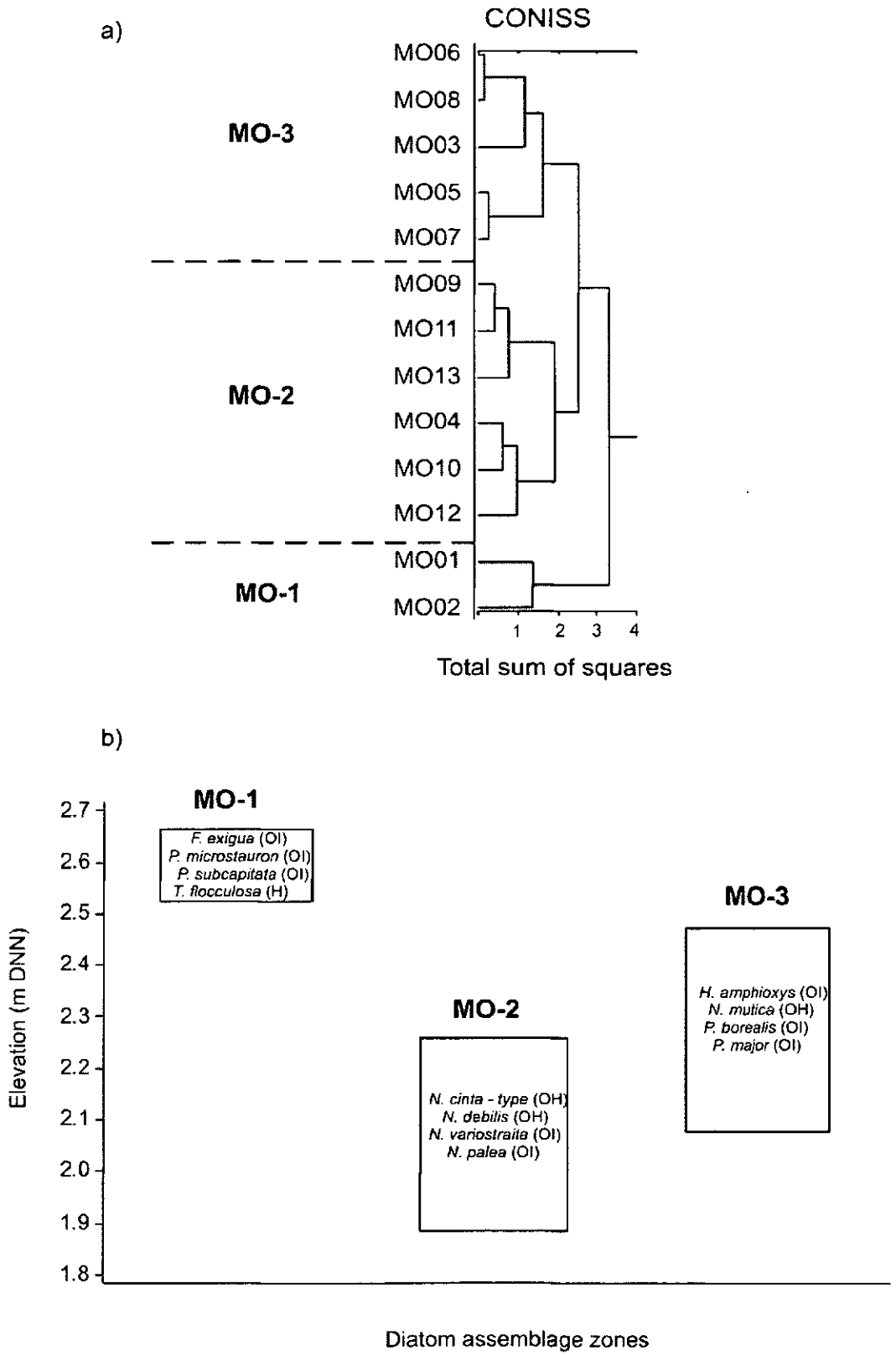

Figure 4.8. a) Results of unconstrained cluster analysis of the Moservå diatom data. Cluster analysis excludes all taxa where relative abundances are < 1%. b) Elevation range and dominant taxa for diatom assemblage zones, identified from unconstrained cluster analysis. Halobian preferences of these taxa are indicated.

Unconstrained cluster analysis divides the modern samples into three diatom assemblage zones (Figure 4.8a). The elevation range and dominant taxa in each zone are presented in Figure 4.8b. The diatom assemblages across the salt-marsh surface at Moservå show some evidence of a vertical zonation, although some samples do not clearly fit this trend. Samples MO1 and MO2 contain noticeably different diatom assemblages to the remaining samples. These samples are highlighted as possible outliers. Cluster analysis has demonstrated the need for further investigation of samples in this transect, with the possible removal of at least some of the samples from the final training set.

Storbæk

Modern diatom data from the salt marsh at Storbæk are presented are Figure 4.9. A total of 144 diatom taxa were identified across the salt marsh at Storbæk, of which 78 taxa were found with relative abundances ≥ 1%. One species, species G1, remains unidentified with a maximum relative abundance of 8.3%. Unidentified diatom taxa, with relative abundances ≥ 1%, are described in Appendix 5. A small number of *Achnanthes* species could not be identified to species level. These species remain grouped together and named as *Achnanthes* sp. Valve preservation was very good across the whole transect and all 13 surface samples analysed returned full counts of more then 300 valves.

The salt marsh at Storbæk is dominated by mesohalobous and oligohalobous taxa such as *Gomphonema parvulum, Navicula cincta* – type, *Navicula peregrina* and *Pinnularia ignobilis* Small abundances (< 5%) of the polyhalobous species *Cymatosira belgica* are found across the entire transect. Unconstrained cluster analysis divides the modern samples into three diatom assemblage zones (Figure 4.10a). The elevation range and dominant taxa in each zone are presented in Figure 4.10b. The diatom assemblages across the salt-marsh surface at Storbæk do not demonstrate a vertical zonation of diatom species with respect to elevation.

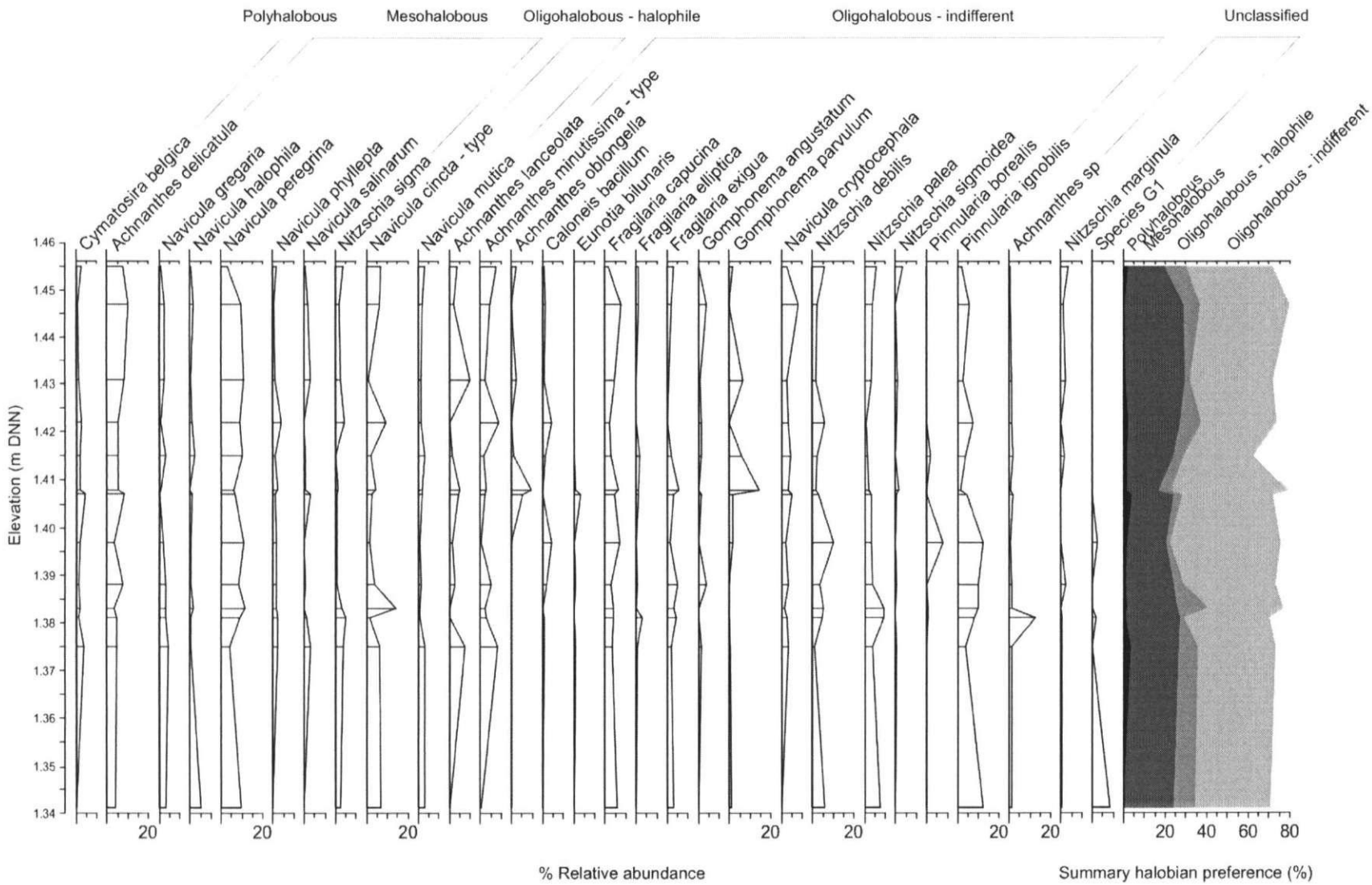

Figure 4.9. Modern diatom data from the salt-marsh surface at Storbæk. Only species with > 3% relative abundance are shown. Summary halobian prefernces only include species with at least 3% relative abundance.

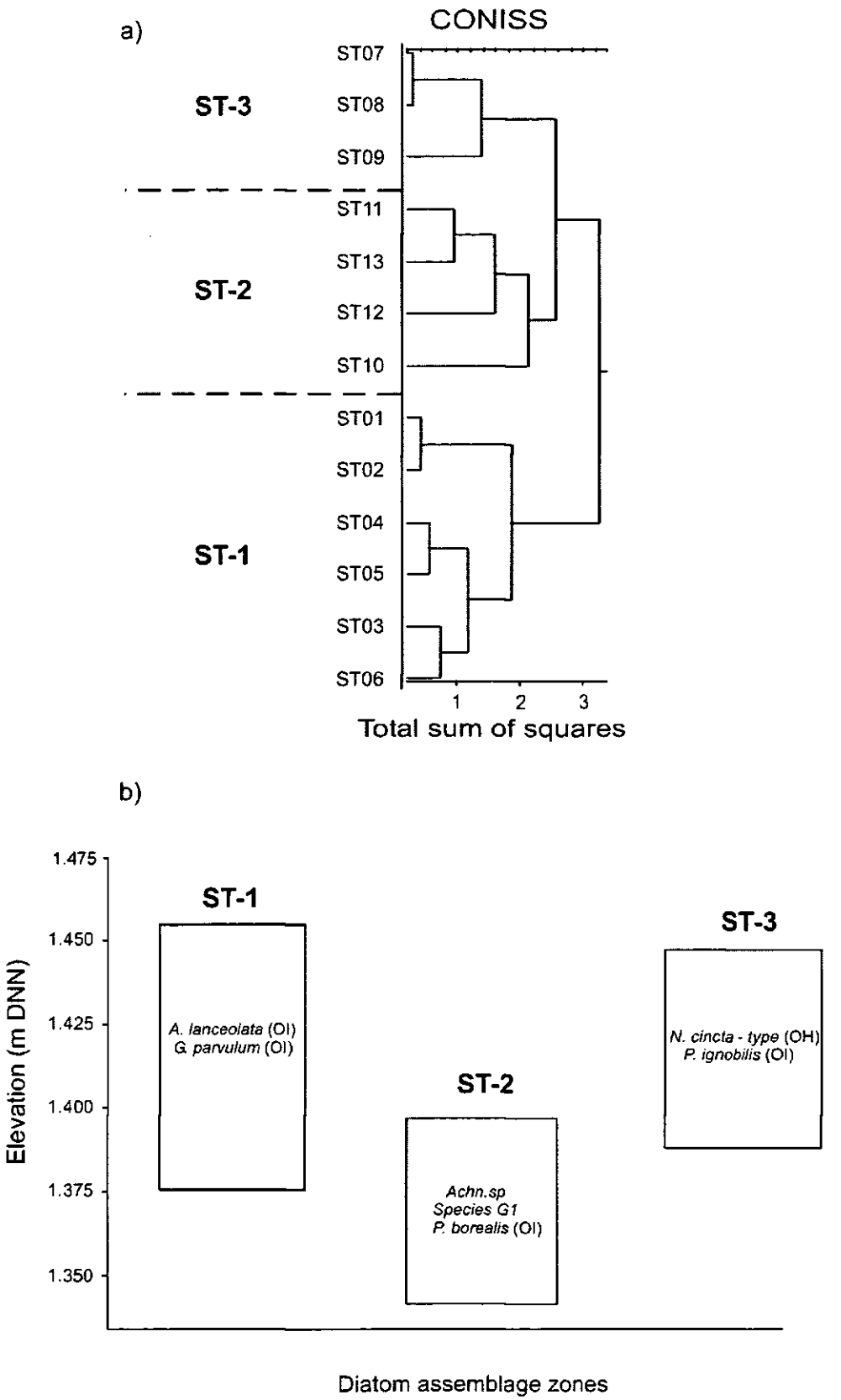

Figure 4.10. a) Results of unconstrained cluster analysis of the Storbæk diatom data. Cluster analysis excludes all taxa where relative abundances are < 1%. b) Elevation range and dominant taxa for diatom assemblage zones, identified from unconstrained cluster analysis. Halobian preferences of these taxa are indicated.

Oksby Enge

Modern diatom data from the salt marsh at Oksby Enge are presented in Figure 4.11. A total of 150 diatom taxa were identified across the salt marsh at Oksby Enge, of which 94 taxa were found with relative abundances ≥ 1%. Two species remain unidentified, Species A1, with a maximum relative abundance of 1.6% and Species G1, with a maximum relative abundance of 8.3%. Unidentified diatom taxa, with relative abundances ≥ 1%, are described in Appendix 5. Valve preservation was very good across the entire transect, although diatom concentrations were low and highly concentrate slides were needed to obtain full counts from some samples. All 22 surface samples analysed returned full counts of more than 300 diatom valves.

The salt marsh at Oksby Enge is dominated by the two oligohalobous groups. Taxa such as *Fragilaria capucina, Nitzschia dissipata, Nitzschia terrestris* and *Nitzschia palea* characterise this transect and are indicative of a fresh to brackish water environment. Increasing abundances of the oligohalobous – halophile taxa, *Navicula cincta* – type, *Navicula mutica* and *Nitzschia debilis* are found towards lower elevations, indicating that the environment is more brackish here. The abundance of polyhalobous and mesohalobous taxa remains low overall but increasing abundances of taxa within these two groups are found at lower elevations. Unconstrained cluster analysis divides the modern samples into four diatom assemblage zones (Figure 4.12a). The elevation range and dominant taxa in each zone are presented in Figure 4.12b. The diatom assemblages across the salt-marsh surface at Oksby Enge show a strong vertical zonation of species with respect to elevation.

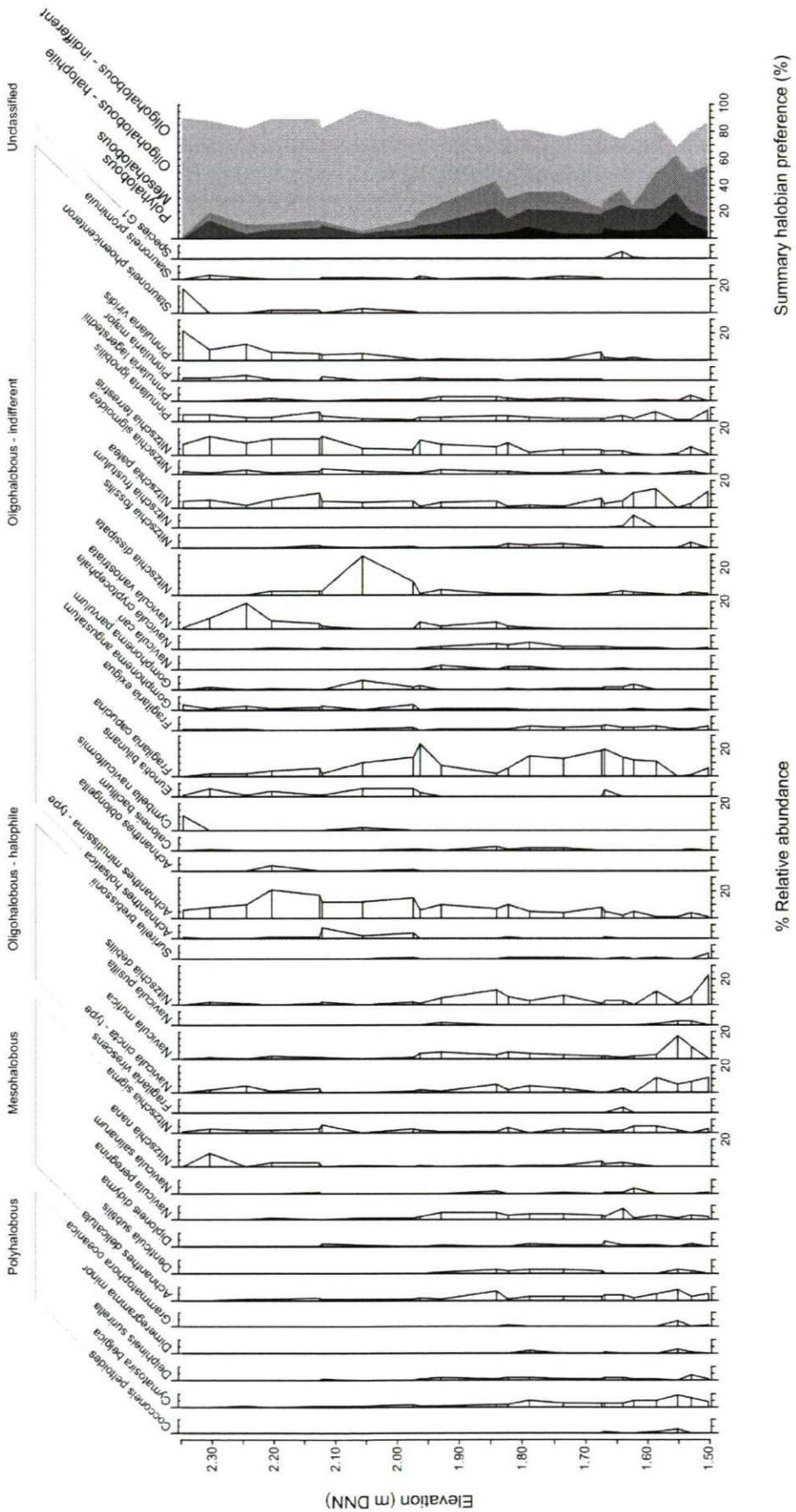

Figure 4.11. Modern diatom data from the salt-marsh surface at Oksby Enge. Only species with > 3% relative abundance are shown. Summary halobian preferences only include species with at least 3% relative abundance.

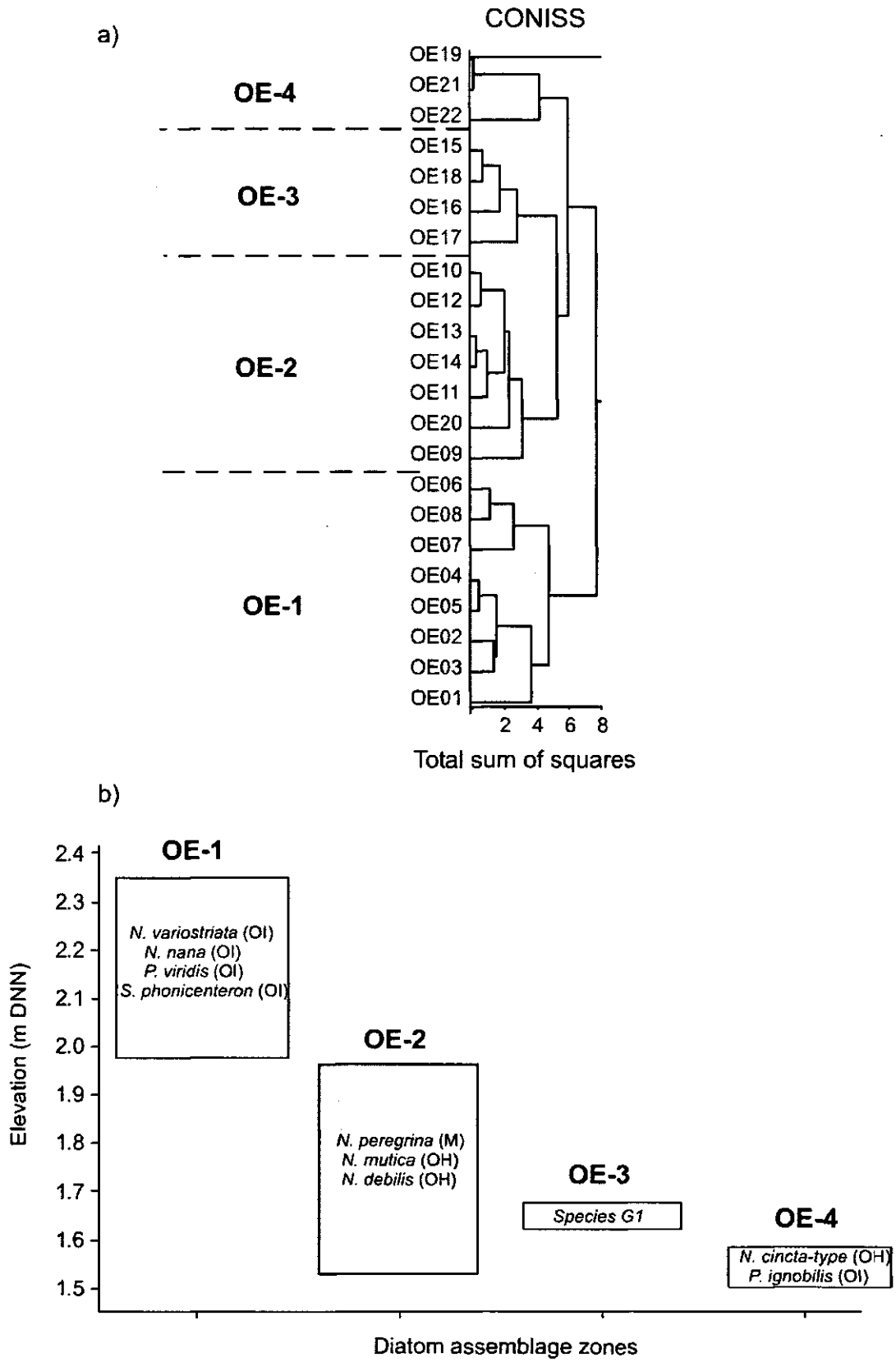

Figure 4.12. a) Results of unconstrained cluster analysis of the Oksby Enge diatom data. Cluster analysis excludes all taxa where relative abundances are < 1%. b) Elevation range and dominant taxa for diatom assemblage zones, identified from unconstrained cluster analysis. Halobian preferences of these taxa are indicated.

Langli North

Modern diatom data from the salt marsh at Langli North are displayed in Figure 4.13. A total of 146 diatom taxa were identified across the salt marsh at Langli North, of which 92 taxa were found with relative abundances ≥ 1%. Seven species remain unidentified: Species B1, C2, D2, E2, G2, I2 and J2, all with relative abundances of < 3%. Unidentified diatom taxa, with relative abundances ≥ 1%, are described in Appendix 5. Valve preservation was variable across the transect but poor overall. In the majority of samples, smaller taxa such *Achnanthes delicatula* were well preserved whilst larger taxa, such as *Diploneis didyma, Navicula digitoradiata and Nitzschia vitrea,* were broken or fragmented. Of the 31 samples analysed, 27 of them returned full counts. In samples which did return full counts, it was mainly broken valves that were counted (See Chapter 3, Section 3.7.4 for a description of the strategy adopted for counting broken valves). Samples LN1, LN7, LN8 and LN20, only returned partial counts due to the extremely poor valve preservation in these samples. These samples have therefore been excluded from the results and subsequent analysis.

The salt marsh at Langli North is dominated by polyhalobous and mesohalobous taxa such as *Cymatosira belgica, Delphineis surirella* and *Achnanthes delicatula*. The oligohalobous – halophile taxa, *Navicula cincta* – type, is also found in high abundances across the transect. Some oligohalobous – indifferent taxa such as *Achnanthes minutissima* – type and *Achnanthes oblongella*, are found at mid elevations in relatively high abundances. At lowest elevations, in samples from the tidal flat, *Achnanthes delicatula* clearly dominates the assemblage. Unconstrained cluster analysis divides the modern samples into three diatom assemblage zones (Figure 4.14a). The elevation range and dominant taxa in each zone are presented in Figure 4.14b. The diatom assemblages across the salt-marsh surface at Langli North demonstrate a strong vertical zonation of species with respect to elevation.

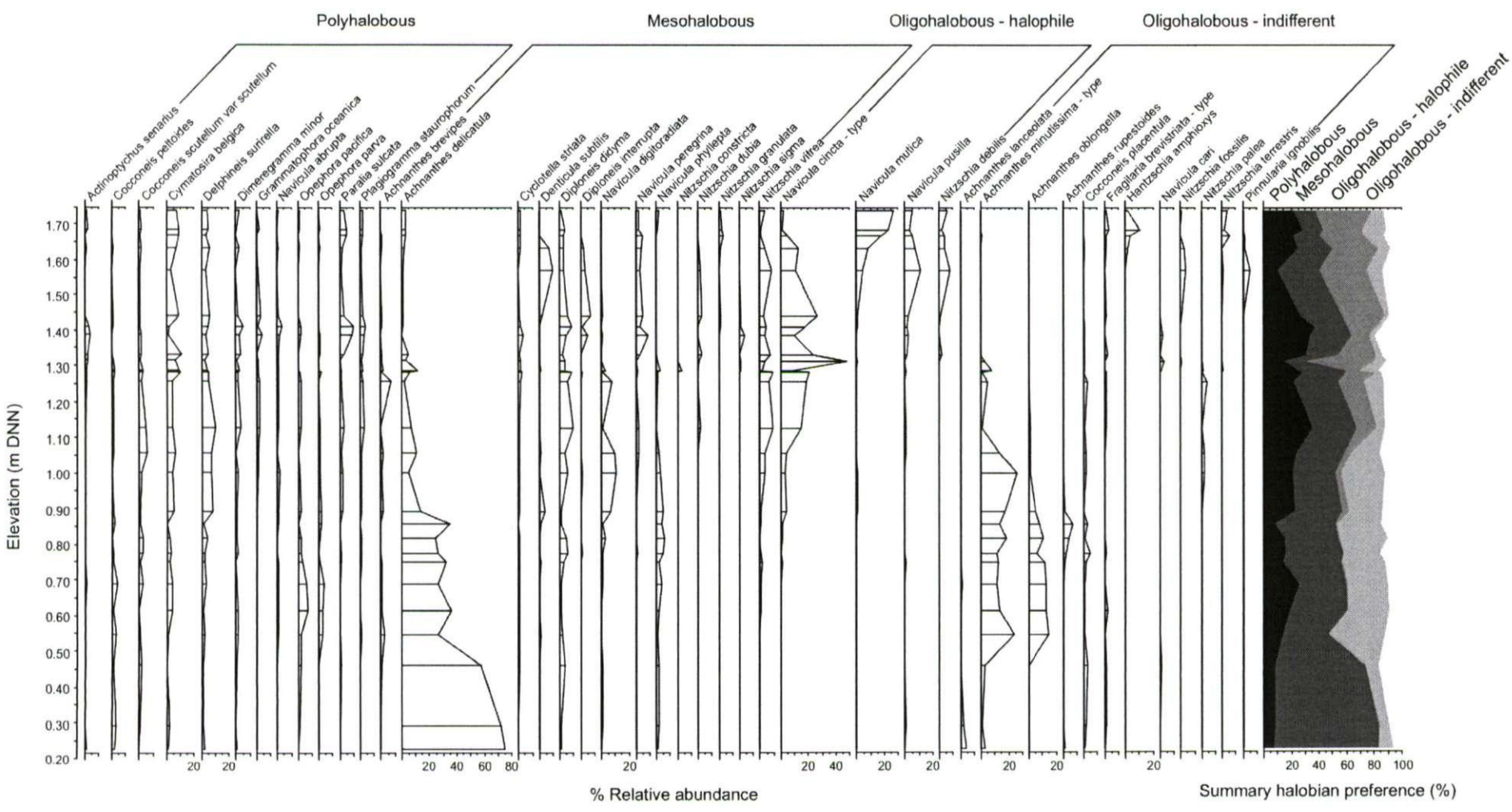

Figure 4.13. Modern diatom data from the salt-marsh surface at Langli North. Only species > 3% relative abundance are shown. Summary halobian prefences only include species with at least 3% relative abundance.

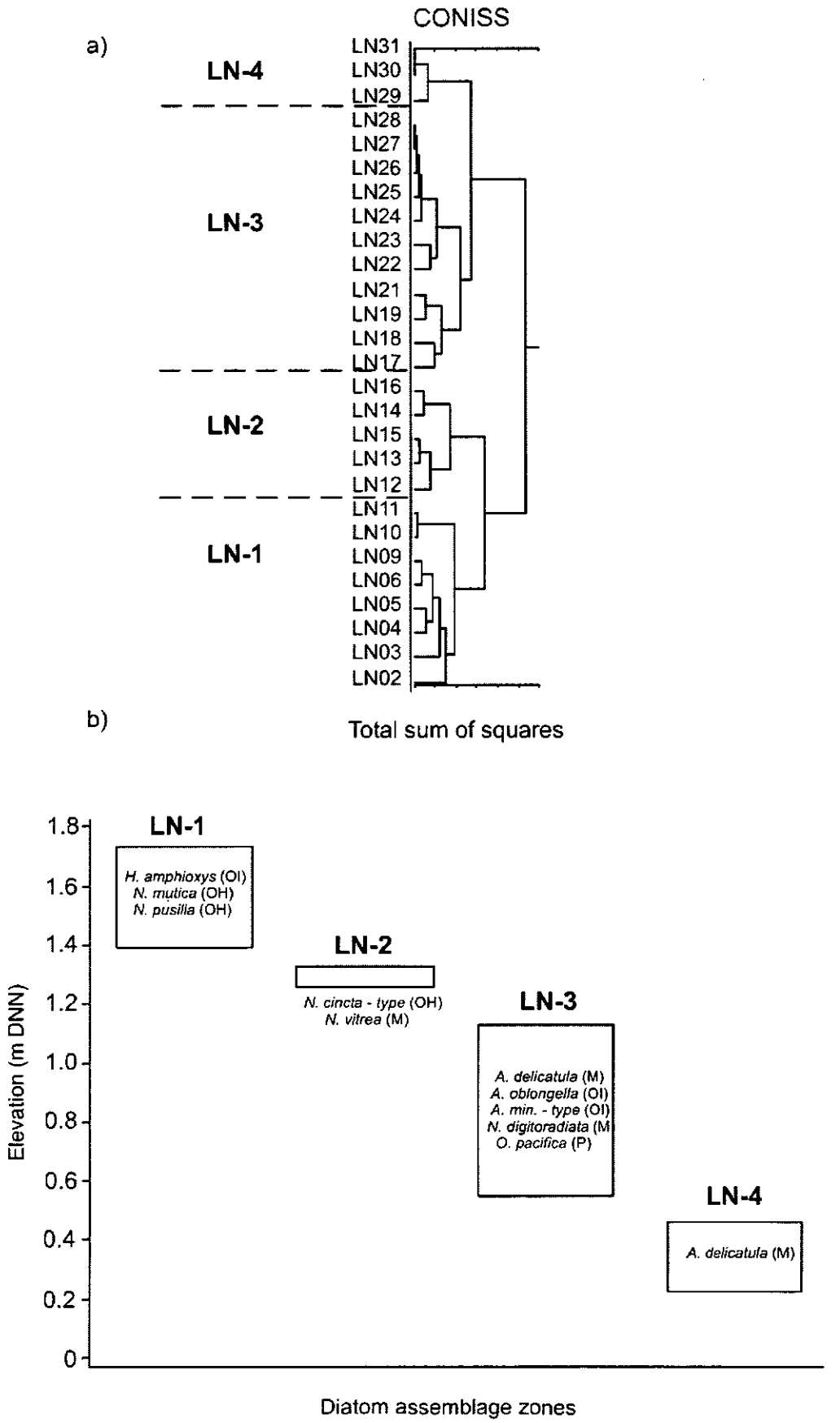

Figure 4.14. a) Results of unconstrained cluster analysis of the Langli North diatom data. Cluster analysis excludes all taxa where relative abundances are < 1%. b) Elevation range and dominant taxa for diatom assemblage zones, identified from unconstrained cluster analysis. Halobian preferences of these taxa are indicated.

Langli South

Modern diatom data from the salt marsh at Langli South are presented in Figure 4.15. A total of 117 diatom taxa were identified across the salt marsh at Langli North, of which 75 taxa were found with relative abundances ≥ 1%. Species B1 remains unidentified with 1.3% maximum relative abundance. Unidentified diatom taxa, with relative abundances ≥ 1%, are described in Appendix 5. Valve preservation was highly variable across the transect. At low elevations and in particularly sandy samples, valve preservation was very poor. Towards higher elevations, valve preservation was much better. Of the 33 samples analysed, 26 returned full counts of more than 300 valves. Samples, LS1, LS2, LS3, LS20, LS22, LS24 and LS26 returned only partial counts due to the extremely poor valve preservation in these samples. These samples have therefore been excluded from the results and subsequent analysis.

The salt marsh at Langli South is dominated by polyhalobous and mesohalobous taxa such as *Cymatosira belgica, Navicula digitoradiata* and *Nitzschia vitrea.* The oligohalobous – halophile taxon, *Navicula cincta* – type, is also dominant across this transect, as is the case in the majority of transects investigated. At lower elevations, in samples from the tidal flat, *Achnanthes delicatula* again dominates the assemblage. At higher elevations, several oligohalobous taxa are identified including *Navicula pusilla, Nitzschia debilis* and *Pinnularia ignobilis*. Unconstrained cluster analysis divides the modern samples into four diatom assemblage zones (Figure 4.16a). The elevation range and dominant taxa in each zone are presented in Figure 4.16b. The diatom assemblages across the salt-marsh surface at Langli South do not demonstrate a vertical zonation of species. Samples in Zone LS-1 (LS31, LS32, LS33) and Zone LS-2 (LS28, LS29, LS30), contain noticeably different diatom assemblages to the remaining samples. These samples in particular are highlighted for further investigation and possible removal from the final training set.

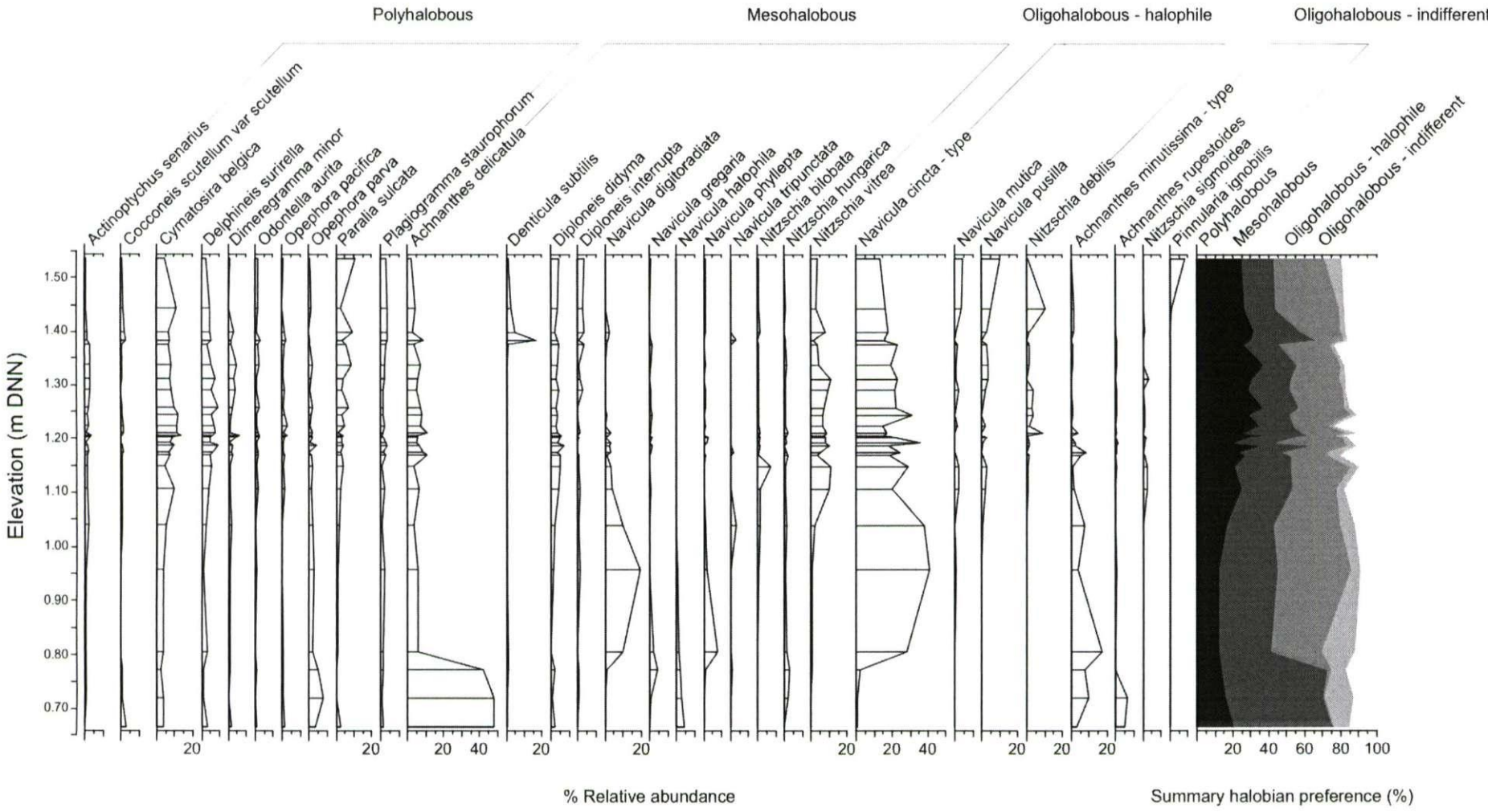

Figure 4.15. Modern diatom data from the salt-marsh surface at Langli South. Only species with > 3% relative abundance are shown. Summary halobian preferences only include species with at least 3% relative abundance.

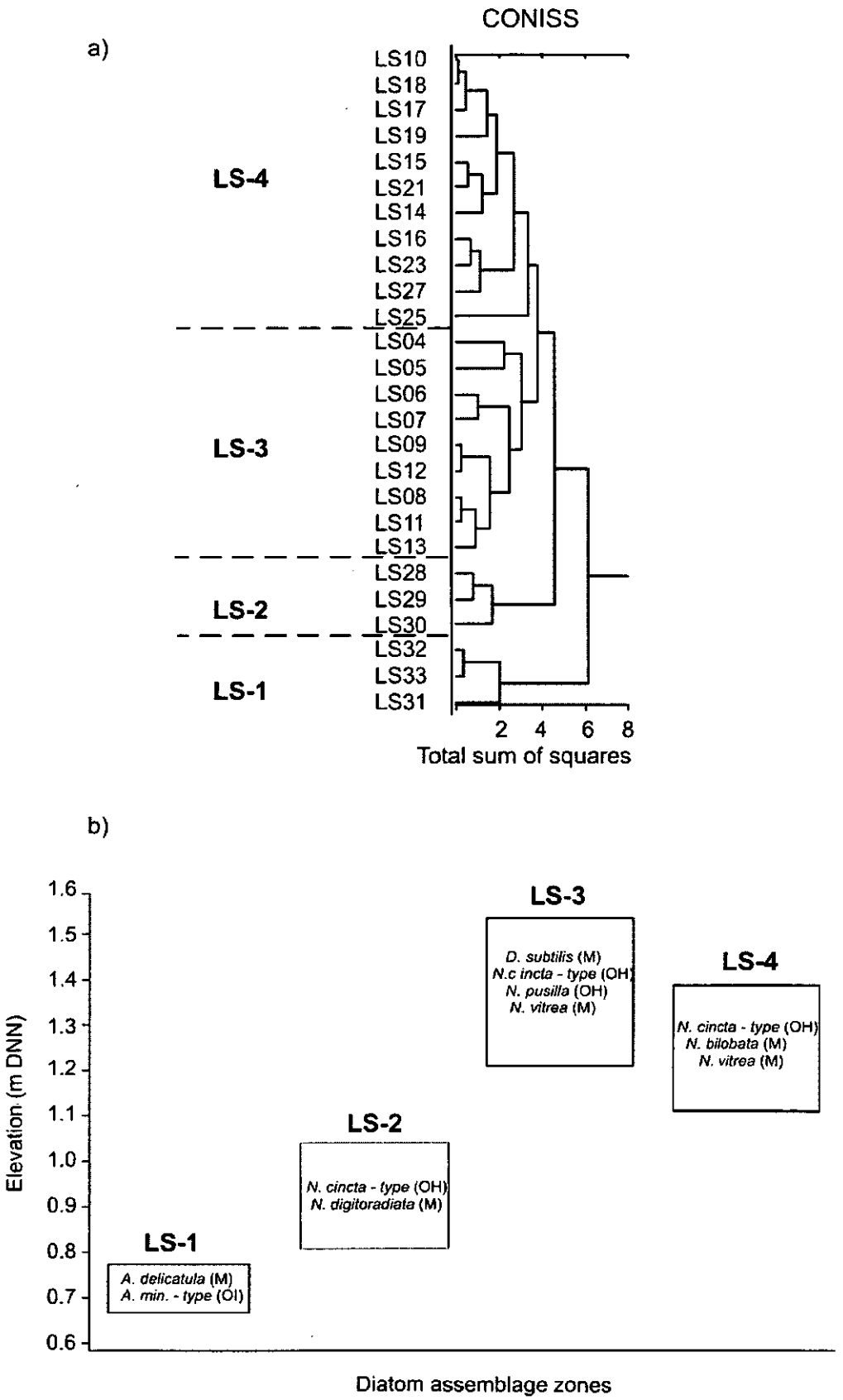

Figure 4.16. a) Results of unconstrained cluster analysis of the Langli South diatom data. Cluster analysis excludes all taxa where relative abundances are < 1%. b) Elevation range and dominant taxa for diatom assemblage zones, identified from unconstrained cluster analysis. Halobian preferences of these taxa are indicated.

4.4 Combined Modern Diatom Data

Diatom data from each of the six modern transects were subsequently combined to form one large, modern diatom data set using the TILIA package (Grimm, 2004). A total of 251 taxa resulted, 166 of which were found with relative abundances of ≥ 1%. Samples where minimum diatoms counts were not obtained (MO14, LN1, LN7, LN8, LN20, LS1, LS2, LS3, LS20, LS22, LS24 and LS26) are excluded from this data set, resulting in a total of 128 samples. The combined modern diatom data are presented in relation to elevation in Figure 4.17. Only species with relative abundances ≥ 5% are presented for ease of visual interpretation.

In general, at low elevations, polyhalobous and mesohalobous taxa such as *Achnanthes delicatula, Cymatosira belgica* and *Navicula digitoradiata* are dominant. At higher elevations, oligohalobous taxa such as *Nitzschia terrestris, Pinnularia borealis, Pinnularia viridis* and *Stauroneis phoenicenteron* are common. Between approximately 1.30 and 1.90 m elevation, the diatom signal is somewhat confusing. The abundance of polyhalobous, mesohalobous and oligohalobous taxa fluctuates greatly and no one group is dominant. The samples identified from anomalous diatom assemblage zones at Kjelst Enge in particular mostly fall within this elevation range.

Results from the six individual transect locations have shown that in some locations the diatom assemblages demonstrate a strong vertical zonation of species with respect to elevation. In other transects, in particular at Kjelst Enge, Moservå, Storbæk and Langli South, the diatoms do not. Unconstrained cluster analysis was repeated for the full combined data set to assess whether the diatom assemblages demonstrated a vertical zonation for the Ho Bugt embayment as a whole. The results are presented in Figure 4.18.

Unconstrained cluster analysis divides the modern samples in the combined data set into five diatom assemblage zones (Figure 4.18). The elevation range and dominant taxa in each zone are presented in Figure 4.19. The modern transect samples which fall within each of these zones are also indicated. The diatom assemblages across the salt-marsh surface in the Ho Bugt embayment as a whole show some evidence to support the concept of a vertical zonation of diatom species. Vertical zonation is demonstrated between Zones COM-1 and COM-2 and also between Zones COM-3, COM-4 and COM-5, but not for the data set as a whole. This is likely to be the result of including some samples from transects

such as Kjelst Enge, Moservå, Storbæk and Langli South which, even at the local scale, do not appear to be vertically zoned. These results suggest that a through exploration of the modern samples, species and environmental data is required before any training set is developed. This is achieved in later sections of this chapter (Section 4.5) via the use of several statistical analyses and ordination techniques.

Unconstrained cluster analysis on the whole data set shows that each transect appears to be associated with its own assemblage composition. In general, samples from the same transect appear to fall within the same cluster on the dendrogram. For example, all samples from Storbæk fall within Zone COM-1, all samples from Moservå fall within Zone COM-2 and all samples from Kjelst Enge fall within Zone COM-5. This is to be expected where samples from different transects cover different elevation ranges. However, in some cases samples from the same elevation range are shown to be associated with very different diatom assemblages (Table 3.1 and Figures 4.5 - 4.15). For example, the majority of samples from Langli North and Langli South fall within Zone COM-4 and are dominated by taxa such as *Navicula mutica, Navicula pusilla, Nitzschia debilis* and *Nitzschia vitrea* (Figure 4.18 and 4.19). The Kjelst Enge samples all fall within Zone COM-5 and cover a similar elevation range to the Langli samples, but are instead dominated by taxa such as *Diploneis didyma, Navicula cincta* and *Nitzschia sigma var. diminuata* (Figure 4.18 and 4.19). These observations have interesting implications with regards to the spatial variability of diatom assemblages within salt marshes, and the subsequent development and application of transfer functions. It is possible that samples from only one of these clusters (Zone COM-4 or Zone COM-5) can be used in the training set, depending on which one is the most representative. These points are explored further in Section 7.2 and are discussed in Section 9.11.

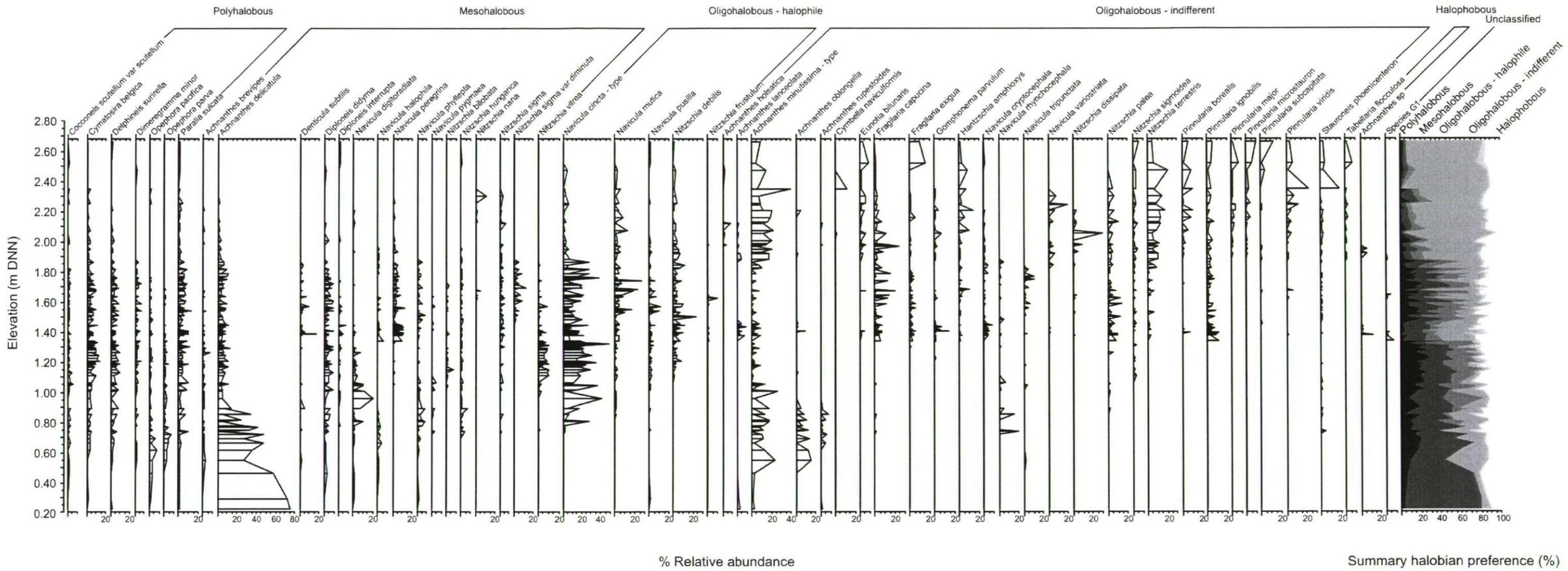

Figure 4.17. Combined modern diatom data from the six transects investigated. Only species with > 5% relative abundance are shown. Summary halobian preferences only included species with at least 5% relative abundance.

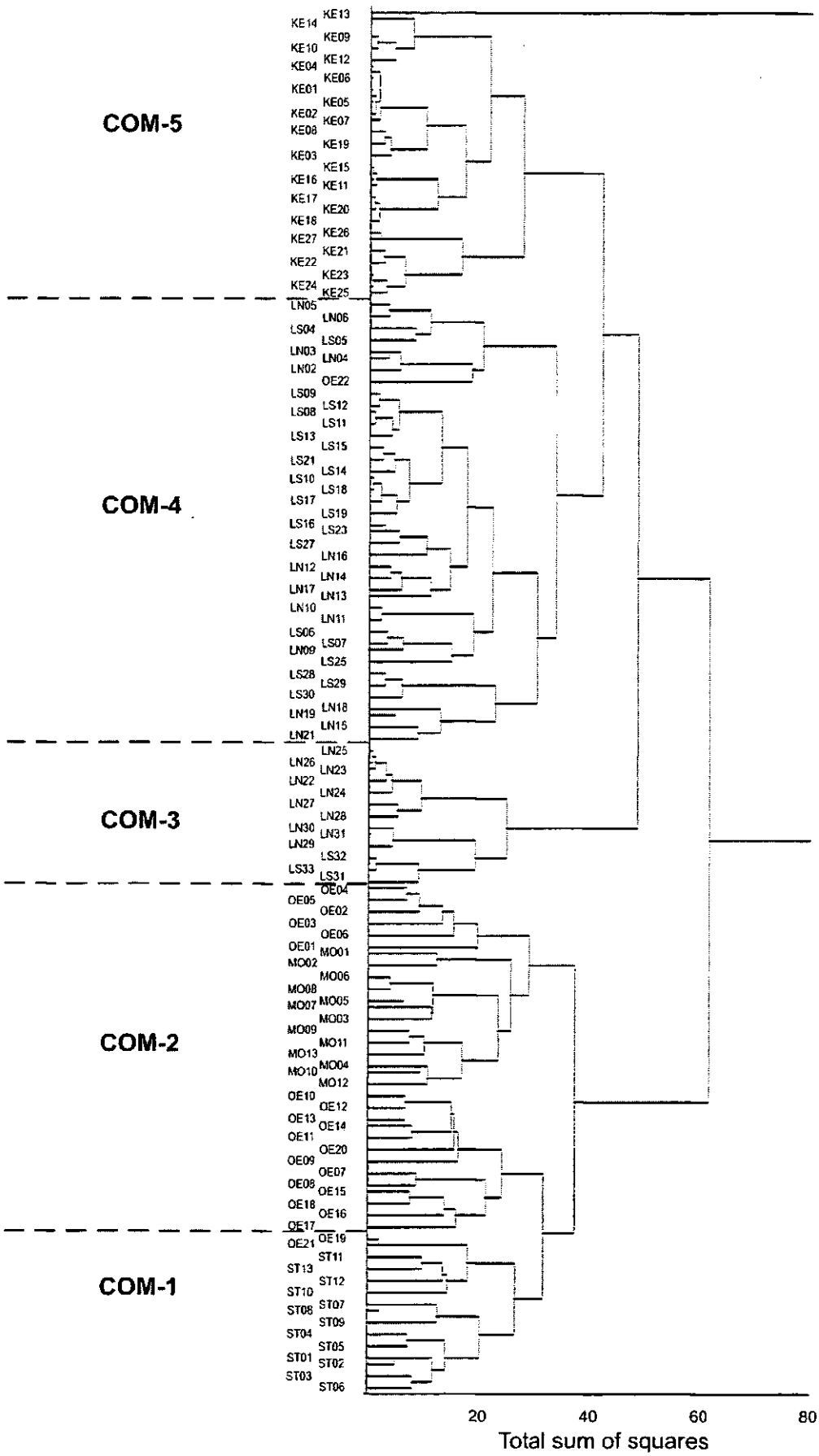

Figure 4.18. Results of unconstrained cluster analysis for the combined modern diatom data. Cluster analysis excludes all taxa where relative abundances are < 1%. Samples which fall within each subsequent diatom assemblage zone are indicated.

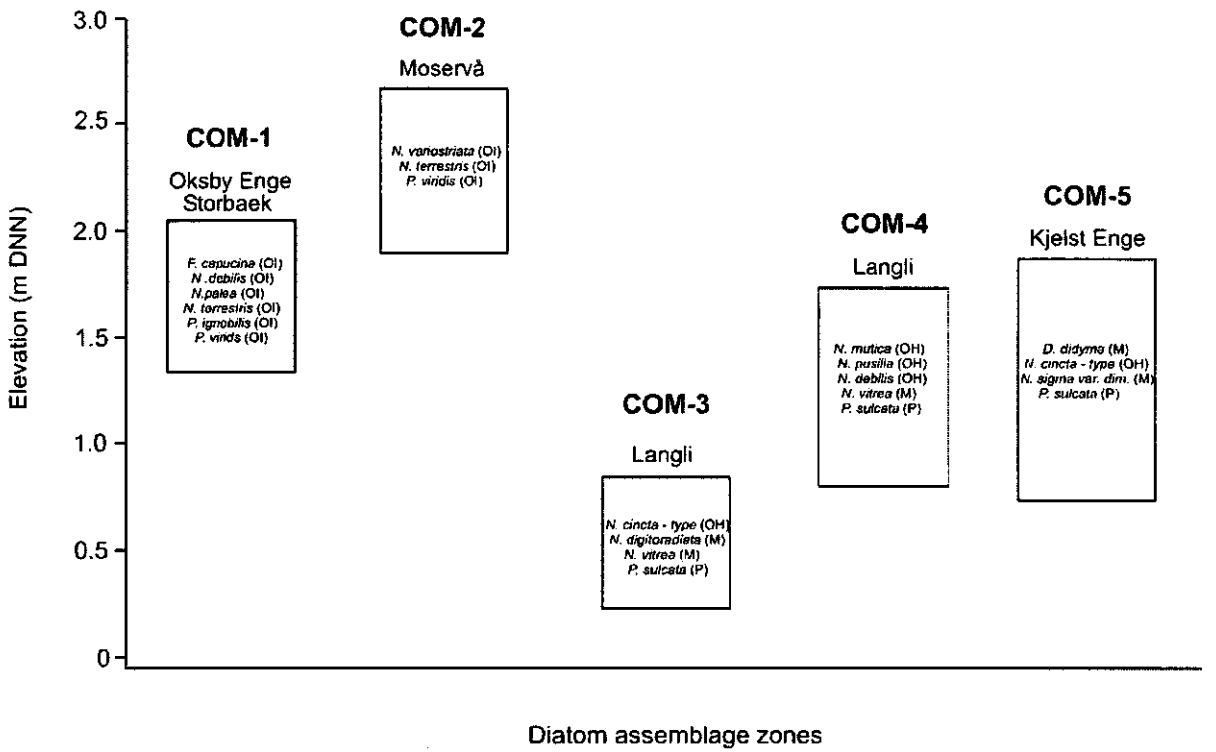

Figure 4.19. Elevation range and dominant taxa for diatom assemblage zones identified from unconstrained cluster analysis for the combined modern diatom data. The modern transect samples that fall into each zone are indicated.

4.5 Statistical Analysis

Initial results obtained from cluster analysis of the modern diatom data have highlighted a number of anomalous samples and suggest that a through exploration of the modern species and environmental data is required before any transfer function can be developed. This section presents the results of both indirect (PCA and DCA) and direct (CCA) gradient analysis, used to explore variation in the species and environmental data.

4.5.1 Inclusion of samples, species and environmental variables

Details of the samples, species and environmental variables included in ordinations are fully detailed in Section 3.8, and summarised in Table 4.2. Two data sets are analysed in the ordinations: DataSetA excludes the Kjelst Enge samples and contains six environmental variables measured from five transects (elevation, pH, salinity, LOI, $CaCO_3$, sand, silt, clay). DataSetB, contains samples from all six transects (127 samples) but only three environmental variables (elevation, pH and salinity). Descriptive statistics for each environmental used in ordinations is presented in Table 4.3. Information for individual transects is presented in Appendix 6.

Data Set	Species cut-off employed	Species before cut-off	Species after cut-off	Samples Included	Transects Included	Environmental Variables
DataSetA	≥ 1% relative abundance & present in > 1 sample	251	152	100	MO, ST, OE, LN and LS	Elevation, pH, salinity, LOI, $CaCO_3$, Sand, Silt, Clay
DataSetB	≥ 1% relative abundance & present in > 1 sample	251	161	127	KE, MO, ST, OE, LN and LS	Elevation, pH, salinity

Table 4.2. Summary details of the species, samples and environmental variables included in the two data sets analysed in ordinations. Full details are given in Section 3.8.

Environmental Variable	Minimum	Maximum	Mean	Median	Standard Deviation
Elevation (m DNN)	0.225	2.666	1.468	1.442	0.473
pH	4.09	8.75	6.652	6.690	1.008
Salinity (g/l^{-1})	0.02	3.360	1.367	1.30	0.837
LOI (%)	1.16	65.46	30.80	30.08	18.82
$CaCO_3$ (%)	0.300	8.41	2.627	2.653	1.228
Sand (%)	4.23	94.15	30.15	22.41	20.83
Silt (%)	5.85	91.02	62.65	69.33	19.51
Clay (%)	< 0.001	12.17	7.204	7.325	2.755

Table 4.3. Descriptive statistics for each environmental variable used in ordinations. Statistics were calculated using MINITAB® Release 14. Information for individual transects is presented in Appendix 6.

4.5.2 Correlations between environmental variables

Results of normality tests on all eight environmental variables are presented in Table 4.4. In this test, the *null* hypothesis (H_0) states that the data follow a normal distribution. Where *p*-values were less than a rejection level of 0.05 (95% confidence), the null hypothesis was rejected and the data were assumed *not* to be normally distributed. Results for elevation, pH and salinity include the Kjelst Enge samples (127 samples); results for all other environmental variables are based on 100 samples (Table 4.2).

Elevation and clay fraction are the only two variables which show a normal distribution prior to transformation. One variable $CaCO_3$, showed a skewed distribution and all other variables displayed bimodal distributions. $CaCO_3$ achieves a normal distribution after a square-root transformation. For the other five environmental variables, transformations do little to alter the bimodal distributions. All environmental data included in ordinations are therefore untransformed. Correlations between pairs of environmental variables were calculated using a Spearman's Rank correlation coefficient, since this test does not require data to be normally distributed. Results are presented in Table 4.5. To aid visual interpretation of relationships, the results are also presented as a scatter plot matrix (Figure 4.20).

Variable	Before transformation (p value)	Normally distributed?	After Log_{10} transformation (p value)	Normally distributed?	After Sqrt transformation (p value)	Normally Distributed?
Elevation	**0.587**	**Yes**	N/A	N/A	N/A	N/A
pH	0.008	No	0.001	No	0.005	No
Salinity	0.040	No	0.000	No	0.000	No
LOI	0.007	No	0.000	No	0.002	No
CaCO3	0.012	No	0.000	No	**0.074**	**Yes**
Sand	0.000	No	0.008	No	0.001	No
Silt	0.000	No	0.000	No	0.000	No
Clay	**0.092**	**Yes**	N/A	N/A	N/A	N/A

Table 4.4. Results of Andersen-Darling normality tests applied to all eight environmental variables. Results for elevation, pH and salinity include the Kjelst Enge samples (127 samples), results for all other environmental variables are based on 100 samples. Attempts to achieve normality through various data transformations and resulting p-values are shown. Normal distributions are highlighted in bold.

	Elevation	**pH**	**Salinity**	**LOI**	**$CaCO_3$**	**Sand**	**Silt**
pH	-0.707 **< 0.001**						Correlation (r_s) *P-value*
Salinity	-0.712 **< 0.001**	0.462 **< 0.001**					
LOI	0.858 **< 0.001**	-0.633 **< 0.001**	-0.617 **< 0.001**				
$CaCO_3$	0.109 0.282	-0.123 0.224	0.134 0.183	0.296 **0.003**			
Sand	-0.631 **< 0.001**	0.634 **< 0.001**	0.316 **0.001**	-0.708 **< 0.001**	-0.473 **< 0.001**		
Silt	0.699 **< 0.001**	-0.674 **< 0.001**	-0.396 **< 0.001**	0.777 **< 0.001**	0.447 **< 0.001**	-0.983 **< 0.001**	
Clay	0.025 0.805	-0.058 0.564	0.143 0.157	0.111 0.272	0.326 **0.001**	-0.507 **< 0.001**	0.373 **< 0.001**

Table 4.5. Spearman's Rank Correlation matrix between all environmental variables. Results for elevation, pH and salinity include the Kjelst Enge samples (127 samples). Results for all other environmental variables are based on 100 samples. Correlation (r_s) and P-values are shown for each pair of environmental variables. Significant ($p < 0.05$) correlations are highlighted in bold.

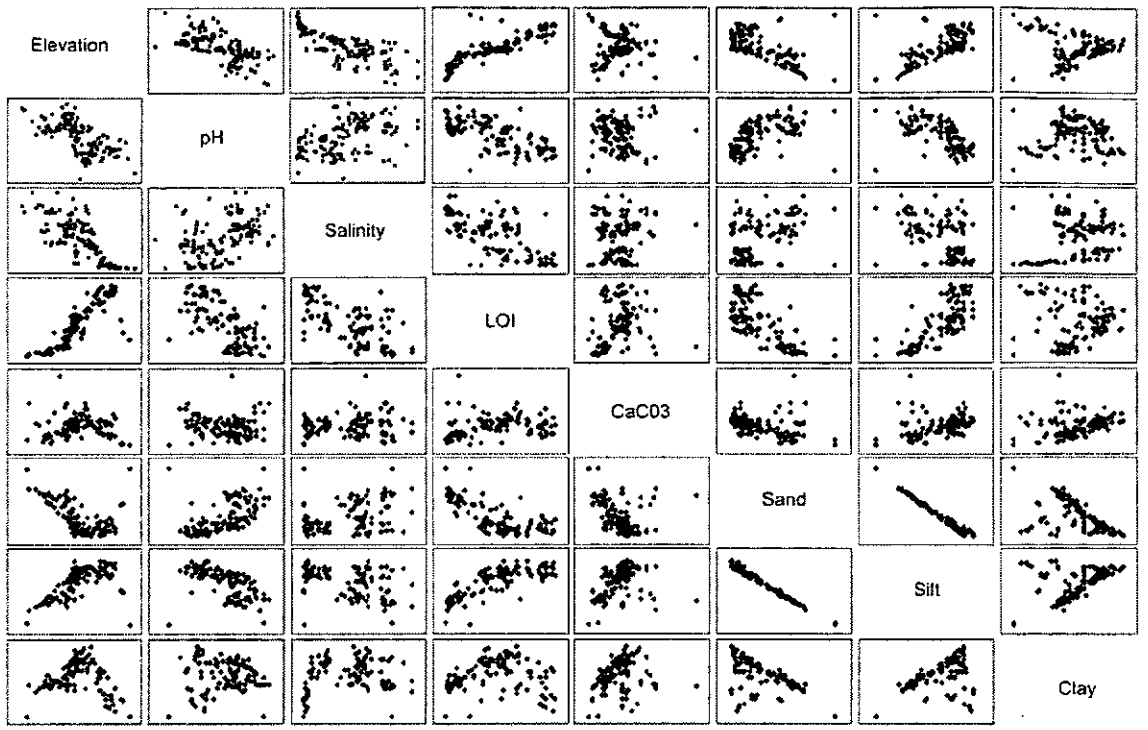

Figure 4.20. Scatter plot matrix between pairs of environmental variables. Results for elevation, pH and salinity include the Kjelst Enge samples (127 samples), results for all other environmental variables are based on 100 samples.

Calculation of the Spearman's Rank correlation coefficient between pairs of environmental variables shows a number of variables to be significantly ($P < 0.05$) or highly significantly ($P < 0.01$) correlated with one another. For the main data set, elevation in particular shows relatively strong ($r_s > 0.7$) and highly significant negative correlations with pH (r_s -0.707) and salinity (r_s -0.712), and strong and highly significant positive relationships with LOI (r_s 0.858) and silt fraction (r_s 0.699). This is not surprising since a number of these variables are influenced, either directly or indirectly, by the duration of tidal flooding, which itself is a function of elevation. A number of other variables are highly significantly correlated with one another, but in the majority of cases the relationships are weaker ($r_s < 7$). LOI shows a strong and highly significant negative relationship with sand (r_s -0.708) and a strong and highly significant positive relationship silt fraction (r_s 0.777). These results suggest that there is a relatively high degree of intercorrelation between the environmental variables measured. In ordinations, variables which are highly correlated essentially describe similar axis of variation in the data. No environmental variables are removed from the data set at this stage, but this exercise has highlighted variables which show strong inter-correlations, and will facilitate removal of such variables in subsequent ordinations and in the interpretation of results. These points are further explored in the following sections of this chapter.

4.5.3 Ordinations

Ordination techniques were used in this study to provide an objective way in which to examine species and environmental data. Preliminary ordinations were performed to highlight samples with extreme environmental characteristics and/or unusual species assemblages (through PCA and DCA, respectively), to identify redundancies in environmental information (through CCA), and to eliminate variables which did not exert an independent influence on diatom distributions (CCA). The following section presents the results of PCA, DCA and CCA ordinations, firstly for DataSetA and secondly for DataSetB.

Principal Components Analysis (PCA) - DataSetA

PCA was used in this study to summarise environmental information and to highlight samples with extreme environmental characteristics. PCA was initially performed on the entire data set (100 samples, 8 environmental variables). Results are presented in Table 4.6 and displayed graphically in Figure 4.21.

Axis	1	2	3	4
Eigenvalue	0.534	0.226	0.101	0.065
Cumulative percentage variance	53.4	76.0 (22.6)	86.0 (10)	92.5 (6.5)

Table 4.6. Results of an initial PCA for DataSetA (100 samples, 8 environmental variables). Numbers in parentheses are individual axes contributions.

The results of an initial PCA show that the percentage variance explained by the first four axes is 92.5%. Axis one reflects the dominant environmental gradient, explaining 53.4% of variance, although the contribution of axes two (22.6%) and three (10%) is also reasonably large. The PCA bi-plot of axis 1 and axis 2 (Figure 4.21a) illustrates that the first axis is positively correlated with sand, pH and to a lesser extent, salinity, and negatively correlated with elevation, LOI and silt. Axis one therefore contrasts high sand, pH and salinity in samples to the right of the diagram, and high elevation, LOI and silt in samples to the left of the diagram. None of the environmental variables appear to be particularly strongly correlated with this axis one. This is most possibly due to the presence of outlier samples within the data set, which are clearly visible on the PCA bi-plot. Axis two is negatively correlated with $CaCO_3$ and clay. Axis three (Figure 4.21b) is negatively correlated with clay and positively correlated with $CaCO_3$. Correlations between a number of the environmental variables is highlighted by the small angles between their

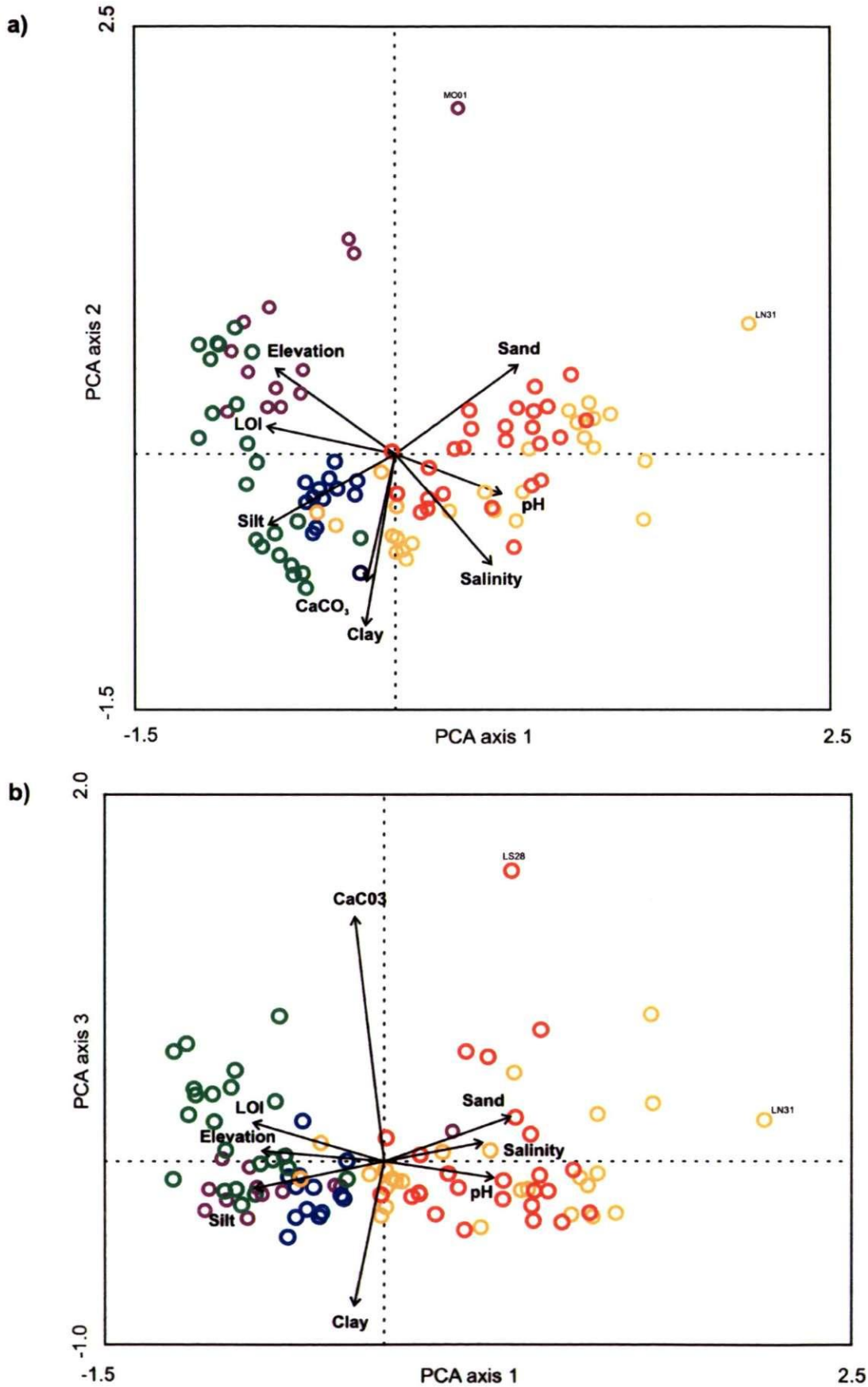

Figure 4.21. Ordiantion bi-plots showing results of PCA on DataSetA illustrating axes a) 1 and 2 and b) 1 and 3 for 100 samples and 8 environmental variables. Samples are colour coded by transect. Moservå = purple, Storbæk = blue, Oksby Enge = green, Langli North = yellow and Langli South = red. Sample labels are not shown for clarity.

environmental vectors and confirmed by the results of Spearman's correlation coefficients (Table 4.5). For example, elevation is positively correlated with LOI and negatively correlated with pH and salinity.

Removal of outlier samples

On examining the PCA bi-plots (Figure 4.21), the following samples are identified as outliers: LN31 (axis 1), MO1 (axis 2) and LS28 (axis 3). These samples are confirmed as outliers by their extremely high axis scores on the respective axes and also upon examination of the environmental data. Samples LN31 and MO1 have high sand fractions (93 and 94% respectively) and correspondingly low clay fractions (0 %). Sample MO1 also has a low $CaCO_3$ value (0.30%). Sample LS28 has a high $CaCO_3$ value (8.4%), almost twice that of any other sample. Whilst these measured values are deemed to be correct, their values are well outside the range of all other samples in the data set. For these reasons they are considered to be outlier samples and are therefore removed from the data set. To some extent, samples MO2 and MO3 also appear to be outliers. However, examination of their axes scores and of the environmental data suggests that the measured environmental values for these samples are within the range of other samples. These two samples are therefore retained in the data set. Following removal of samples LN31, MO1 and LS28, one species, *Eunotia exigua*, was also excluded from the corresponding diatom data set as it no longer met the aforementioned abundance criteria (Table 4.2).

Removal of samples LN31, MO1 and LS28 therefore reduces the data set to 97 samples, 8 environmental variables and 151 taxa. Results of a PCA run using this reduced data set are presented in Table 4.7 and Figure 4.22. The percentage of variance explain by the first four axes is now 0.9% higher than for the full data set. The contribution of each individual axis is also shown to increase. Axis one, reflecting the dominant environmental gradient, now accounts for 55.8% of variation in the data. 2.4% more than when the PCA was run on the full data set. Examination of the PCA bi-plot (Figure 4.22) shows that the removal of the three outliers does not significantly alter the position of remaining sites on the ordination diagram. The orientation, length and relative positions of the bi-plot arrows also remains fairly consistent, with the exception of pH which now has the strongest correlation with axis one. This suggests that the removal of the three outlying samples does not significantly alter the overall interpretations but results in a small increase in the percentage of variance explained.

Axis	1	2	3	4
Eigenvalue	0.558	0.213	0.098	0.066
Cumulative percentage variance	55.8	77.1 (21.3)	86.9 (9.8)	93.4 (96.5)

Table 4.7. Results of PCA for DataSetA on a reduced data set (97 samples, 8 environmental variables). Samples LN31, MO1 and LS28 are removed. Numbers in parentheses are individual axes contributions.

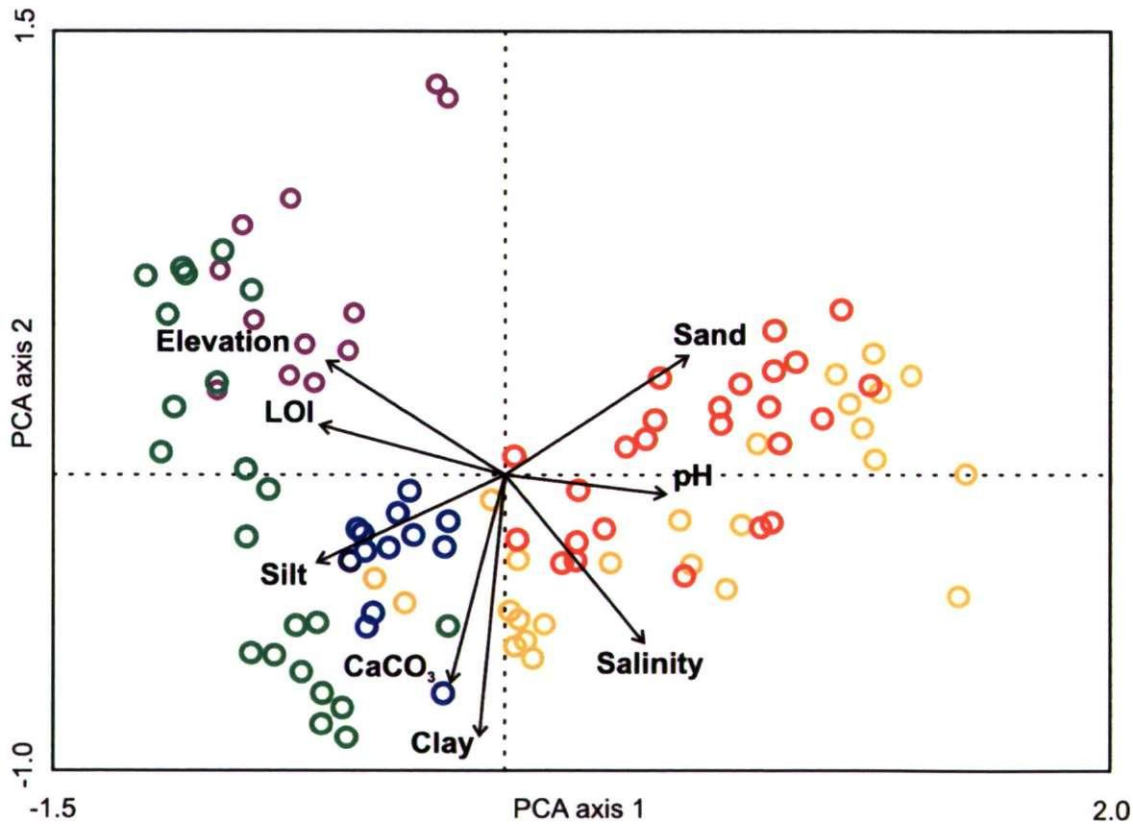

Figure 4.22. Ordination bi-plot showing the results of PCA on reduced data set (97 samples). The orientation, length and relative positions of the bi-plot arrows remains fairly consistent but a higher percentage of variance is now explained with the removal of the three outliers. Samples are colour coded by transect. Moservå = purple, Storbæk = blue, Oksby Enge = green, Langli North = yellow and Langli South = red. Sample labels are not shown for clarity.

Detrended Correspondence Analysis (DCA) – DataSetA

DCA was used in this study to reveal major patterns in the diatom species data, to highlight samples with unusual diatom assemblages and to determine whether linear or unimodal methods were suitable for further exploration of the modern training set. DCA was initially performed on the full data set (97 samples and 151 taxa). Results are presented in Table 4.8 and Figure 4.23.

Axis	1	2	3	4
Eigenvalue	0.489	0.306	0.171	0.084
Lengths of gradient (SD units)	3.342	2.612	2.174	2.034
Cumulative percentage variance of species data	16.4	26.6 (10.2)	32.3 (5.7)	35.1 (2.8)

Table 4.8. Results of DCA for DataSetA (97 samples, 151 taxa). Numbers in parentheses are individual axes contributions.

The gradient length of the longest axis, axis one, is reasonably long (3.34 SD units) indicating that most species in the data set can be approximated by a unimodal response model. This confirms the choice of DCA for the examination of species data and indicates that unimodal ordination methods (CCA) are suitable for the subsequent analysis of species-environment relations (Lepš and Šmilauer, 2003). The first two axes account for 26.6% of the variance in the diatom species data. This relatively low value is in common with several other studies and is considered 'typical' of noisy data sets with a large numbers of zero values (e.g., Stevensen et al., 1991; Bennion 1994; Burgess, 2004).

Examination of the ordination bi-plots (Figures 4.23) reveals a general trend in the diatom data. The samples from Moservå and Oksby Enge, found towards the left of the diagram, are predominantly associated with oligohalobous diatom taxa and fresh water conditions. Taxa such as *Eunotia arcus, Nitzschia terrestris, Pinnularia gibba, Pinnularia viridis* and *Stauroneis phoenicenteron* are associated with these samples. These findings are consistent with the fact that the samples from Moservå and Oksby Enge are mainly from the fresh water and high salt marshes. Towards the right of the diagram, samples from Langli North and Langli South are associated with polyhalobous and mesohalobous diatom taxa, characteristic of brackish and marine conditions. Taxa such as *Diploneis didyma, Diploneis interrupta, Nitzschia navicularis* and *Nitzschia vitrea* are associated with these samples. These samples are mainly from the middle and low salt marshes and their association with

these taxa is expected. These general trends suggest that axis one is most probably associated with elevation and/or salinity.

One cluster of samples, towards the bottom right of the diagram is distinct from the remaining samples in terms of their diatom assemblages (e.g., samples LN23, LN24, LS31, LS32, and LS33). These samples are associated with diatom species such as *Achnanthes delicatula, Achnanthes oblongella, Cocconeis placentula, Navicula phyllepta, Opephora parva* and *Opephora pacifica*. The position of these samples on the ordination diagram is determined by the high abundance of such species at these sites. For example, *A. delicatula* is found with an abundance of > 50% in most of the samples in this cluster. This cluster of samples is from the tidal flat.

Removal of outlier samples

No visible outliers with unusual diatom assemblages are detected from the DCA. The cluster of samples in the bottom right of the ordination diagram are not considered to be outliers despite their distinct diatom assemblages. The samples here are the only samples analysed from the tidal flat and their association with a slightly different diatom assemblage is expected. Removal of these samples, at this stage of the analysis, would result in a significant loss of information.

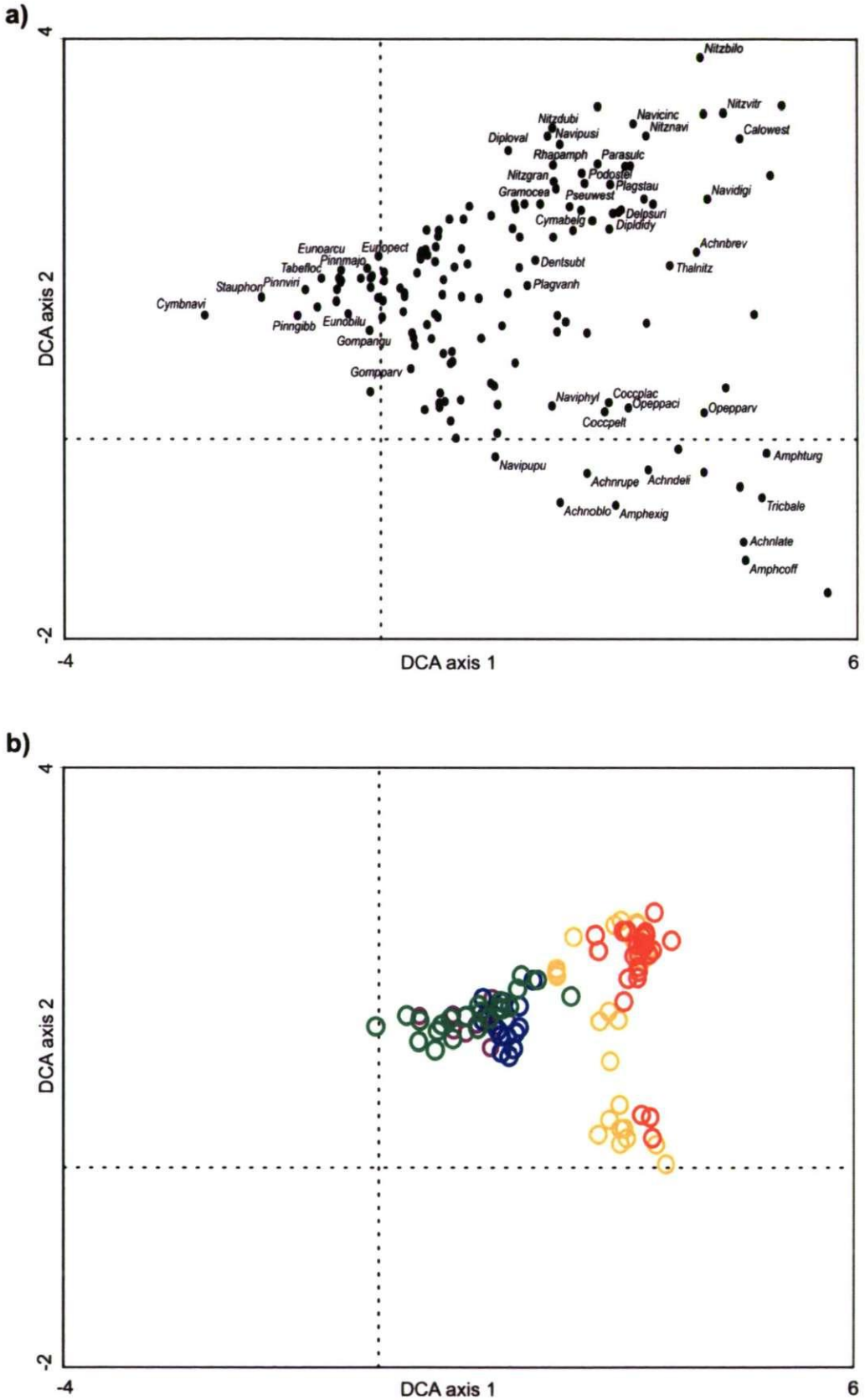

Figures 4.23. Ordination bi-plots showing the results of DCA on DataSet A (97 samples and 151 taxa), showing a) species and b) samples. Species mentioned in text and those best illustrating the general trend are labelled (see text). See Appendix 7 for a conversion of species codes to full names. Samples are colour coded by transect. Moservå = purple, Storbæk = blue, Oksby Enge = green, Langli North = yellow and Langli South = red. Sample labels are not shown for clarity.

Canonical Correspondence Analysis (CCA) – DataSetA

A DCA axis 1 gradient length of 3.34 SD units (Table 4.8) has indicated that most species in this data set can be approximated by a unimodal response model (Lepš and Šmilauer, 2003). A unimodal ordination method (CCA) was therefore subsequently used to explore species-environment relations in the data set. Prior to the implementation of CCA, PCA highlighted three samples (MO1, LN21 and LS28) with extreme environmental characteristics. These samples are excluded from all CCA ordinations. Following removal of these samples, one species, *Eunotia exigua*, was also excluded from the corresponding diatom data set as it no longer met the aforementioned abundance criteria (Table 4.2). Results of DCA indicated that there were no outlying samples with atypical diatom assemblages. The data set analysed by an initial CCA therefore consisted of 97 samples and 151 taxa. Results are presented in Table 4.9 and Figure 4.24

Axis	1	2	3	4	Total inertia
Eigenvalue	0.457	0.221	0.165	0.060	
Species-environment correlations	0.971	0.836	0.838	0.708	
Cumulative percentage variance:					
of species data	15.3	22.7 (7.4)	28.2 (5.5)	30.2 (2)	
of species-environment relation	45.3	67.3 (22)	83.3 (16)	89.6 (6.3)	
Sum of all eigenvalues					2.986
Sum of all canonical eigenvalues					1.007

Table 4.9. Results of an initial CCA for DataSetA (97 samples, 151 taxa, 8 environmental variables). Numbers in parentheses are individual axes contributions.

CCA axis 1 and axis 2 together explain 22.7% of the variance in the diatom species data. This percentage is very close to that obtained by the DCA in an unconstrained analysis (21.9 compared to 22.7%), and suggests that the environmental variables measured are those responsible for explaining the variation in the species data (Lepš and Šmilauer, 2003). The species-environment correlations are very high for axis 1 (0.971) and are also reasonably high for axes 2, 3 and 4. Together the 8 environmental variables explain 33.7% of the variance in the diatom data. Associated Monte Carlo permutation tests demonstrate that the first axis and all canonical axes are significant (p = 0.008 and 0.008 respectively, with 499 permutations under a reduced model, restricted for spatial structure (Birks, *pers. comm.*)).

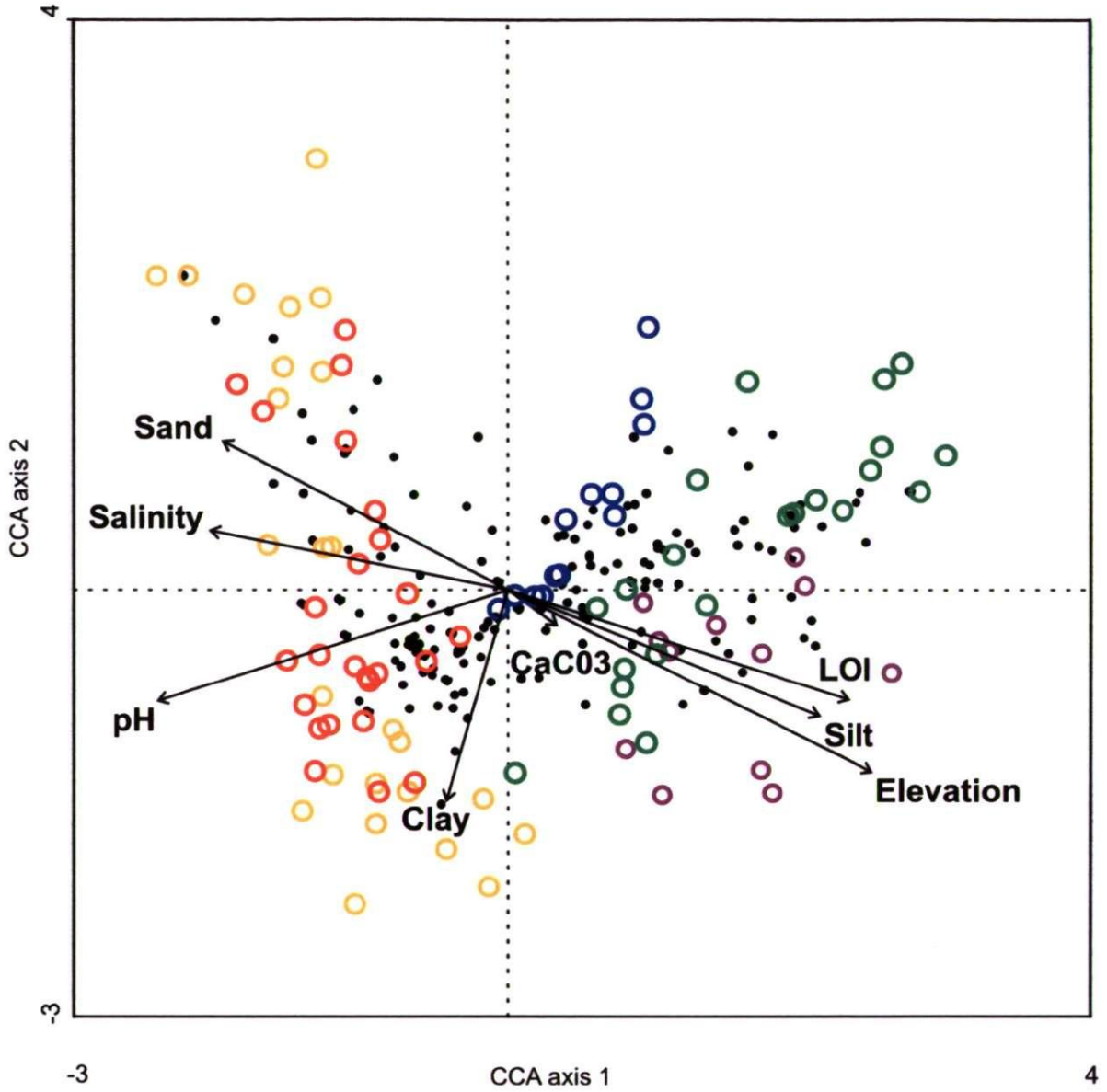

Figure 4.24. CCA tri-plot for DataSetA with 8 environmental variables, 97 samples and 151 taxa. Species (black dots) are not labelled for clarity, samples are colour coded by transect. Samples are colour coded by transect. Moservå = purple, Storbæk = blue, Oksby Enge = green, Langli North = yellow and Langli South = red. Sample labels are not shown for clarity.

Examination of the CCA tri-plot shows the majority of environmental variables are associated with axis 1. Clay fraction is associated with axis 2. Axis 1 therefore represents the major gradient in the data, from high salt marsh (high elevation, high LOI and low salinity) plotted on the right, to low salt marsh (low elevation, low LOI and high salinity) plotted on the left. Those variables with longer arrows, such as elevation, are more strongly correlated with the ordination axes (Jongman et al., 2002). $CaCO_3$ shows a weak correlation with the axes and is likely to be a redundant environmental variable. The proximity of a number of the environmental variable arrows to one another indicates a high degree of intercorrelation within the environmental data. Earlier results of Spearman's correlation confirm this (Table 4.5).

Removal of outlying samples

Samples with environmental variables with extreme influence or 'leverage' (Montgomery and Peck, 1982) can have a greater influence on the ordination results. In this study any sample with > 5x SD influence was considered to be outlying (Birks et al., 1990a). One sample (MO2) was identified with 4.3x SD influence in the initial CCA but was retained in the analysis. No other outlier samples were detected.

Constrained CCAs

Results of a series of constrained CCAs are presented in Table 4.10. Out of the eight environmental variables, six are shown to exert an independent and statistically significant influence on diatom distributions ($P < 0.05$). Sand and $CaCO_3$ are statistically insignificant and are removed from the analysis. Elevation is considered the most important variable in explaining the variance in the diatom data, shown by the high eigenvalue ratio (1.10) and the amount of variability explained (13.7%). pH is also shown to be important (eigenvalue ratio 1.12, variability explained 12.5%). This result is not unexpected since a number of palaeolimnological studies have demonstrated a strong relationship between diatom species and pH (e.g., Birks et al., 1990b). The low relative importance of salinity in explaining the variance in the diatom data is, however, somewhat surprising. The salinity measurements taken in this study are only point measurements (Section 3.3) and probably do not reflect the true variability of salinity that occurs over tidal cycles. Had salinity been measured on a variety of temporal scales, it is highly likely that the diatom assemblages would show a stronger relationship with this variable. The low relative importance of salinity in explaining the variation in the diatom data may also be linked to the proximity

of drainage systems which have lead to a highly spatially variable pattern of salinity across the Ho Bugt marshes.

Variable	λ_1	λ_2	λ_1/λ_2	% Variance explained	*P* - value
Elevation	**0.410**	**0.372**	**1.10**	**13.7**	**0.008**
pH	**0.375**	**0.335**	**1.12**	**12.5**	**0.008**
LOI	**0.343**	**0.361**	**0.95**	**11.5**	**0.008**
Silt	**0.322**	**0.379**	**0.84**	**10.8**	**0.038**
Sand	0.299	0.394	0.76	10.0	0.162
Salinity	**0.279**	**0.355**	**0.79**	**9.3**	**0.024**
Clay	**0.177**	**0.480**	**0.37**	**5.9**	**0.030**
$CaCO_3$	0.088	0.484	0.18	2.9	0.380

Table 4.10. Results of a series of constrained CCAs for DataSetA. Variables are ordered by the greatest amount of variance explained. Significant ($p < 0.05$) variables are highlighted in bold. Sand and $CaCO_3$ do not exert an independent influence on diatom distributions and are therefore removed from the analysis.

Results of a CCA run on a reduced data set of six environmental variables (sand, $CaCO_3$ excluded) are presented in Table 4.11. By removing two environmental variables the eigenvalues for axes one and two are slightly reduced, as is the overall percentage of variance explained (32% cf. 34% Table 4.9). These results suggest that the removal of two environmental variables has not significantly reduced the explanatory power of the ordination.

Axis	1	2	3	4	Total inertia
Eigenvalue	0.454	0.221	0.158	0.051	
Species-environment correlations	0.969	0.836	0.825	0.703	
Cumulative percentage variance:					
of species data	15.2	22.6 (7.4)	27.9 (5.3)	29.6 (1.7)	
of species-environment relation	47.3	70.4 (23.1)	86.8 (16.4)	92.1 (5.3)	
Sum of all eigenvalues					2.986
Sum of all canonical eigenvalues					0.960

Table 4.11. Results of CCA for DataSetA performed on a reduced data set with only 6 environmental variables (97 samples, 151 taxa). Numbers in parentheses are individual axes contributions.

Intercorrelation between environmental variables

Earlier results of a Spearman's correlation coefficient have demonstrated that a high degree of correlation and intercorrelation exist within the data set (Table 4.5). For example, elevation is correlated with salinity, pH, LOI and silt, and salinity is itself correlated with LOI and silt. Upon examination of the inter-set correlations between the variables and the ordination axes (Table 4.12), a number of these intercorrelated variables are also shown to correlate with axis one in the CCA. This suggests that some of these variables may be multicollinear and potentially redundant. Highly intercorrelated variables, which also showed high correlation with axis one, were selected as a subset group to be tested in a partially constrained CCA. This subset group consisted of the following variables: elevation, pH, salinity, LOI and silt.

Variable	Axis 1	Axis 2	Axis 3
Elevation	0.88	-0.32	0.14
Salinity	-0.72	0.10	-0.14
pH	-0.84	-0.20	0.25
LOI	0.82	-0.19	-0.00
Silt	0.75	-0.23	-0.37
Clay	-0.15	-0.38	-0.71

Table 4.12. Inter-set correlations between the environmental variables and the ordination axes. A number of variables are highly correlated with axis one and are also highly intercorrelated (See also Spearman's correlation coefficients, Table 4.5).

Partially constrained CCAs

Table 4.13 shows the results of a series of partially constrained CCAs. Elevation was selected as the sole constraining environmental variable based on the results of a preliminary CCA with automatic forward selection (Elevation, *Lambda1* = 0.41). Highly significant *P*-values (< 0.01) were obtained for all variables tested in partially constrained CCAs. Despite these variables being intercorrelated and all having a strong correlation with axis one, each of these intercorrelated variables is still seen to exert a statistically significant and independent influence on diatom distributions.

Variable	λ_1	λ_2	λ_1/λ_2	*P* - value
Elevation				**Sole variable**
pH	0.241	0.303	0.80	**0.008**
LOI	0.127	0.359	0.35	**0.008**
Silt	0.221	0.370	0.60	**0.008**
Salinity	0.194	0.355	0.55	**0.008**

Table 4.13. Results of partially constrained CCAs for DataSetA using elevation as the sole representative of the group of intercorrelated variables. Intercorrelated variables were tested in turn as sole covariables in the CCA.

Examination of VIFs

Examination of the VIFs for the remaining six environmental variables showed that all variables had VIFs < 20. Sand and silt originally had extremely high VIFs (> 100) in the initial CCA. Removal of sand and $CaCO_3$ from the analysis reduced the VIF for silt and resulted in all remaining VIFs being under 20.

CCA with manual forward selection

Summary results obtained from a CCA using manual forward selection of environmental variables are shown in Table 4.14. Elevation and pH are shown to be the most important variables in the model in terms of the amount of variance they explain. Monte Carlo permutation tests show all variables, except LOI, to be significant. LOI is therefore excluded from the final model. Results of a final CCA with manual forward selection are shown in Table 4.15 and Figure 4.25. By removing another environmental variable (LOI), the eigenvalues for axes 1 and 2 are almost the same as when six environmental variables were included in the model (Table 4.11). The overall percentage variance explained is now 31%, only slightly less than the original CCA with eight environmental variables (33.7%, Table 4.9). The first four axes explain 30% of the variation in the species data and 95% of the species-environment relation. Axis one now explains 49% of the species-environment relation. Associated Monte Carlo permutation tests demonstrate the first axis and all canonical axes are significant (P = 0.008 and 0.008 respectively, with 499 permutations under a reduced model, restricted for spatial structure (Birks, *pers. comm.*)).

Variable	*P*-value	Included in final model?
Elevation	**0.006**	Yes
pH	**0.012**	Yes
Clay	**0.014**	Yes
Salinity	**0.028**	Yes
LOI	0.126	No
Silt	**0.022**	Yes

Table 4.14. Summary results obtained from manual forward selection of environmental variables. Variables are listed in order of the extra variance each one explains when included in the model. Significant ($P = < 0.05$) results are shown in bold.

Axis	1	2	3	4	Total inertia
Eigenvalue	0.454	0.221	0.158	0.050	
Species-environment correlations	0.969	0.835	0.825	0.704	
Cumulative percentage variance:					
of species data	15.2	22.6 (7.4)	27.9 (5.3)	29.6 (1.7)	
of species-environment relation	49.0	72.9 (23.9)	89.9 (17)	95.4 (5.5)	
Sum of all eigenvalues					2.985
Sum of all canonical eigenvalues					0.926

Table 4.15. Summary results obtain from a final CCA for DataSetA (5 environmental variables, 97 samples, 151 diatom taxa). The inclusion of environmental variables in this final CCA is based on using manual forward selection (Table 4.14). Numbers in parentheses are individual axes contributions.

The final CCA ordination tri-plot (Figure 4.25) shows salinity, pH, elevation and silt to be associated with axis one. Clay fraction is associated with axis two. Although all five variables have been shown to exert an independent and statistically significant influence on diatom distributions, there is still one clear environmental gradient in the data. Samples and species associated with the high salt-marsh environment (high elevation and low salinity, low pH) are plotted on the right of the diagram and those associated with the low salt-marsh environment (low elevation and high salinity, high pH) are plotted on the left of the diagram.

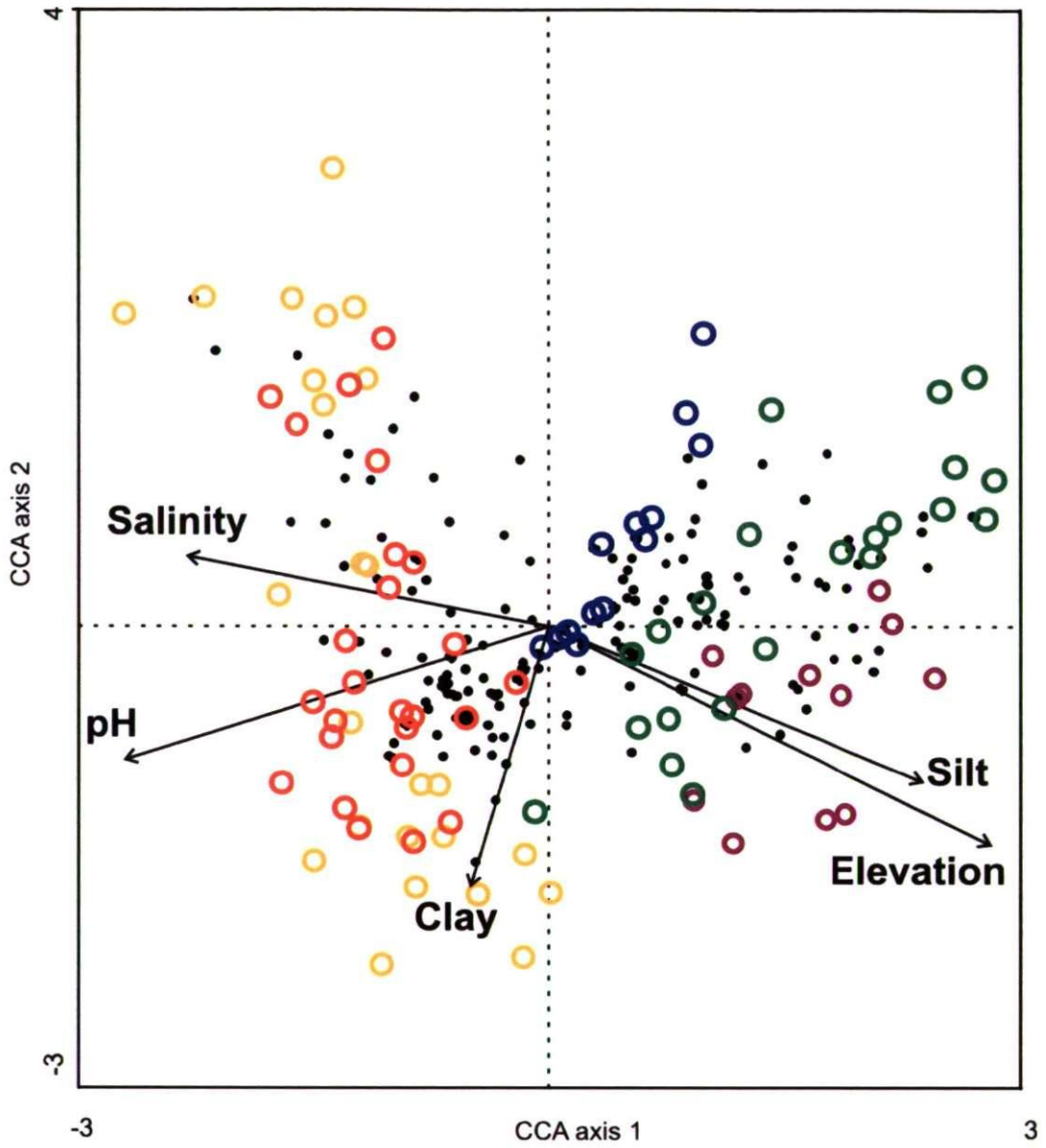

Figure 4.25. Final CCA tri-plot with five environmental variables, 97 samples and 151 taxa. Selection of environmental variables in the final CCA is based on the results of manual forward selection (Table 4.14). Species (black dots) are not labelled for clarity. Samples are colour coded by transect. Moservå = purple, Storbæk = blue, Oksby Enge = green, Langli North = yellow and Langli South = red. Sample labels are not shown for clarity.

Variance partitioninig

Figure 4.26 displays the results of variance partitioning. Of the total explained variance (31%), the unique contributions of elevation and pH are the highest (15.5 and 16.3% respectively). The high contribution of pH is a little surprising. Although several palaeolimnological studies have demonstrated a strong relationship between diatom taxa and pH, the contribution of pH in this data set was expected to be weaker than that of elevation. The contribution of salinity is less important (7.2%). It is important to note that both pH and salinity were measured from single spot samples (Section 3.3). These measurements probably do not reflect the true temporal or spatial variability of these variables across the Ho Bugt salt marshes. Elevation was also measured from a single spot sample but is less likely to have varied over similar temporal scales. A total of 42.5% of the explained variance in the data is attributed to associations between the five environmental variables.

Initial results of variance partitioning suggest that both pH and elevation are suitable variables to reconstruct. However, given the nature of the point sampling method used (Section 3.3) pH values obtained in this study are unlikely to reflect the true temporal or spatial variability of pH. On this basis, elevation is argued to be the more suitable of the two variables to reconstruct.

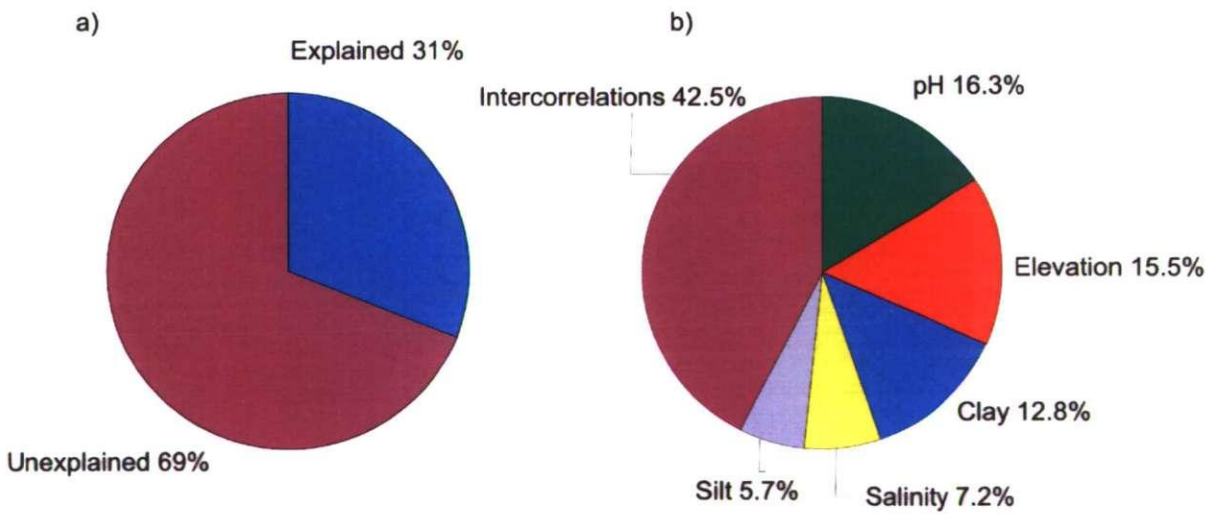

Figure 4.26. Variance partitioning pie charts for DataSetA, showing a) the total variation of the diatom data explained by the final CCA model and b) the total variation explained by each of the components and the interactions between variables.

Principal Components Analysis (PCA) - DataSetB

PCA was again used on this data set to summarise environmental information and to highlight any samples with extreme environmental characteristics. PCA was initially performed on the entire data set (127 samples, including the Kjelst Enge samples, 3 environmental variables); results are presented in Table 4.16 and displayed graphically in Figure 4.27.

Axis	1	2	3
Eigenvalue	0.730	0.201	0.069
Cumulative percentage variance	73.0	93.1 (20.1)	100.0 (6.9)

Table 4.16. Results of an initial PCA for DataSetB (127 samples and 3 environmental variables). Numbers in parentheses are individual axes contributions.

The results of an initial PCA on DataSetB shows that axis one explains a large proportion of variance in the data (73%) and represents the dominant environmental gradient. The PCA bi-plot of axis one and two (Figure 4.27) illustrates that the first axis is positively correlated with elevation and negatively correlated with pH and salinity. Axis one therefore contrasts high elevation, low salinity and low pH in samples to the right of the diagram and low elevation, high salinity and high pH in samples to the left of the diagram. The correlation between axis one and elevation is very strong, much stronger than that seen for DataSetA (Figure 4.21). Axis two is positively correlated with salinity and negatively correlated with pH.

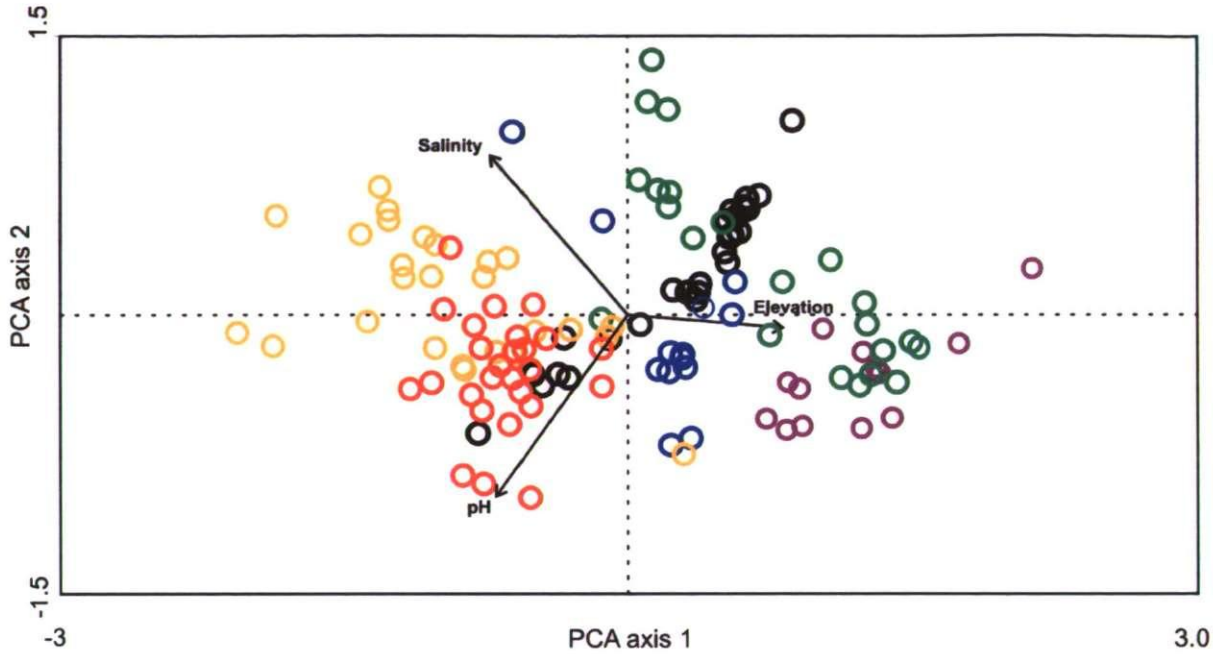

Figure 4.27. Ordination bi-plot showing results of PCA on DataSetB (127 samples, 3 environmental variables). Samples are colour coded by transect. Moservå = purple, Storbæk = blue, Oksby Enge = green, Langli North = yellow and Langli South = red, Kjelst Enge = black. Sample labels are not shown for clarity.

Removal of outlying samples

On examining the PCA bi-plot (Figure 4.27) and the corresponding axes scores, none of the samples appear to be outliers. Sample MO1 has a slightly higher axis score on axis one when compared to other samples. This sample has a higher elevation (2.67 m DNN), than any other sample in the data set and so the relative positioning of this sample is somewhat expected. An exploratory PCA run with sample MO1 removed changed the relative positioning and direction of bi-plot arrows and resulted in a lower percentage of variance explained. For these reasons this sample is retained in the analysis.

Detrended Correspondence Analysis (DCA) – DataSetB

DCA was again used on this data set to reveal major patterns in the diatom species data, to highlight samples with unusual diatom assemblages and to determine whether linear or unimodal methods were suitable for further exploration of the modern training set. DCA was initially performed on the full data set (127 samples and 161 taxa). Results are presented in Table 4.17 and Figure 4.28.

Axis	1	2	3	4
Eigenvalue	0.476	0.222	0.161	0.123
Lengths of Gradient (SD units)	3.065	2.972	2.101	1.957
Cumulative percentage variance of species data	15.4	22.5 (7.1)	27.7 (5.2)	31.7 (4.0)

Table 4.17. Results of an initial DCA for DataSetB (127 samples, 161 taxa). Numbers in parentheses are individual axes contributions.

The gradient length of the longest axis, axis one, is reasonably long (3.065 SD units) indicating that most species in the data set can be approximated by a unimodal response model. As with DataSetA, this confirms the choice of DCA for the examination of the species data and indicates that unimodal ordination methods (CCA) are suitable for the subsequent analysis of the species-environment relations (Lepš and Šmilauer, 2003). The first two axes account for 15.4% of the variance in the diatom species data. This value is lower than that obtained for DataSetA but is likely to be the result of including more samples in the data set resulting in increased 'noise.' Examination of the ordination bi-plots (Figure 4.28) reveals a general trend in the diatom data. As with DataSetA, samples from Moservå and Oksby Enge, found towards the left of the diagram are predominately associated with oligohalobous diatom taxa and fresh water conditions. Towards the right of the diagram, samples are associated with polyhalobous and mesohalobous diatom taxa, characteristic of brackish and marine conditions.

Interestingly, the Kjelst Enge samples all plot within one cluster towards the bottom right of the diagram. This is somewhat surprising because these samples span a large elevation range (0.73 – 1.86 m DNN), and cover a range of salt-marsh environments (Table 4.1) yet they all appear to be associated with similar diatom taxa. Two reasons are hypothesised for these results. Firstly, the presence and reasonably high abundance of polyhalobous (and often allochthonous) diatom taxa along much of the Kjelst Enge transect (Figure 4.5)

means that many of these samples are similar in terms of their overall diatom assemblages. Samples from the high salt marsh, containing a high abundance of polyhalobous taxa, will plot alongside samples from the tidal flat, where these taxa are more commonly found. Secondly, the presence of several fresh water taxa in the low salt marsh because of the proximity of the fresh water drainage channel (Section 4.3) emphasises this similarity between samples from high and low elevations. Samples from the low salt marsh containing a high abundance of oligohalobous taxa will plot alongside samples from the high salt marsh, where oligohalobous taxa are more common (e.g., Figure 4.11). The implications of including these Kjelst Enge samples in any transfer function development are further explored in Chapter 7.

Earlier vertical zonation results (Figures 4.18 and 4.19) indicated that the Kjelst Enge and Langli samples covered similar elevation ranges, but are associated with different dominant diatom taxa. DCA (Figure 4.28) provides more detailed information on this relationship. The Kjelst Enge samples are shown to have similar diatom assemblages to the Langli North samples, but different diatom assemblages to the Langli South samples. The Langli South samples cover a similar elevation range to the Kjelst Enge samples. Again, these observations have interesting implications with regard to the spatial variability of diatom assemblages across the salt marshes.

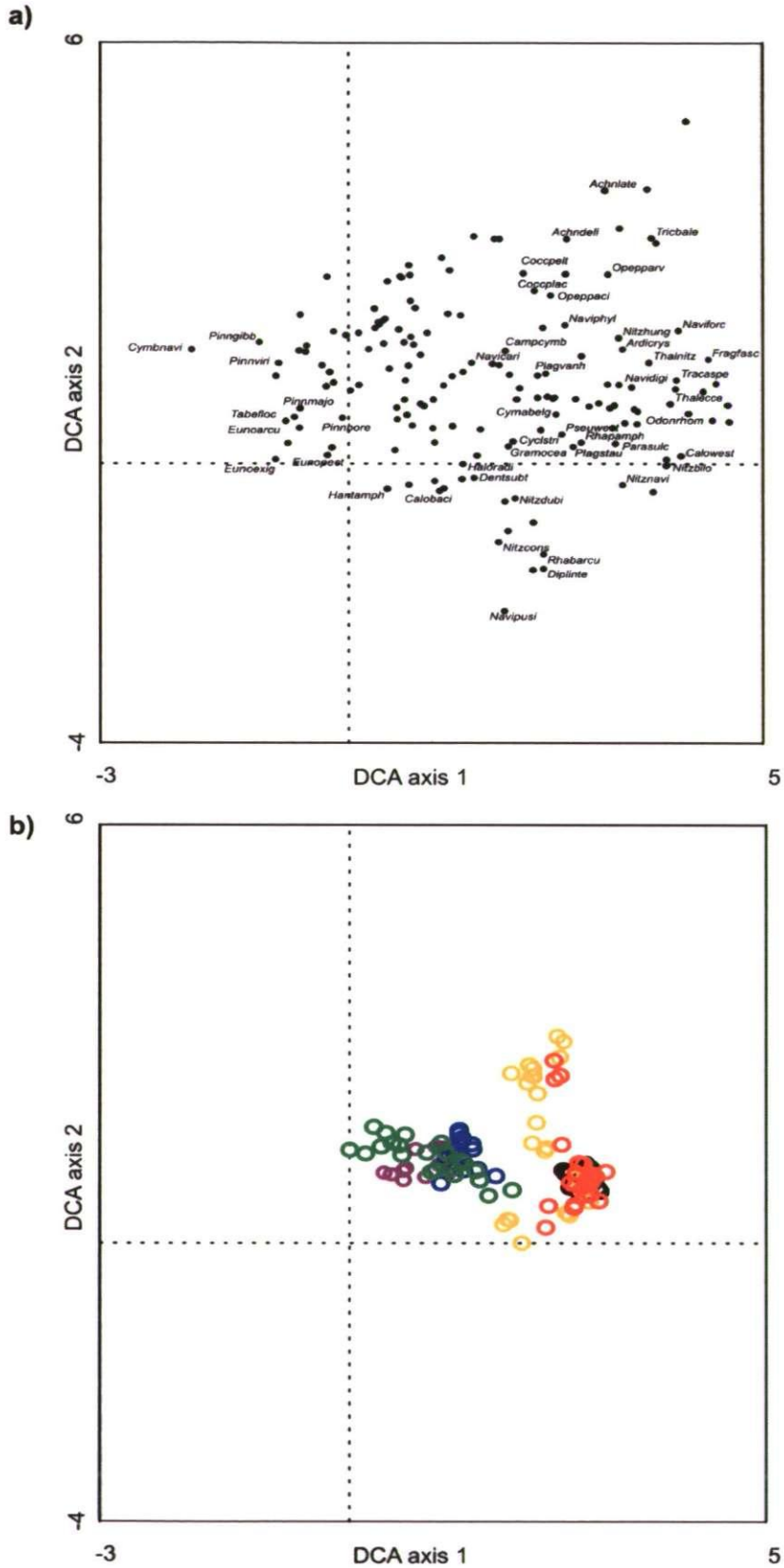

Figures 4.28. Ordination bi-plots showing the results of DCA on DataSetB (127 samples and 161 taxa), showing a) species and b) samples. Species mentioned in text and those best illustrating the general trend are labelled (see text). See Appendix 7 for a conversion of species codes to full names. Samples are colour coded by transect. Moservå = purple, Storbæk = blue, Oksby Enge = green, Langli North = yellow and Langli South = red. Sample labels are not shown for clarity.

Removal of outlying samples

No visible outlying samples with unusual diatom assemblages are detected from the DCA. However, the similarity between all of the Kjelst Enge samples, which come from a wide elevation range, suggests that caution needs to be employed when including these samples in any training set. This issue is further explored in Section 7.2.

Canonical Correspondence Analysis (CCA) – DataSetB

A DCA axis 1 gradient length of 3.065 SD units (Table 4.17) has indicated that most species in this data set can be approximated by a unimodal response model (Lepš and Šmilauer, 2003). The unimodal ordination method of CCA was therefore subsequently used to explore species-environment relations in the data set. Results of PCA and DCA analysis indicated that there were no outlying samples with extreme environmental variables or atypical diatom assemblages. The data set analysed by an initial CCA therefore consisted of 127 samples and 161 taxa. Results are presented in Table 4.18 and Figure 4.29.

Axis	1	2	3	Total inertia
Eigenvalue	0.347	0.117	0.053	
Species-environment correlations	0.914	0.758	0.707	
Cumulative percentage variance:				
of species data	11.2	15.0 (3.8)	16.7 (1.7)	
of species-environment relation	67.1	89.7 (22.6)	100.0 (10.3)	
Sum of all eigenvalues				3.098
Sum of all canonical eigenvalues				0.517

Table 4.18. Results of an initial CCA for DataSetB (127 samples, 161 taxa, 3 environmental variables). Numbers in parenthesis indicate individual axes contributions.

CCA axes one and two together explain only 15% of the variance in the diatom species data and the total variance explained is 16.7%. This suggests that the measured environmental variables (elevation, pH and salinity) only account for a small proportion of the variation in the diatom data, but given some of the differences between transects already noted this is not unexpected. Together the three environmental variables analysed in this data set explain only 17% of the total variance in the diatom data. Associated Monte Carlo permutations tests demonstrate the first axis and all canonical axis to be significant (P = 0.008 and 0.004, respectively, with 499 permutations under a reduced model, restricted for spatial structure (Birks, *pers. comm.*)).

Examination of the CCA tri-plot (Figure 4.29) shows elevation and salinity to be associated with axis one and pH to be associated, although less strongly, with axis two. Axis one therefore represents the major environmental gradient in the data from high salt marsh (high elevation, low salinity) plotted on the right of the diagram, to low salt marsh (low elevation, low salinity) plotted on the left of the diagram. Despite their atypical diatom assemblages, the samples from Kjelst Enge generally conform to this pattern.

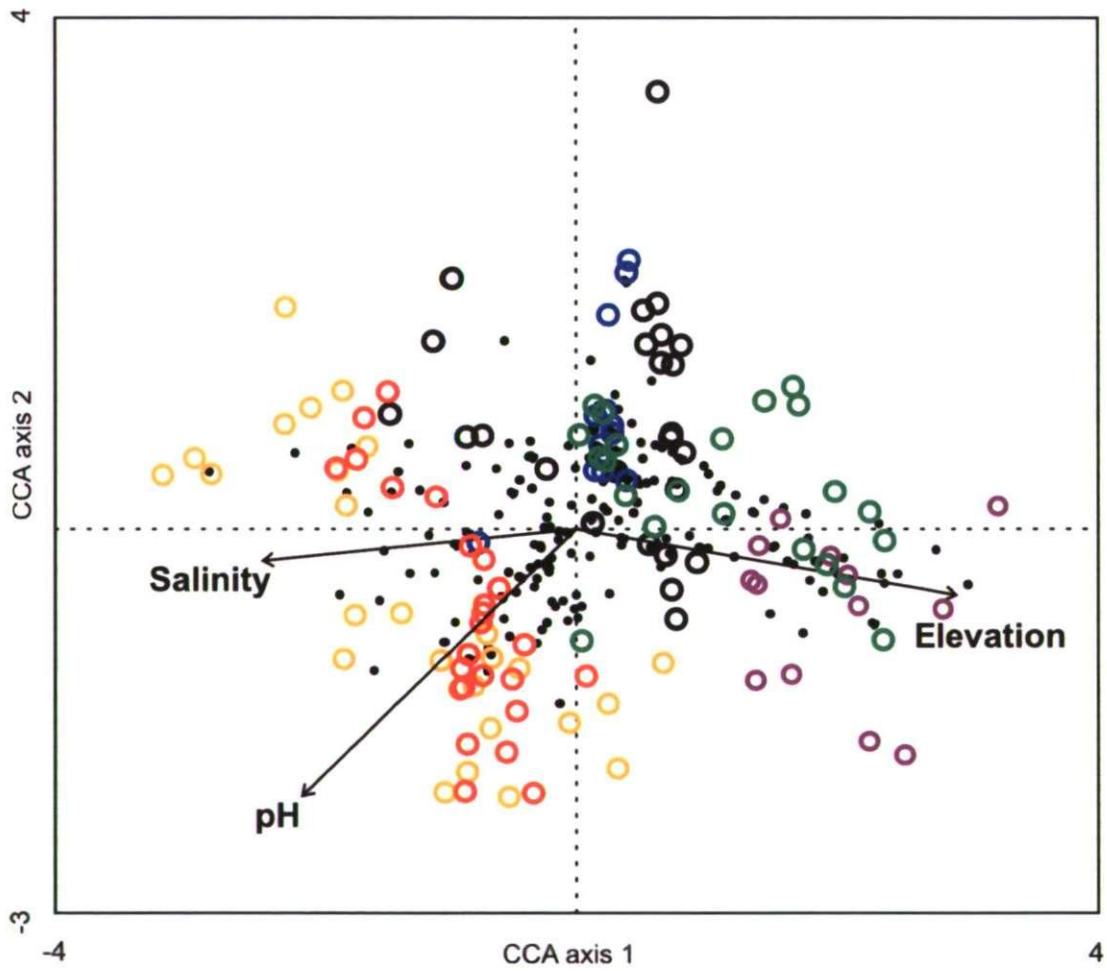

Figure 4.29. CCA tri-plot for DataSetB with three environmental variables, 127 samples and 161 taxa. Species (black dots) are not labelled for clarity. Samples are colour coded by transect. Moservå = purple, Storbæk = blue, Oksby Enge = green, Langli North = yellow and Langli South = red. Sample labels are not shown for clarity.

Removal of outlying samples

One sample KE03 was identified with a 3.1 x SD influence in the initial CCA. This sample was retained in the analysis because the influence of this sample was below the 5 x SD cut-off.

Constrained CCAs

Results of a series of constrained are presented in Table 4.19. Out of three environmental variables, only elevation is shown to exert an independent and statistically significant influence on modern diatom distributions ($P = < 0.05$). Elevation is therefore considered the most important variable in explaining the variance in the diatom data, shown by the highest eigenvalue ratio (0.85) and the amount of variability explained (10.9%).

Variable	λ_1	λ_2	λ_1 / λ_2	% Variance explained	*P* - value
Elevation	**0.337**	**0.398**	**0.85**	**10.9**	**0.040**
pH	0.245	0.391	0.63	7.9	0.070
Salinity	0.222	0.404	0.55	7.2	0.062

Table 4.19. Results of a series of constrained CCAs for DataSetB. Variables are ordered by the greatest amount of variance explained. Significant ($P < 0.05$) variables are highlighted in bold.

With only one remaining environmental variable in the model, no further screening techniques or analysis were employed for DataSetB. Analysis of this data set has indicated that elevation is the most important variable in explaining diatom distributions. The results obtained for this data set are somewhat different from those obtained for DataSetA. The inclusion of the Kjelst Enge samples has clearly had significant implications for the species-environment relations. This is especially true for the relationship between species and pH and salinity. Results of CCA have demonstrated that elevation is still the most important variable in influencing diatom distributions but results of DCA have suggested that the diatom assemblages in samples from Kjelst Enge are complex. Careful consideration will be given as to whether these samples should be included in any training set and subsequent transfer function development. These points are further explored in Section 7.2.

4.6 Chapter summary

This chapter has presented the results from the investigations into the modern salt-marsh environment. The first part of the chapter described the topography and vegetation zonation of the salt-marsh environment at each of the transect locations samples. Modern diatom data was presented alongside the analysis of a number of environmental variables. The vertical zonation of diatom species with respect to the tidal frame was tested via the use of unconstrained cluster analysis. These results have highlighted several key points:

- The diatom assemblages at Oksby Enge and Langli North were found to display a strong vertical zonation of diatom species with respect to elevation.

- The diatom assemblages from the remaining four transects (Kjelst Enge, Moservå, Storbæk and Langli South) did not display a clear vertical zonation.

- For the combined modern diatom data, some evidence of a vertical zonation is apparent but clearly there are several groups of samples which do not fit this pattern.

- Samples from Langli and Kjelst Enge, which cover similar elevation ranges, were seen to be associated with different dominant diatom taxa.

These results suggested that a thorough exploration of the modern species and environmental data was needed before any training set and subsequent transfer function could be developed. This was achieved through the use of several ordination techniques. Two data sets were analysed in ordinations and the results have highlighted several key points:

For DataSetA, which included a smaller number of samples but a larger number of environmental variables (100 samples, 152 taxa and 8 environmental variables):

- PCA identified three samples with extreme environmental characteristics that were subsequently removed from the data set.
- DCA highlighted the samples from the tidal flat at Langli North and Langli South as being associated with a different diatom assemblage from the remaining samples

- CCA established that both pH and elevation exert strong, independent and statistically significant influences on modern diatom assemblages, suggesting that diatom-based training sets can be developed for both these variables
- Concerns regarding the nature of the sampling method used to measure pH (Section 3.3), means that elevation is the more suitable variable to reconstruct. The point sampling method used is unlikely to reflect the true temporal and spatial variability of pH over tidal cycles.

For DataSetB, which included a larger number of samples but a smaller number of environmental variables (127 samples, 161 taxa and 3 environmental variables):

- DCA has demonstrated that the samples from Kjelst Enge are all associated with similar diatom assemblages. This is surprising given the fact that these samples span a relatively large elevation range (+0.7 – +1.9 m DNN) and come from a range of salt-marsh environments.
- DCA has shown that samples from Langli South and Kjelst Enge cover similar elevations ranges but are associated with different diatom taxa.
- CCA established that only elevation was shown to exert an independent and statistically significant influence on diatom distributions. This suggests that the inclusion of the Kjelst Enge samples has strong implications for the species-environment relations.
- Careful consideration needs to be given as to whether the samples from Kjelst Enge should therefore be included in any training set and subsequent transfer function development.

For both DataSetA and DataSetB:

- Elevation exerts a strong, independent and statistically significant influence on modern diatom distributions in the Ho Bugt embayment and is therefore the most appropriate environmental variable to reconstruct.

These points are further discussed in Chapter 7 alongside the detailed development of a diatom-based transfer function for reconstructing changes in palaeomarsh-surface elevation. The next two chapters present the results from the investigations of the palaeoenvironment.

Chapter 5

Palaeoenvironments - Lithostratigraphy

Following the description and discussion of the modern salt-marsh environment in the previous chapter, this chapter presents the first results from the palaeoenvironment. The lithostratigraphy of the Ho Bugt salt marshes is presented alongside the detailed sedimentological characteristics of the master core sequence (core RØ1 from Røgel salt marsh). Justification for this choice of core is given in Section 3.4.3. The results of investigations focussing specifically on the humified black layer in this core are also presented. Chronological control is provided by ^{14}C, OSL and $^{210}Pb/^{137}Cs$ dates. The modelling of these dates to produce a series of age-depth models for the various core sequences is detailed and discussed in Section 8.7.

5.1 Salt-marsh lithostratigraphy

Cores and monolith sections were collected from 8 transects across the salt marshes along the northern and western side of the Ho Bugt embayment (Figure 3.1). Radiocarbon dates were obtained from stratigraphic sections at Kjelst, Bredmose, Røgel and Oksby Enge. OSL dates were obtained from sections at Røgel and Oksby Enge. $^{210}Pb/^{137}Cs$ age estimates were obtained from Bredmose, Kjelst and Røgel. Dates are presented alongside lithostratigraphy and are fully detailed in Tables 5.1 – 5.3. $^{210}Pb/^{137}Cs$ ages are presented and modelled in Section 8.7. Transects are described from north to south.

5.1.1 Kjelst Enge (Figure 5.1a)

At Kjelst Enge, a *Phragmites* peat forms the basal unit of the Holocene sequence overlying sand, presumably of Saalian age and of glacial origin (Aagard et al., 1995). The deepest basal peat was found at a depth of - 5.85 m DNN. This basal peat unit is up to 2 m thick. The sharp upper basal contact suggests that the peat has been eroded in places. In the most landward of the cores the transition to the overlying clay is conformable. Here, the basal peat reaches a level of + 0.5 m DNN. Overlying the basal peat lays an extensive clay unit within which a bed of clayey *Phragmites* peat is found in the most landward of the cores. This unit, found between 0 and approximately + 1 m DNN, is variable in thickness but is up to one metre thick at its greatest extent. The upper most unit at Kjelst consists of a peaty clay.

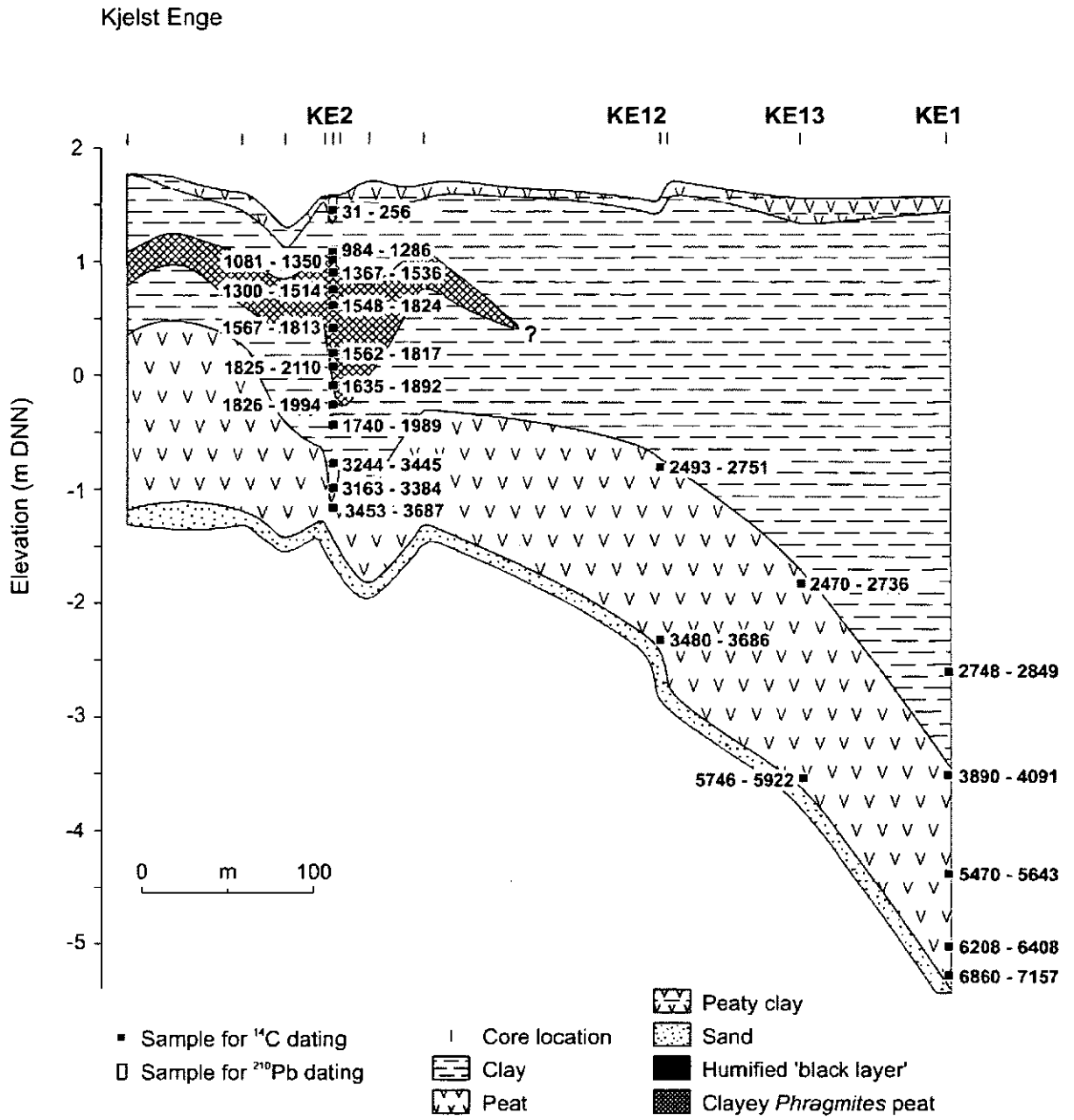

Figure 5.1. Stratigraphy of Kjelst Enge salt marsh. Radiocarbon ages show the full 2σ calibrated age range. Full details are provided in Table 5.1.

A series of radiocarbon dates have been obtained from cores at Kjelst (Table 5.1). Radiocarbon dates from core KE2 were obtained as part of the HOLSMEER Project (Gehrels et al., 2006a). Additional radiocarbon dates from the basal peat unit found in cores KE12, KE13 and KE1, were obtained as part of this project (Table 5.2). Radiocarbon dates from core KE2 indicate that the basal peat in this core was formed between 3500 and 3200 cal. yr BP. Erosion has removed the upper part of the basal peat and one dated sample in the overlying clay unit is reworked from the basal peat. The clay unit was deposited between 2000 and 1700 cal. yr BP. Ages on the upper *Phragmites* peat range from 1400 to 1000 cal. yr BP. One sample in the upper clay unit has been dated and this returned a near modern age.

In core KE1, radiocarbon dates suggest that the basal peat in this core was formed between 7200 and 3800 cal. yr BP. This core contains the oldest radiocarbon dates obtained from the Ho Bugt salt marshes. In core KE13, the basal peat was formed between 5900 and 2500 cal. yr BP and in core KE12 between 3700 and 2500 cal. yr BP. Erosion has removed the upper part of the peat in these cores. The two uppermost dates obtained from the basal peat in core KE1 (Table 5.2. nos. 37 & 38), suggest that the peat here has been somewhat compacted. This is especially obvious when compared with the basal dates from core KE13. Although deeper in sequence, these two samples returned younger ages than the basal date from core KE13, indicating that some down core movement has taken place. The issue of core compaction and the implications for this study are further explored in Section 9.1. One sample from the overlying clay unit in core KE1 was dated. This returned an age of 2700 – 2800 cal. yr BP.

Kjelst core KE2							
Sample number	**Laboratory Code**	**Sample Depth (cm)**	**Elevation (m DNN)**	**Material dated**	**Conventional Radiocarbon Age (^{14}C yr BP)**	**Calibrated Radiocarbon Age 2 sigma (cal. yr BP)**	**Median age (cal. yr BP)**
1	AAR-8891	0.12	+1.46	Detrital plant material	25 ± 39	31 – 256	69
2	AAR-8892	0.50	+1.08	Detrital plant material	1191 ± 41	984 – 1286	1118
3	AAR-8048	0.56	+1.02	Detrital plant material	1330 ± 65	1081 – 1350	1249
4	AAR-8049	0.68	+0.90	Detrital plant fragment	1562 ± 40	1367 – 1536	1460
5	AAR-8050	0.82	+0.76	Detrital plant fragment	1487 ± 42	1300 - 1514	1372
6	AAR-8051	0.96	+0.62	Detrital *Phragmites*	1772 ± 57	1548 – 1824	1693
7	AAR8052	1.16	+0.42	*Juncus* nodule	1763 ± 42	1567 – 1813	1673
8	AAR-8053	1.38	+0.20	Detrital *Juncus* fragment	1765 ± 50	1562 - 1817	1679
9	AAR-8054	1.51	+0.07	Detrital *Phragmites*	1995 ± 55	1825 – 2110	1949
10	AAR-8055	1.67	-0.09	Detrital plant fragment	1853 ± 46	1635 – 1892	1788
11	AAR-8056	1.84	-0.26	Detrital plant fragment	1965 ± 39	1826 – 1994	1917
12	AAR-8057	2.01	-0.42	Detrital plant fragment	1930 ± 43	1740 – 1989	1879
13	AAR-8058	2.35	-0.77	Detrital *Phragmites*	3122 ± 44	3244 – 3445	3349
14	AAR-8059	2.57	-0.99	Detrital *Phragmites*	3073 ± 44	3163 – 3384	3293
15	AAR-8060	2.75	-1.17	Detrital plant fragment	3332 ± 48	3453 – 3687	3565
Bredmose core BR1							
Sample number	**Laboratory Code**	**Sample Depth (cm)**	**Elevation (m DNN)**	**Material dated**	**Conventional Radiocarbon Age (^{14}C yr BP)**	**Calibrated Radiocarbon Age 2 sigma (cal. yr BP)**	**Median age (cal. yr BP)**
16	AAR-8067	1.77	-0.09	*Phragmites* fragment	1577 ± 41	1378 – 1547	1466
Bredmose core BR12							
Sample number	**Laboratory Code**	**Sample Depth (cm)**	**Elevation (m DNN)**	**Material dated**	**Conventional Radiocarbon Age (^{14}C yr BP)**	**Calibrated Radiocarbon Age 2 sigma (cal. yr BP)**	**Median age (cal. yr BP)**
17	AAR-8068	1.53	+0.65	Detrital fragment	1880 ± 41	1714 – 1918	1823
Bredmose core BR2							
Sample number	**Laboratory Code**	**Sample Depth (cm)**	**Elevation (m DNN)**	**Material dated**	**Conventional Radiocarbon Age (^{14}C yr BP)**	**Calibrated Radiocarbon Age 2 sigma (cal. yr BP)**	**Median age (cal. yr BP)**
18	AAR-8069	1.60	-0.02	Detrital plant fragment	2360 ± 100	2153 – 2719	2431

Table 5.1. Radiocarbon data obtained by AMS ^{14}C dating as part of the HOLSMEER Project (Gehrels et al., 2006a). Samples were analysed at the AMS ^{14}C Dating Laboratory, University of Århus. All ages are corrected for δ^{13}C. Calibrated ages are based on the non-marine INTCAL04 calibration curve (Reimer et al., 2004).

Røgel core RØ1							
Sample number	**Laboratory Code**	**Sample Depth (cm)**	**Elevation (m DNN)**	**Material dated**	**Conventional Radiocarbon Age (^{14}C yr BP)**	**Calibrated Radiocarbon Age 2 sigma (cal. yr BP)**	**Median age (cal. yr BP)**
19	SUERC-9253	51	+1.09	Unid. Plant remains	1026 ± 34	802 – 1051	945
20	SUERC-9254	68	+0.92	*Phragmites*	1464 ± 34	1302 – 1404	1351
21	SUERC-9255	72	+0.88	*Phragmites*	1683 ± 34	1524 – 1694	1590
22	SUERC-9256	81	+0.79	*Phragmites*	1271 ± 31	1093 – 1287	1221
23	SUERC-9257	92	+0.68	Unid. Plant remains	1532 ± 34	1351 – 1518	1420
24	SUERC-9259	168	-0.08	Unid. Plant remains	2698 ±33	2753 – 2855	2800
25	SUERC-9262	189	-0.29	*Juncus*(?) stem	3015 ± 36	3079 – 3338	3226
26	SUERC-9263	215	-0.55	*Phragmites*	3890 ± 37	4162 – 4421	4329
27	SUERC-9264	219	-0.59	Unid. Plant remains	3882 ± 37	4160 – 4419	4322
28	SUERC-9265	222	-0.62	Unid. Plant fragment	3939 ± 34	4253 – 4515	4384
Røgel core RØ1 Monolith							
Sample number	**Laboratory Code**	**Sample Depth (cm)**	**Elevation (m DNN)**	**Material dated**	**Conventional Radiocarbon Age (^{14}C yr BP)**	**Calibrated Radiocarbon Age 2 sigma (cal. yr BP)**	**Median age (cal. yr BP)**
29	SUERC-9266	55	+1.05	*Phragmites*	968 ± 34	791 – 936	860
30	SUERC-9267	60	+1.00	*Phragmites*	1193 ± 32	1005 – 1236	1119
Oksby Enge Monolith A							
Sample number	**Laboratory Code**	**Sample Depth (cm)**	**Elevation (m DNN)**	**Material dated**	**Conventional Radiocarbon Age (^{14}C yr BP)**	**Calibrated Radiocarbon Age 2 sigma (cal. yr BP)**	**Median age (cal. yr BP)**
31	SUERC-9268	124	+0.38	*Phragmites*	1835 ± 35	1698 – 1868	1773
32	SUERC-9269	152	+0.10	Unid. Plant remains	2718 ± 32	2758 – 2868	2814
Oksby Enge OEB5							
Sample number	**Laboratory Code**	**Sample Depth (cm)**	**Elevation (m DNN)**	**Material dated**	**Conventional Radiocarbon Age (^{14}C yr BP)**	**Calibrated Radiocarbon Age 2 sigma (cal. yr BP)**	**Median age (cal. yr BP)**
33	SUERC-9272	18	+1.61	*Phragmites* (rhizome?)	Modern	n/a	n/a
34	SUERC-9274	82	+0.97	*Phragmites*	744 ± 34	658 – 730	684
35	SUERC-9275	101	+0.78	*Phragmites*	1318 ± 34	1178 – 1298	1257
Kjelst core KE1 (2004)							
Sample number	**Laboratory Code**	**Sample Depth (cm)**	**Elevation (m DNN)**	**Material dated**	**Conventional Radiocarbon Age (^{14}C yr BP)**	**Calibrated Radiocarbon Age 2 sigma (cal. yr BP)**	**Median age (cal. yr BP)**
36	SUERC-9276	416	-2.59	Unid. Plant fragment	2680 ± 35	2748 – 2849	2785
37	SUERC-9277	515	-3.58	*Juncus* (?) stem	3667 ± 37	3890 – 4091	3998
38	SUERC-9278	598	-4.41	*Phragmites*	4821 ± 39	5470 – 5643	5527
39	SUERC-9279	654	-4.97	*Phragmites*	5514 ± 55	6208 – 6408	6317
40	SUERC-9282	683.5	-5.27	Unid. Plant remains	6101 ± 42	6860 – 7157	6976
Kjelst core KE12							
Sample number	**Laboratory Code**	**Sample Depth (cm)**	**Elevation (m DNN)**	**Material dated**	**Conventional Radiocarbon Age (^{14}C yr BP)**	**Calibrated Radiocarbon Age 2 sigma (cal. yr BP)**	**Median age (cal. yr BP)**
41	SUERC-9283	235	-0.83	*Phragmites*	2549 ± 35	2493 – 2751	2631
42	SUERC-9285	380	-2.28	*Phragmites*	3352 ± 34	3480 – 3686	3592
Kjelst core KE13							
Sample number	**Laboratory Code**	**Sample Depth (cm)**	**Elevation (m DNN)**	**Material dated**	**Conventional Radiocarbon Age (^{14}C yr BP)**	**Calibrated Radiocarbon Age 2 sigma (cal. yr BP)**	**Median age (cal. yr BP)**
43	SUERC-9286	333.5	-1.75	*Phragmites*	2507 ± 55	2470 – 2736	2586
44	SUERC-9287	508	-3.49	*Phragmites*	5101 ± 40	5746 – 5922	5820

Table 5.2. Radiocarbon data obtained by AMS ^{14}C dating (this study). Samples were prepared at the NERC Radiocarbon Laboratory, East Kilbride and analysed at the SUERC AMS Facility for ^{14}C analysis. All ages are corrected for δ^{13}C. Calibrated ages are based on the non-marine INTCAL04 calibration curve (Reimer et al., 2004).

5.1.2 Røgel (Figure 5.2)

At Røgel the basal peat unit is found between -0.8 and +0.3 m DNN and is again underlain by sands. Towards the seaward end of the transect the basal peat is clearly eroded. In the landward cores, the basal peat forms a more gradual transition to the overlying clay. *Phragmites* roots are found in the uppermost part of the clay unit. Overlying the clay is a very distinct amorphous black organic unit. It is found approximately 0.5 m below the surface in the landward cores but dips slightly towards the sea. Towards the landward part of the transect, the black layer merges into a clayey peat. Here the unit is very similar to the clayey peat unit in the Kjelst transect. The uppermost unit at Røgel is a peaty clay, within which is contained a 5 – 10 cm thick layer of fine, well-sorted sands. The sand unit thickens towards the dune system that borders the marsh along its western margin (Figure 5.3), suggesting a possible aeolian origin. In the landward part of the transect, the sand directly overlies the clayey peat.

A series of radiocarbon dates from core RØ1 (Table 5.2) indicates that the basal peat in this core was formed between 4500 and 2800 cal. yr BP. Although no dates are available from the base of the clay unit, it is estimated to have been deposited between 1100 and 1600 cal. yr BP. This estimate is based on ages from the same clay unit in the KE2 core. Several dates obtained from this unit do not conform to stratigraphic order, suggesting that some reworking of the clay has taken place. This is very similar to the situation found in core KE2 from the Kjelst transect (Section 5.1.1). Three dates were obtained from the lower black layer contact and these suggest that the initial formation of the black layer in this core took place between 1200 and 700 cal. yr BP. No datable material was found in the black layer itself, or in the overlying peaty clay unit.

In addition to the radiocarbon ages, two OSL ages were obtained from the upper sand unit at Røgel (Table 5.3). Dates from the top and bottom of the sand unit returned ages of 396 ± 30 and 486 ± 40 yr BP, respectively. The top 18 cm of Røgel core RØ1 was also subjected to ^{210}Pb and ^{137}Cs analyses. Here the peaty clay is dated to between 100 and -50 yr BP. These ages agree reasonably well with the OSL chronology and are presented and discussed in Section 8.7.

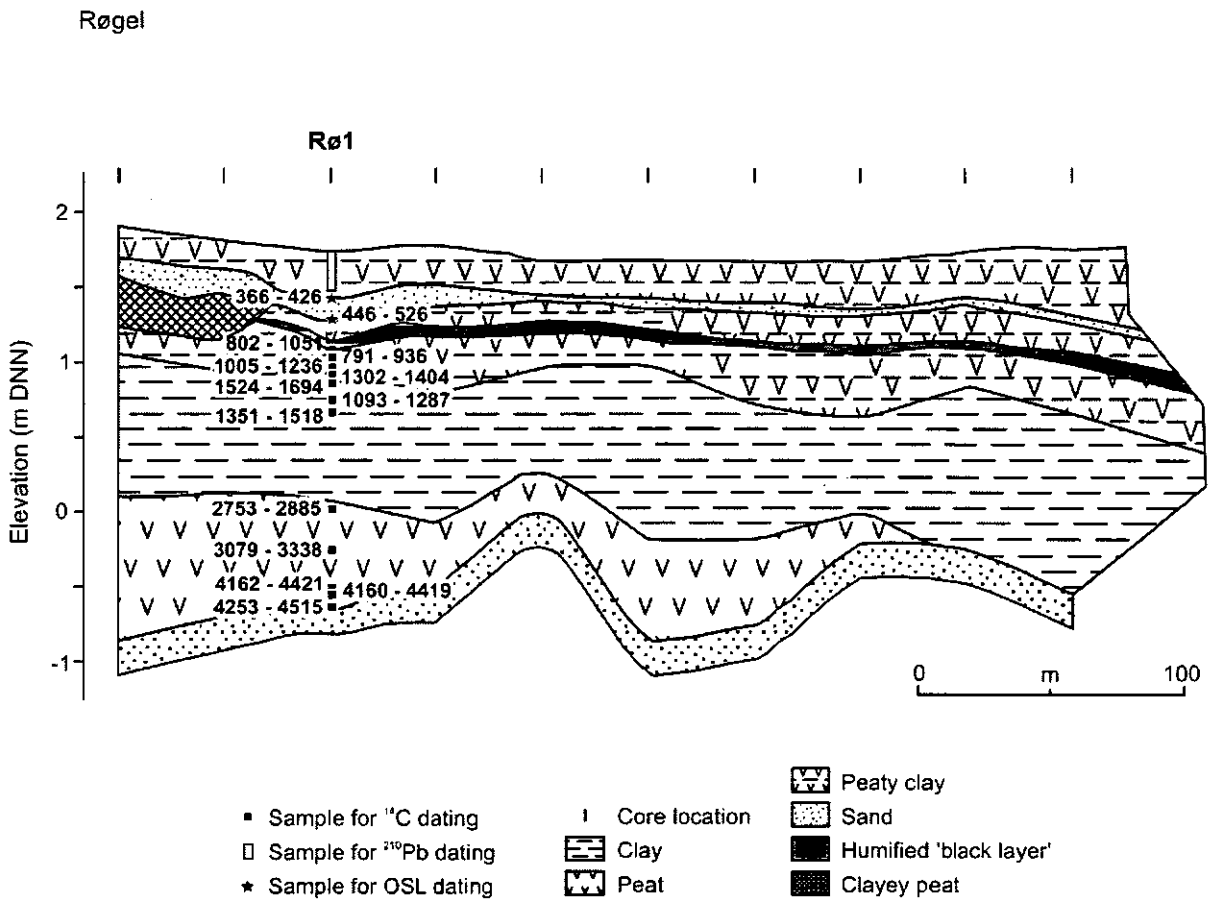

Figure 5.2. Stratigraphy of Røgel salt marsh. Radiocarbon ages show the full 2σ calibrated age range. Full details are provided in Table 5.2.

Sample number	Core	Laboratory Code	Sample Depth (m)	Elevation (m DNN)	Age (yr BP)
45	Røgel monolith (RØ1)	Risø 052803	23	+1.37	396 ± 30
46	Røgel monolith (RØ1)	Risø 052804	33	+1.27	486 ± 40
47	Oksby Enge OEB5	Risø 052802	33	+1.46	436 ± 30
48	Oksby Enge Monolith A	Risø 052801	152	+0.08	5626 ± 340

Table 5.3. OSL data for samples taken from the salt marshes at Røgel and Oksby Enge. Samples were prepared and analysed at the Risø National Laboratory for Luminescence dating, Roskilde, Denmark. Errors are analytical laboratory errors.

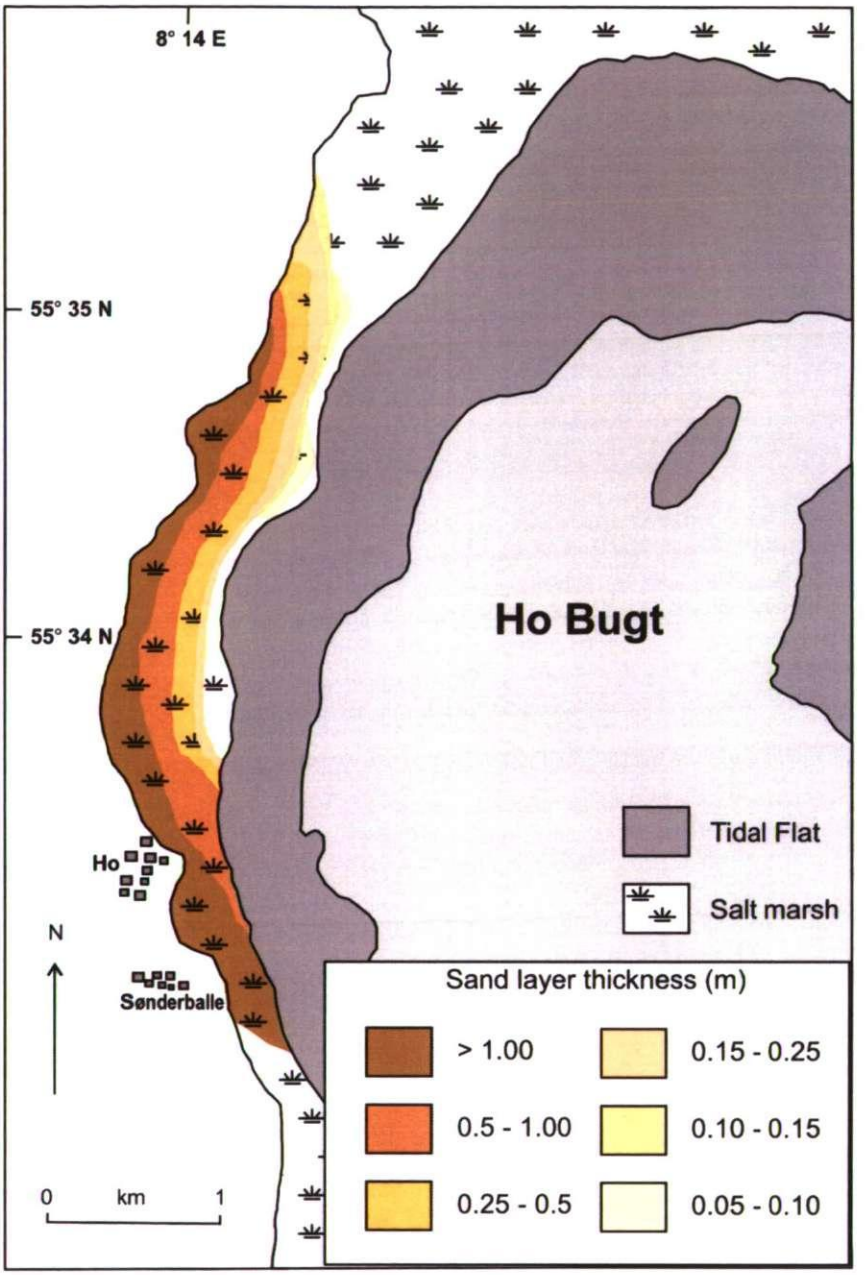

Figure 5.3. Map of Ho Bugt salt marshes showing location and thickness of the sand unit. The unit is seen to thicken in a landward direction. To the west the marshes are backed by a former dune ridge system which has now been stabilised by plantations (Jepsen, 1996).

5.1.3 Oksby Enge A (Figure 5.4a)

The basal peat unit at Oksby Enge A is found around - 2 m DNN. Here the unit is up to 2 metres thick in places and reaches an elevation of + 0.5 m DNN. In the most landward cores, where the basal peat unit is thinner, the transition to the overlying clay unit is very sharp and indicative of an erosional contact. The stratigraphy above the basal peat is similar to that found at Oksby Enge B. The black layer and sand layer are clearly present. Here, as is the case at Røgel, the sand layer thickens in a landward direction (Figure 5.3).

5.1.4 Oksby Enge B (Figure 5.4b)

The stratigraphy at Oksby Enge B is very similar to that at Røgel. Here however, the basal peat unit is thin suggesting that it has been eroded. The black layer is found between +0.7 and +1.2 m DNN and varies between 5 and 11 cm in thickness. The sand unit at Oksby Enge B thickens in a landward direction (Figure 5.3) and is up to one metre thick in the most landward core. A second sand unit is identified c. -0.5 m DNN in the most landward core.

Five radiocarbon dates were obtained from cores at Oksby Enge B (Table 5.2). Three dates from core OEB5 and two dates from monolith OEA. In core OEB5, one date from the top of the sand layer returned a 'modern' age (Table 5.2. no.33). This age is much younger than expected. Laboratory notes reflect some doubt over the nature of the plant macrofossil used for dating, suggesting the possibility that an *in-situ* rhizome was dated. This sample is therefore excluded for any further analysis in this study. One dated sample from the bottom of the black layer (Table 5.2. no. 34) returned an age of 670 – 730 cal. yr BP. This is slightly younger than the age for the black layer obtained at Røgel. From the clay unit, one dated sample returned an age of 1180 – 1300 cal. yr BP. One OSL sample from the upper sand unit returned an age of 406 – 466 yr BP (Table 5.3), agreeing well with the OSL ages from Røgel.

In Monolith OEA, two radiocarbon dates suggest that the basal peat unit in this monolith was formed between 2800 and 1700 cal. yr BP. Clearly some erosion of the peat has taken place in the core. One OSL sample from the underlying basal sand in this core (Table 5.3) returned an age of 5626 ± 340 yr BP. This date provides a maximum age for the formation of the basal peat unit at Oksby Enge.

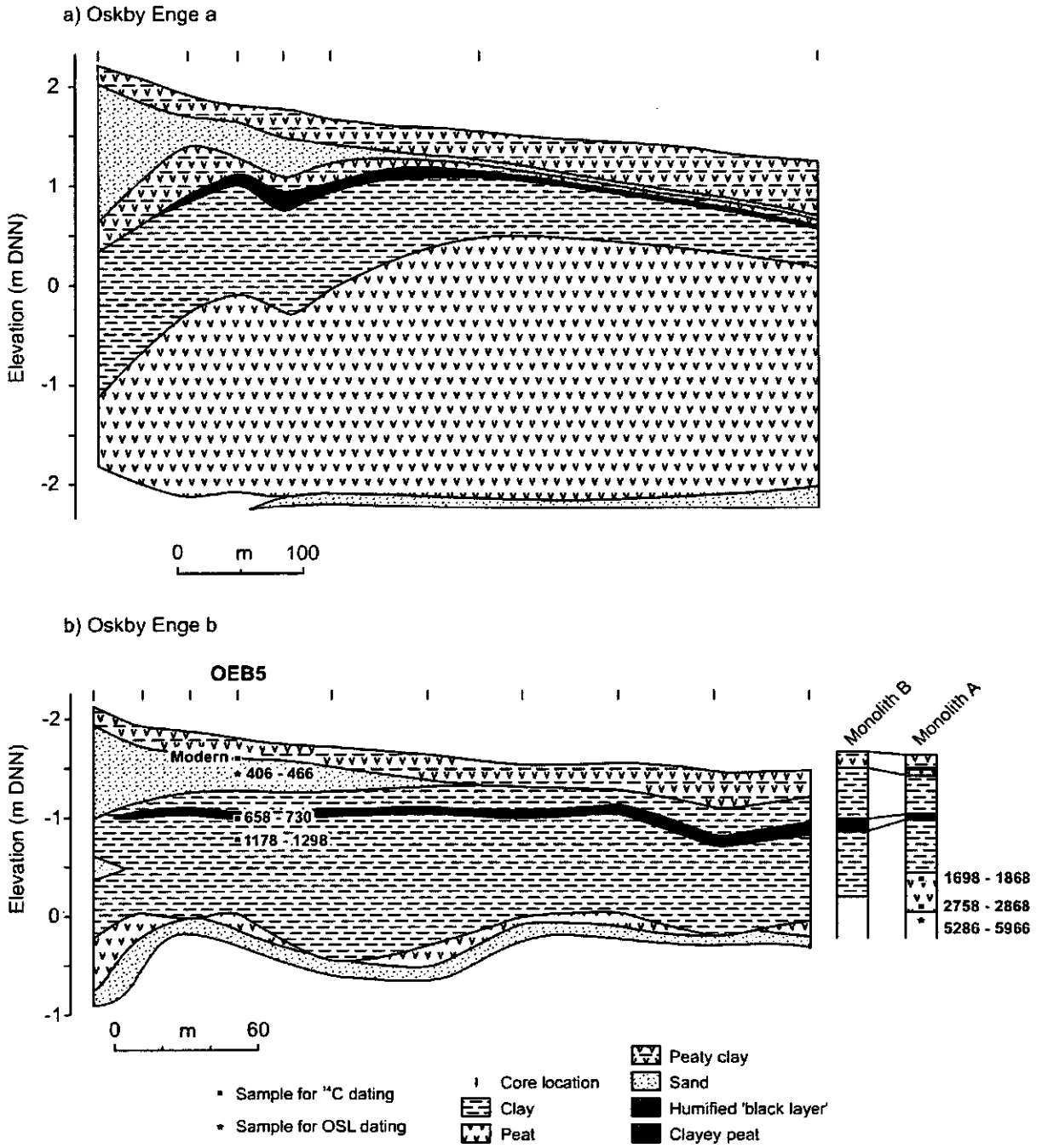

Figure 5.4. Stratigraphy of salt marshes at a) Oksby Enge A, and b) Oksby Enge B. Radiocarbon ages show the full 2σ calibrated age range. Full details are given in Table 5.2.

5.1.5 Bredmose (Figure 5.5a)

At Bredmose, the basal peat unit is up to 2 metres thick. In core BR12 it is found up to a level of + 1m DNN, higher than found at any other location in Ho Bugt. The overlying stratigraphy is similar to the Oksby Enge transects. The black layer is found between + 1.4 and + 0.6 m DNN and is around 10 cm in thickness. The sand layer is found between + 2.46 and + 0.95 m DNN and again thickens considerably towards the landward part of the transect where the dunes are located. In the most landward cores, the sand layer is almost 1 metre thick (Figure 5.3).

Three radiocarbon dates were obtained from cores along the Bredmose transect as part of the HOLSMEER Project (Table 5.1) (Gehrels et al., 2006a). In core BR12 the basal peat unit is dated to the 1700 to 1900 cal. yr BP. In core BR2, a slightly lower date on the basal peat returned an age of 2200 – 2700 cal. yr BP. In core BR1, where the overlying clay unit encroaches upon the underlying sands an age of 1400 – 1500 cal. yr BP was obtained. This last sample (no. 16, Table 5.1) returned a younger than expected age. Again, laboratory notes reflect some doubt over the nature of the sample used for dating, suggesting the possibility that an *in*-situ rhizome was dated. This sample is therefore excluded for any further analysis in this study.

5.1.6 Nørballe (Figure 5.5b)

At Nørballe, the *Phragmites* basal peat is again of variable thickness and is eroded in places. The black layer is found between + 1.2 and - 0.6 m DNN. The sand unit is up to 0.5 m thick and is marginally thicker in the most landward of the cores. In the most seaward core, a second sand layer was found around 0 m DNN but was not identified in any other core.

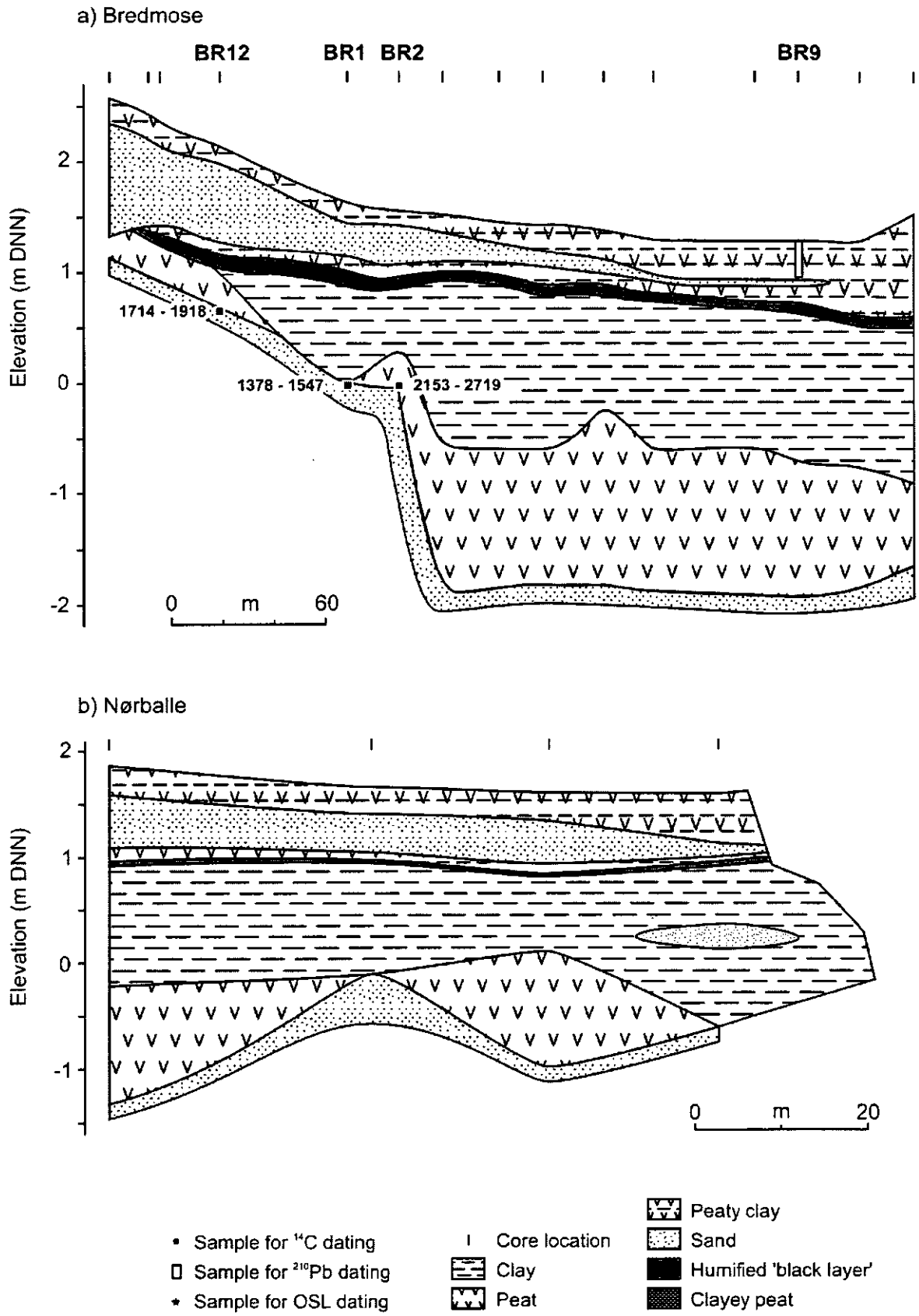

Figure 5.5. Stratigraphy of salt marshes at a) Bredmose and b) Nørballe. Radiocarbon ages show the full 2σ calibrated age range. Full details are provided in Table 5.1.

5.1.7 Sønderballe (Figure 5.6)

At Sønderballe, as is the case elsewhere, the basal peat unit reaches an elevation of around 0 m DNN and is overlain by a thick clay unit. A second sand layer is contained within this clay unit and, in the most seaward of the cores, is directly overlain by the black layer. Here the black layer is found between - 0.63 and + 1.08 m DNN. The main sand unit, found between + 1 and + 1.6 m DNN, is very extensive at Sønderballe and in most cores is around 0.5 m thick (Figure 5.3).

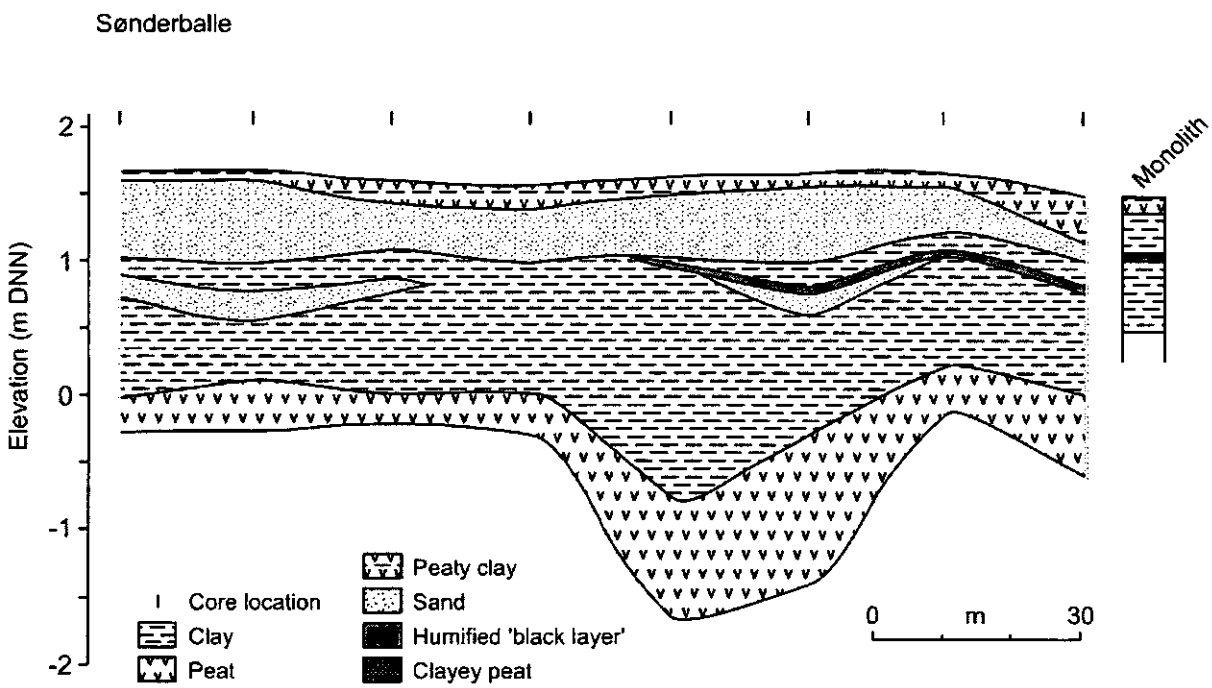

Figure 5.6. Stratigraphy of Sønderballe salt marsh.

5.1.8 Langli Island

On Langli Island, the salt marshes sediments were found to be very shallow. In most cases, impenetrable sediments were reached after less than 1 m and consequently the stratigraphy is not presented. Overlying the basal sand unit is clay which contains orange staining in the lower most section. The upper most unit at Langli is a peaty clay topsoil which varies between 0.35 and 0.05 m in thickness. No evidence for the sand layer or the black layer was found on Langli Island, presumably because the sediments here are too young.

5.2 Røgel Master Core Sequence (core RØ1)

Core RØ1 from Røgel salt marsh was selected as the master sequence for analysis of diatoms and sedimentological characteristics. Justification for this choice of core is given in Section 3.4.3. In addition, detailed investigations focussing specifically on the humified black layer in this core were also undertaken. The sedimentological characteristics and results from investigations of the black layer are presented here. The biostratigraphy of core RØ1 is presented in Chapter 6. The ^{14}C, OSL and $^{210}Pb/^{137}Cs$ ages associated with this core are described in context above and are presented in Tables 5.1 – 5.3 and also in Figure 5.7a.

5.2.1 Core RØ1 – Lithostratigraphy

The detailed lithostratigraphy of this core is shown in Figure 5.7a. In this core the basal peat unit is found between 1.48 – 2.25 m core depth (between + 0.12 and - 0.65 m DNN). The lower most peat section (core depth 1.74 – 2.25 m), is a *Phragmites* peat. The upper transition to clay is fairly sharp, suggesting an erosional contact, but not as sharp as in the most seaward cores along this transect. The overlying clay unit is found between core depths 0.52 and 1.48 m (+ 1.08 and + 0.12 m DNN). *Phragmites* remains are found throughout the clay, with numerous *Phragmites* roots visible in the uppermost part. Between core depths 0.47 and 0.52 m (+ 1.13 and + 1.08 m DNN) the black layer is found. The lower contact of the black layer is diffuse with some black staining and black mottles visible down to 0.60 m core depth (+ 1.0 m DNN). The transition from the black layer to the overlying peaty clay unit is very sharp, the change occurring over a depth of less than 0.01 m. The uppermost unit is a peaty clay. Within this peaty clay, the sand layer is well preserved and extends from 0.18 – 0.33 m core depth. (+ 1.42 to + 1.27 m DNN). Both the upper and lower contacts of the sand layer are found to dip slightly in a seaward direction. These dipped contacts are shown in situ in the salt marsh in Figure 5.7.

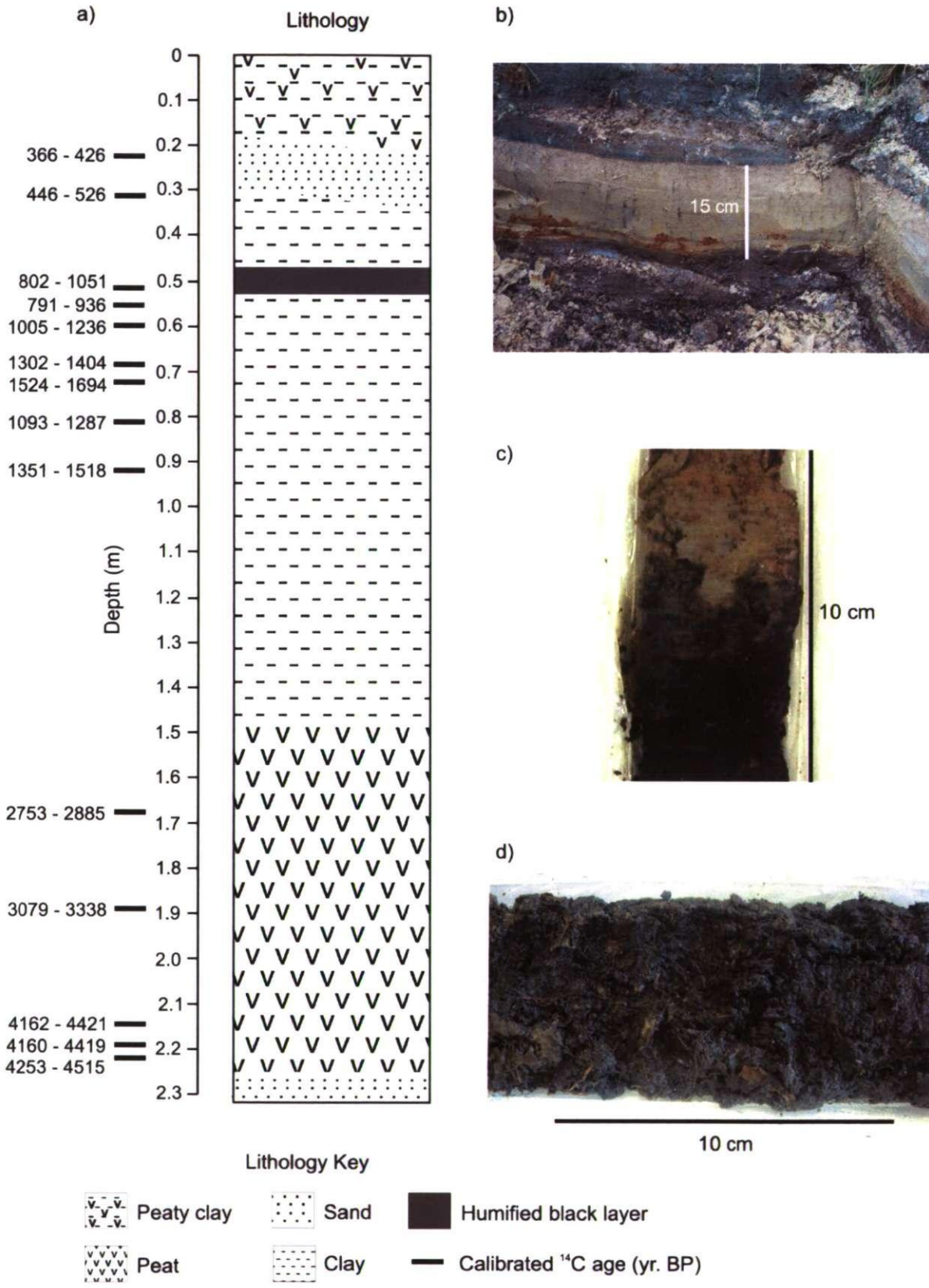

Figure 5.7. a) Detailed lithology of Røgel master core sequence (core RØ1). b) The dipping upper and lower sand layer contacts in situ in the salt marsh, c) the reasonably sharp transition from peat to clay at 1.48 m core depth, and d) *Phragmites* basal peat found in this core.

5.2.2 Core RØ1 – Sedimentological characteristics

A number of sedimentological parameters were investigated from core RØ1 in order to characterise the nature of the sediments. These included: bulk density, loss on ignition, carbonate content and grain size (sand, silt and clay fractions). The results of these investigations are presented below.

Dry Bulk Density

A total of 194 samples were analysed from core RØ1 for dry bulk density. Results are presented in Figure 5.8. Values are found to range from 0.14 to 1.28 g/cm^3. Changes in dry bulk density correlate well with the lithostratigraphy. Bulk density is low but consistent in the basal peat, here values range from 0.14 to 0.42 g/cm^3. In the overlying clay unit bulk densities are higher but are again fairly consistent, ranging from 0.54 to 1.11 g/cm^3. A distinct change in bulk density is noted with transition from the clay into the black layer. Here bulk density values are low but extremely consistent, ranging from 0.24 to 0.39 g/cm^3, and are comparable to those values found in the basal peat. Below the sand layer, bulk densities in the peaty clay unit are comparable to those found in the lower clay unit.

The sand layer did not preserve well in the Røgel monolith section and so bulk density results are not available from this layer. The peaty clay above the sand layer shows considerable variation in dry bulk density. Values here range from 0.25 to 1.28 g/cm3. There is a noticeable down core increase in dry bulk density values in this upper lithological unit, which indicate that some compaction of the core sequence has taken place here. The remaining parts of the core appear largely unaffected by compaction, as suggested by the bulk density record. The issue of core compaction and the possible implications for this study are further discussed in Section 9.1.

Loss on Ignition

A total of 148 samples from core RØ1 were analysed using the loss on ignition method (Ball, 1964; Folk, 1965) to establish organic content. Results are presented in Figure 5.8. As with previous measurements, samples from core depths 0.25 – 0.28 m were not analysed since the sand layer sediments at this depth were not preserved intact. Samples were analysed at 1 cm resolution in the top 1 m of the core, at 2 cm resolution between core depths 1.0 and 1.60 m, at 4 cm resolution between core depths 1.6 and 2.0 m and at 8

cm resolution from core depth 2.0 m to the bottom of the sequence. Samples were taken alongside diatom samples.

LOI values vary greatly throughout the core sequence with values ranging from 0 – 80%. Changes in LOI correlate well with lithostratigraphy. The highest LOI values are found in the basal peat. Here values range from 55 – 80% organic matter. LOI values are also high in the black layer with values ranging from 50 – 70% organic matter. Lower LOI values dominate in the clay unit (5 – 20% organic matter). The lowest LOI values are found in the sand layer. Here, the organic component accounts for less than 5% of material in each of the samples analysed. LOI values are higher in the upper peaty clay compared unit with the lower clay unit, reflecting the higher organic content of these samples.

Calcium Carbonate Content

The samples used to establish LOI were further analysed to establish the calcium carbonate content. The results are presented in Figure 5.8. Calcium carbonate values are expressed as a percentage of the original material. Changes in the calcium carbonate content are found to correlate well with changes in lithostratigraphy. Throughout the majority of the core, calcium carbonate values are low and remain fairly consistent within each lithological unit. However, in the basal peat calcium carbonate values are more variable ranging from 0.7 – 14%. This is probably a result of in-washing events. Flooding of the basal peat, by an extreme high tide or similar event, will result in higher calcium carbonate values as carbonate rich material is in-washed (Kirby, *pers. comm.*). The two highest peaks in calcium carbonate values in this unit occur just before the upper basal peat contact, suggesting that the peat was flooded several times before finally being transgressed.

In the overlying clay unit, calcium carbonate values vary between 2.5 and 5%. Above 0.92 m core depth, calcium carbonate values in the clay unit increase and range from 5 - 10.5 %. In the peaty clay immediately below the sand layer, calcium carbonate values are slightly lower than those found in the clay unit, varying between 2 and 3%. In the sand layer, calcium carbonate values are the lowest (< 0.5%).

Grain Size (sand, silt and clay fractions)

The results of grain size analysis are presented in Figure 5.8. A total of 220 samples from core RØ1 were analysed for sand, silt and clay fractions. These samples were taken at 1 cm resolution throughout the entire core sequence. Samples from core depths 0.25 – 0.28 m were not analysed since the sand layer sediments at this depth were not well preserved. Of these 220 samples three samples, from core depths 2.20, 2.24 and 2.25 m, produced unreliable results. It is speculated that some remaining organic material in these samples distorted the grain size distribution graphs and produced these poor results. Repeat analyses of these samples also resulted in the same problem; hence these samples have been removed from the analysis. Since the organic component is removed from samples during preparation, all percentages are expressed as a percentage of the minerogenic fraction.

Changes in grain size distribution are found to correlate well with changes in lithostratigraphy. The basal peat unit in core RØ1 is dominated by silt (40 – 80%) and sand (c. 30 – 40%) fractions. Only very small amounts of clay (<10%) are found in this unit. The overlying clay unit is dominated by silt (c. 80%) with some clay (c. 10 – 15%) and only minimal amounts of sand (< 10%). The grain size distribution of the black layer is very similar to that of the underlying clay unit. Here also, the silt fraction is the most dominant grain size fraction (c. 90%) with the remaining minerogenic component of these samples comprised of clay (c. 10%), and only very minimal amounts of sand (< 5%). The sand layer, contained within this unit, has a distinctly different grain size distribution to the remainder of the core. Here, as expected, the sand fraction is the most dominant (> 95%), with minimal amounts of silt (< 5%). Within this unit the grain size is also fairly uniform, suggesting rapid deposition.

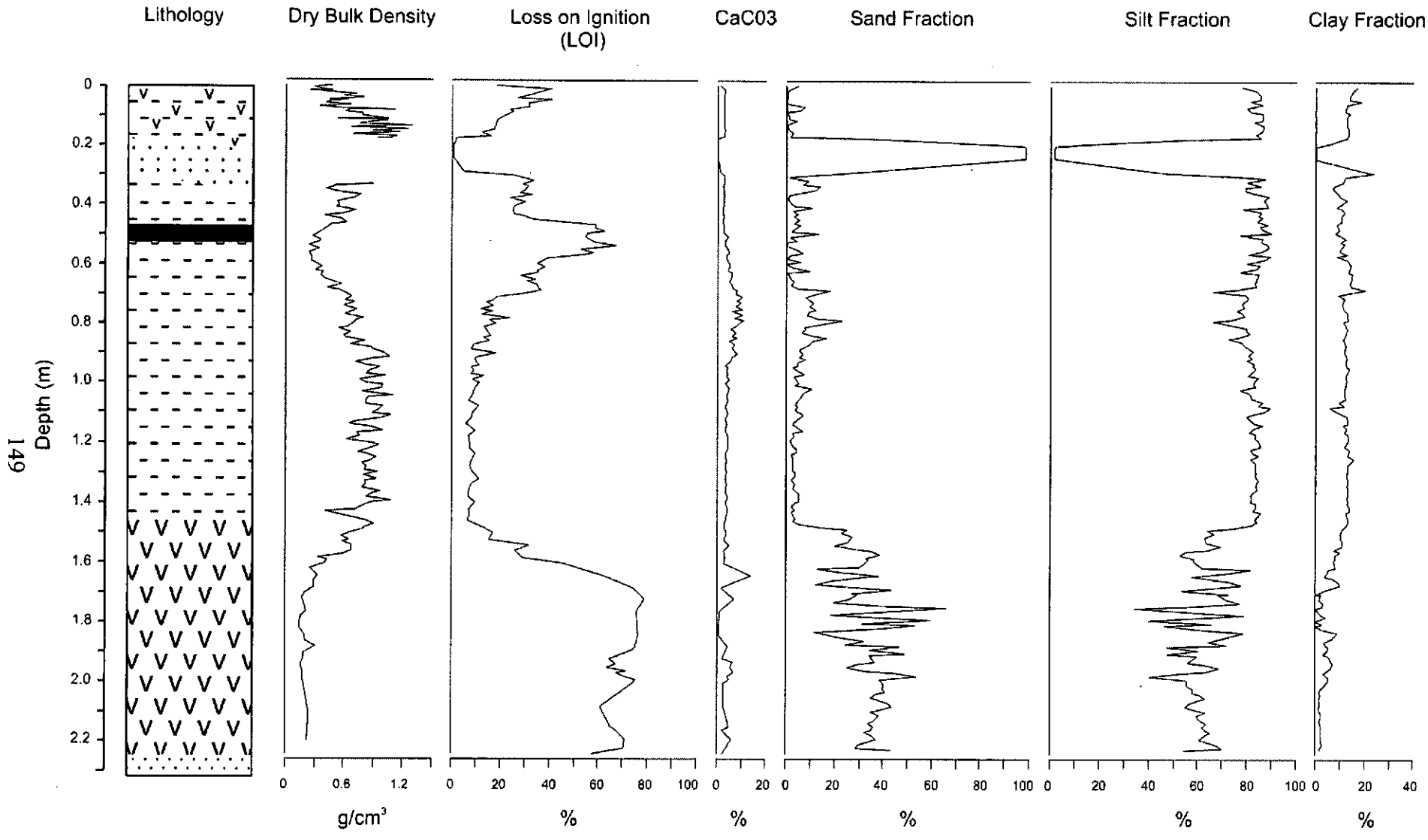

Figure 5.8. Sedimentological characteristics of core RØ1 alongside lithology. Key to lithology is given in Figure 5.7.

5.2.3 Core RØ1 - Black layer investigations

Several analyses were conducted on the Røgel master section as an aid in determining the nature of the humified black layer. In the Baltic similar black layers have been interpreted to be the result of temporary reversals in relative sea level (Lampe and Janke, 2004; Lampe, 2005). In the Tønder salt marsh, along the North Sea coast of southernmost Denmark, a distinct black horizon is associated with embankment in 394 cal. yr BP (Jacobsen, 1964). However, there is no evidence to suggest that the Ho Bugt marshes were ever diked. In this study the hypothesis that the black layer resulted from a temporary reversal in relative sea level was therefore initially explored. Iron (Fe), Calcium (Ca), Magnesium (Mg) and Manganese (Mn) concentrations, Total Organic Carbon (TOC) and the amount of humic substances insoluble in sodium hydroxide (NaOH) were analysed for the upper 72 cm of the Røgel master core (RØ1). These variables were selected to enable direct comparisons to be made with the investigations in the Baltic (Lampe, *unpublished data*). In addition, the black layer from the Røgel master section was analysed for microscopic charcoal. The results of these investigations are presented below.

Geochemistry

The results of Fe, Ca, Mg and Mn measurements are presented in Figure 5.9. Changes in the concentration of the various elements are found to correlate well with changes in lithostratigraphy. Fe, Ca, and Mg concentrations are found to be fairly high throughout this core section. Fe concentrations in particular are found to be extremely high with concentrations reaching 40 g/kg^{-1}. Mn concentrations are found to be much lower than the other elements investigated. Of the four elements investigated, only calcium shows any noticeable change associated with the black layer. This is in contrast to data from the Baltic where black layers are associated with higher Fe values (Lampe, *unpublished data*), a result of oxidation and reduction processes. A distinct peak in calcium is observed correlating with the black layer and here values reach a maximum of 6.4 g/kg^{-1}. This is possibly related to the high microscopic charcoal content of this layer (see below). Higher calcium values in sediments after fire events have been observed in several contemporary studies (e.g. Neff et al., 2005). The lowest concentration of all four elements is found in the sand unit.

Total Organic Carbon (TOC)

The results of total organic carbon measurements are presented in Figure 5.9. Changes in the amount of total organic carbon are found to correlate well with changes in lithostratigraphy. In the clay unit below the black layer, TOC values range from 8 to 20%. Values are shown to increase with movement up core towards the black layer. Samples from the black layer are found to have the highest TOC values. Here values range from 20 – 28% TOC.

Humification

The results of the humification experiments are presented in Figure 5.9. The results obtained show some agreement with the lithostratigraphy. Lowest light transmission values, indicating greater humification, are found in the black layer. Here, light transmission values range between 40 and 60%. The highest light transmission values are found in the sand layer. Here, light transmission values are close to 100%. Two of the samples from the sand layer returned light transmission values over 100%. This is probably a reflection of the inappropriateness of the method used in this part of the core. The higher minerogenic component of some sediments, such as this sand unit, can distort light transmission values resulting in higher than expected results (Hazell, 2004). It is also possible that quartz grains in these samples acted as reflectors, distorting the beam of light and producing incorrect results (Solman, *pers. comm.*). Light transmission values in the clay and peaty clay units vary between 70 and 95%. However, once again these results must be interpreted with caution. Higher light transmission values may be a reflection of increased minerogenic component rather than indication of a lesser degree of humification (Hazell, 2004). Although it is possible to correct for this (e.g. Hazell, 2004), humification was analysed in this investigation only an exploratory basis and this was not considered necessary.

Microscopic Charcoal

A total of 13 samples were examined for microscopic charcoal. The results are presented in Figure 5.9. A clear peak in charcoal concentration is associated with the black layer. The concentration of charcoal is approximately six times greater in the black layer compared to that of the neighbouring clay and peaty clay units.

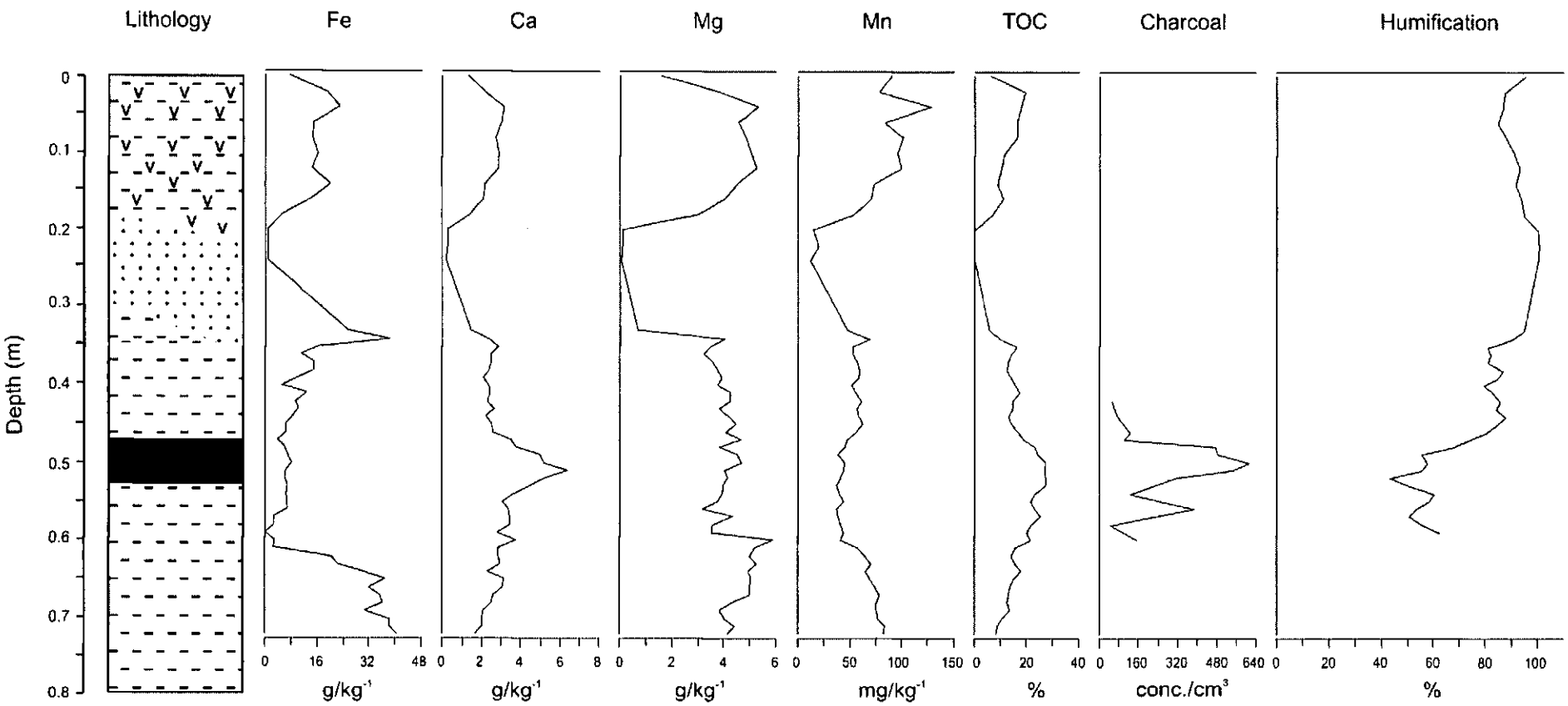

Figure 5.9. Results of Røgel black layer investigations alongside lithology. Key to lithology is given in Figure 5.7.

5.3 Chapter summary

In this chapter, the lithostratigraphy of the Ho Bugt salt marshes has been presented alongside the detailed sedimentological characteristics of the master core sequence (core RØ1 from Røgel salt marsh). ^{14}C, OSL and $^{210}Pb/^{137}Cs$ ages have been described in context of the salt-marsh lithostratigraphy. The results of investigations focussing on the humified black layer in this core have also been presented. The lithostratigraphy of the Ho Bugt marshes is characterised by several key lithological units:

1) An extensive basal peat unit, formed between approximately 7000 and 2000 cal. yrs BP and containing numerous *Phragmites* remains.
2) A clay unit formed between approximately 2000 and 1200 cal. yr BP.
3) A humified black layer formed between approximately 1200 and 650 cal. yr BP and found around 0.5 m below the surface. This unit is up to 10 cm thick in places and is correlative to a clayey peat found along the Kjelst transect in the northern most part of the embayment.
4) An extensive sand unit formed between approximately 450 and 400 cal. yr BP and found around 0.2 m below the surface. This unit is up to 1 m thick in places and is thickest towards the landward extent of the transect, where the salt marsh borders onto a former dune ridge system. The geometry of this sand unit strongly suggests an aeolian origin (Figure 5.3).

The interpretation of these units is discussed alongside biostratigraphical data in Chapter 9. Changes in the sedimentological characteristics of the master core sequence (core RØ1), have been found to correlate well with changes in the lithostratigraphy. Noticeable changes in dry bulk density, LOI and grain size are correlated with the black layer and the sand layer. Detailed investigations focussing on the black layer in this core have shown that this layer is characterised by a peak in Ca values and a six-fold increase in charcoal abundance. ^{14}C, OSL and $^{210}Pb/^{137}Cs$ ages are found to agree well with one another and have provided chronological control for the various lithological units. The modelling of these dates to produce a series of age depth models for each of the core sequences are presented in Section 8.7. The biostratigraphy of core RØ1 and other core and monolith sections investigated is presented in the next chapter.

Chapter 6

Palaeoenvironments – Biostratigraphy

In the previous chapter, the lithostratigraphy of the Ho Bugt salt marshes was presented alongside the detailed sedimentological characteristics of the master core sequence (core RØ1). In this chapter, the biostratigraphy of the core and monolith sections is presented. Low resolution diatom analyses of several core and monolith sections provide an overview of the main biostratigraphical changes in the Ho Bugt salt marshes. A high resolution diatom record from the master core sequence (core RØ1) provides a detailed record of biostratigraphical changes from which a high resolution local water-level history can be established. Justification for this choice of core is given in Section 3.4.3. This local water-level history is later compared with that established from the existing master core sequence from Kjelst Enge (core KE2), analysed as part of the HOLSMEER Project.

6.1 Salt-marsh biostratigraphy

Sample core and monolith sections were collected from six locations within the Ho Bugt embayment and analysed for diatoms. Justification for the choice of core and monolith sections selected for diatom analysis, and the sampling resolution chosen, is given in Chapter 4 and summarised below. Where appropriate, the radiocarbon and OSL dates presented in the previous chapter are shown alongside the biostratigraphy. Core and monolith sections are described from north to south. The location of all core and monolith sections are shown in Figure 3.1.

6.2 Kjelst Enge (KE2)

Core KE2 from the salt marsh at Kjelst Enge was analysed as part of the HOLSMEER Project by Dr J. Kirby. The results are presented here since they form an integral part of this investigation. From 0 to 0.90 m core depth (1.58 – 0.68 m DNN), samples for diatom analyses were counted at 4 cm resolution. Below 0.90 m, samples were analysed at 8 cm resolution. In the majority of samples the diatoms were well preserved and minimum counts of 250 – 300 diatom valves were obtained. In the bottom of the core, diatom preservation was very poor. The bottom samples at 2.82 and 2.90 m core depth were barren, whilst the sample at 2.74 m contained only the occasional broken diatom fragment. The biostratigraphy of core KE2 is presented in Figure 6.1.

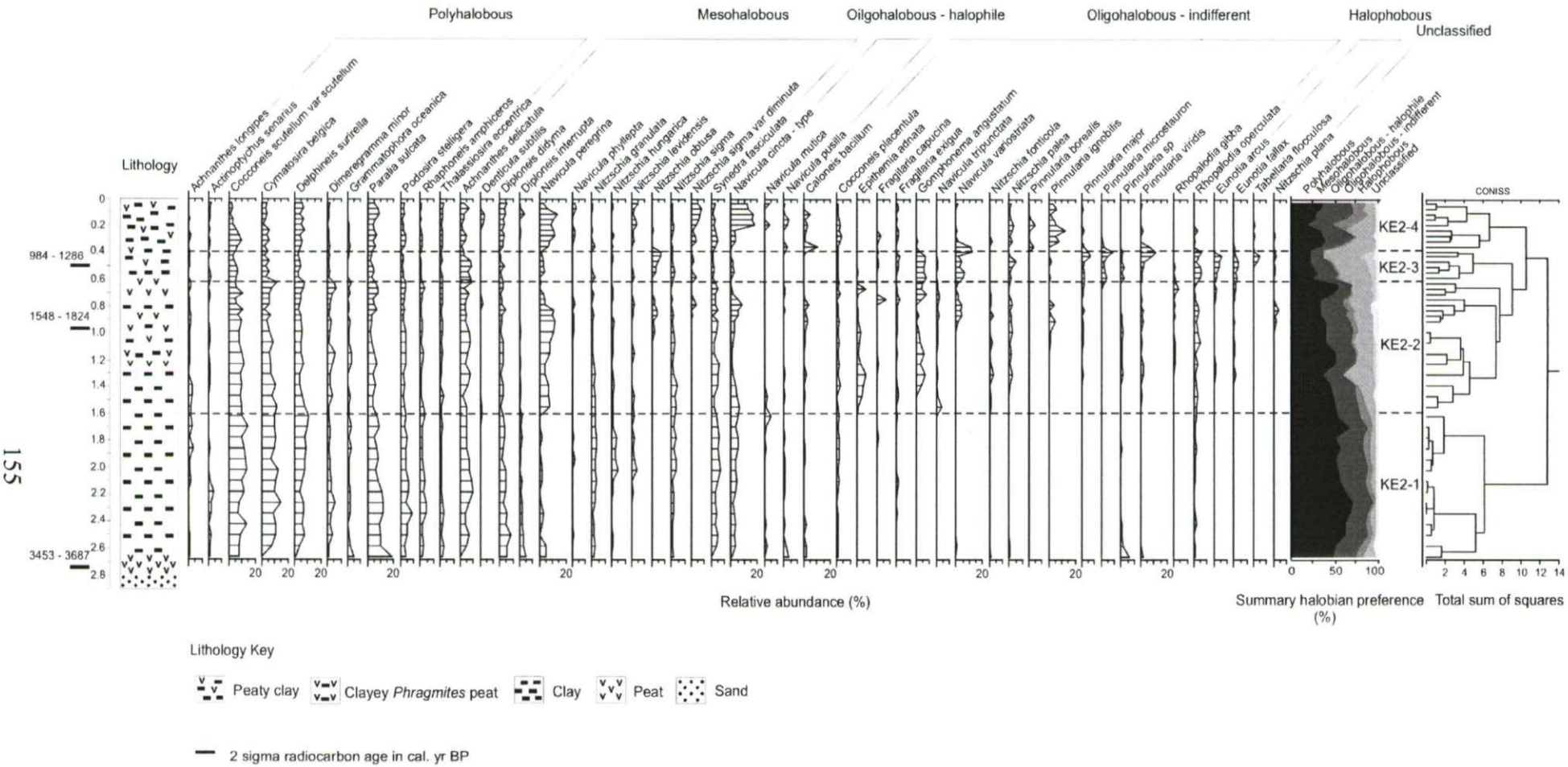

Figure 6.1. Diatom stratigraphy of core KE2. Samples were counted by J.R. Kirby. Only species with at least 3% relative abundance are shown. Cluster analysis, based on a square root transformation of species data, and summary halobian preferences exclude all taxa where relative abundances are < 1%.

A total of 110 diatom taxa were identified throughout core KE2, 87 with relative abundances ≥ 1%. Constrained cluster analysis (CONISS; Grimm, 1987), divides the samples into four diatom assemblage zones. The lowest sample to return a complete count is at 2.66 m core depth, at the eroded contact of the basal peat and the clay. This sample is dominated entirely by polyhalobous species, including *Paralia sulcata*, *Grammatophora oceanica*, *Cocconeis scutellum var scutellum* and *Diploneis didyma*, indicative of a marine environment. Several of the dominant taxa identified in this sample are allochtonous (transported), and their occurrence is most probably associated with the flooding and reworking of the upper part of the basal peat.

Zone KE-1 (2.66-1.60 m depth) corresponds with the lower clay unit and is mainly dominated by polyhalobous species, including *Cymatosira belgica*, *Delphineis surirella* and *P.sculcata*. Several mesohalobous taxa such as *Achnanthes delicatula, D. didyma* and *Synedra fasciculata* also present. The diatom taxa in this zone are indicative of a marine environment. Zone KE-2 (0.60-1.60 m depth) corresponds with the upper part of the lower clay unit and with the lower part of the upper *Phragmites* peat. Dominant taxa such as *Navicula peregrina, Epithemia adnata* and *Gomphonema angustatum* are indicative of a brackish to fresh water environment. Indicator species for Zone KE-3 (0.37-0.60 m depth) include *Pinnularia microstauron*, *Pinnularia viridis*, *Eunotia arcus, Eunotia fallax* and *Tabellaria flocculosa*. The indicator species for this zone suggest a predominately freshwater environment. Zone KE-3 spans the upper part of the *Phragmites* peat and the lower part of the overlying peaty clay. Zone KE-4 (0-0.35 m depth) is characterized by increasing occurrences of *N. peregrina*, *Navicula cincta - type* and *Pinnularia ignobilis*, indicating the return to slightly brackish conditions. Zone KE-4 corresponds with the upper part of the upper clay unit. The biostratigraphy generally corresponds with lithostratigraphical changes, but some differences are noticeable. For example, the freshwater conditions that are prevalent throughout the upper *Phragmites* peat unit persist well into the overlying clay unit.

6.3 Bredmose (BR9)

Core BR9 from the salt marsh at Bredmose was analysed for diatoms to meet two objectives:

i) To provide a high resolution diatom record from the upper core section for which a $^{210}Pb/^{137}Cs$ chronology was available (HOLSMEER project).

ii) To establish the paleoenvironmental significance of the black layer.

Diatom samples were analysed at 1 cm resolution in the upper 0.3 m of the core. The black layer in this core is 3 cm thick and extends from 0.755-0.785 m core depth (+0.595-0.565 m DNN). Diatom samples were analysed at 1 cm resolution from 0.74-0.82 m depth, and then at 2 cm resolution down to 0.88 m depth. Three samples were analysed from the black layer itself, three from the clay unit below the black layer and two from the clay unit overlying the black layer.

In the upper section of this core the diatoms were well preserved and minimum counts of 300 diatom values were obtained from all samples. Diatom preservation was highly variable throughout the black layer section, with numerous broken fragments visible. Minimum counts of 300 diatom values were obtained from all eight samples counted however, most of these counts comprised of broken fragments.

Figure 6.2 presents the diatom stratigraphy of a section through the black layer in core BR9. A total of 88 diatom taxa were identified in this core section, of which 48 were found with relative abundances of $\geq$ 1%. Constrained cluster analysis divides the samples into three diatom assemblage zones (Figure 6.2). Zone BRBLK-1 corresponds to the clay unit directly below the black layer, extending from 0.785 to 0.81 m core depth. This zone is dominated by several polyhalobous species including *Dimeregramma minor, C. belgica* and *P. sculcata.* These species are all allochtonous (transported) and are found in relatively high abundances throughout much of this clay layer. Several mesohalobous and oligohalobous species are also present in Zone BRBLK-1, including *N. peregrina* and *Epithemia turgida.* The diatom assemblage in this zone is indicative of a marine to brackish water environment.

Zone BRBLK-2 (0.755-0.795 m depth) corresponds with the black layer and with the upper part of the lower clay unit. The diatoms in Zone BRBLK-2 show a distinct freshening of the environment, characterized by an increase in several *Pinnularia* species, including *Pinnularia borealis*, *Pinnularia major* and *P. viridis*. Zone BRBLK-3 (0.74 – 0.755 m depth) corresponds to the upper clay unit. The diatom flora here is again indicative of a more marine environment, dominated by species such as *Diploneis smithii* and *Diploneis interrupta*. Very few *Pinnularia* species are identified in this zone. Although only a few samples were analysed in this section of the core, the changes in biostratigraphy are shown to correlate reasonably well with the changes in the lithostratigraphy. In particular, a distinct fresh water diatom assemblage appears to be associated with the black layer.

Figure 6.3 presents the diatom stratigraphy of the upper 0.3 m of core BR9. A total of 137 diatom taxa were identified in this section of the core, of which 82 were found with relative abundances of ≥ 1%. Three of these species remain unidentified. Species G1 has a maximum relative abundance of 9.6%, the other two unidentified species occur with only minor (< 3%) relative abundances. Unidentified diatom taxa, with relative abundances ≥ 1%, are described in Appendix 5. In this relatively short core section, corresponding with the upper peaty clay unit, several major changes in the diatom assemblage are noted which are not identified in the lithostratigraphy. Constrained cluster analysis divides the samples into three diatom assemblage zones (Figure 6.3). Zone BR9-1 (0.175-0.30 m depth) is dominated by mesohalobous taxa such as *Denticula subtilis, D. interrupta, N. peregrina* and the oligohalobous – halophile taxon *N. cincta* – type. These taxa are indicative of a brackish water environment. Indicator species for Zone BR9-2 (0.055 – 0.175 m depth) include a number of oligohalobous - indifferent taxa such as *Fragilaria capucina, Nitzschia fonticola* and *Achnanthes clevei*. These taxa are mostly absent from the rest of this core section. Mesohalobous taxa such as *Navicula phyllepta* and *Navicula pygmaea* are also dominant in this zone. The taxa in this zone are indicative of a brackish to fresh water environment. In Zone BR9-3 (0-0.055 m depth), the relative abundance of oligohalobous – indifferent taxa decreases. The mesohalobous taxon *Navicula phyllepta* and the oligohalobous – halophile taxa *N.cincta* – type and *Nitzschia debilis*, are dominant in this zone. These taxa indicate a return to brackish water conditions.

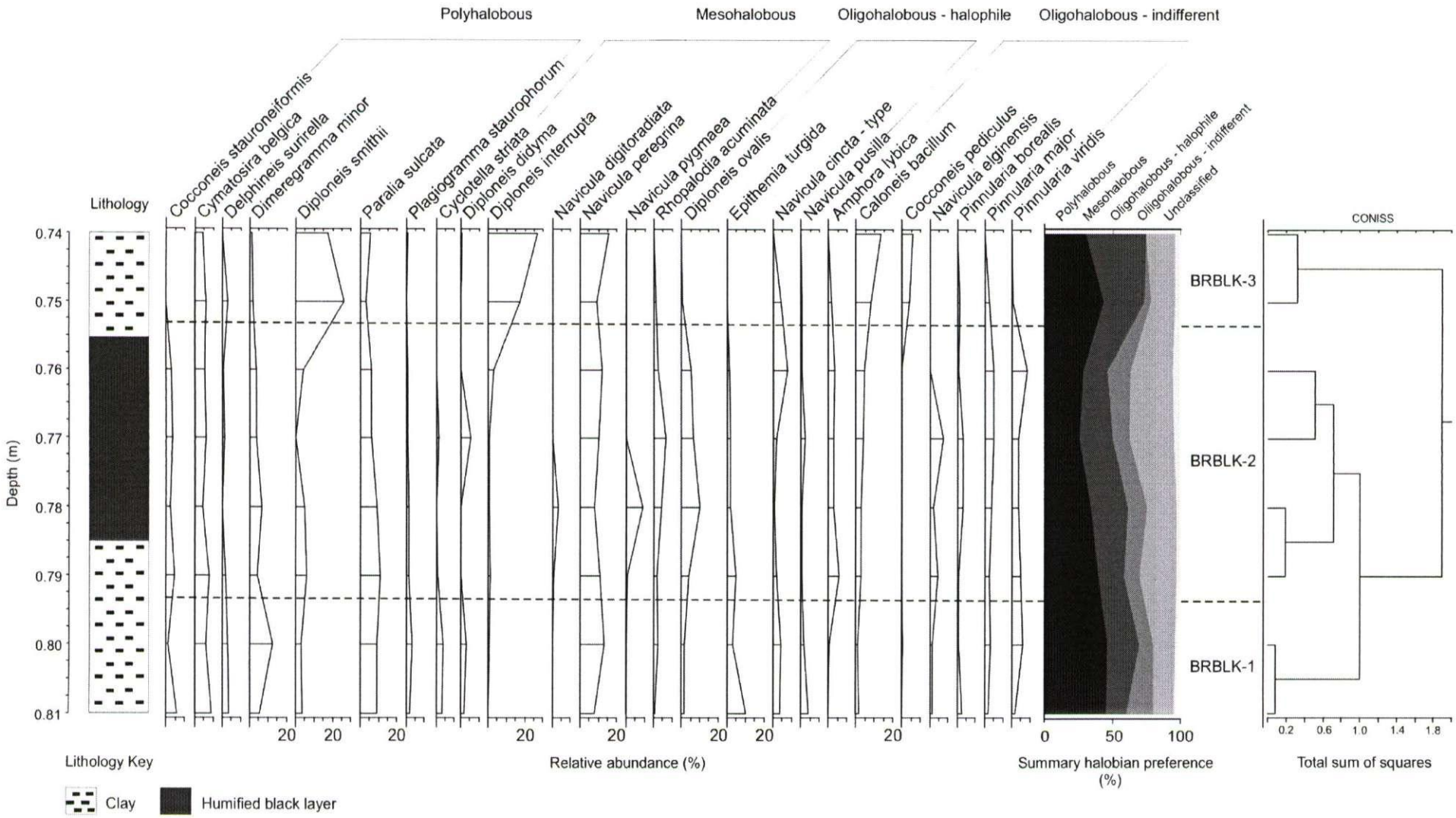

Figure 6.2. Diatom stratigraphy of a section through the black layer in core BR9. Only species with at least 3% relative abundance are shown. Cluster anlaysis, based on a square root transformation of species data, and summary halobian preferences exclude all taxa where relative abundances are < 1%.

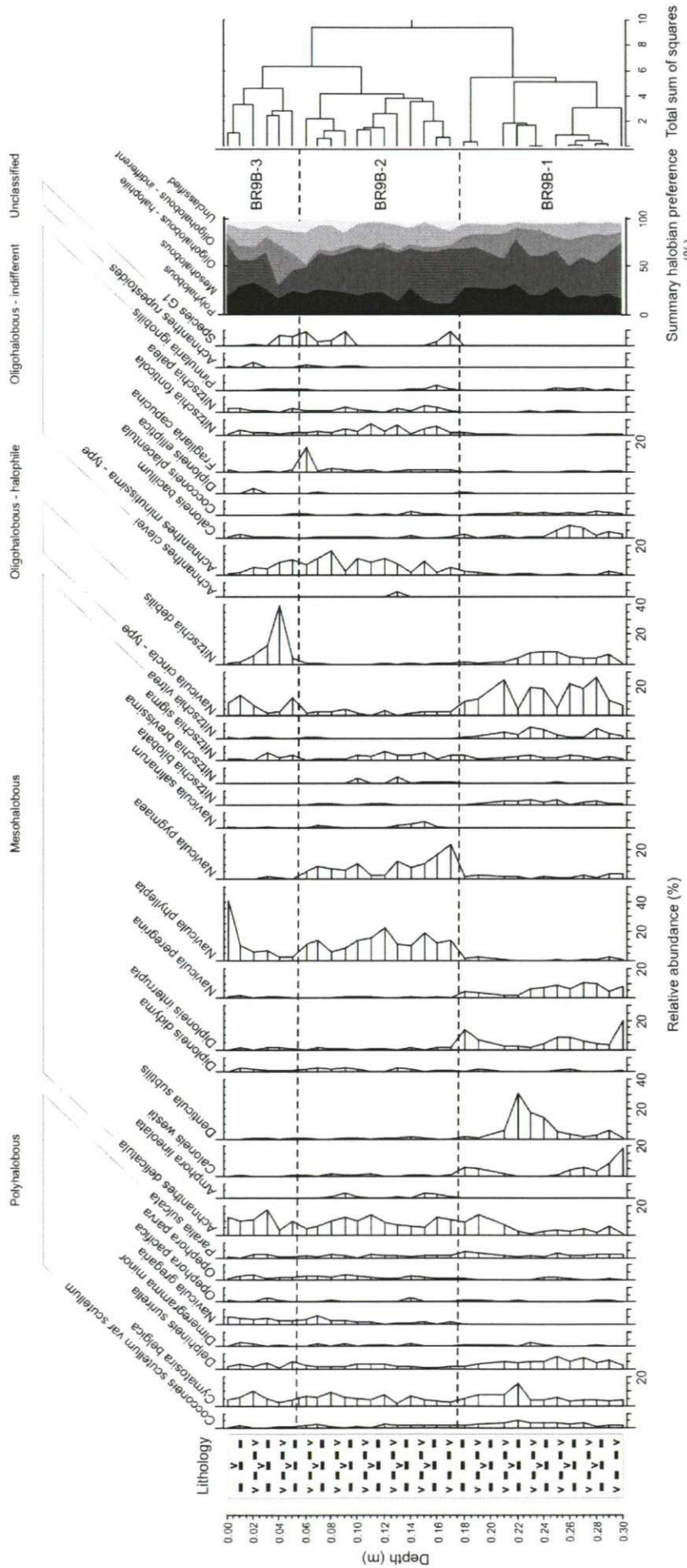

Figure 6.3. Diatom stratigraphy of the upper part of core BR9B. Only species with at least 3% relative abundance are shown. Cluster analysis, based on a square root transformation of species data, and summary halobian preferences exclude all taxa where relative abundances are < 1%. Key to lithology is given in Figure 6.1.

6.4 Røgel (RØ1)

Diatom analysis was conducted on Core RØ1 from the salt marsh at Røgel to provide a high resolution diatom record to compare with the existing record from the salt marsh at Kjelst Enge (core KE2, Figure 6.1). Diatom samples were initially analysed at 8 cm resolution. In sections of the core where interesting changes in the abundance and presence of several taxa were noted, samples were then analysed at a higher resolution. Diatom samples were analysed at 1 cm resolution down to a depth of 0.80 m, at 2 cm resolution to a depth of 1.0 m, at 4 cm resolution to a depth of 1.60 m and then at 8 cm resolution to the bottom of the core (2.25 m). Additional samples were analysed from stratigraphic levels that were ^{14}C dated. Samples from the upper 0.5 m were taken from Røgel monolith. Between 0.19 and 0.33 m core depth, the sand layer was not well preserved and consequently no diatom data is available for this part of the record.

The diatom stratigraphy of core RØ1 is presented in Figure 6.4. Diatom preservation was highly variable throughout the core. In the lowest part of the basal peat, from 2 m depth down to the bottom of the core, samples were barren. The last sample to return a complete count is at 1.92 m depth. In the upper part of the basal peat, diatoms were found to be reasonably well preserved, although numerous broken and partially dissolved fragments were observed. Around 1.6 m core depth several samples did not return full counts. The upper contact of the basal peat is at 1.48 m depth. It is possible that erosion and reworking of the upper part of the basal peat has affected diatom preservation in this section of the core. From 0.60 – 1.60 m depth, diatom preservation was very good and full counts were obtained from all samples within this section of the core. This section corresponds to the lower clay unit.

Between 0.46 and 0.60 m depth, diatom preservation was highly variable. In samples from core depths 0.47, 0.50, 0.51, 0.53, 0.54 and 0.56 m, only a few broken diatom fragments were observed, even when highly concentrate slides were examined. Consequently these samples have been excluded from the results. Samples from 0.46, 0.49, 0.52, 0.55, 0.57 and 0.59 m depth, returned partial counts of between 180 and 300 diatom valves. These samples are included in the results at this stage. Samples from 0.48, 0.58 and 0.60 m depth were the only samples within this section of the core to return full counts. The black layer in core RØ1 extends from 0.47 – 0.52 m depth. It is important to note that the samples

which did not return counts, or returned only partial counts, are mainly concentrated within this layer (Figure 6.5).

Diatom preservation in the samples from 0.33 – 0.45 m depth was also very good (Figure 6.6) and minimum counts were again obtained from all samples in this section of the core. This section corresponds to the upper clay unit. Although it was not possible to sample accurately the sand layer (0.18 – 0.33 m depth) due to poor preservation, pilot samples taken from this layer indicated that the diatoms were not preserved here. In the peaty clay unit in the upper part of the core (0 – 0.17 m depth) diatom preservation was again very good.

A total of 194 diatom taxa were identified in this core, of which 132 had relative abundances ≥ 1%. Six species remain unidentified. Five of these unidentified species were found with relative abundances of < 2% and one with a relative abundance of < 3%. Unidentified diatom taxa, with relative abundances ≥ 1%, are described in Appendix 5. Some major changes in the diatom assemblages are noted throughout this core. The most interesting changes are, however, concentrated in the upper 0.80 m, the focus of the very high resolution analysis

Constrained cluster analysis divides the samples into four diatom assemblage zones (Figure 6.4). Zone RØ1-1 (0.715-1.92 m depth) is the largest of the four zones, spanning the upper part of the basal peat and lower part of the lower clay unit. This zone is dominated by polyhalobous and mesohalobous taxa such as *C. belgica, D. interrupta* and *Navicula digitoradiata*. Several taxa from the oligohalobous groups such as *N. cincta* – type, *Navicula mutica* and *Caloneis bacillum*, are also present in high abundances. The absence of oligohalobous – indifferent and halophobous taxa, indicative of a fresh water environment, throughout much of the basal peat is somewhat surprising. Laboratory notes indicate that numerous broken and partially dissolved diatom fragments were observed in these samples. It is likely that the autochthonous (*in situ*) diatom population is not well preserved in this section of the core and as a consequence, the counts reflect a mostly allochtonous (transported) population. This is confirmed by the high abundance of numerous allochtonous taxa such as *C. belgica, D. surirella, G. oceanica* and *P. sulcata* throughout the basal peat, and the high $CaCO_3$ values found in this part of the core (Section 5.2.2 and Figure 5.7). Higher $CaCO_3$ values are indicative of in-washing and tidal

flooding events (Kirby *pers. comm*). The presence of allochothonous marine taxa in this section of the core is likely to be linked to the gradual transgression of the basal peat unit.

Zone RØ1-2 (0.47-0.715 m depth) corresponds with the upper part of the lower clay unit and with the black layer. An increasing number of oligohalobous taxa such as *E. adnata, Navicula amphibola, Navicula ryhnchocephala* and *P. minor* are identified in this zone and are associated with the black layer samples. These species are indicative of a fresh water environment. Alongside these taxa, an increase in the number of polyhalobous and allochtonous taxa is also noted. High relative abundances of *C. scutellum var scutellum, D. minor, G. oceanica* and *P. sulcata* are also found in these samples. Diatom preservation was particularly poor in this part of the core and, as is the case for the basal peat, it is likely that the autochthonous population is not well preserved and that the counts again reflect a mostly allochtonous population. The presence of these allochtonous taxa also suggests that the fresh water environment, under which it is likely that the black layer was created, may have been reflooded at some point in time.

In Zone RØ1-3 (0.105-0.47 m depth), mesohalobous and oligohalobous taxa are dominant. This zone is characterised by high abundances of taxa such as *C. bacillum, Fragilaria brevistriata* – type, *Fragilaria exigua, Fragilaria pinnata* and *P. viridis*, indicative of a fresh water environment. This zone corresponds to the upper part of the lower clay unit, and with the peaty clay above the sand layer. No diatom data are available for the sand layer. However, from the diatom data presented, it is clear that sand layer formation began at a time when fresh water conditions prevailed. The upper part of the core, Zone RØ1-4 (0-0.105 m depth) corresponds with the upper part of the peaty clay. Here the diatom taxa are again indicative of a brackish water environment.

In general the biostratigraphy of core RØ1 generally corresponds with the lithostratigraphical changes, but some differences are noticeable. For example, the (fresh water?) conditions under which the black layer formed appear to be initiated in the top 0.17 m of the underlying clay unit.

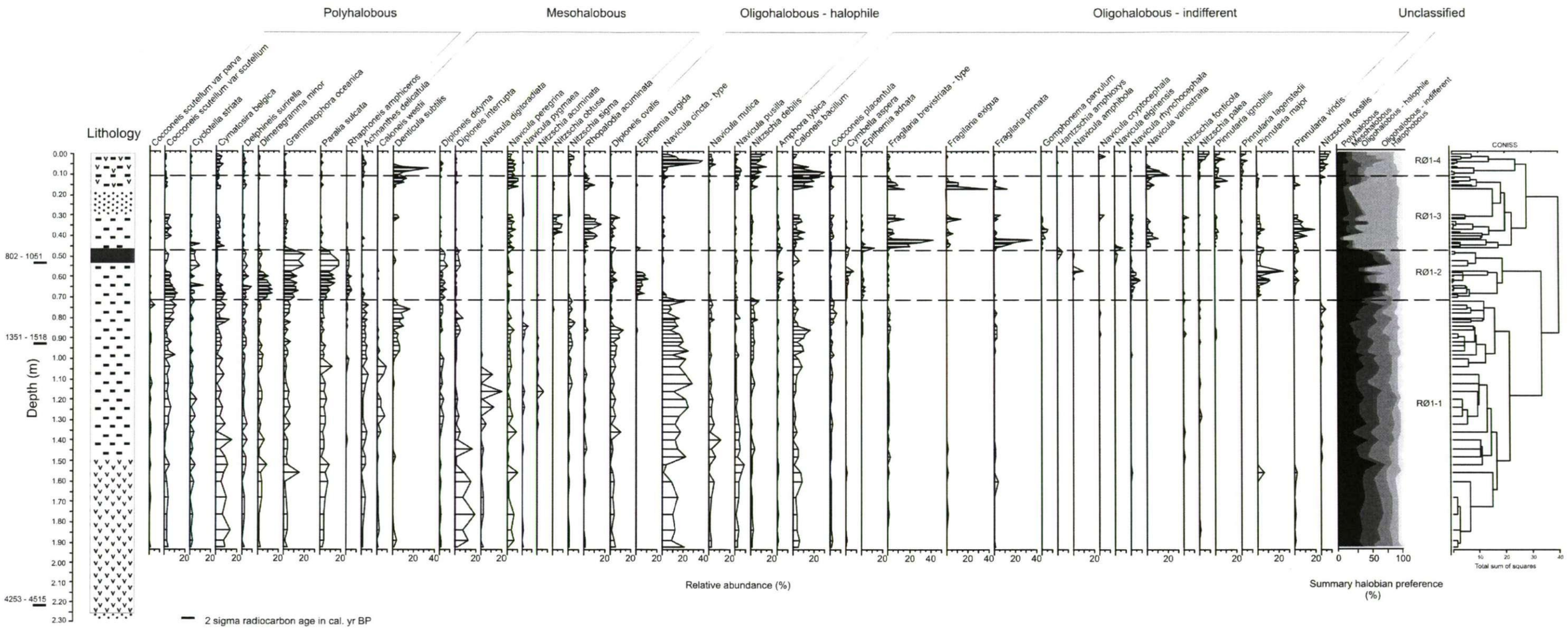

Figure 6.4. Diatom stratigraphy of core RØ1. Only species with at least 5% relative abundance are shown. Cluster analysis, based on a square root transformation of species data, and summary halobian preferences exclude all taxa where relative abundances are < 1%. Key to lithostratigraphy is given in Figure 5.7.

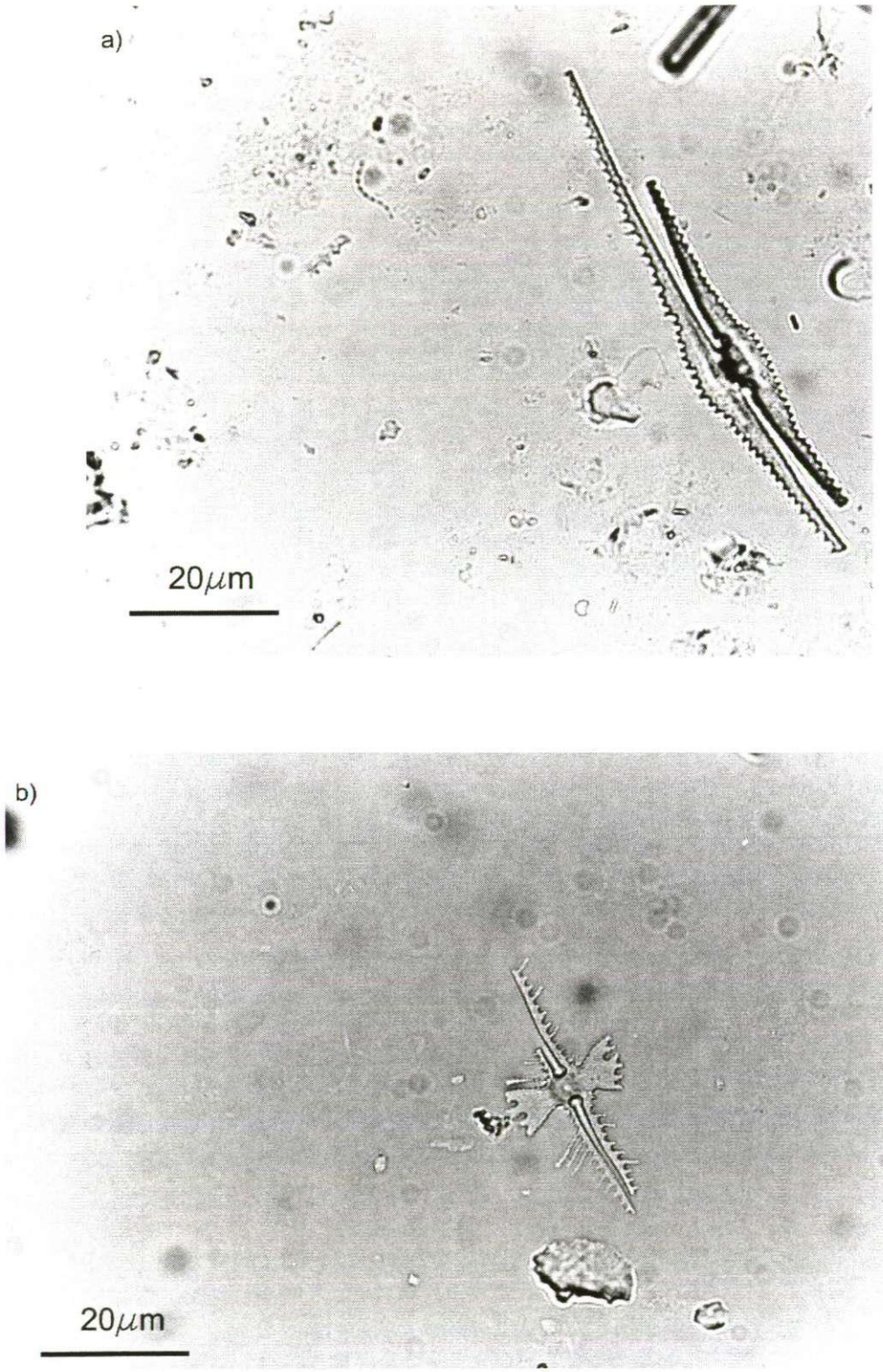

Figure 6.5. Examples of the poor preservation of diatoms in the black layer of core RØ1. a) *Cymbella aspera* (?) and b) *Navicula amphibola* (?).

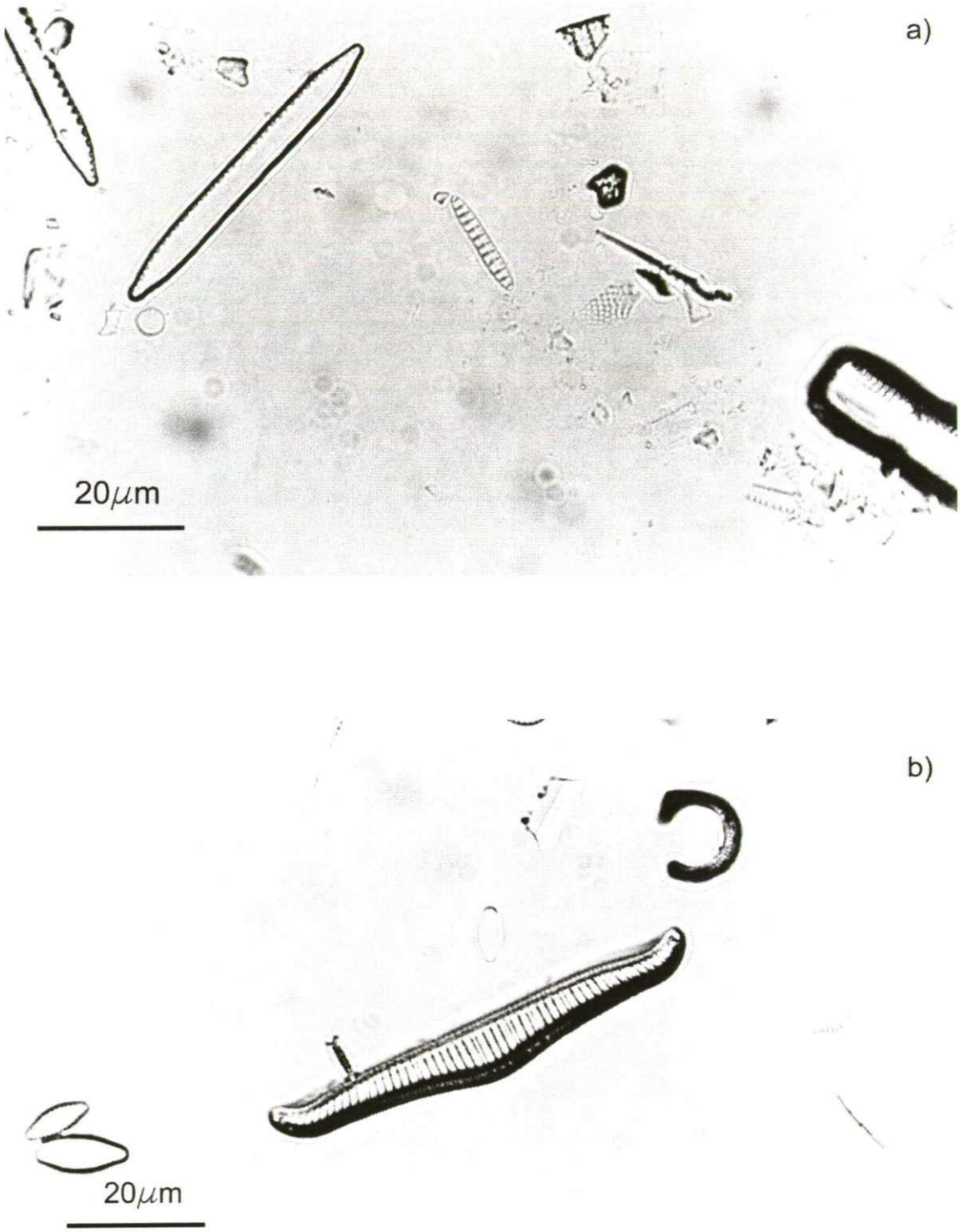

Figure 6.6. Examples of the good preservation of diatoms in the upper peaty clay unit of core RØ1. a) *Denticula subtilis, Nitzschia terrestris* and *Diploneis interrupta* (girdle view) and b) *Rhopalodia gibba*.

6.5 Oksby Enge (OEB5 and OEA)

Diatom analysis was conducted on two monolith sections from Oksby Enge, OEB5 and OEA. Samples were analysed at 8 cm resolution to provide a general overview of the biostratigraphical changes occurring at these locations. Additional samples were analysed to assess the preservation of diatoms in the black layer and the sand layer, and from stratigraphic levels that were dated.

6.5.1 OEB5

Diatom preservation was generally very good in monolith OEB5 and full counts were obtained from the majority of samples down to a depth of 1.20 m. One sample taken from the upper contact of the black layer (0.72 m depth) also returned a full count, although laboratory notes indicate that diatom preservation was very poor in this slide. In this monolith, a thin (< 0.5 cm) organic horizon is observed within the sand layer. The diatom sample from this unit (0.33 m core depth) returned a full count. Samples immediately above and below (at 0.32 and 0. 34 m core depth) returned partial counts of between 100 and 200 valves. The remaining few pilot samples taken from the sand layer were barren of diatoms.

Figure 6.7 presents the diatom stratigraphy of monolith OEB5. A total of 134 diatom taxa were identified in samples from this monolith, of which 83 were found with relative abundances of ≥ 1%. Two species remain unidentified but were found with very low (< 1%) relative abundances. Unidentified diatom taxa, with relative abundances ≥ 1%, are described in Appendix 5. Constrained cluster analysis divides the samples into four diatom assemblage zones. Zone OEB5-1 (0.75-1.20 m depth) corresponds to the lower clay unit. This zone is mainly dominated by polyhalobous and mesohalobous taxa such as *C. scutellum var scutellum, C. belgica, D. subtilis* and *Nitzschia vitrea*. High abundances of *N. cincta* – type are also noted. The diatom taxa in this zone are indicative of a marine to brackish water environment.

Zone OEB5-2 (0.695-0.75 m depth) corresponds with the black layer. Indicator species in this zone include *N. amphibola*, *P. minor* and *P. viridis*. These taxa are indicative of a fresh water environment. Zone OEB5-3 (0.25-0.695 m depth) corresponds with the upper clay unit and also includes the samples from the organic horizon within the sand layer. This zone is dominated by mesohalobous and oligohalobous taxa including *D. subtilis*, *C.*

bacillum and *Pinnularia lagerstedtii*. These taxa indicate a return to slightly brackish water conditions. The few samples analysed from the organic horizon within the sand layer, indicate that this layer is associated with predominately fresh water conditions. Zone OEB5-4 corresponds with the peaty clay layer at the top of the monolith. The diatom assemblage in this zone is again indicative of brackish to fresh water environment. Indicator taxa for this zone are *C. bacillum*, *Navicula pusilla*, and *Navicula variostriata*.

6.5.2 OEA

Diatom preservation was very good in this monolith and full counts of 300 diatom valves were obtained from most of the samples. The one sample taken from immediately below the black layer (0.66 m depth) also returned a full count. Samples from below 1.20 m depth, taken from the basal peat, were barren of diatoms and only a few broken fragments were observed in these samples.

Figure 6.8 presents the diatom stratigraphy of OEA. A total of 115 taxa were identified in samples from this monolith, of which 73 were found with relative abundances of $\geq$ 1%. Two species remain unidentified. Species C, which occurs with a maximum relative abundance of 6.3% and Species G, which occurs with a maximum relative abundance of 2.7%. Unidentified diatom taxa, with relative abundances $\geq$ 1%, are described in Appendix 5. Constrained cluster analysis divides the samples into three diatom assemblage zones. Zone OEA-1 (0.76-1.20 m depth), corresponds to the lower clay unit. This zone is dominated mainly by polyhalobous and mesohalobous taxa indicative of a marine environment. Taxa such as *C. belgica, D. minor, Cyclotella straita* and *D. interrupta* are common in this zone. Some oligohalobous taxa such as *N. cincta* – type and *Fragilaria exigua*, are also identified. Zone OEA-2 (0.45-0.76 m depth), corresponds to the upper part of the lower clay unit and with the black layer. Mesohalobous taxa dominate this zone. A number of oligohalobous – indifferent taxa such as *N. variostriata, P. borealis, P. microstauron* and *P. viridis* are associated with the sample from immediately below the black layer. These taxa are indicative of a fresh water enviornment. The diatom taxa in Zone OEA-3 (0 -0.45 m depth) are indicative of a brackish water environment. This zone is charterised by taxa such as *A. delicatula, N. cincta* – type and *N. pusilla*. This zone corresponds with the upper part of the upper clay unit and with the peaty clay at the very top of the core.

6.6 Additional fossil samples

Diatom samples were also analysed from stratigraphic levels that were ^{14}C dated in a number of additional cores, to establish the water-level relationships of the facies for the sea-level reconstruction. The determination of the 'indicative meaning' for each of these samples is discussed in Section 8.5.

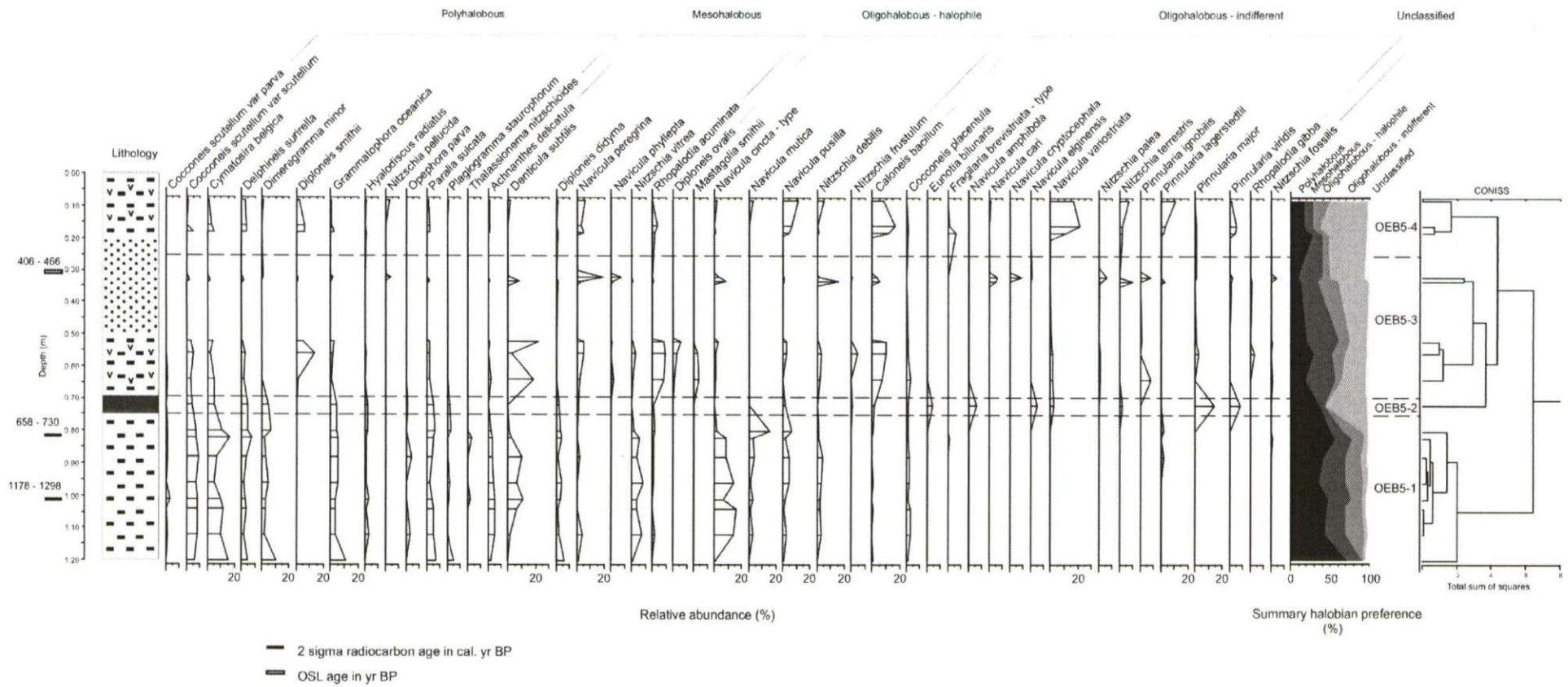

Figure 6.7. Diatom stratigraphy of core OEB5. Only species with at least 3% relative abundance are shown. Cluster analysis, based on a square root transformation of species data, and summary halobian preferences exclude all taxa where relative abundances are < 1%.Key to lithology is given in Figure 5.7

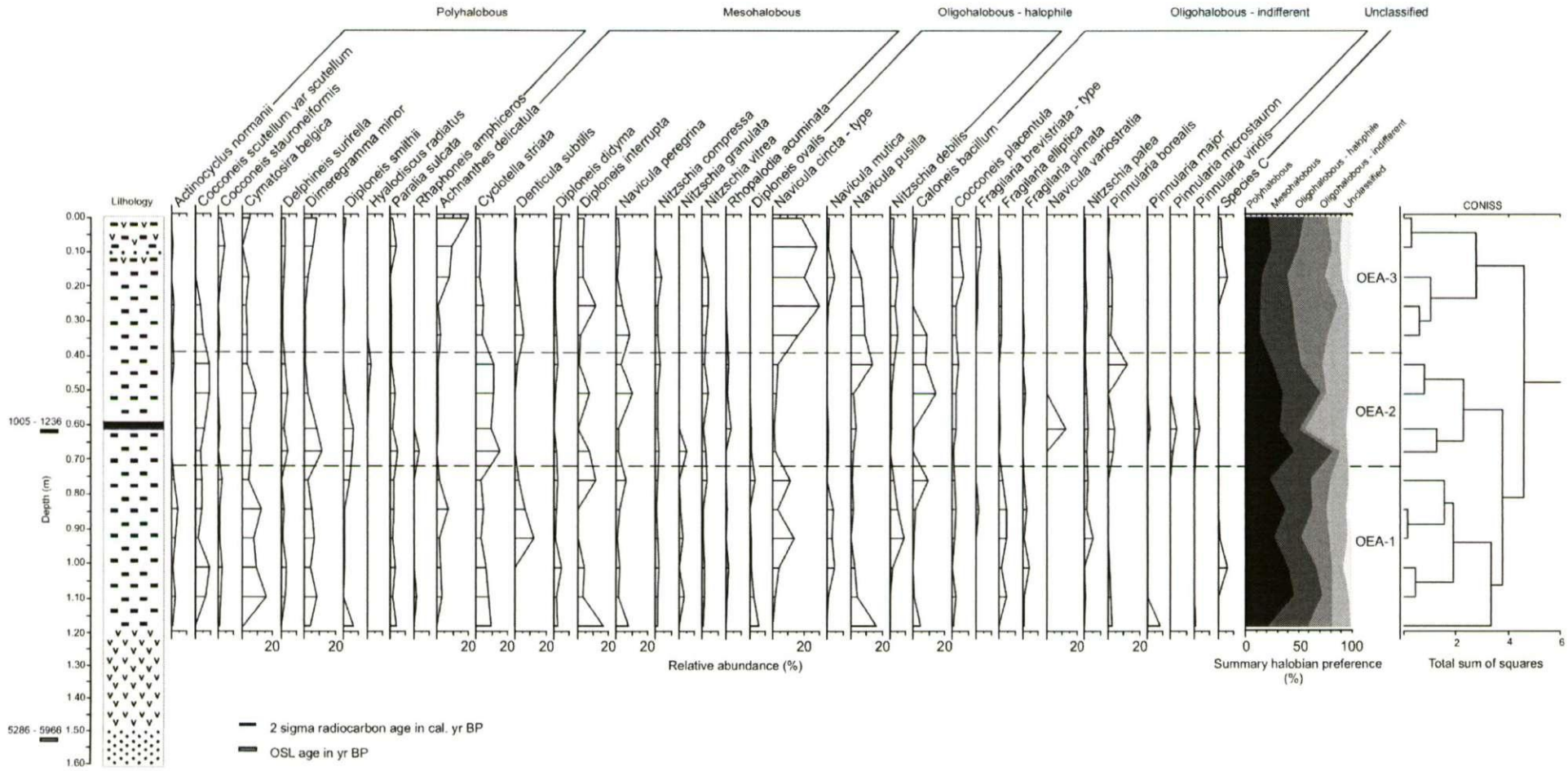

Figure 6.8. Diatom stratigraphy of monolith OEA. Only species with at least 3% relative abundance are shown. Cluster analysis, based on a square root transformation of species data, and summary halobian preferences exclude all taxa where relative abundances are < 1%. Key to lithology is given in Figure 5.7.

6.7 Chapter summary

This chapter has presented the results from the biostratigraphical investigations of several core and monolith sections from the Ho Bugt salt marshes. In general the biostratigraphy in all sections investigated has been shown to correlate well with lithostratigraphical changes. Some exceptions to this are noted, in particular in cores KE2 and RØ1, where the highest resolution analyses were conducted. Across all of the sections investigated some key points can be noted:

- Diatom preservation in many of the basal peat sections was found to be poor. Where counts were obtained, the results reflect a mainly allochtonous (transported) population.
- Diatoms were found to be best preserved in the clay units across all cores. These units are associated with polyhalobous and mesohalobous taxa, indicative of a marine environment.
- Samples analysed from cores BR9, RØ1, and monoliths OEB5 and OEA, indicate that the black layer is associated with a predominantly fresh water diatom assemblage. Results from core RØ1 suggest that these fresh water conditions were initiated sometime before the formation of this layer. High abundances of allochtonous taxa in these samples also suggest that the black layer may have been reflooded at some point in time, at least in this location.
- Whilst diatom data from the sand layer are sparse, samples from core RØ1 and monolith OEB5, indicate that the initial formation of this layer began during a time when fresh water conditions prevailed.
- Diatoms were also found to be well preserved in the upper peaty clay unit across all cores. This unit is associated with mesohalobous taxa, indicative of a brackish water environment, and consistent with present day salt marsh conditions. High resolution diatom analyses of this unit in core BR9 has indicated that some changes in the diatom assemblage occur within this layer
- Diatom stratigraphy is fairly consistent across the Ho Bugt marshes. Identified lithostratigrphical units in the various cores have similar diatom populations, suggesting that dated sections are representative.

The next chapter details the development of a diatom-based transfer function for reconstructing changes in palaeomarsh-surface elevation in a number of the cores investigated.

Chapter 7

The development of a diatom-based transfer function

Results presented in Chapter 4 demonstrate that elevation exerts a strong, independent and statistically significant influence on modern diatom distributions in the Ho Bugt embayment. This chapter details the development of a series of diatom-based transfer functions (DBTFs) using regression models, to reconstruct changes in palaeomarsh-surface elevation based on this strong relationship. Regression models are initially created using Maximum Likelihood (ML), Weighted-Averaging (WA) and Weighted-Averaging Partial Least Squares (WA-PLS) and also by use of the Modern Analogue Technique (MAT). The performance and predictive abilities of each of the models is discussed with the aim of determining whether robust transfer function models can be derived from the Ho Bugt training set. The previous chapter highlighted the presence and high abundance of several allochthonous taxa in many of the core sections investigated. Such taxa are likely to present problems in the application of any transfer function. The second part of this chapter therefore explores the development of a transfer function which excludes allochthonous diatom taxa.

7.1 Justification for transfer function construction

Chapter 4 presented the results of a detailed investigation into the modern salt-marsh environment within the Ho Bugt embayment. A thorough exploration of the modern diatom and environmental data was achieved through the use of several ordination techniques. Two data sets were analysed in ordinations: DataSetA (100 samples, 8 environmental variables) and DataSetB, which includes the Kjelst Enge samples (127 samples, 3 environmental variables). For both data sets, elevation was shown to exert a strong, independent and statistically significant influence on modern diatom distributions, suggesting that DBTFs can be developed to reconstruct changes in palaeomarsh-surface elevation. The analysis of DataSetB highlighted the anomalous nature of the samples from Kjelst Enge and suggested that careful consideration should be given as to whether these samples should be included in any training set and subsequent transfer function development. This point is discussed further below.

7.2 Inclusion of Samples

After careful consideration and exploratory analysis it was decided to exclude the Kjelst Enge samples from the training set. These samples are excluded for the following reasons:

- The Kjelst Enge transect is dominated by polyhalobous (and often allochthonous) diatom taxa, even at high elevations (Figure 4.5).
- The relatively high abundance of several oligohalobous diatom taxa (e.g., *Navicula rhynchocephala*, *Stauroneis phoenicenteron*) at low elevations (samples KE21-KE27) is linked to the proximity of these samples to the nearby *Storbæk* drainage channel and complicates the species-environment relationship (Figures 4.2 and 4.5).
- Unconstrained cluster analysis of the entire modern diatom data demonstrates that samples from similar elevation ranges at Kjelst Enge and Langli are associated with very different diatom assemblages (Figure 4.19).
- DCA analysis of the Kjelst Enge diatom data (Section 4.5.3, pp.123) shows all 27 samples to be associated with similar diatom taxa (Figure 4.28), despite spanning a relatively large elevation range (0.73 – 1.86 m DNN) and covering a range of salt-marsh environments (Table 4.1).
- Early experimentation with transfer function development (Szkornik et al., 2005) suggested that the inclusion of the Kjelst Enge samples led to erroneous predictions for many of the core samples. This was primarily because of the presence of fresh water taxa (mainly *Navicula rhynchocephala*) at low elevations in the modern Kjelst Enge samples (Figure 4.5). Although this was not a problem for cores where such taxa were absent (e.g., core KE2; Szkornik et al., 2006) problems arose when the transfer function was applied to cores where such taxa were present (e.g., Røgel core RØ1).

In addition, the screening process implemented in Chapter 4 identified three outlier samples, LN31, MO1 and LS28, with extreme environmental characteristics (identified through PCA). These samples are likely to have anomalous diatom assemblages associated with their extreme environmental characteristics and are therefore excluded from transfer function development.

7.3 Inclusion of species

As was the case in earlier statistical analysis (Chapter 4) species are only included in transfer function development if a) their relative abundance is ≥ 1%, and b) the species is present in more than one sample. In coastal environments, species with relative abundances of < 1% are likely to be allochthonous and are not often used in interpretation (Nelson and Kashima, 1993). In this study allochthonous taxa remain a major problem both as a result of their presence in the modern training set and also due to their high relative abundance in many of the core sections investigated (Chapter 6). Attempts to develop a DBTF which excludes allochthonous taxa, and the problems associated with such an approach, are discussed below in Section 7.6.3.

7.4 Inclusion of environmental data

All elevation data included in training set development is untransformed. Results of Andersen-Darling normality tests (Table 4.3) illustrated that the elevation data used in this study are normally distributed.

7.5 Linear versus unimodal models

Statistical methods used to develop DBTFs fall into two categories: linear and unimodal (Birks, 1995). The ordination technique of Detrended Canonical Correspondence Analysis (DCCA) was used as a tool for determining which type of model was most suitable for use in subsequent transfer function development. Where gradient lengths are short (< 2 SD), the majority of taxa are behaving monotonically along the environmental gradient and linear models are usually more appropriate. Where gradient lengths are long (> 2 SD) unimodal models of regression and calibration are deemed more appropriate (Birks, 1995). A DCCA, using elevation as the sole constraining environmental variable (ter Braak and Juggins, 1993; Birks, 1995), was performed on the entire data set (97 samples and 151 taxa) to establish gradient length in SD units. An axis one gradient length of 3.5 SD was obtained (Table 7.1) indicating the suitability of unimodal regression models.

Axis	1	2	3	4
Eigenvalue	0.410	0.263	0.135	0.071
Lengths of gradient	**3.539**	**2.557**	**2.153**	**1.617**
Species-environment correlations	0.943	0.000	0.000	0.000
Cumulative percentage variance: of species data	13.7	22.5	27.1	29.5

Table 7.1. Results of a DCCA performed on a data set of 97 samples, 156 taxa, using elevation as the sole constraining environmental variable (ter Braak and Juggins, 1993; Birks, 1995).

7.6 Development of DBTFs for elevation

Unimodal models were initially developed for the entire data set (97 samples, 151 taxa) based on ML, WA and WA-PLS regression models. An additional model was developed using the MAT which does not have an underlying statistical model (Birks, 1995). Models were developed using both untransformed and square-root transformed species data. A square-root transformation of species data is often used when developing regression models to stabilise the variances (Prentice, 1980). For all models 'jack-knifing' was used to cross-validate the training set. Jack-knifing is the simplest method of cross-validation and gives a good measure of the overall predictive abilities of the training set (ter Braak and Juggins, 1993). All prediction errors in this study are therefore expressed as 'cross-validated' ($_{jack}$) estimates. All models were developed using the computer programme C^2 version 1.4.3 (Juggins, 2003 – 2006).

The performance of the various regression models was assessed in terms of the root-mean squared error of prediction ($RMSEP_{jack}$) and the maximum bias (max $bias_{jack}$). The most appropriate model is one with a low cross-validated RMSEP, a measure of the random error in the model (Altman and Bland, 1983, Birks, 1998), and a relatively low maximum bias (ter Braak and Juggins, 1993). Many studies (e.g., Horton et al., 2003; 2006) commonly quote the coefficient of determination (r^2) as an important performance statistic. However, this statistic is dependent on the range of the observed environmental gradient and is not considered as independent as the $RMSEP_{jack}$ and max $bias_{jack}$ (Oksanen et al., 1990; Altman and Bland, 1983; Birks, 1998). The r^2 is most important when comparing models for different environmental variables (Gasse et al., 1995). In addition to selecting a model with the best performance statistics, it was also necessary to follow the principle of parsimony in statistics and select the 'minimum adequate model' (Birks, 1998, *sensu* Crawley, 1993).

Table 7.2 highlights the performance of the ML, WA, WA-PLS and MAT regression models initially developed for the full data set (97 samples, 151 taxa). Most WA-PLS and MAT models perform slightly better when a square-root transformation of species data (√species) is used, although the differences are minimal. WA models perform best when untransformed species data are used. ML, WA-PLS (two components) and MAT models are shown to perform best when $RMSEP_{jack}$ and max $bias_{jack}$ statistics are compared. The WA-PLS √species (two component) model performs slightly better then the WA-PLS (two component) model when $RMSEP_{jack}$ are compared (0.127 m cf 0.129 m respectively), but has a slightly higher max $bias_{jack}$ (0.177 m cf 0.127 m). On this basis, and because the improvement on $RMSEP_{jack}$ is only minimal, the model using untransformed species data is considered most appropriate.

ML and WA-PLS (two components) were selected as the models to develop further on the basis of their low $RMSEP_{jack}$ (0.147 m and 0.129 m, respectively) and their relatively low maximum $bias_{jack}$ (0.182 m and 0.127 m, respectively) values. Although MAT also performs very well, this method has come under criticism in the recent literature because of issues related to spatial autocorrelation (Telford and Birks, 2005). Spatial autocorrelation describes the tendency of sites located close to one another to resemble each other ecologically (Legendre and Fortin, 1989; Legendre, 1993; Telford and Birks, 2005). Although this issue has been considered for sometime in ecology and biogeography (e.g., Griffith, 1987; 1992; Legendre and Fortin, 1989; Legendre, 1993) it has only recently been acknowledged as a major issue in transfer function development. Telford and Birks (2005) and Telford (2006) argue that MAT is particularly sensitive to this problem and that models based on unimodal methods, such as ML and WA-PLS, are more robust. For these reasons the MAT transfer function is not developed further in this study.

Model	Apparent RMSE (m)	Apparent r^2	Max Bias (m)	$RMSEP_{jack}$ (m)	r^2_{jack}	Max Bias $_{jack}$ (m)
ML	0.126	0.937	0.080	**0.147**	**0.909**	**0.182**
WA (Inverse)	0.146	0.907	0.171	0.159	0.891	0.235
WA (Inverse) √ Species	0.171	0.872	0.339	0.186	0.849	0.411
WA (Classical)	0.153	0.907	0.077	0.166	0.892	0.139
WA (Classical) √ Species	0.183	0.872	0.229	0.193	0.851	0.306
WA TOL (Inverse)	0.131	0.925	0.174	0.178	0.864	0.345
WA TOL (Inverse) √ Species	0.156	0.895	0.309	0.224	0.780	0.512
WA TOL (Classical)	0.136	0.925	0.122	0.177	0.865	0.277
WA TOL (Classical) √ Species	0.164	0.895	0.249	0.229	0.781	0.432
WA-PLS (component 1)*	0.146	0.907	0.172	0.159	0.891	0.236
WA-PLS (component 2)	**0.106**	**0.951**	**0.104**	**0.129**	**0.928**	**0.127**
WA-PLS (component 3)	**0.092**	**0.963**	**0.092**	**0.131**	**0.926**	**0.125**
WA-PLS (component 4)	**0.079**	**0.973**	**0.066**	**0.138**	**0.918**	**0.120**
WA-PLS (component 5)	**0.071**	**0.978**	**0.066**	**0.147**	**0.907**	**0.129**
WA-PLS (component 1)* √ Species	0.0.172	0.872	0.355	0.187	0.849	0.424
WA-PLS (component 2) √ Species	**0.103**	**0.954**	**0.115**	**0.127**	**0.930**	**0.177**
WA-PLS (component 3) √ Species	**0.081**	**0.971**	**0.110**	**0.135**	**0.921**	**0.200**
WA-PLS (component 4) √ Species	**0.066**	**0.981**	**0.067**	**0.149**	**0.904**	**0.217**
WA-PLS (component 5) √ Species	0.055	0.987	0.036	0.161	0.889	0.162
MAT (mean)				**0.134**	**0.930**	**0.328**
MAT (weighted-mean)				**0.126**	**0.938**	**0.286**
MAT (mean) √ Species				**0.123**	**0.939**	**0.305**
MAT (weighted-mean) √ Species				**0.118**	**0.944**	**0.286**

Table 7.2. Performance of ML, WA and WA-PLS (unimodal) and MAT regression models using both untransformed and square-root transformed species data (√ Species). Best performing models (models with $RMSEP_{jack} < 0.15$) are highlighted in bold. * WA-PLS one component reduces to simple WA (Birks, 1995).

7.6.1 Development of a ML regression model

The performance of the initial ML regression model (based on 97 samples and 151 taxa) is shown in Table 7.2 and displayed graphically in Figure 7.1. A relatively strong relationship is noted between observed and ML predicted elevation. This is confirmed by the high r^2_{jack} value (0.909, Table 7.2). Examination of the observed versus ML predicted elevation plot (Figure 7.1a) demonstrates this strong relationship. Increased scatter is noted at both ends of the environmental gradient (i.e. for samples with both low and high elevations), suggesting that the model performs less well here. This is confirmed by the residual plot (Figure 7.1b) which shows higher residual values for samples from the highest and lowest elevations. The residual plot also indicates that there may be outlier samples, with high residual values, within this model. Within environmental data sets there are often samples which show a poor relationship to the environmental variable of interest (Jones and Juggins, 1995). These outlier samples can have a strong influence within the model and can significantly reduce the predictive abilities of the transfer function (Martens and Naes, 1989). Further screening to remove these samples is therefore needed and is likely to improve the predictive abilities of the dataset.

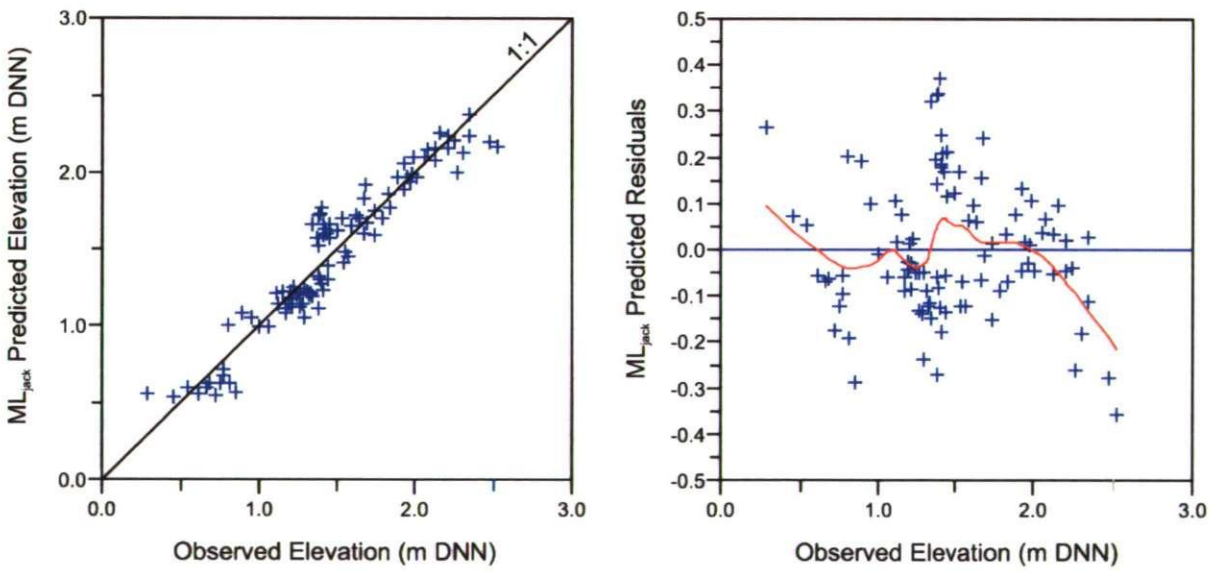

Figure 7.1 Scatter plots showing a) observed elevation versus model predicted elevation and b) residual plot, using a ML model based on 97 samples and 151 taxa. Trend lines are 1:1 and LOWESS smooth fits (stiffness = 0.4).

Removal of outlying samples

Outlier samples were determined where the absolute residual (observed elevation minus ML predicted elevation) was found to be greater than one standard deviation of the observed elevation (Jones and Juggins, 1995). Although several samples were found to have reasonably high residuals (e.g., samples MO2, ST10), no samples were found with a residual greater in absolute value than 0.48, the standard deviation of the observed elevation (m DNN). All samples are therefore retained in the model and no further improvements were made. The final performance of the ML model is therefore shown in Table 7.2.

7.6.2 Development of a WA-PLS regression model

The performance of the initial WA-PLS (two components) regression model (based on 97 samples and 151 taxa) is shown in Table 7.2 and displayed graphically in Figure 7.2. A very strong relationship is noted between observed and WA-PLS predicted elevation and is confirmed by the high r^2_{jack} value (0.926). Examination of the observed versus WA-PLS predicted elevation plot (Figure 7.2a) demonstrates this strong relationship. The WA-PLS regression model appears to perform well along the entire length of the gradient. The majority of samples lie close to the 1:1 line, even at the high and low ends of the environmental gradient. Examination of the residual plot (Figure 7.2b) confirms this point. The LOWESS smooth fit is not as deflected at the extreme ends of the gradient as in the ML model (Figure 7.1b). This suggests that the WA-PLS model performs much better than the ML model at the extremes of the environmental gradient (i.e. for samples with the highest and lowest elevations).

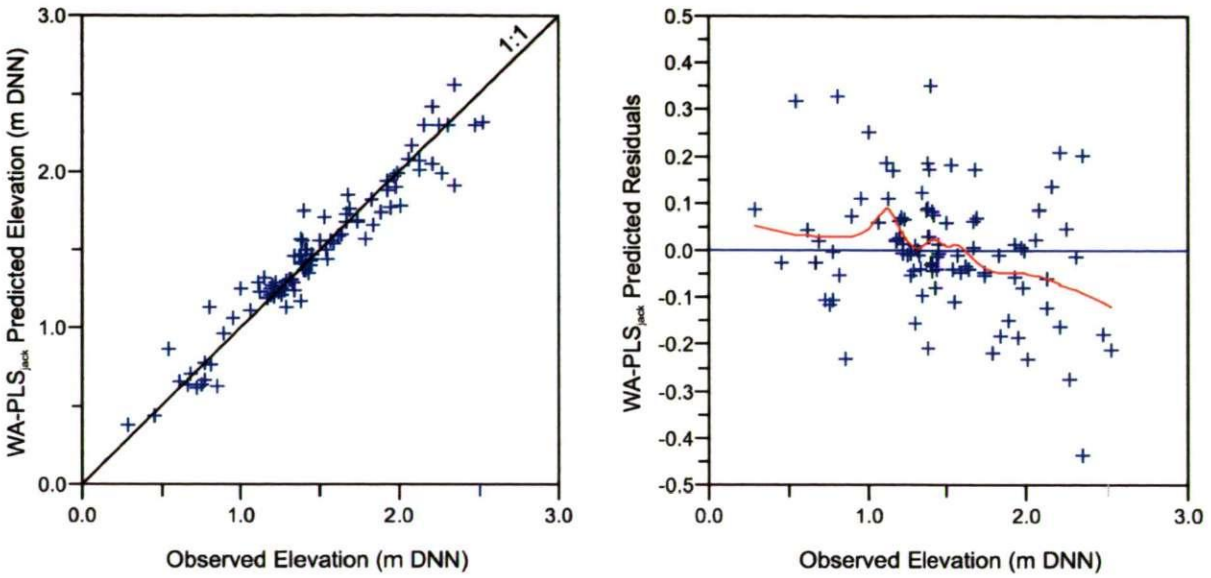

Figure 7.2 Scatter plots showing a) observed elevation versus model predicted elevation and b) residual plot, using a WA-PLS (two components) model based on 97 samples and 151 taxa. Trend lines are 1:1 and LOWESS smooth fits (stiffness = 0.4).

Removal of outlying samples

As with the ML model, outlying samples were determined where the absolute residual was found to be greater than one standard deviation of the observed elevation (Jones and Juggins, 1995). No samples were found with a residual greater in absolute value than 0.48, the standard deviation of the observed elevation (m DNN). Sample MO5 was found to have a residual value close to this (-0.44) and plots as a clear outlier on the residual plot (Figure 7.2b). Sample MO5 contains a high abundance of *Achnanthes minutissima* (39.5%) which is 16% higher than any other sample in the training set. *A. minutissima* is well represented in the training set in samples which show a stronger relationship to elevation. Removal of this sample is therefore unlikely to have any adverse affect on the species coefficients. Re-running the WA-PLS regression model with this sample removed resulted in a slight improvement in the performance statistics. Sample MO5 was therefore excluded from the final WA-PLS model. Following removal of this sample, the species data was re-checked to ensure all species still fulfilled the aforementioned abundance criteria (Section 7.3). A summary of the final performance of the WA-PLS model is shown in Table 7.3. The WA-PLS two component model is still found to perform the best. The three component model also performs very well but the addition of this component to the model does not result in any reduction in the $RMSEP_{jack}$. Ter Braak and Juggins (1993) and Brooks and Birks (1999) argue that a component should only be considered 'useful' if the addition of that component to the model results in a reduction of the $RMSEP_{jack}$ of 5% or more of the $RMSEP_{jack}$ for the one component model.

Model	Apparent RMSE (m)	Apparent r^2	Max Bias (m)	$RMSEP_{jack}$ (m)	r^2_{jack}	Max Bias $_{jack}$ (m)
WA-PLS (1 component)	0.141	0.912	0.180	0.153	0.897	0.245
WA-PLS (2 components)	**0.100**	**0.955**	**0.097**	**0.122**	**0.934**	**0.109**
WA-PLS (3 components)	0.084	0.968	0.085	0.122	0.934	0.118
WA-PLS (4 components)	0.071	0.977	0.058	0.125	0.931	0.102
WA-PLS (5 components)	0.062	0.983	0.061	0.131	0.925	0.123

Table 7.3. Performance of the final WA-PLS regression model based on 96 samples and 151 taxa. Sample MO5 is removed. Best performing model (WA-PLS 2 components) is highlighted in bold.

Given that the WA-PLS model performs better than the ML model when $RMSEP_{jack}$ and max $bias_{jack}$ statistics are compared (Table 7.2 and 7.3), and the WA-PLS model is seen to perform better at the ends of the environmental gradient (Figures 7.1a and 7.2a), the WA-PLS (two component) model is chosen as the final transfer function model for the full training set. The development of a transfer function which excludes allochthonous taxa is explored in the next sections of this chapter.

7.6.3 Development of regression models which exclude allochthonous taxa

Initial application of the ML and WA-PLS regression models to the core and monolith sections analysed in this study, suggested that the presence, and high abundance, of allochthonous taxa in many of the core sections may be a potential problem. This is particularly true for the black layer in Røgel core RØ1. Here a high abundance of allochthonous taxa (Section 6.4 and Figure 6.4) such as *Paralia sulcata, Cocconeis placentula* and *Dimeregramma minor*, potentially the result of a re-flooding event, coupled with the poor preservation of many *in situ* freshwater taxa, is likely to lead to erroneous transfer function predictions. For these reasons attempts were made to develop a diatom-based transfer function which excludes all allochthonous taxa. Although $RMSEP_{jack}$ and max $bias_{jack}$ statistics for these models (not shown) suggested that they performed very well, and were comparable to those for the full training set, application of these models to the various core sections greatly increased the number of fossil taxa without a modern analogue (the 'no analogue problem'). For example, for core KE2, application of the transfer function which excludes allochthonous taxa increased the number of fossil taxa

without a modern analogue from 29 to 44% (Section 8.2). These problems are further illustrated in Sections 8.2 – 8.5. Such results were considered unacceptable and the development of a transfer function which excludes allochthonous taxa was not further pursued. Further discussion on the problems of allochthonous taxa encountered throughout this study can be found in Section 9.9.

7.7 Comparing the performance with published models

Compared to other microfossils commonly used to develop transfer functions for reconstructing changes in palaeomarsh-surface elevation and relative sea level, such as foraminifera, the development of diatom-based transfer functions has been more limited. Studies by Zong and Horton (1998, 1999) were the first to use the relationship between diatoms and elevation to develop diatom-based transfer functions for reconstructing changes in palaeomarsh-surface elevation and relative sea level. More recently, diatom-based transfer functions have been developed to assess changes in palaeomarsh-surface elevation and relative sea-level to provide insights into the earthquake deformation cycle (e.g., Hamilton and Shennan 2005) and to assess palaeoseismic changes along the Pacific coast of Japan (Sawai et al., 2004). Other studies have compared the relative performance of foraminifera, testate amoebae and diatoms as sea-level indicators by investigating the potential of multiproxy transfer function models (Gehrels et al., 2001). The relative performance of these published models is compared with those produced in this study in Table 7.4.

Examination of the data presented in Table 7.4 implies that the models developed in this study compare favourably in terms of $RMSEP_{jack}$ with those published in the literature. Comparison of max $bias_{jack}$ statistics is not possible because the majority of authors do not state this. Although the performance statistics indicate that the models developed in this study perform equally as well as those already published, the true predictive abilities of a model cannot be fully assessed until it is applied to fossil data. The application of the final WA-PLS transfer function developed here is applied to data in fossil cores in the next chapter.

Author(s)	Study area	Regression model	RMSEP (m)	r^2	Average tidal range (m)
Hamilton and Shennan (2005)	Cook Inlet, Alaska	Full data set = WA-PLS (2 components)	0.214	0.75	8.8
		SWLI* > 180 = WA-PLS (3 components)	0.078	0.89	
		SWLI > 225 = WA-PLS (3 components)	0.023	0.93	
Zong and Horton (1998)	UK regional	WA (Tol) Inverse	0.195	0.71	5.4
		WA (Tol) Classical	0.214	0.72	
Gehrels et al (2001)	UK regional	WA-PLS	0.054	0.78	5.7
Sawai et al (2004)	Pacific coast, Japan	WA-PLS (2 component)	0.29	0.84	~ 1.7
Szkornik (this study)	Ho Bugt, Denmark	WA-PLS (2 components)	0.122	0.934	~ 1.5

Table 7.4. Comparison of the performance of published diatom-based transfer functions for reconstructing changes in palaeomarsh-surface elevation and relative sea level with that produced by this study. * Standardised Water Level Index (SWLI) is used to enable elevation data to be compared between sites with different tidal ranges (Horton 1997). All studies use jack-knifing as the method of cross-validation.

7.8 Chapter Summary

This chapter has detailed the development of a series of diatom-based transfer functions for reconstructing changes in palaeomarsh-surface elevation, based on the strong, independent and statistically significant relationship between diatoms and elevation demonstrated in Chapter 4. Unimodal models were initially developed for the entire data set (97 samples, 151 taxa) based on ML, WA and WA-PLS regression. An additional model was developed using the Modern Analogue Technique (MAT) but was not developed further due to issues with spatial autocorrelation. ML and WA-PLS (2 component) models were found to perform best when $RMSEP_{jack}$ and max $bias_{jack}$ statistics were compared. The WA-PLS (two components) model was selected as the final transfer function model for the following reasons:

- $RMSEP_{jack}$ and max $bias_{jack}$ statistics for the final WA-PLS model (Table 7.3) are slightly better than for the ML model (Table 7.2)

- The WA-PLS model is seen to perform best at the extremes of the environmental gradient (i.e. for samples with very high or very low elevations) (Figures 7.1a and 7.2a). This is especially important in this study where samples from fresh water basal peats (Section 8.5) are likely to lie close to the upper extreme or beyond the range of the measured environmental gradient.

The second part of this chapter explored the development of regression models which exclude allochthonous diatom taxa. However, exploratory application of such methods to the fossil cores (Sections 8.2 – 8.5) resulted in a large increase in the number of fossil taxa with no modern analogue. For these reasons the development of a transfer function which excludes allochthonous taxa was not further pursued.

In the next chapter the final WA-PLS transfer function model (Table 7.3) is applied to a series of cores to reconstruct changes in palaeomarsh-surface elevation. Following construction of reliable age-depth models (Section 8.7), these changes are linked to former local water level and the data are plotted as a series of time-height diagrams of local water-level change. These water-level curves are integrated with the results of litho- and biostratigraphical investigations in Chapter 9 to explore the evolution of the Ho Bugt embayment.

Chapter 8

Reconstruction of local water-level changes

In the previous chapter, a WA-PLS transfer function was developed based on the strong and significant relationship between diatoms and elevation established in Chapter 4. In this chapter, diatom data from the various core sections analysed (Chapter 6) are calibrated using the WA-PLS transfer function to reconstruct changes in palaeomarsh-surface elevation. The reliability of these reconstructions is assessed via the use of goodness of fit and analogue statistics. Following development of age-depth models using the available ^{210}Pb, ^{137}Cs, ^{241}Am, ^{14}C and OSL ages, the palaeomarsh-surface records are linked to local water level and the data are plotted in a series of time-height diagrams of local water-level change. Reconstructions from the past two centuries are compared with the observations from the nearby tide gauge at Esbjerg.

8.1 Methodology

The final WA-PLS transfer function is presented in Table 7.3. In the following sections of this chapter, diatom data from the various core sections analysed (KE2, BR9, RØ1) are calibrated using this WA-PLS transfer function. For each diatom sample analysed the WA-PLS transfer function calculates the palaeomarsh-surface elevation at which the sample was formed (known as the 'indicative meaning'). The indicative meaning of a sample describes the vertical relationship between the environment in which it accumulated and a contemporary reference water level, in this case DNN (Shennan, 1982; 1986; van de Plassche, 1986). For all reconstructions, sample-specific root mean squared errors of prediction for each of the fossil samples are estimated by bootstrapping (1000 bootstrap cycles) using the computer programme C^2 (Birks et al., 1990a; Line et al., 1994). For the purposes of sea-level reconstructions, these errors are treated as the 'indicative range' (Shennan, 1982, 1986a, 1986b).

8.1.1 Inclusion of species and samples

Only taxa with relative abundances $\geq 1\%$ and present in more than one sample in each core section are used in calibration. This is to ensure consistency with the cut-off levels defined for the modern training set (Section 3.8.2). Only samples where counts of at least 250 valves were obtained are included in the calibration.

8.1.2 Assessing the reliability of the reconstructions

The reliability of each of the reconstructions was assessed via 'goodness of fit' and 'analogue' statistics (Birks et al., 1990a, Birks, 1998). Goodness of fit statistics for each of the fossil samples were assessed by fitting these samples passively into ordination space (e.g., Laird et al., 1996). A CCA ordination was run using elevation as the sole constraining environmental variable in order to calculate the squared residual distance of each fossil sample from the elevation axis (Birks, 1990a; Laird et al., 1996). Following Birks et al. (1990a) and Laird et al (1996) fossil samples with residual distances larger than the residual distance of the extreme 10% of the training set (samples with squared residual length > 5.75) were considered to have a 'poor fit' and samples with residual distances larger than the residual distance of the extreme 5% of the training set (samples with squared residual length > 6.2) were considered to have a 'very poor' fit. All other samples were considered to have a 'good fit'.

The MAT was used in addition to the goodness-of-fit statistics as a second independent method for assessing the reliability of the reconstructions. Although the MAT can be used to model relationships in the modern training set, as explored in Chapter 7 of this thesis (Table 7.2), it is used here as a tool for comparing the similarity (or dissimilarity) between fossil and modern samples. MAT compares numerically the assemblages in each of the fossil samples with assemblages in the modern training set (Birks, 1995). If fossil samples have good modern analogues in the training set then the reconstructions are likely to be more reliable (ter Braak, 1995). MAT was performed in the computer programme C^2, using the squared chord distance as the dissimilarity coefficient and based on the 10 closest modern analogues (Prentice, 1980; Overpeck et al., 1985). The MAT produces a series of dissimilarity values for percentiles of the modern training set and a minimum dissimilarity coefficient (Min. DC), measured as the squared chord distance, for each of the reconstructed fossil samples. Following Birks et al. (1990a), Bartlein and Whitlock (1993) and Lotter (1998), cut-off values for 'no close' and no 'good analogue' are based on the second (27.77) and fifth percentiles (36.09) of the distribution of the dissimilarities of samples in the modern training set. Fossil samples with squared chord distances greater than these values are defined as having 'no close' and 'no good' analogue respectively.

Although there are several examples of the use of such techniques to evaluate reconstructions within palaeolimnology (e.g., Birks et al., 1990a, Lotter et al., 1998, Juggins et al., 1994), there are few examples of the employment of such techniques to assess reconstructions in the sea-level literature. Some exceptions to this include the work of Edwards and Horton (2002) and Hamilton and Shennan (2005a), who use the MAT to evaluate their reconstructions. It is, however, important to note that although these statistical techniques offer one way of evaluating a reconstruction, they do not necessarily provide the only answer. One of the most powerful ways to assess the reliability of a reconstruction is to compare the reconstruction with historical or observational records (Birks and Birks, 2006). For sea-level reconstructions this commonly involves comparison with tide-gauge records (e.g., Gehrels et al., 2002; 2005). These comparisons are explored in the latter parts of this chapter (Section 8.8).

8.2 Palaeomarsh-surface reconstruction of core KE2 (Kjelst Enge)

Diatom data in core KE2 from the salt marsh at Kjelst Enge were calibrated using the WA-PLS transfer function. The resulting palaeomarsh-surface reconstruction is presented in Figure 8.1. Reconstructed palaeomarsh-surface elevations range from 1.27 – 2.2 m and sample-specific standard errors of prediction for the fossil samples range from 0.124 – 0.151 m (Table 8.1). Highest sample-specific errors are for those samples with the highest reconstructed elevations.

In general, the reconstruction appears to correspond well with changes in the litho- and biostratigraphy. The lowest reconstructed elevations are found to correspond with diatom zone KE-1 and the lower clay unit. Here, reconstructed elevations are around 1.3 m DNN. Around 0.6 m core depth a significant increase in oligohalobous – indifferent and halophobous diatom taxa is noted, which indicates a 'freshening' of the salt-marsh environment. This change is also reflected in the reconstruction. Higher salt-marsh surface elevations (up to 2.2 m) are found to correspond with the increase in oligohalobous – indifferent taxa between 0.62 and 0.42 m core depth. At the very top of the core, reconstructed elevations decrease once again to c. 1.5 m and correlate with a return to more brackish water conditions as indicated by the diatom record and the lithostratigraphy.

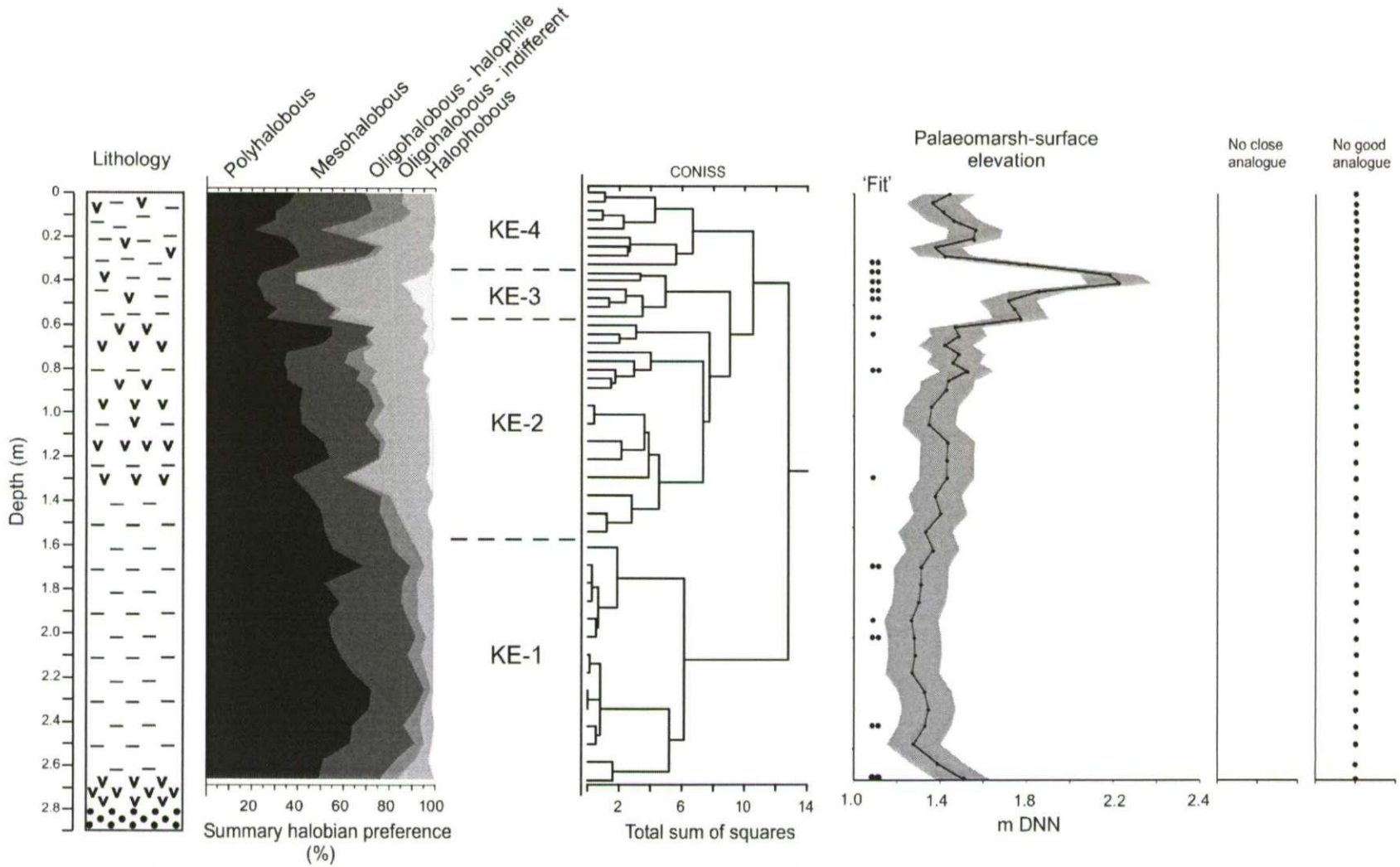

Figure 8.1. Palaeomarsh-surface reconstruction of KE2 (Kjelst Enge) alongside lithology, summary halobian groups and diatom zones. Cluster analysis and summary halobian groups only include taxa with at least 1% relative abundance. The full diatom record for this core is presented in Chapter 6. Errors on the reconstruction are sample-specifc bootstrap standard errors. Fossil samples with a poor (.) and very poor (..) fit to the modern diatom data, and fossil samples with no good modern analogue are indicated. Key to lithology is presented in Figure 6.1.

Sample Depth (m)	WA-PLS predicted palaeomarsh-surface elevation (m) (Indicative meaning)	Bootstrap standard error (m) (Indicative range)	Goodness of fit	Min DC	Analogue
0.02	1.44	0.124	Good	62.763	No Good
0.06	1.362	0.124	Good	61.236	No Good
0.10	1.409	0.124	Good	55.096	No Good
0.14	1.460	0.125	Good	59.797	No Good
0.18	1.561	0.127	Good	67.427	No Good
0.22	1.552	0.127	Good	82.384	No Good
0.26	1.372	0.125	Good	81.482	No Good
0.30	1.420	0.126	Good	81.819	No Good
0.34	1.825	0.129	Very Poor Fit	83.315	No Good
0.38	2.177	0.138	Very Poor Fit	89.966	No Good
0.42	2.226	0.151	Very Poor Fit	74.430	No Good
0.46	1.847	0.132	Very Poor Fit	76.010	No Good
0.50	1.710	0.134	Very Poor Fit	90.176	No Good
0.54	1.742	0.129	Good	82.807	No Good
0.58	1.77	0.130	Very Poor Fit	81.283	No Good
0.62	1.465	0.126	Good	77.618	No Good
0.66	1.484	0.129	Poor Fit	81.336	No Good
0.70	1.420	0.128	Good	77.449	No Good
0.74	1.486	0.126	Good	75.378	No Good
0.78	1.456	0.125	Good	81.043	No Good
0.82	1.522	0.126	Very Poor Fit	83.493	No Good
0.86	1.432	0.125	Good	82.576	No Good
0.90	1.426	0.125	Good	85.388	No Good
0.98	1.358	0.125	Good	78.808	No Good
1.06	1.346	0.125	Good	74.187	No Good
1.14	1.433	0.127	Good	85.396	No Good
1.22	1.429	0.127	Good	85.191	No Good
1.30	1.429	0.128	Poor Fit	87.609	No Good
1.38	1.375	0.125	Good	75.700	No Good
1.46	1.401	0.126	Good	67.405	No Good
1.54	1.330	0.126	Good	61.990	No Good
1.62	1.366	0.125	Good	62.991	No Good
1.70	1.311	0.127	Very Poor Fit	67.438	No Good
1.78	1.310	0.125	Good	65.389	No Good
1.86	1.300	0.126	Good	61.217	No Good
1.94	1.267	0.126	Poor Fit	67.452	No Good
2.02	1.279	0.126	Very Poor Fit	68.130	No Good
2.10	1.282	0.126	Good	58.808	No Good
2.18	1.270	0.126	Good	60.458	No Good
2.26	1.327	0.126	Good	45.425	No Good
2.34	1.346	0.126	Very Poor Fit	61.401	No Good
2.42	1.328	0.126	Very Poor Fit	68.748	No Good
2.50	1.277	0.126	Good	61.685	No Good
2.58	1.383	0.125	Good	63.794	No Good
2.66	1.515	0.126	Very Poor Fit	61.190	No Good

Table 8.1. Summary of the WA-PLS predictions (m) and bootstrap errors (m) generated by the WA-PLS transfer function for fossil samples from core KE2. Output is compared with goodness of fit statistics, produced by fitting samples passively into ordination space (Figure 8.2) and dissimilarity coefficients (Min DC), produced by MAT.

Although in general the reconstruction agrees well with both the litho- and biostratigraphy, some significant differences are noted. For example, around 1.3 m core depth an increase in oligohalobous – indifferent diatom taxa is observed which correlates with diatom zone KE2 and corresponds to the *Phragmites* peat unit. The lithology and diatom taxa of this zone indicate 'freshening' conditions. Surprisingly, only a small corresponding increase in reconstructed palaeomarsh-surface elevations is noted. A second example is highlighted towards the top of the core. Here the freshwater conditions that are prevalent throughout the upper part of the *Phragmites* peat are seen to persist well into the overlying peaty clay unit. The highest reconstructed elevation (2.25 m) is found within the upper peaty clay unit and not within the *Phragmites* peat as might be expected. Not surprisingly, the reconstructed palaeomarsh-surface record appears to correlate better with the biostratigraphical changes than with the lithostratigraphy.

8.2.1 Reliability of the reconstruction

KE2 fossil samples fitted passively into ordination space are shown in Figure 8.2. Fossil samples from core KE2 with a poor or very poor fit to the modern data and those with 'no close' and 'no good' analogue are indicated in Figure 8.1 and Table 8.1.

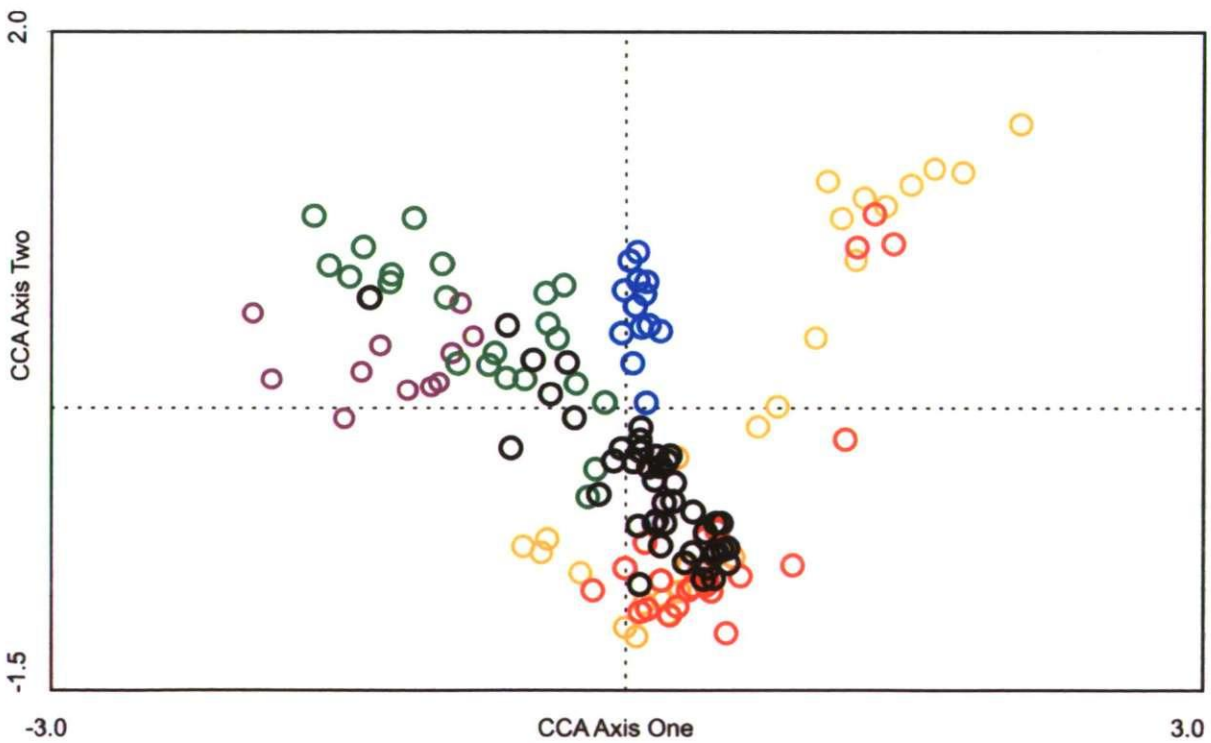

Figure 8.2. Fossil samples from core KE2 fitted passively into ordination space. Colour coding for samples is as per previous ordinations: Moservå =purple, Storbæk =blue, Oksby Enge =green, Langli North =yellow, Langli South =red, KE2 fossil samples =black.

Out of a total of 45 fossil samples, 10 (22%) are considered to have a very poor fit and 3 (7%) are considered to have a poor fit to the modern data (Figure 8.1 and Table 8.1). The majority of samples with a very poor fit are those samples with the highest predicted palaeomarsh-surface elevations. In this particular section of the core (core depth 0.34 – 0.58 m), the fossil samples are dominated by a number of fresh water taxa such as *Eunotia arcus, Eunotia, fallax, Rhopalodia operculata* and *Tabellaria flocculosa. E. fallax* and *R. operculata* are not represented in the modern training set and although *E. arcus* and *T. flocculosa* are, their occurrences are sparse and their relative abundances low (generally < 5%). Results of MAT show that all 45 fossil samples from core KE2 do not possess a good modern analogue (Figure 8.1 and Table 8.1). As with the goodness of fit statistics, the results of MAT are clearly influenced by poor representation (< 10% occurrences (Birks, 1998)) and missing taxa in the modern training set. Out of a total of 86 taxa in the KE2 fossil samples, 25 (29%) do not have a modern analogue. For taxa which do have a modern analogue, the distribution of these taxa in the training set is often sparse and overall abundances are relatively low (< 10%). Calibrating the data in this core using a transfer function which excludes allochthonous taxa (Section 7.6.3) results in 38 (44%) of fossil taxa with no modern analogue, and even further reduces the reliability of the reconstruction.

These results indicate that the reconstruction of core KE2 should be interpreted with caution, but it is important to place this limitation in context. Although many fossil samples have no 'good analogue' with the modern training set, this does not mean that they have no analogue at all. It is highly likely that given 'better' fresh water analogues and by improving the representation of taxa in the modern training set, the overall trends demonstrated by the palaeomarsh-surface record would remain the same. In some cases these trends would be amplified (i.e. high palaeomarsh-surface elevations would become 'higher'). The current reconstruction gives a valuable insight into changes in palaeomarsh-surface elevation that have occurred and is of value as long as the limitations are acknowledged.

It is worth noting that the inclusion of the modern surface samples from Kjelst Enge (Section 7.2) into the training set does not improve the results. With the inclusion of these samples, an additional four taxa gain a modern analogue. However, the relative abundances of these taxa are again low (< 5%).

8.3 Palaeomarsh-surface reconstruction of core BR9 (Bredmose)

Diatom data from the upper 0.3 m of core BR9 from the salt marsh at Bredmose were calibrated using the WA-PLS transfer function. The resulting palaeomarsh-surface reconstruction is presented in Figure 8.3. Reconstructed palaeomarsh-surface elevations range from 0.863 – 1.476 m DNN. Sample-specific standard errors of prediction for each of the fossil samples range from 0.125 – 0.139 m (Table 8.2). In general the reconstruction corresponds well with changes in litho- and biostratigraphy, although, as noted previously (Chapter 6), some significant changes in biostratigraphy occur within this single peaty clay unit. These changes are reflected in the reconstruction. In the lower part of the core section from 0.18 – 0.30 m core depth, reconstructed palaeomarsh-surface elevations are around 1.4 m DNN. At 0.18 m core depth reconstructed values decrease to around 1.2 m DNN. This change corresponds with the shift from diatom zone BR1 to diatom zone BR2. At 0.04 m core depth, the highest reconstructed value is obtained (1.476 m) with values then decreasing towards the top of the core. The sample with the lowest predicted palaeomarsh-surface elevation (0.863 m) is at the very top of the core. Here the WA-PLS transfer function under-predicts the surveyed elevation for the core top (1.35 m DNN).

Although changes in the reconstructed palaeomarsh-surface elevations appear to correspond well with changes in litho- and biostratigraphy some important differences are noted. For example, diatom zone BR2 corresponds with the highest abundance of oligohalobous - indifferent taxa, indicative of fresh water conditions. However, the palaeomarsh-surface record shows the lowest predicted elevations for this zone. In addition, the highest predicted palaeomarsh surface elevation does not correspond to the diatom sample with the highest percentage of fresh water diatom taxa.

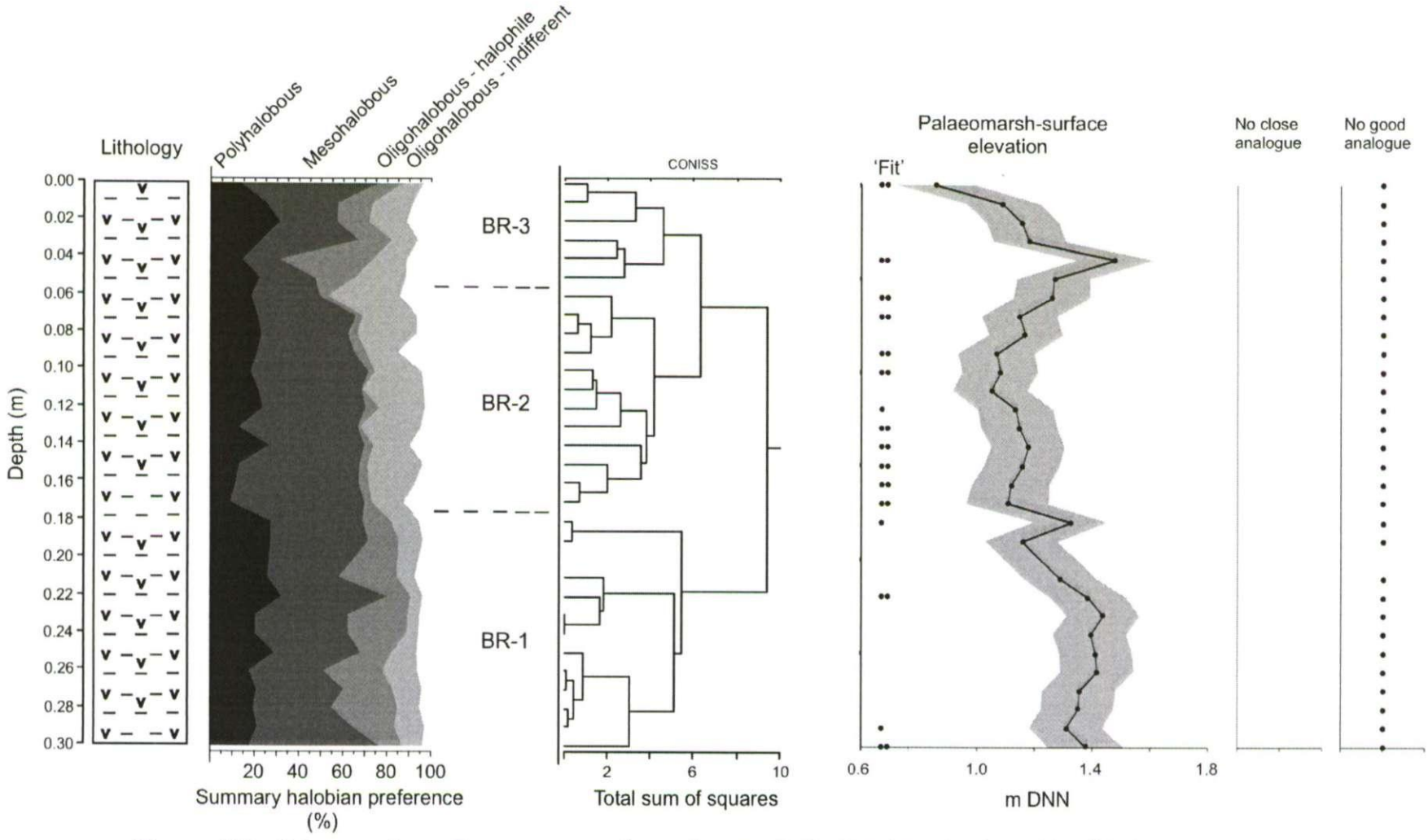

Figure 8.3. Palaeomarsh surface reconstruction of core BR9 (Bredmose) alongside lithology, summary halobian groups and diatom zones. Cluster analysis and summary halobian groups only include taxa with at least 1% relative abundance. The full diatom record for this core is presented in Chapter 6. Errors on the reconstruction are sample-specifc bootstrap standard errors. Fossil samples with a poor (.) and very poor (..) fit to the modern diatom data, and fossil samples with no good modern analogue are indicated. Key to lithology is presented in Figure 6.2.

Sample Depth (m)	WA-PLS predicted elevation (m) (Indicative meaning)	Bootstrap standard error m) (Indicative range)	Goodness of fit	Min DC	Analogue
0.00	0.863	0.137	Very Poor	71.405	No Good
0.01	1.091	0.125	Good	48.901	No Good
0.02	1.157	0.125	Good	49.711	No Good
0.03	1.182	0.125	Good	55.222	No Good
0.04	1.476	0.132	Very Poor	61.373	No Good
0.05	1.266	0.127	Good	53.607	No Good
0.06	1.260	0.132	Very Poor	72.719	No Good
0.07	1.145	0.129	Very Poor	61.850	No Good
0.08	1.168	0.128	Good	58.375	No Good
0.09	1.066	0.130	Very Poor	62.968	No Good
0.10	1.081	0.129	Very Poor	59.451	No Good
0.11	1.046	0.129	Good	57.851	No Good
0.12	1.133	0.129	Poor	52.334	No Good
0.13	1.146	0.130	Very Poor	69.16	No Good
0.14	1.177	0.127	Very Poor	64.391	No Good
0.15	1.157	0.129	Very Poor	61.279	No Good
0.16	1.118	0.131	Very Poor	73.43	No Good
0.17	1.106	0.139	Very Poor	83.695	No Good
0.18	1.326	0.125	Poor	57.246	No Good
0.19	1.155	0.126	Good	36.299	No Good
0.21	1.287	0.126	Good	40.817	No Good
0.22	1.384	0.134	Very Poor	52.776	No Good
0.23	1.437	0.128	Good	42.622	No Good
0.24	1.392	0.127	Good	47.758	No Good
0.25	1.411	0.126	Good	45.630	No Good
0.26	1.416	0.126	Good	48.556	No Good
0.27	1.355	0.127	Good	53.258	No Good
0.28	1.350	0.126	Good	38.464	No Good
0.29	1.309	0.126	Poor	47.952	No Good
0.30	1.378	0.130	Very Poor	57.738	No Good

Table 8.2 Summary of the WA-PLS predictions (m) and bootstrap errors (m) generated by the WA-PLS transfer function for fossil samples from core BR9. Output is compared with goodness of fit statistics, produced by fitting samples passively into ordination space (Figure 8.4) and dissimilarity coefficients (Min DC), produced by MAT.

8.3.1 Reliability of the reconstruction

BR9 fossil samples fitted passively into ordination space are shown in Figure 8.4. Fossil samples from core BR9 with a poor or very poor fit to the modern data and those with 'no close' and 'no good' analogue are indicated in Figure 8.3 and Table 8.2.

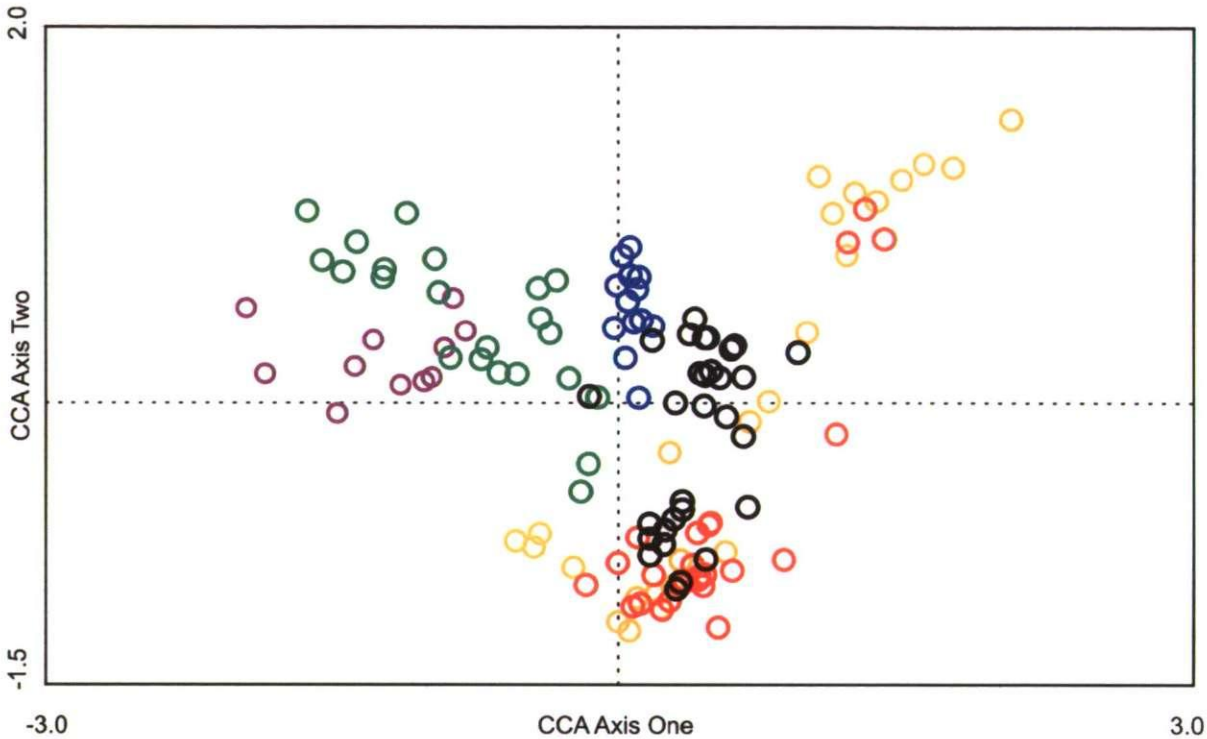

Figure 8.4. Fossil samples from core BR9 fitted passively into ordination space. Moservå = purple, Storbæk = blue, Oksby Enge = green, Langli North = yellow, Langli South = red, BR9 fossil samples = black.

Out of a total of 30 fossil samples in core BR9, 10 (33%) have a very poor fit and 3 (10%) have a poor fit (Figure 8.3 and Table 8.2). Although the majority of taxa that occur in the fossil samples in core BR9 do have a modern analogue, many of the fossil taxa are under-represented in the modern training set. For these species, calibration parameters will be poorly estimated and the resulting reconstructed values are likely to be unreliable (Birks, 1990). Of the 80 taxa present in the fossil samples, only 5 of them (6.3%) do not have a modern analogue. This is a significantly smaller figure than occurred in the Kjelst Enge reconstruction. Fossil samples with a very poor fit are dominated by *Navicula phyllepta, Navicula pygmaea, Nitzschia fonticola* and *Diploneis interrupta*. All of these taxa are represented in the modern training set but generally occur with relative abundances of < 3% (N. *pygmaea* < 8%). Results of MAT show that all 30 fossil samples from core BR9 do not posses a good modern analogue (Figure 8.3 and Table 8.2). For this reconstruction, the issue of under-representation of taxa is a bigger problem than that of no analogues and

reduces the reliability of the reconstruction. Calibrating the data in this core using a transfer function which excludes allochthonous taxa (Section 7.6.3) results in 17 (21%) of fossil taxa with no modern analogue, and even further reduces the reliability of the reconstruction.

As with the reconstruction of core KE2, these results indicate that the reconstruction of core BR9 should be interpreted with caution, but does not mean that the reconstruction is entirely meaningless. As argued previously, increasing the representiveness of taxa in the modern training set is likely to result in the same general pattern of reconstructed elevations. This is especially true for the BR9 core where the majority of taxa do have a modern analogue, albeit one that is poorly represented in the modern training set.

8.4 Palaeomarsh-surface reconstruction of core RØ1 (Røgel)

The WA-PLS transfer function was calibrated to core RØ1 from the salt marsh at Røgel. Samples from 0.52 and 0.55 m core depth were excluded from the calibration because these samples only returned partial diatom counts of 186 and 220 valves, respectively. The resulting palaeomarsh-surface reconstruction is presented in Figure 8.5. Reconstructed palaeomarsh-surface elevations range from 2.08 – 1.16 m DNN. Sample-specific standard errors of prediction for each of the fossil samples range from 0.124 – 0.191 m (Table 8.3).

In general, the reconstruction shows agreement with the litho- and biostratigraphy. In the lowermost section of the core (below 1.0 m core depth), reconstructed elevations vary between 1.2 and 1.6 m, corresponding to the upper part of the basal peat and lower clay unit. Re-working of the upper part of the eroded basal peat is likely to explain the similarity between diatom assemblages in the upper part of the peat unit and those in the overlying clay unit. Above 0.80 m core depth, reconstructed values show a fluctuating but gradual increase in elevation up to a maximum of 2.08 m DNN at 0.37 m core depth. Highest diatom-predicted elevations correspond with the upper part of the lower clay unit and the overlying black layer. This is in agreement with the biostratigraphy (Chapter 6) which indicates that the (fresh water?) conditions under which the black layer formed are initiated in the top 0.17 m of the underlying clay unit. A second phase of higher diatom-predicted elevations is noted immediately below the sand layer, corresponding with earlier biostratigraphical results (Chapter 6) which indicated that the initial formation of the sand layer began during a time when fresh water conditions prevailed.

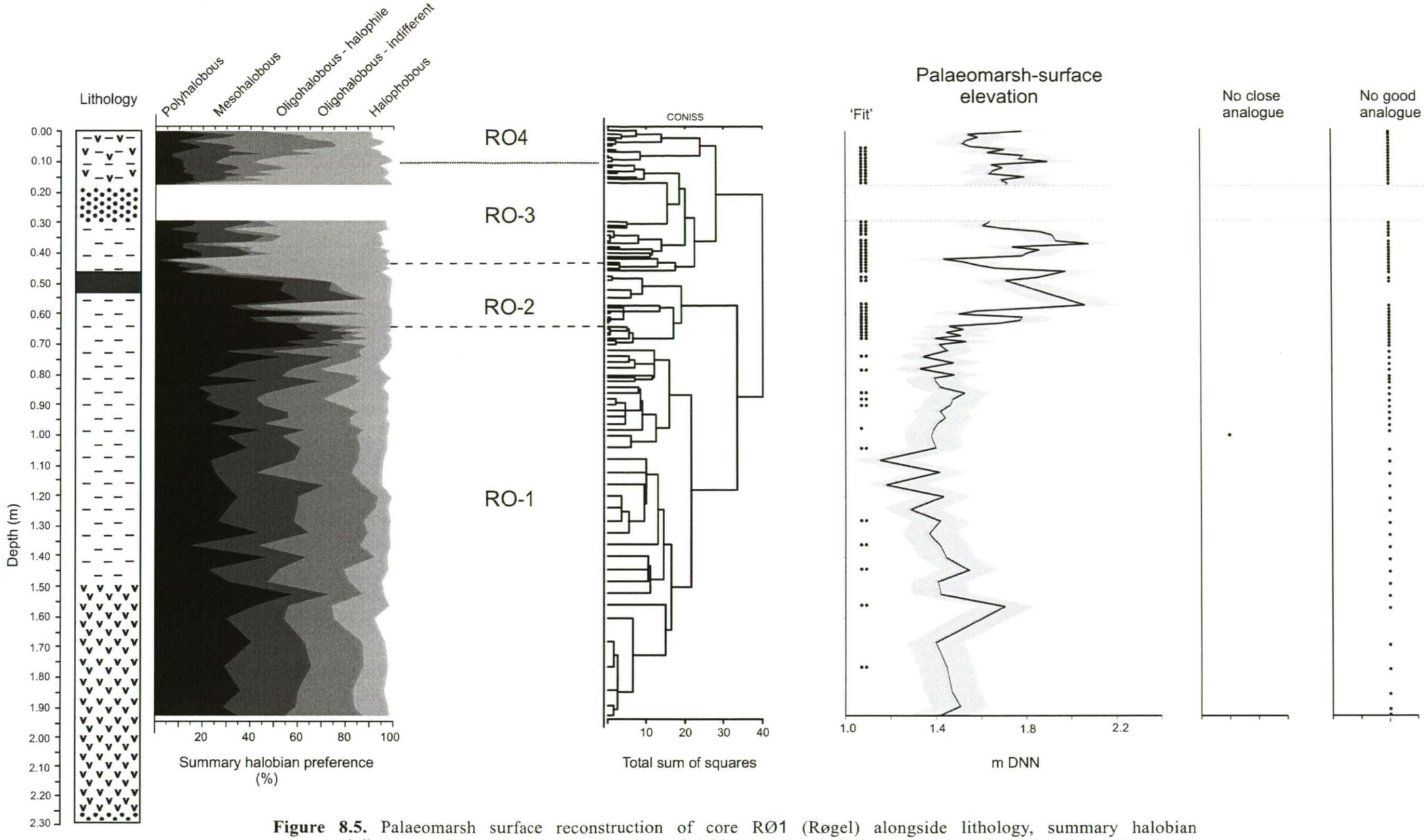

Figure 8.5. Palaeomarsh surface reconstruction of core RØ1 (Røgel) alongside lithology, summary halobian groups and diatom zones. Cluster analysis and summary halobian groups only include taxa with at least 1% relative abundance. The full diatom record for this core is presented in Chapter 6. Errors on the reconstruction are sample-specifc bootstrap standard errors. Fossil samples with a poor (.) and very poor (..) fit to the modern diatom data, and fossil samples with no good modern analogue are indicated. Key to lithology is presented in Figure 5.7.

Sample Depth (m)	WA-PLS predicted elevation (m) (Indicative meaning)	Bootstrap standard error (m) (Indicative range)	Goodness of fit	Min DC	Analogue
0.00	1.785	0.127	Good	42.53	No Good
0.01	1.546	0.126	Good	46.20	No Good
0.02	1.590	0.127	Good	38.78	No Good
0.03	1.536	0.127	Good	54.37	No Good
0.04	1.520	0.126	Good	43.19	No Good
0.05	1.558	0.125	Good	40.07	No Good
0.06	1.704	0.132	Very Poor	52.37	No Good
0.07	1.631	0.136	Very Poor	46.95	No Good
0.08	1.785	0.135	Very Poor	53.43	No Good
0.09	1.769	0.140	Very Poor	65.02	No Good
0.10	1.895	0.137	Very Poor	70.60	No Good
0.11	1.65	0.134	Very Poor	54.58	No Good
0.12	1.696	0.133	Very Poor	69.51	No Good
0.13	1.653	0.136	Very Poor	74.63	No Good
0.14	1.640	0.136	Very Poor	82.19	No Good
0.15	1.777	0.135	Very Poor	98.29	No Good
0.16	1.691	0.138	Very Poor	71.42	No Good
0.17	1.72	0.189	Very Poor	106.8	No Good
0.30	1.639	0.133	Very Poor	88.81	No Good
0.31	1.610	0.129	Very Poor	77.48	No Good
0.32	1.707	0.144	Very Poor	111.70	No Good
0.33	1.862	0.128	Very Poor	98.70	No Good
0.34	1.917	0.134	Very Poor	103.09	No Good
0.36	1.936	0.134	Very Poor	107.10	No Good
0.37	2.080	0.130	Very Poor	88.19	No Good
0.38	1.740	0.134	Very Poor	93.95	No Good
0.39	1.862	0.132	Very Poor	100.40	No Good
0.40	1.806	0.129	Very Poor	108.30	No Good
0.41	1.783	0.130	Very Poor	101.14	No Good
0.42	1.432	0.167	Very Poor	141.60	No Good
0.43	1.53	0.145	Very Poor	110.04	No Good
0.44	1.591	0.140	Very Poor	116.39	No Good
0.45	1.669	0.133	Very Poor	102.47	No Good
0.46	1.972	0.145	Very Poor	117.99	No Good
0.48	1.851	0.131	Very Poor	75.34	No Good
0.49	1.710	0.132	Very Poor	84.36	No Good
0.57	2.061	0.159	Very Poor	95.66	No Good
0.58	1.835	0.145	Very Poor	93.16	No Good
0.59	1.583	0.139	Very Poor	81.86	No Good
0.60	1.503	0.129	Very Poor	71.60	No Good
0.61	1.783	0.130	Very Poor	100.06	No Good
0.62	1.777	0.132	Very Poor	93.73	No Good
0.63	1.685	0.131	Very Poor	83.22	No Good
0.64	1.460	0.128	Very Poor	74.50	No Good
0.65	1.525	0.128	Very Poor	75.58	No Good
0.66	1.449	0.129	Very Poor	64.46	No Good
0.67	1.513	0.130	Very Poor	66.08	No Good
0.68	1.400	0.129	Very Poor	66.38	No Good
0.69	1.399	0.128	Good	68.63	No Good

0.70	1.414	0.128	Good	46.47	No Good
0.72	1.450	0.125	Good	49.94	No Good
0.74	1.345	0.127	Very Poor	55.29	No Good
0.76	1.479	0.128	Good	55.73	No Good
0.78	1.332	0.126	Good	51.95	No Good
0.80	1.480	0.126	Good	49.14	No Good
0.81	1.394	0.125	Good	50.75	No Good
0.82	1.396	0.125	Good	44.79	No Good
0.84	1.4190	0.126	Good	47.52	No Good
0.86	1.5270	0.129	Very Poor	63.06	No Good
0.88	1.474	0.127	Very Poor	60.62	No Good
0.90	1.460	0.126	Very Poor	50.45	No Good
0.92	1.4190	0.125	Good	50.05	No Good
0.94	1.443	0.125	Good	42.39	No Good
0.96	1.406	0.126	Good	48.48	No Good
0.98	1.388	0.125	Poor	42.97	No Good
1.00	1.383	0.125	Good	30.95	No close
1.04	1.399	0.126	Very Poor	47.49	No Good
1.08	1.154	0.128	Good	43.09	No Good
1.12	1.417	0.125	Good	46.02	No Good
1.16	1.182	0.129	Good	46.92	No Good
1.20	1.434	0.125	Good	36.94	No Good
1.24	1.290	0.127	Good	45.57	No Good
1.28	1.418	0.125	Very Poor	41.60	No Good
1.32	1.373	0.124	Good	37.51	No Good
1.36	1.420	0.126	Very Poor	56.12	No Good
1.40	1.447	0.125	Good	32.76	No Good
1.44	1.548	0.127	Very Poor	60.64	No Good
1.48	1.409	0.125	Good	41.32	No Good
1.52	1.421	0.126	Good	53.71	No Good
1.56	1.706	0.128	Very Poor	62.47	No Good
1.68	1.398	0.125	Good	40.85	No Good
1.76	1.447	0.125	Very Poor	40.88	No Good
1.84	1.471	0.125	Good	39.20	No Good
1.89	1.506	0.125	Good	44.87	No Good
1.92	1.416	0.124	Good	38.58	No Good

Table 8.3. Summary of the WA-PLS predictions (m) and bootstrap errors (m) generated by the WA-PLS transfer function for fossil samples from core RØ1. Output is compared with goodness of fit statistics, produced by fitting samples passively into ordination space (Figure 8.6) and dissimilarity coefficients (Min DC), produced by MAT.

8.4.1 Reliability of the reconstruction

RØ1 fossil samples fitted passively into ordination space are shown in Figure 8.6. Fossil samples from core RØ1 with a poor or very poor fit to the modern data and those with 'no close' and 'no good' analogue are indicated in Figure 8.5 and Table 8.3.

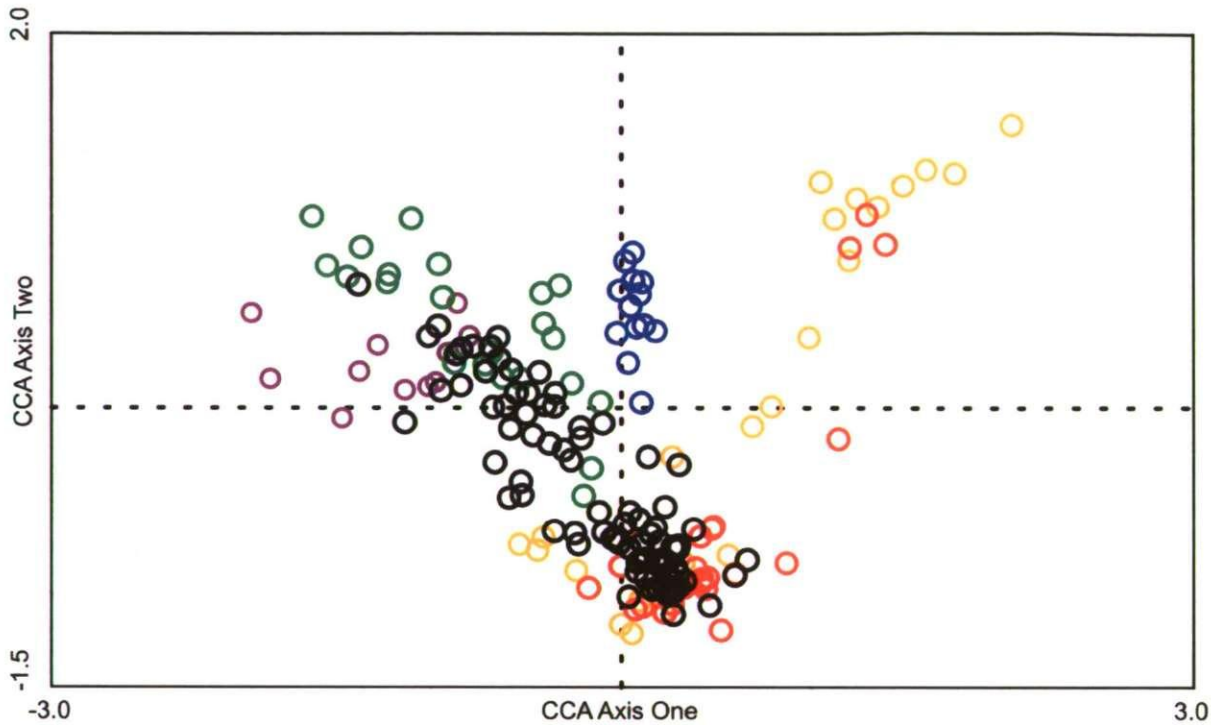

Figure 8.6. Fossil samples from core RØ1 fitted passively into ordination space. Moservå = purple, Storbæk = blue, Oksby Enge = green, Langli North = yellow, Langli South = red, RØ1 fossil samples = black.

Out of a total of 86 fossil samples from core RØ1, 52 (60.5%) have a very poor fit and one sample has a poor fit. In general, samples in the lower part of the core have a better fit to the modern samples than those in the upper parts of the core, apart from the uppermost six samples. The major bio- and lithostratigraphical changes that occur in the upper 0.80 m of this core have probably resulted in assemblages that are very different to those found in the modern surface samples, explaining the dissimilarity of these samples. Samples immediately below the black layer and those samples on either side of the sand layer have a very poor fit to the modern data. Samples immediately below the black layer are dominated by four main taxa: *Cocconeis scutellum var. scutellum, Cymatosira belgica, Grammatophora oceanica* and *Paralia sulcata*, all of which are allochthonous. *C. scutellum var scutellum* and *G. oceanica* are present in the modern training set but they are poorly represented with relative abundances not exceeding 5%. *C. belgica* and *P. sulcata*

are also present in the modern training set but they occur across the whole range of modern samples and their abundances are highly variable. Samples on either side of the sand layer are dominated by *Rhopalodia acuminata, Caloneis bacillum, Fragilaria brevistriata* and *Fragilaria exigua. R. acuminata* is not present in the modern training set and *C. bacillum, F. brevistriata and F. exigua* do not occur with relative abundances > 5% (*F. exigua* 15% in sample MO2).

Results of MAT show that of the 86 fossil samples in core RØ1, 85 have no good modern analogue and 1 has no close modern analogue. Of the 126 diatom taxa present in the fossil samples, 21 (16.7%) do not possess a modern analogue. Although the majority of taxa in the core without a modern analogue only occur with low relative abundances (< 5%), several of these taxa are more dominant. Maximum relative abundances of dominant taxa in the core without a modern analogue include: *R. acuminata* (17%), *Epithemia turgida* (11%), *Epithemia adnata* (11%) and *Navicula amphibola* (11%). As a result, many of the fossil samples are significantly different from the samples in the modern training set (as illustrated by the Min DC, Table 8.3) and consequently are considered to have 'no good analogue'. Calibrating the data in this core using a transfer function which excludes allochthonous taxa (Section 7.6.3) results in 36 (28%) of fossil taxa with no modern analogue, and even further reduces the reliability of the reconstruction.

As with the cores from Kjelst Enge and Bredmose, no analogue species and poorly represented taxa in the modern training set have greatly influenced the reliability of the reconstruction. In the reconstruction of core RØ1, the additional problem of taxa in the modern training set which span a range of environments and results in 'multiple analogues' has further exacerbated these issues. The absence of several dominant core taxa from the modern training set makes this reconstruction more unreliable than previous ones but again does not mean that the reconstruction is entirely meaningless. The majority of these missing taxa are fresh water taxa (e.g., *E. turgida, E. adnanta* and *N. amphibola*) and inclusion of such taxa into the training set is likely to amplify existing trends. In particular the 'fresh water' sections of the core are likely to become more 'fresh.' From this perspective the reconstruction can still be considered valuable as long as the limitations are acknowledged.

8.5 Reconstruction of additional diatom samples

Diatom data from a series of additional fossil samples from which ^{14}C and OSL ages were obtained were also calibrated using the WA-PLS transfer function in order to establish an indicative meaning for these samples (Tables 8.4, 8.5 and 8.6). Establishment of the indicative meanings for these samples is important because they are used to reconstruct the millennial-scale sea-level history of the Ho Bugt embayment (Chapter 9). Core KE2 was sampled and dated as part of the HOLSMEER Project. For this core, samples were not taken from depths at which datable material was obtained and because there was no remaining material from which to take new samples, the indicative meaning is calculated from the average of the two nearest samples, or interpolated from the nearest sample. In most cases, the nearest samples are two cm either side of the depth at which the ^{14}C date was obtained (e.g., the indicative meaning for the ^{14}C sample at 0.12 m depth is the average of the indicative meanings for samples at 0.10 and 0.14 m core depth). For the Bredmose core, also dated as part of the HOLSMEER Project, archived material was available from which to take new samples and these were counted as part of this study.

Although the samples from core RØ1 are presented previously (Table 8.3), they are again presented here to place them in context with the indicative meanings for other ^{14}C samples. For the two OSL ages from Røgel (Table 8.3), the indicative meanings are inferred from the nearest diatom sample. For the age at 0.23 m core depth, the indicative meaning is inferred from the diatom sample at 0.17 m core depth. For the age at 0.33 m core depth, a diatom sample was also counted at this depth from which to infer the indicative meaning (Table 8.3). This is also true for the OSL sample from core OEB5 at 0.33 m core depth. One sample (no. 4, Table 5.3), taken from the basal sand unit in monolith OEA is excluded from further analyses because no diatom data are available for this sample, and the sample could not be related to a modern environment (Table 8.7).

Sample No.	Laboratory Code	Sample depth (m)	WA-PLS predicted elevation (m) (Indicative meaning)	Bootstrap standard error (m) (Indicative range)	Fit	Min. DC	Analogue
KE2							
1	AAR-8891	0.12	1.43	± 0.12	N/A	N/A	N/A
2	AAR-8891	0.50	1.71	± 0.13	N/A	N/A	N/A
3	AAR-8048	0.56	1.76	± 0.13	N/A	N/A	N/A
4	AAR-8049	0.68	1.45	± 0.12	N/A	N/A	N/A
5	AAR-8050	0.82	1.52	± 0.13	N/A	N/A	N/A
8	AAR-8051	0.96	1.37	± 0.12	N/A	N/A	N/A
7	AAR8052	1.16	1.43	± 0.13	N/A	N/A	N/A
8	AAR-8053	1.38	1.38	± 0.13	N/A	N/A	N/A
9	AAR-8054	1.51	1.34	± 0.13	N/A	N/A	N/A
10	AAR-8055	1.67	1.31	± 0.13	N/A	N/A	N/A
11	AAR-8056	1.84	1.30	± 0.13	N/A	N/A	N/A
12	AAR-8057	2.01	1.28	± 0.13	N/A	N/A	N/A
13	AAR-8058	2.35	1.35	± 0.13	N/A	N/A	N/A
14	AAR-8059	2.57	1.38	± 0.12	N/A	N/A	N/A
15	AAR-8060	2.75	2.30**	± 0.40**	N/A	N/A	N/A
BR12							
17	AAR-8068	1.53	1.52	0.13	Good	75.83	No Good
BR2							
18	AAR-8069	1.60	1.46	0.13	Very Poor	51.09	No Good

Table 8.4. Indicative meanings for samples dated by ^{14}C as part of the HOLSMEER Project, predicted using a WA-PLS transfer function, except the samples marked by double asterisks (**) which have been estimated by surveyed heights of present day marsh environments because no diatom data are available (Table 8.7). One dated sample (no. 16, Table 5.1) has previously been excluded because it returned a much younger than expected age (Section 5.1.5). The reliability of samples from core KE2 are not statistically assessed. The indicative meaning for these samples is calculated from the average of the two nearest samples, or interpolated from the nearest sample. The reconstruction of these neighbouring samples has been previously assessed in Section 8.2.1.

Sample No.	Laboratory Code	Sample depth (m)	WA-PLS predicted elevation (m) (Indicative meaning)	Bootstrap standard error (m) (Indicative range)	Fit	Min. DC	Analogue
RØ1							
19	SUERC-9253	0.51	1.70**	± 0.20**	N/A	N/A	N/A
20	SUERC-9254	0.68	1.40	± 0.13	Very Poor	85.67	No Good
21	SUERC-9255	0.72	1.45	± 0.13	Good	58.18	No Good
22	SUERC-9256	0.81	1.39	± 0.13	Good	55.04	No Good
23	SUERC-9257	0.92	1.42	± 0.13	Good	54.63	No Good
24	SUERC-9259	1.68	1.40	± 0.13	Good	47.74	No Good
25	SUERC-9262	1.89	1.51	± 0.13	Good	45.06	No Good
26	SUERC-9263	2.15	2.30**	± 0.40**	N/A	N/A	N/A
27	SUERC-9264	2.19	2.30**	± 0.40**	N/A	N/A	N/A
28	SUERC-9265	2.22	2.30**	± 0.40**	N/A	N/A	N/A
Røgel Monolith							
29	SUERC-9266	0.55	1.57	± 0.13	Very Poor	76.91	No Good
30	SUERC-9267	0.60	1.50	± 0.13	Very Poor	82.28	No Good
OEA							
31	SUERC-9268	1.24	2.01	± 0.14	Very Poor	92.20	No Good
32	SUERC-9269	1.52	2.30**	± 0.40**	N/A	N/A	N/A
OEB5							
34	SUERC-9274	0.82	1.37	± 0.13	Good	39.81	No Good
35	SUERC-9275	1.01	1.39	± 0.13	Poor	47.16	No Good
KE1 (2004)							
36	SUERC-9276	4.16	1.55	± 0.13	Very Poor	71.18	No Good
37	SUERC-9277	5.15	1.73	± 0.17	Very Poor	150.34	No Good
38	SUERC-9278	5.98	1.69	± 0.15	Very Poor	96.50	No Good
39	SUERC-9279	6.54	2.00	± 0.14	Very Poor	108.92	No Good
40	SUERC-9282	6.84	1.78	± 0.15	Very Poor	101.27	No Good
KE12							
41	SUERC-9283	2.35	1.62	± 0.13	Very Poor	77.95	No Good
42	SUERC-9285	3.80	2.17	± 0.14	Very Poor	83.32	No Good
KE13							
43	SUERC-9286	3.34	1.83	± 0.13	Very Poor	81.42	No Good
44	SUERC-9287	5.08	1.77	± 0.13	Very Poor	97.75	No Good

Table 8.5. Indicative meaning for samples dated by ^{14}C (this study) predicted using a WA-PLS transfer function, except the samples marked by double asterisks (**) which have been estimated by surveyed heights of present day marsh environments because no diatom data are available (Table 8.7). One dated sample (no. 33, Table 5.2) has previously been excluded because it returned a much younger than expected age (Section 5.1.3).

Sample No.	Core	Laboratory Code	Sample Depth (m)	WA-PLS predicted elevation (m) (Indicative meaning)	Bootstrap standard error (m) (Indicative range)	Fit	Min. DC	Analogue
1	RØ1	Risø 052803	0.23	1.72	0.19	Very Poor	106.83	No Good
2	RØ1	Risø 052804	0.33	1.86	0.12	Very Poor	98.70	No Good
3	OEB5	Risø 052802	0.33	1.74	0.13	Good	58.57	No Good

Table 8.6. Indicative meaning for samples dated by OSL predicted using the WA-PLS transfer function. Indicative meanings and indicative ranges are inferred from the nearest WA-PLS predicted diatom sample (see text). One sample (no. 4, Table 5.3) taken from the basal sand unit is excluded because no diatom data are available for this sample and the sample could not be related to a modern environment (Table 8.7).

Surface environment	m DNN
Freshwater marsh	2.30 ± 0.40
Salt marsh to freshwater marsh transition	1.90 ± 0.20
High salt marsh	1.70 ± 0.20
High salt marsh to low salt marsh transition	1.50 ± 0.20
Low salt marsh	1.10 ± 0.40
Low salt marsh to tidal flat transition	0.75 ± 0.20
Tidal flat	<0.75

Table 8.7. Indicative meaning of lithofacies and lithostratigraphical contacts based on survey of modern salt-marsh environments (Gehrels et al., 2006a). This information is used to infer the indicative meanings for samples for which no diatom data are available.

8.5.1 Reliability of the reconstructions

Additional fossil samples fitted passively into ordination space are shown in Figure 8.7. Samples for core KE2 are not assessed. The indicative meaning for these samples is calculated from the average of the two nearest samples, or interpolated from the nearest sample. No diatom data is available from these exact depths to enable the samples to be analysed in the ordinations. Goodness of fit and MAT statistics for the original samples used in these calculations are shown in Table 8.2 and give some idea of how reliable the reconstructed values may be. Samples where the indicative meaning is inferred from surveyed heights of modern salt-marsh environments are also not assessed. Again, no diatom data are available for these samples to enable them to be entered into the ordination. Reconstructed values for all other samples in Tables 8.4, 8.5 and 8.6 are all assessed via goodness of fit and analogue statistics. Fossil samples with a poor or very poor fit to the modern data and those with 'no close' and 'no good' analogue are indicated in Tables 8.4, 8.5 and 8.6.

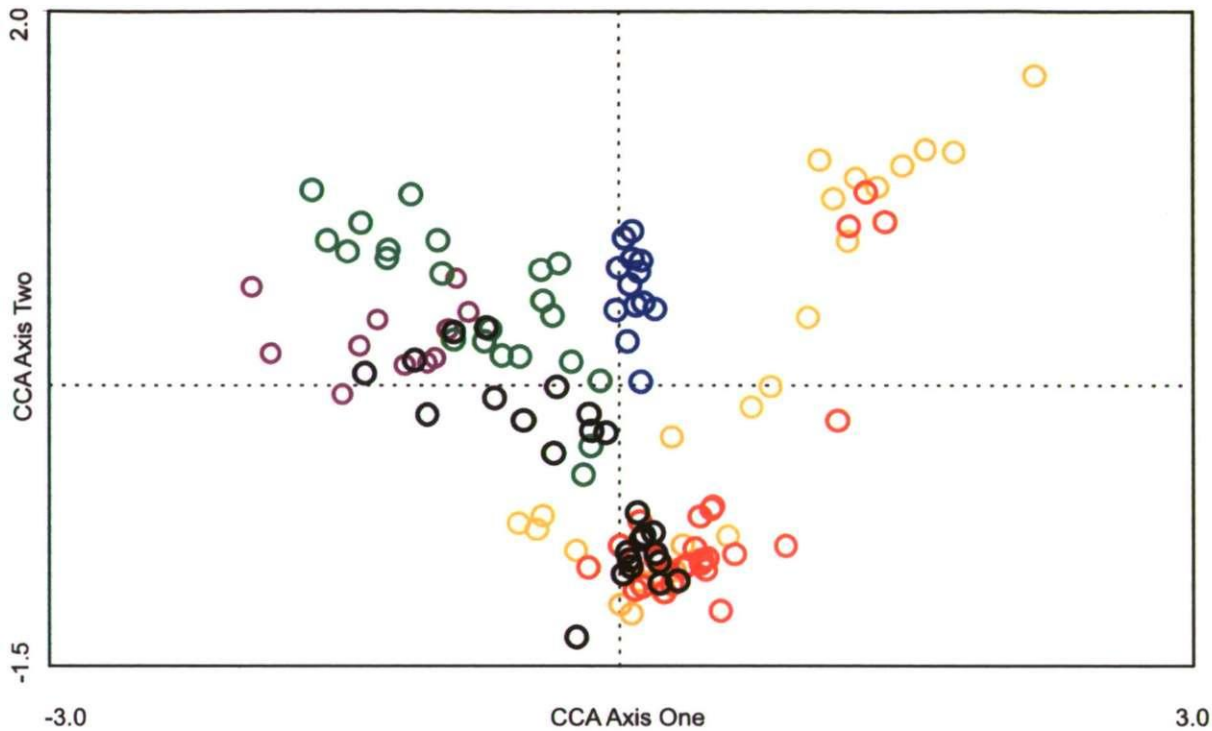

Figure 8.7. Additional fossil samples fitted passively into ordination space. Sample numbers 17-18, 20-25, 29-31 (Table 8.4) and 34-44 (Table 8.5) and 1-3 (Table 8.6) are plotted. Samples where the indicative meaning is inferred from the surveyed heights of modern salt-marsh environments are not assessed (see text). Moservå = purple, Storbæk = blue, Oksby Enge = green, Langli North = yellow, Langli South = red, fossil samples = black.

The results of goodness of fit and MAT suggest that several of the inferred indicative meanings need to be interpreted with caution. A number of fossil samples are shown to have a very poor fit to the modern samples and all diatom-inferred indicative meanings are shown to have no good analogue. These results are not surprising given that a number of these additional fossil samples are from basal peat deposits (e.g., sample numbers 37 - 44, Table 4.5), that formed under a fresh water environment. Previous reconstructions have already highlighted the lack of fresh water analogues and under-representation of such taxa in the modern training set. The modern training set extends to a height of 2.53 m DNN and although it does include samples from the high and fresh water marshes, the highest elevation is still probably lower than the height at which the basal peat unit formed. Dominant taxa found in these fossil samples include *Fragilaria pinnata, Fragilaria virescens, Epithemia adnanta* and *Epithemia turgida*. *E. adnanta* and *E. turgida* have no modern analogue and *F. pinnata* and *F. virescens* only occur with relative abundances < 5% in the modern training set. As was the case for previous reconstructions, under representation of taxa and lack of modern analogues has reduced the reliability of the diatom inferred indicative meanings.

8.6 Comments on the reliability of the reconstructions

From the assessment of the various reconstructions, it is clear that there are concerns regarding the reliability of the reconstructed values but it is important to place these findings in context. Lack of modern analogues, under-representation of taxa and multiple analogues have all contributed to reducing the reliability of the reconstructed values. However, for many of the core sections under representation of taxa, rather than a complete lack of analogues, is the biggest problem. This is particularly true of the fresh water taxa. The use of statistical methods such as goodness of fit and MAT, provide only one way of assessing the reliability of a reconstruction. It is important to assess the reliability of a reconstruction alongside litho- and biostratigraphical information as well as by using statistical techniques. These points are further explored in Chapter 9.

The next part of this chapter presents the development of a series of age-depth models. The diatom-inferred palaeomarsh-surface records presented here are linked to local-water level and the data are plotted in a series of time-height diagrams of local water-level change. These diatom-predicted local water-level curves are compared with observational data from the nearby tide gauge record at Esbjerg to provide further assessment on their reliability.

8.7 Age-depth models

To provide chronological control on the relative sea-level records and to enable comparison between records, age-depth models were developed using the available ^{210}Pb, ^{137}Cs, ^{241}Am, OSL and ^{14}C ages for all core sections from which reconstructions were attempted (cores KE2, BR9 and RØ1). Selecting a suitable age-depth model for each of the cores is important as subtle changes in salt-marsh accretion can greatly affect the accuracy of the water-level reconstruction (Gehrels et al., 2005). In developing an age-depth model it is often convenient to have a single, central point estimate of a ^{14}C date (Telford et al., 2004a). For ^{14}C dates this is not a problem however, calibrated ^{14}C ages, as used in this study, often display multi-modal and non-normal errors (Telford et al., 2004a; Gehrels et al., 2005). One of the most frequently used methods for gaining a point estimate of a calibrated ^{14}C age is the intercept, i.e. where the mean or median of the ^{14}C date intercepts the calibration curve (e.g., Stuiver and Reimer, 1993, Seierstad et al., 2002). However, such a method has been criticised in the literature because small variations in the calibration curve can greatly affect the point estimates (Telford et al., 2004a). In this study, the median age is used to provide a point estimate but the full 2σ range (95% confidence intervals) is also presented as horizontal error bars. Although this is not the only possible option, presentation of the full 2σ range provides some assessment of the uncertainty in the radiocarbon result (Bowman and Leese, 1995; Telford et al., 2004a). Such a method is also consistent with the HOLSMEER ages previously published in Gehrels et al. (2006a).

A number of different approaches to age-depth modelling have been presented in the literature (Telford et al., 2004b). Some of the more common methods include linear interpolation and linear regression models (e.g., Bennett, 1994), mixed effect models (e.g., Heegard, 2003; Heegard et al., 2005) and weighted-average probability density functions (e.g., Telford et al., 2004; Gehrels et al., 2005, 2006c). In this study, selecting one linear regression model for each of the core sections modelled was considered erroneous as the cores contains several lithological units which are likely to have been deposited under different sedimentation rates. The development of mixed effect models and weighted-average probability density functions, such as those employed by Heegard et al. (2005) and Gehrels et al. (2005, 2006c) respectively, were beyond the scope of this present study but are potential areas to explore in future work. The age-depth models established for cores KE2, BR9 and RØ1 are presented in the next section of this chapter.

8.7.1 Kjelst Enge core KE2

Chronology

The age-depth model for core KE2 is based on ^{210}Pb, ^{137}Cs and fifteen ^{14}C ages. The first two techniques were used to establish a chronology for the youngest part of the sequence. A definitive chronology based on an assessment of all the radiometric data (^{210}Pb and ^{137}Cs) for this part of the core was calculated using the methods described in Appleby (2001). Total ^{210}Pb activity was found to reach equilibrium with the supporting ^{226}Ra at a depth of about 15 cm (Figure 8.8). The ^{137}Cs activity versus depth (Figure 8.8) was found to have three relatively distinct peaks. The upper peak at 5 cm is likely to be attributed to the Chernobyl accident in 1986. Several studies have identified the Chernobyl peak in the ^{137}Cs record in the Danish Wadden Sea (e.g., Pedersen, 2004; Ehlers et al., 1993; Andersen et al., 2000) and the amount of ^{137}Cs represented by this peak in core KE2 (c. 180 Bq/kg-1) is comparable with these studies. The two lower peaks at 7.5 and 9.5 cm may be attributed to the same event and result from down core movement of ^{137}Cs as documented by other studies in the Danish Wadden Sea (e.g., Bartholdy et al., 2004; Pedersen, 2004). It is also possible that one of these peaks could be attributed to atomic weapons testing, which began in 1953 and reached a maximum in 1963. Measurements of ^{241}Am measurements are not available for this core to support this link.

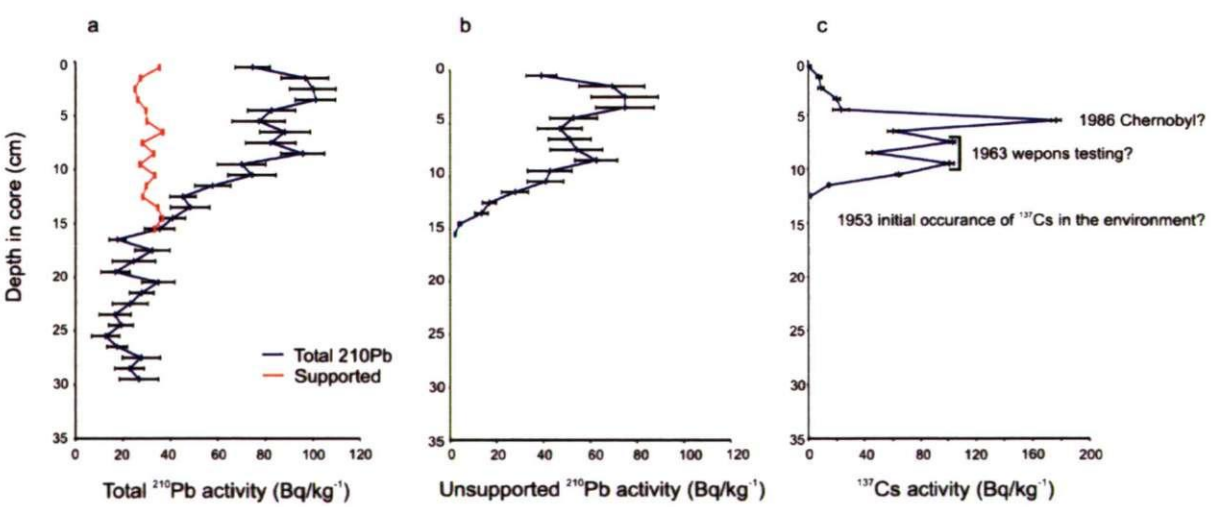

Figure 8.8. Isotopic data plotted against core depth for core KE2 showing a) total and supported ^{210}Pb activity, b) unsupported (excess) ^{210}Pb activity and c) ^{137}Cs activity.

Raw ^{210}Pb dates were calculated using the constant rate of supply (CRS) dating model (Equation 8.1; Appleby, 2001). Although this method is considered most reliable in sediments where uniform sedimentation rates prevail, several studies have demonstrated the use of such a model on salt-marsh cores, where non-uniform accumulation rates are more common (e.g., Gehrels et al., 2002, 2005; Pedersen, 2004; Horton et al., 2006). Age of sediments at depth (m) is calculated as:

$t = 1/\lambda \, Ln \, (A(0)/A)$ **Equation 8.1**

Where t = age

λ = ^{210}Pb radioactive decay constant (0.03114 y^{-1})

A(0) = total inventory of unsupported ^{210}Pb at depth where activity is negligible,

A = difference between A(0) and cumulative input at that depth.

Raw ^{210}Pb dates calculated using the CRS dating model place 1963 at a depth of 0.08 m and 1986 at a depth of 0.05 m, in both cases in good agreement with the depths suggested by the ^{137}Cs record. On this basis the CRS ^{210}Pb ages are accepted.

Age-depth model

The age-depth model for core KE2 is based on the following assumptions:

- Sedimentation rates within each lithological unit are likely to have remained constant, except in the upper 10-20 cm where there is less likelihood of compaction.

- The top of the basal peat is eroded as evidenced by the sharp boundary between the peat and the overlying clay (Section 5.1.1).

- The clay unit accumulated very rapidly as a result of infill, following the excavation of the top of the basal peat. This is supported by the series of radiocarbon ages in the lower clay unit, all of which are overlapping in calibrated ages.

- Following stabilisation of the salt-marsh surface, the sedimentation rate within the peaty clay unit appears to have slowed, as suggested by the radiocarbon ages in the upper peaty clay unit.

The age-depth model for core KE2, based on ^{210}Pb, ^{137}Cs and 14 calibrated ^{14}C ages, is presented in Figure 8.9. One ^{14}C dated sample (no. 13, Table 5.2) is in the clay unit, but its age indicates that it is an eroded basal peat fragment (Gehrels et al., 2006a). The age of this sample is close to that of the basal peat, and a number of cores show that the basal peat is eroded, as evidenced by the sharp upper basal contact (Section 5.1.1). This re-worked sample is excluded from further analysis. Some age reversals are apparent in the central part of the clay unit. This unit represents a low marsh to tidal flat environment and sedimentation rates would have been very high. The age-reversals in this unit are relatively small and are the result of rapid infill. The radiocarbon ages from the upper part of the peaty clay unit suggest some slowing of accumulation rates following the initial rapid infill. Given the lack of dates in the lower part of the clay, inferred ages in this part of the core are much less certain, but are estimated here by extrapolating the accumulation rate from the upper part of the profile.

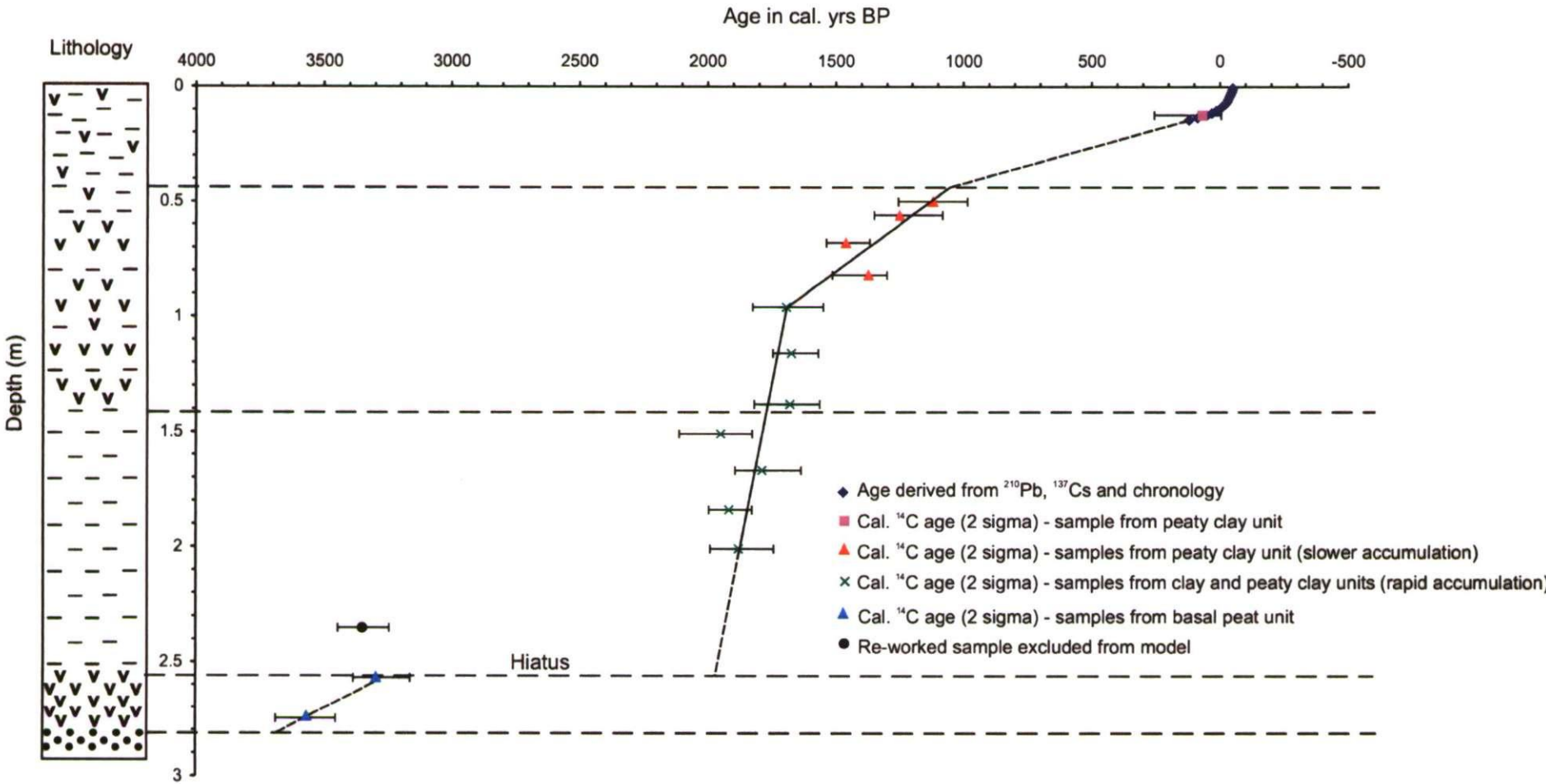

Figure 8.9. Age-depth model for core KE2 from Kjelst Enge. Key to lithology is given in Figure 6.1.

8.7.2 Bredmose core BR9

The age-depth model for Bredmose core BR9 is based solely on ^{210}Pb and ^{137}Cs ages. These two techniques were used to establish a chronology for the upper 0.30 m of this core for which a diatom record has also been established. Total ^{210}Pb activity was found to reach equilibrium with the supporting ^{226}Ra at a depth of about 23 cm (Figure 8.10). The ^{137}Cs activity versus depth (Figure 8.10) was found to have two possible peaks at 12.5 and 14.5 cm. It is possible that the first peak at 12.5 cm results from the Chernobyl accident (1986) and that the second results from nuclear weapons testing (1963). However, in both the Røgel and Kjelst Enge cores the Chernobyl peak is usually the larger of the two (Figures 8.8 and 8.11), which is not the case for this core. Since these two peaks are only 2 cm apart is it also possible that they represent one peak relating to either the Chernobyl accident (1986) or the result of nuclear weapons testing (1963) and that some down core movement of ^{137}Cs has taken place. Post-depositional mobility of ^{137}Cs in coastal sediments has been documented by several authors (e.g., Bartholdy et al., 2004; Foster et al., 2006; Pedersen, 2004). ^{241}Am measurements are not available for this core to support either argument. Attributing the peak at 14.5 cm to Chernobyl would result in an accumulation rate of around 1 cm/yr, which seems too high. It seems more likely that this peak is the result of nuclear weapons testing (1963) and that the Chernobyl peak is 'blurred.' Raw ^{210}Pb dates calculated using the CRS dating model place 1986 at a depth of 9 cm and 1963 at a depth of 14.5 cm. Given the uncertainty associated with the ^{137}Cs record for this core, assessment of the raw ^{210}Pb chronology is very difficult. However, on the basis of a lack of any other information the CRS ^{210}Pb record is accepted.

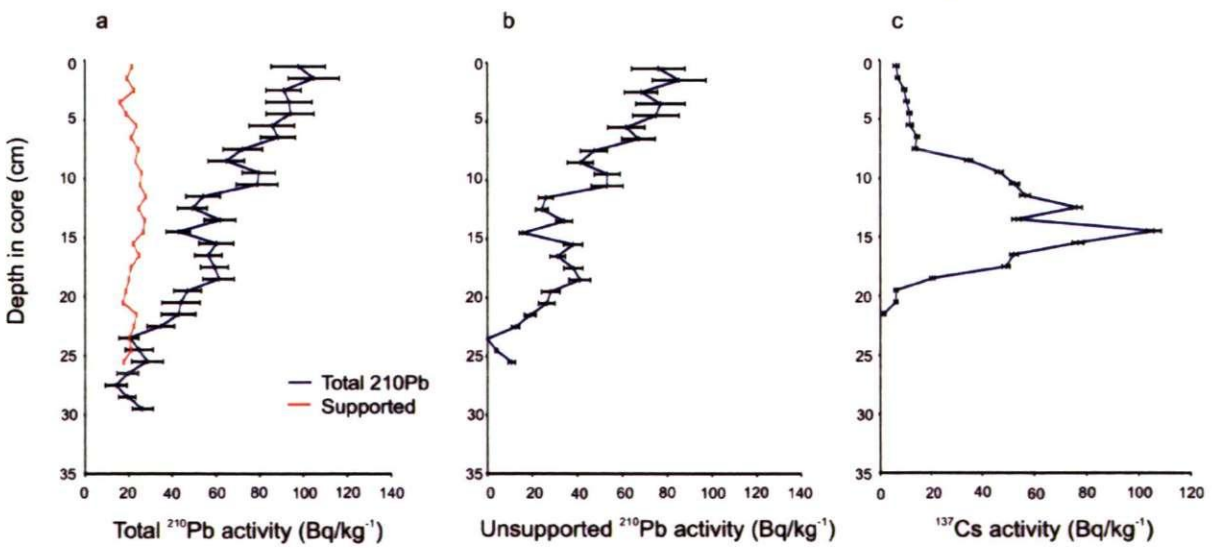

Figure 8.10. Isotopic data plotted against core depth for core BR9 showing a) total and supported ^{210}Pb activity, b) unsupported (excess) ^{210}Pb activity and c) ^{137}Cs activity.

8.7.3 Røgel core RØ1

Chronology

The age-depth model for core RØ1 is based on ^{210}Pb, ^{137}Cs, ^{241}Am, 10 calibrated ^{14}C and two OSL ages. The first three techniques were used to establish a chronology for the youngest part of the sequence and were modelled by Appleby and Piliposian (2006). Total ^{210}Pb activity was found to reach equilibrium with supporting ^{226}Ra at a depth of about 12 cm (Figure 8.11). The ^{137}Cs activity versus depth (Figure 8.11) has two relatively distinct peaks. The more recent, at 4.75 cm, may record fallout from the 1986 Chernobyl accident. The earlier peak, at 6.75 cm, may record the 1963 fallout maximum from the atmospheric testing of nuclear weapons. Traces of ^{241}Am confirm the presence of weapons test fallout in this part of the core, though the record is not sufficiently distinct to be certain of the above attributions.

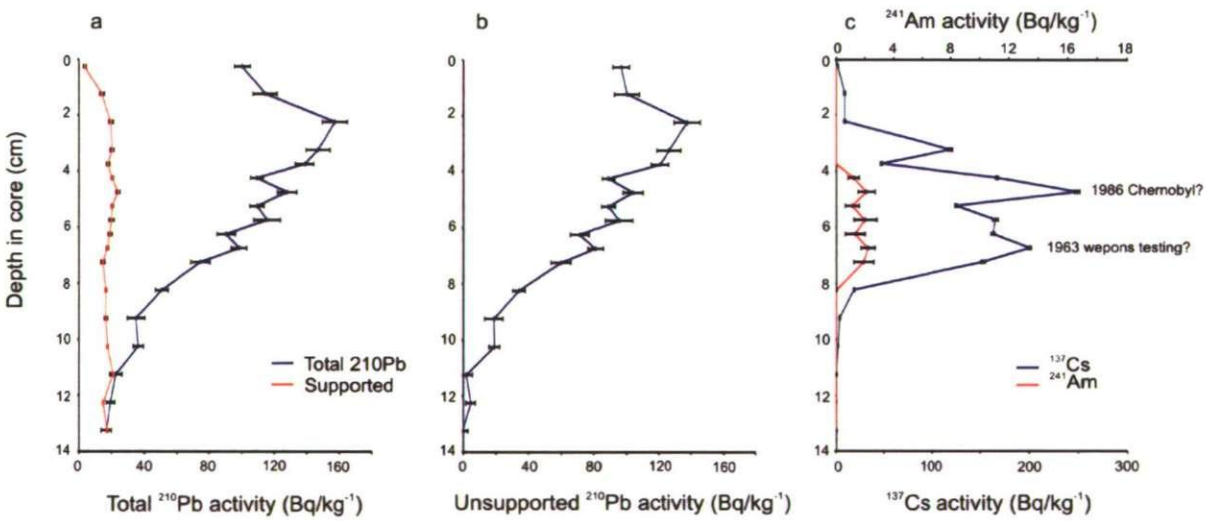

Figure 8.11. Isotopic data plotted against core depth for core RØ1 showing a) total and supported ^{210}Pb activity, b) unsupported (excess) ^{210}Pb activity and c) ^{137}Cs and ^{241}Am activity.

Raw ^{210}Pb dates calculated using the CRS dating model place 1963 at a depth of 6 cm and 1986 at a depth of 3.75 cm, in both cases about 1 cm above the depths suggested by the ^{137}Cs record. This suggests some discrepancy between the ^{137}Cs and ^{210}Pb ages. Calculation of the ^{210}Pb flux suggested that it was relatively uniform up to the mid-1980s (with a mean value of 107 Bq m^{-2} y^{-1}), but increased significantly after this date, resulting in a mean value of 183 Bq m^{-2} y^{-1} in the last 20 years. Appleby and Piliposon (2006) use a corrected chronology, calculated by applying the CRS model (Equation 8.1) in a piecewise manner using the lower value of the ^{210}Pb flux for pre-1986 sediments and the higher value

for the post-1986 sediments. This technique of correcting the ^{210}Pb chronology on the basis of ^{137}Cs peaks has been successfully used in lake sediment cores in Denmark (Appleby, 2001).

Age –Depth Model

The age-depth model for core RØ1 is based on the following assumptions:

- Sedimentation rates with each lithological unit are likely to have remained constant, except in the upper 10-20 cm where there is less likelihood of compaction.
- The top of the basal peat is eroded (Chapter 5), but not as significantly as in core KE2, and only a small hiatus is identified. In core RØ1 the stratigraphic contact between the basal peat and the overlying clay unit is more diffuse than in core KE2 (Section 5.2.1).
- The clay unit accumulated very rapidly as a result of infill, following the excavation of the top of the basal peat
- A change in sedimentation rate is hypothesised following deposition of the black layer.

The age-depth model for core RØ1, based on ^{210}Pb, ^{137}Cs, ^{241}Am, 2 OSL and 10 calibrated ^{14}C ages, is presented in Figure 8.12. Between 0.92 and 1.68 m core depth no datable material was found in this core (Appendix 4) and as a result a large gap in the age depth model is noted. As was the case for the KE2 core, several age reversals are apparent, particularly between 0.5 and 1 m core depth, which result from rapid infill. Here, the 5 dates which form the steepest trend are included in the model and the remaining two dates in this unit are considered too old. Given the lack of dates in the lower part of the clay, inferred ages in this part of the core are much less certain, but are estimated here by extrapolating the accumulation rate from the upper part of the profile.

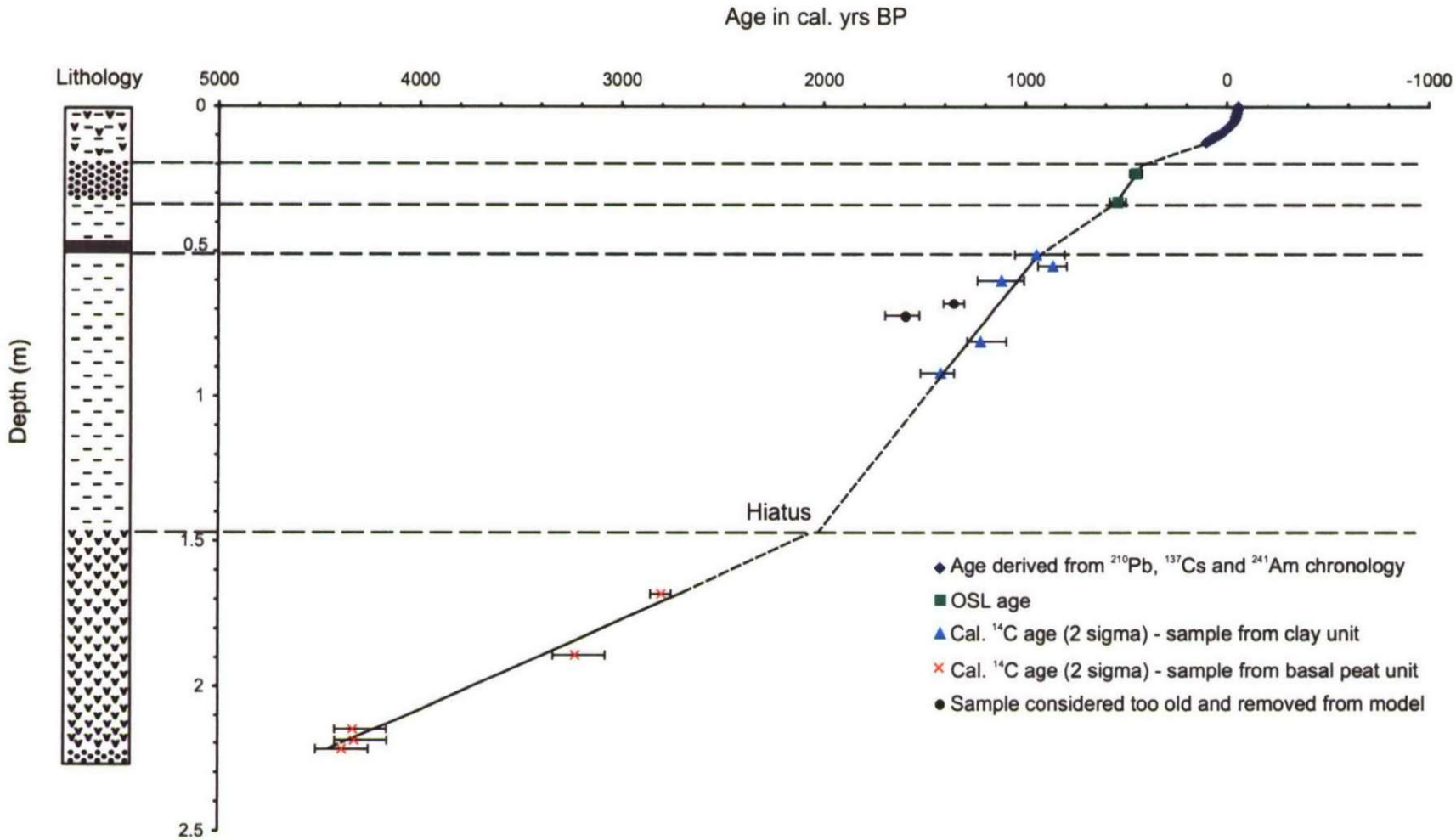

Figure 8.12. Age-depth model for Røgel core RØ1. Key to lithology is given in Figure 5.7.

8.8 Reconstruction of local water levels

For each diatom sample analysed the WA-PLS transfer function has calculated the palaeomarsh-surface elevation at which the sample was formed (the 'indicative meaning') (Sections 8.2-8.5). Although goodness of fit and MAT statistics have indicated that some of the reconstructed palaeomarsh-surface elevations are unreliable, it would be erroneous to exclude samples solely on the basis of these results. It is important to assess the reliability of a reconstruction alongside litho- and biostratigraphical information as well as by using statistical techniques. This is explored and discussed in the next chapter where local water-level curves are compared with the results of litho- and biostratigraphical investigations to explore the evolution of the Ho Bugt embayment. All diatom-inferred samples are therefore retained in the analysis at this stage. Local water-level curves are presented for Kjelst Enge, Bredmose and Røgel salt marshes in the following sections of this chapter. The most recent parts of these records are compared with observational data from the nearby tide gauge at Esbjerg to provide further assessment on the reliability of the reconstructions. The tide gauge at Esbjerg has recorded sea-level change since 1890 (data available from the Permanent Service for Mean Sea Level at http://www.pol.ac.uk/psmsl/) and provides a useful test of the reconstructed records.

To reconstruct local water-level changes, all diatom-inferred data points are plotted in a time-height diagram using the relationship:

$$\mathrm{LWL} = H - I, \qquad \textbf{Equation 8.2}$$

where *LWL* is the local water level, *H* is the sample height relative to DNN and *I* is the diatom-inferred indicative meaning of the sample, calculated from the WA-PLS transfer function. The age (and age error) of each sample is estimated from the respective age-depth model to produce a relative sea-level chronology. Ages are interpolated for samples within each stratigraphic unit using the equation of the appropriate trend line plotted in Figures 8.9 and 8.12. Sample-specific bootstrap errors established for each sample (the 'indicative meaning') (Section 8.2-8.5) are applied as vertical (height) errors in the water-level reconstruction. Samples which have an indicative meaning and an age that is *not* interpolated are known as sea-level index points (SLIPs) (Shennan, 1982, 1986a, 1986b).

8.8.1 Kjelst Enge core KE2

Two water-level curves for core KE2 from Kjelst Enge are presented in Figures 8.13 and 8.14. The first of these presents only SLIPs, and the second presents SLIPs and all age-interpolated data points. As only three data points are available from the most recent part of this core, this record is not considered sufficient enough to make a valid comparison with the nearby tide-gauge record at Esbjerg.

The two water-level curves for core KE2 show a rise in local water level of around 3.5 m in approximately 4000 years. In Figure 8.14 a period of rapid rise is observed around 1900 cal. yr BP. Here the water level appears to rise by approximately 1 m in only a few hundred years. Concerns regarding the statistical reliability of many of the diatom-inferred reconstructed points have already been highlighted (Section 8.2.1). Here, however, the steepness of the rise is primarily the result of the age-depth model used. Reconstructed points in this particular section of the core are all from the clay unit. Whilst it is accepted that the clay unit is likely to have accumulated very rapidly, as a result of infill, a number of age reversal are apparent in this particular section of the core (core depth 0.96 – 2.0 m). In addition, the lack of dates in the lower part of the clay means that inferred ages in this part of the core are much less certain. Age-interpolated data points in this particular section of the water-level curve can therefore be considered less reliable.

In Figure 8.14 a period of slightly lower water level around 900 cal. BP is observed. However, this is constrained by only a few data points. The lack of data points between approximately 1000 and 200 cal. yr BP is probably insufficient to infer sub-millennial scale fluctuations in this section of the curve. Importantly, at no stage in the last 4000 years did the local water level in core KE2 appear to reach above present day levels.

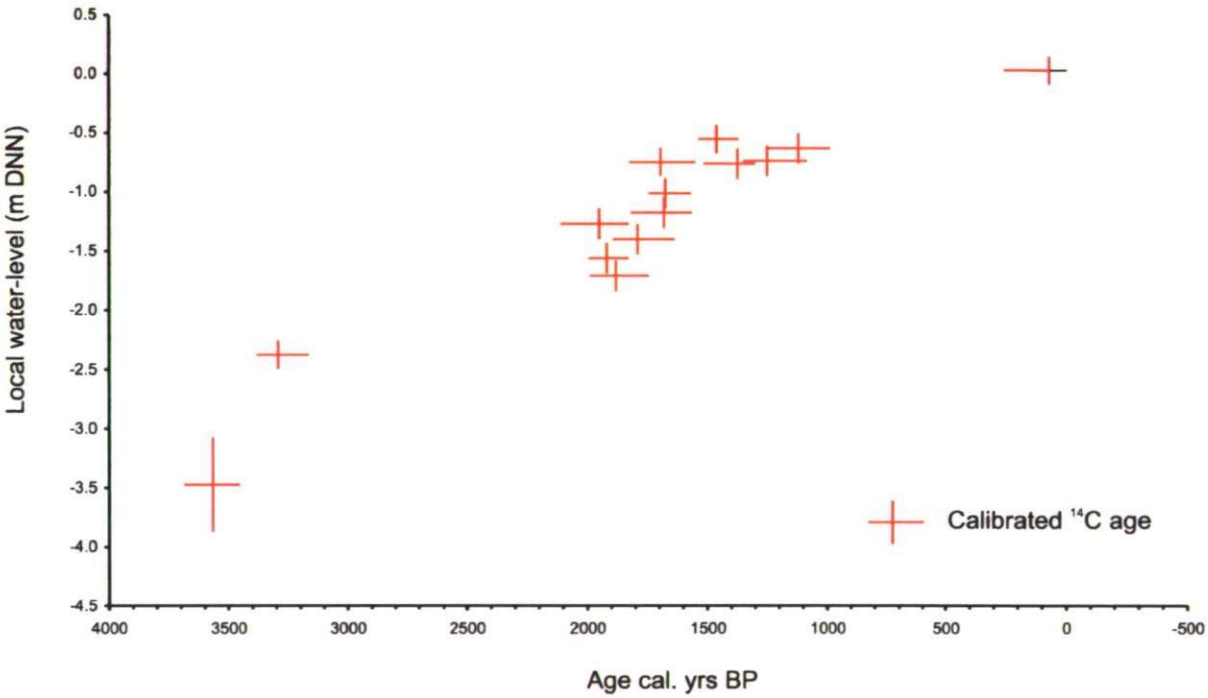

Figure 8.13. Local water-level history of core KE2 from Kjelst Enge showing only SLIPs. The median age of the 2σ calibrated radiocarbon age ranges are plotted, and the full 2σ range is shown by the x-axis error bars. Vertical (height) error bars represent the indicative meaning.

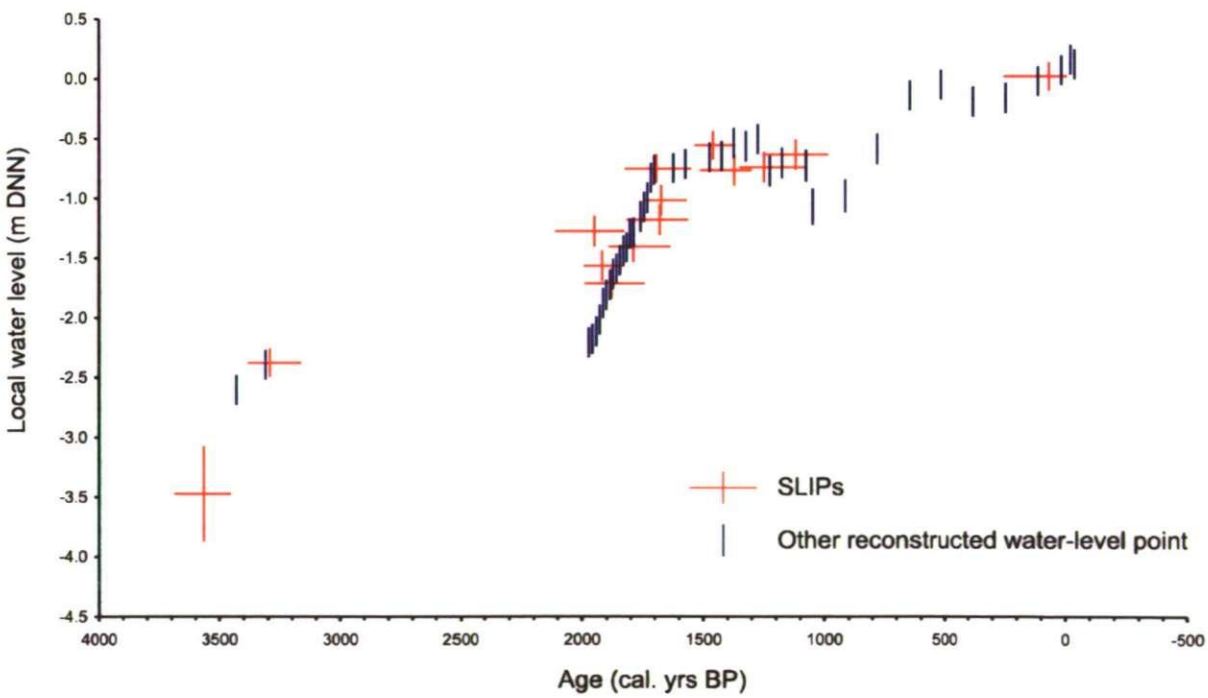

Figure 8.14. Local water-level history of core KE2 from Kjelst Enge showing SLIPs and all diatom-inferred reconstructed sea-level points. Age-errors for interpolated ages are not shown. These errors are at least as large as those from adjacent calibrated ^{14}C ages. Age-errors on ^{210}Pb age estimates were not provided by the laboratory. Vertical (height) error bars represent the indicative meaning.

8.8.2 Bredmose core BR9

On the basis of ^{210}Pb and ^{137}Cs age estimates the local water-level history for the past two centuries from core BR9 is reconstructed in Figure 8.15. The reconstruction for this core is compared with the observations from the tide-gauge record at Esbjerg. For clarity the data in this figure are plotted against age in calendar years (AD). The observed trend of relative sea-level rise since 1890 is reasonably matched by the reconstruction, although some discrepencies are noted. For example prior to 1930 the reconstructed points under-predict the relative sea level. After 1930 the reconstruction tends to over-predict relative sea level.

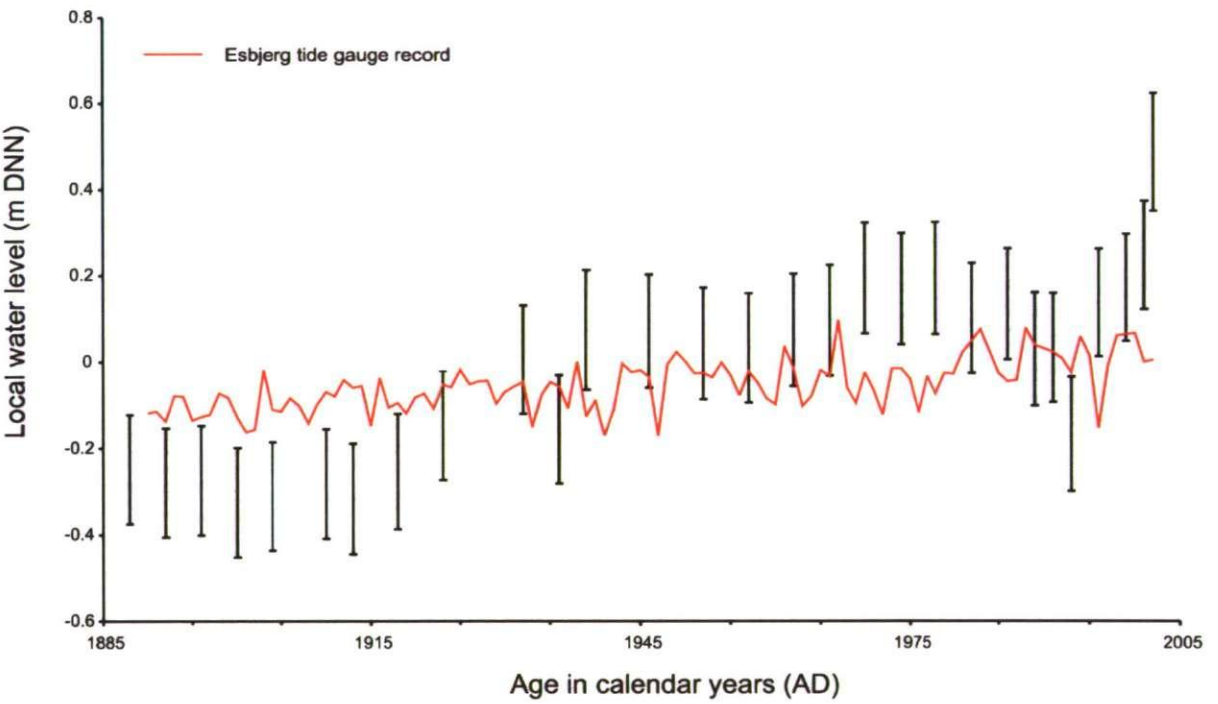

Figure 8.15. Local water-level history of core BR9 from Bredmose showing all diatom-inferred reconstructed water-level points and the Esbjerg tide-gauge record. Age-error bars for ^{210}Pb ages were not provided by the laboratory. Vertical (height) error bars represent the indicative meaning.

8.8.3 Røgel core RØ1

Local water-level curves for core RØ1 from Røgel salt marsh are presented in Figures 8.16 and 8.17. Again, the first of these curves presents only SLIPs. The second presents SLIPs and all age-interpolated data points. The two curves for core RØ1 show a rise in local water level of around 3 m in approximately 4500 years and are in general agreement with the record from Kjelst Enge. One major exception to this is noted. Around 1900 cal. yr BP, the rise in local water level in the RØ1 record does not appear to be as rapid as that identified in the KE2 record (Figure 8.14). However, once again some concern regarding the age-depth model used must be highlighted. Given the lack of dates in the lower part of the clay unit in core RØ1 (Figure 8.12), inferred ages in this part of the core are again less certain. These two records from Røgel and Kjelst Enge are further compared and discussed in the next chapter.

In Figure 8.17, two periods of slightly lower water level are identified. The first around 1000 cal. yr BP, and the second around 500 - 600 cal. yr BP. However, these trends are not particularly well constrained and considerable scatter is noted during these periods. It is possible that the lower water levels around 1000 and 500 cal. yr BP relate to the formation of the black layer and the sand layer, respectively. However, an absence of diatom data from the black layer in this core means that the water-level history between approximately 900 and 600 cal. yr BP is very poorly constrained. These points are further discussed in the next chapter where the local water-level curves are integrated with the results of litho- and biostratigraphical analyses.

On the basis of ^{210}Pb, ^{137}Cs and ^{241}Am age estimates the water-level history for the past two centuries is reconstructed in Figure 8.18. The fifteen youngest samples in core RØ1 span the period from 1790 until the present (2004) and they are plotted together with the tide-gauge data in Figure 8.18. For clarity the data in this figure are again plotted against age in calendar years (AD). The reconstructed sea-level record shows reasonable agreement with the tide-gauge observations. The observed trend of relative sea-level rise since 1890 is matched by the reconstruction for the past 50 years, but the older part of the record (prior to AD 1955) appears to be under-estimated. This is also the case at Bredmose.

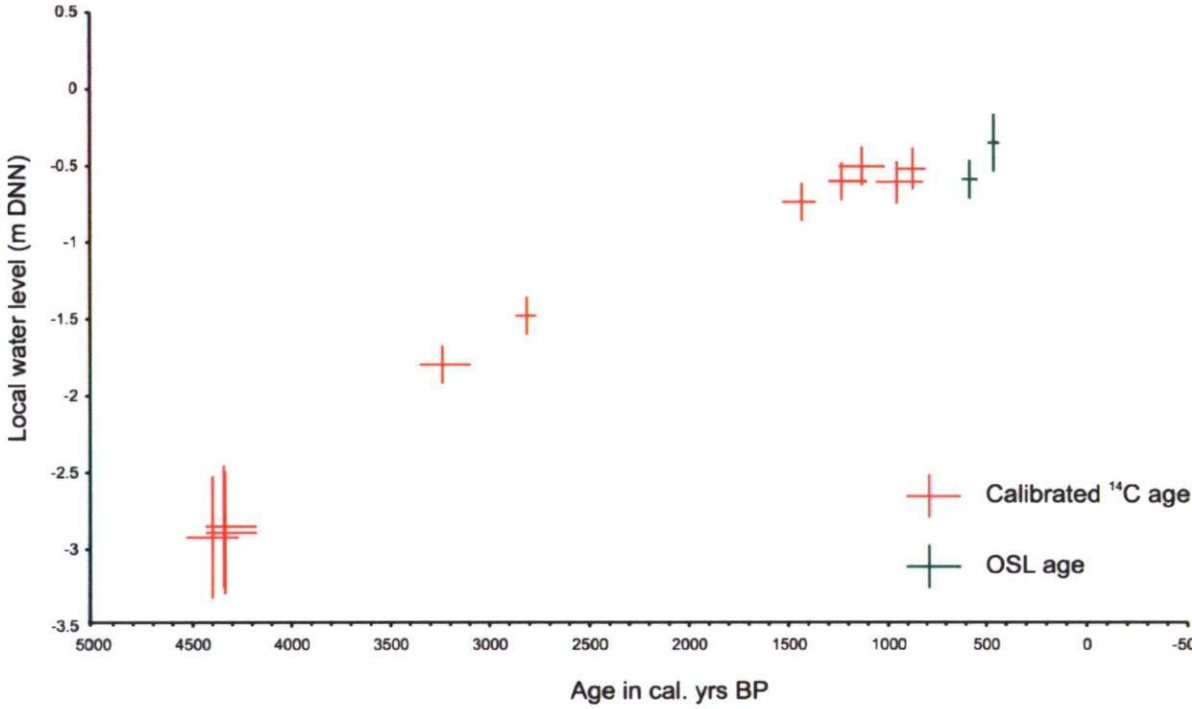

Figure 8.16. Local water-level history of core RØ1 from Røgel showing only SLIPs. The median age of the 2σ calibrated radiocarbon age ranges are plotted, and the full 2 σ range is shown by the x-axis error bars. Vertical (height) error bars represent the indicative meaning.

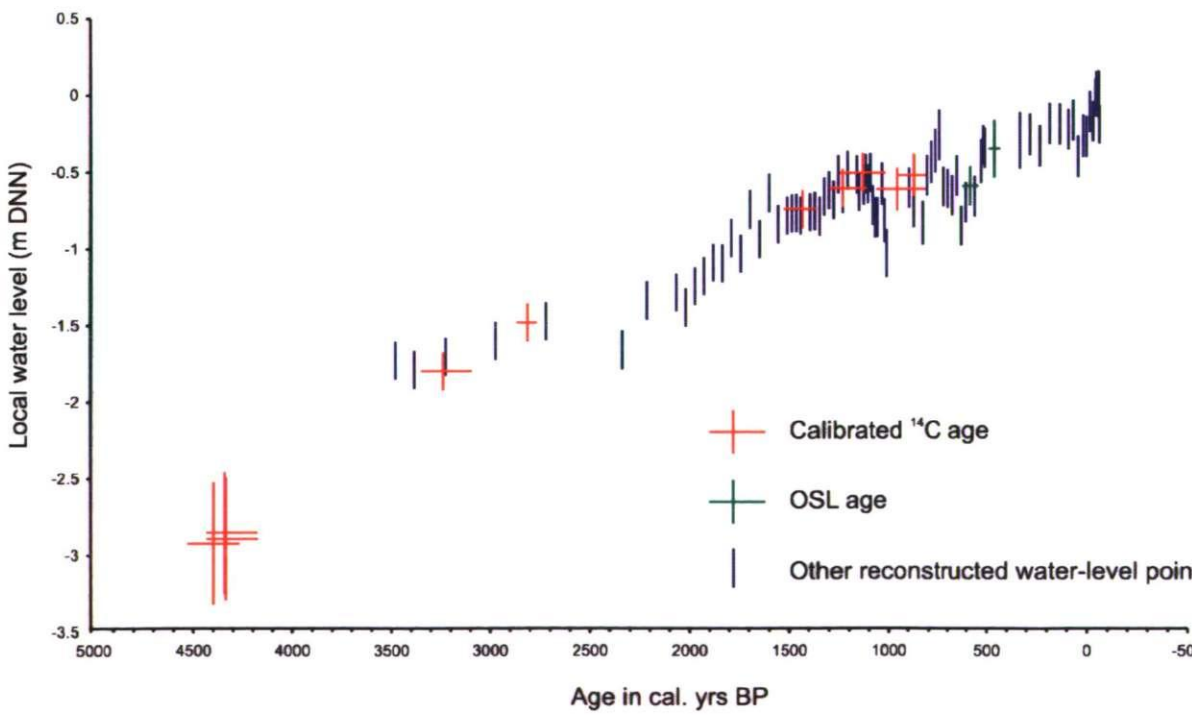

Figure 8.17. Local water-level history of core RØ1 from Røgel showing SLIPs and all diatom-inferred reconstructed sea-level points. Age-errors for interpolated ages are not shown. These errors are at least as large as those from adjacent calibrated ^{14}C ages, except for the uppermost samples where age-errors on ^{210}Pb age estimates are between 2 and 10 yr and are too small to show. Vertical (height) error bars represent the indicative meaning.

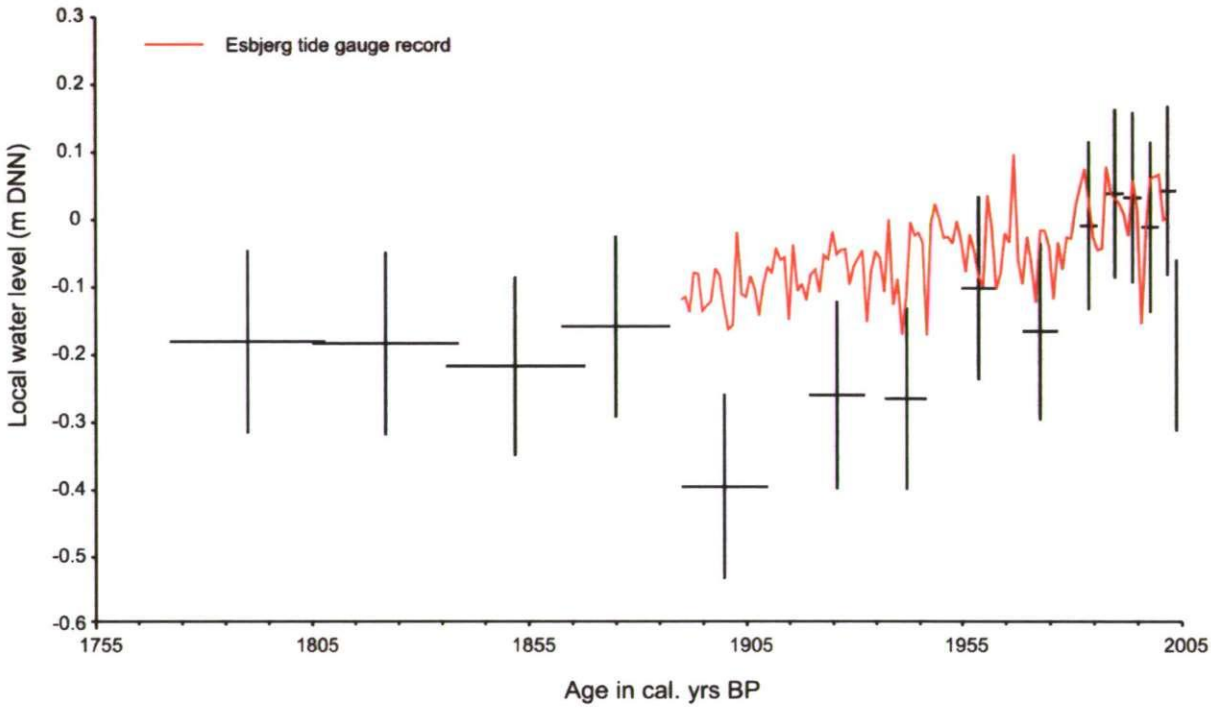

Figure 8.18. Local water-level history of core RØ1 from Røgel showing the 15 youngest diatom-inferred reconstructed water-level points and the Esbjerg tide-gauge record.

8.9 Chapter summary

This chapter has presented the palaeomarsh-surface reconstruction of three core sections (BR9, KE2 and RØ1) using the WA-PLS transfer function developed in Chapter 7. The reliability of the reconstructions was assessed via the use of goodness of fit statistics after fitting the samples passively into ordination space and the MAT. In all reconstructions these statistics have indicated that many of the reconstructed values should be interpreted with caution. Under representation of taxa in the modern training set is the main reason affecting the reliability of these reconstructions, although the absence of several key fresh water taxa has also been noted. However, it is highly likely that given 'better' fresh water analogues and by improving the representation of taxa in the modern training set, the overall trends demonstrated by the palaeomarsh-surface records would remain the same. In some cases these trends would be amplified. This is especially true of the fresh water basal samples for which the indicative meanings are likely to be under-estimated.

In the second part of this chapter age-depth models were developed for each of the core sections investigated using available OSL, calibrated ^{14}C, ^{137}Cs, ^{210}Pb and ^{241}Am ages. The indicative meaning for each diatom sample, calculated from the WA-PLS transfer function,

was then linked to local water level and plotted in a time-height diagram of local water-level change. Given the lack of dates and the age reversals in the lower part of the clay unit in both cores KE2 (Figure 8.9) and RØ1 (Figure 8.12), inferred ages in these units are much less certain and the corresponding sections of the resulting water-level curves need to be interpreted with caution. The water-level reconstructions for the past two centuries at Røgel and Bredmose were compared with the nearby tide-gauge record from Esbjerg to provide further assessment on the reliability of the reconstructions. From these reconstructions the following key points can be highlighted:

- The local water-level records from Kjelst and Røgel both demonstrate around 4 m of rise in the last 4000 yr. These records are further compared in the next chapter
- The records from cores BR9 and RØ1 for the past two centuries generally show good agreement with the tide-gauge data from Esbjerg since 1950, but appear to underestimate relative sea-level in the early parts of the record.

Comparisons between the local water-level curves are discussed in the next chapter where they are placed in the context of litho- and biostratigraphical results to investigate the evolution of the Ho Bugt embayment. The millennial-scale relative sea-level history of the Ho Bugt embayment is established, and the dominant process controlling relative sea-level change in the Ho Bugt embayment is explored through comparison of the relative sea-level data with predictions from a series of geophysical models.

Chapter 9

Integration and Discussion

In this chapter, sea-level index points (SLIPs) from a number of cores are plotted on one diagram to reconstruct the millennial-scale sea-level history of the Ho Bugt embayment. The local water-level curves established in Chapter 8 are compared and discussed and placed in the context of litho- and biostratigraphical results obtained throughout this study. Particular focus is given to comparing the local water-level history of the master sequence established in this study (core RØ1) with that previously established as part of the HOLSMEER Project (core KE2). The second part of this chapter draws together the results of litho- and biostratigraphical investigations, alongside the local water-level histories to explore the evolution of the Ho Bugt salt marshes. The value of obtaining relative sea-level data from this area is demonstrated by comparing sea-level data established by this study with predictions based on geophysical models. These models provide some insight into the controls on relative sea-level change in the Ho Bugt embayment during the mid- to late Holocene. In the final section of this chapter, the implications of this study for a number of broader themes are discussed.

9.1 The millennial-scale relative sea-level history of the Ho Bugt embayment

In order to document the longer-term relative sea-level history of the Ho Bugt embayment, all available diatom-inferred SLIPs are plotted on one time-height diagram of relative sea-level change (Figure 9.1). This diagram plots only samples for which an age has been established by either ^{14}C or OSL ('true' SLIPs). Table 9.1 shows the ^{14}C and OSL samples that have been previously excluded from analyses, and the reason for their rejection. These samples are not included in this diagram. The ^{14}C and OSL samples that are used to document the millennial-scale relative sea-level history of the Ho Bugt embayment are shown in Table 9.2. Relative sea-level change is calculated using the relationship:

$$RSL = H - I, \qquad \textbf{Equation 9.1}$$

where *RSL* is the relative sea level, H is the sample height relative to DNN and I is the diatom-inferred indicative meaning of the sample, calculated from the WA-PLS transfer function (Table 9.2).

Sample number	Core	Sample depth (m)	Elevation (m DNN)	Material dated	Reason for rejection
16	BR1	1.77	-0.09	*Phragmites* fragment	Returned younger than expected age.
33	OEB5	0.18	+1.61	*Phragmites* (rhizome?)	Returned younger than expected age.
13	KE2	2.35	-0.77	Detrital *Phragmites*	Sample re-worked from basal peat
20	RØ1	0.68	+0.92	*Phragmites*	Sample considered too old, removed from age-depth model
21	RØ1	0.72	+0.88	*Phragmites*	Sample considered too old, removed from age-depth model
48	OEA	1.52	+0.08	Sand	No diatom data and sample could not be related to a modern environment.

Table 9.1. Details of the ^{14}C and OSL samples that have been previously excluded from analyses, and the reason for their rejection. These samples are also excluded from the millennial-scale relative sea-level history of the Ho Bugt embayment. Sample numbers correspond to those in Tables 5.1, 5.2 and 5.3.

The millennial-scale relative sea-level history of the embayment is presented in Figure 9.1. Basal SLIPs are differentiated from non-basal SLIPs in order to assess the degree to which non-basal samples have been affected by sediment compaction. Basal SLIPs are usually considered superior compared to non-basal SLIPs, as the former are collected from the base of peat where it directly overlies an incompressible substrate and vertical displacement by compaction can therefore be ruled out (Gehrels et al., 2006a). However, in this study diatom-inferred indicative meaning estimates for many of the older, fresh water basal samples may under estimate elevation. These points are further explored in Section 9.4.

The reconstructed millennial-scale relative sea-level history for the Ho Bugt embayment (Figure 9.1) shows that in Ho Bugt, sea level has risen by about 7 m during the past 7000 yr. In the last 2000 yr, the rise in sea level has been slower than in the preceding 5000 yr. At no point during the last 7000 cal. yr BP does the Ho Bugt relative sea-level history show evidence for above present day sea level. Non-basal SLIPs older than 4000 cal. yr BP appear to have been affected by core compaction as these SLIPs plot lower than the basal SLIPs. For the more recent part of the curve (post 4000 cal. yr BP) the non-basal SLIPs plot within the trend suggested by the basal SLIPs suggesting that the more recent SLIPs have not been affected by compaction. SLIPs from the two master sections investigated in this study (KE2 and RØ1) fall within this latter part of the curve. Interpretation of the millennial-scale record suggests that neither of these two sequences have been particularly affected by sediment compaction.

Sample No.	Lab Code	Core	Depth in core (m)	Elevation (m DNN)	Calibrated ^{14}C age (2 sigma)	Indicative meaning (m)	Indicative range (m)	RSL (m DNN)	Indicative meaning (m)	Indicative range (m)	RSL (m DNN)
1	AAR-8891	KE2	0.12	+1.46	31-256	1.43	0.12	0.03	1.70	0.2	-0.24
2	AAR-8892	KE2	0.50	+1.08	984-1286	1.71	0.13	-0.63	2.30	0.4	-1.22
3	AAR-8048	KE2	0.56	+1.02	1081-1350	1.76	0.13	-0.74	2.30	0.4	-1.28
4	AAR-8049	KE2	0.68	+0.90	1367-1536	1.45	0.12	-0.55	1.90	0.2	-1.0
5	AAR-8050	KE2	0.82	+0.76	1300-1514	1.52	0.13	-0.76	1.70	0.2	-0.94
6	AAR-8051	KE2	0.96	+0.62	1548-1824	1.37	0.12	-0.75	1.50	0.2	0.88
7	AAR-8052	KE2	1.16	+0.42	1567-1813	1.43	0.13	-1.01	1.50	0.2	-1.08
8	AAR-8053	KE2	1.38	+0.20	1562-1817	1.38	0.13	-1.18	1.70	0.2	-1.50
9	AAR-8054	KE2	1.51	+0.07	1825-2110	1.34	0.13	-1.27	1.50	0.2	-1.43
10	AAR8055	KE2	1.67	-0.09	1635-1892	1.31	0.13	-1.40	1.10	0.4	-1.19
11	AAR-8056	KE2	1.84	-0.26	1826-1994	1.30	0.13	-1.56	1.10	0.4	-1.36
12	AAR-8057	KE2	2.01	-0.42	1740-1989	1.28	0.13	-1.70	1.10	0.4	1.52
14	AAR-8059	KE2	2.57	-0.99	3163-3384	1.38	0.12	-2.37	2.30	0.4	-3.29
15	AAR-8060	KE2	2.75	-1.17	3453-3687	2.30*	0.4*	-3.47	2.30	0.4	-3.47
17	AAR-8068	BR12	1.53	+0.65	1714-1918	1.51	0.13	-0.86	2.30	0.4	-1.65
18	AAR-8069	BR2	1.60	-0.02	2153-2719	1.46	0.12	-1.48	2.30	0.4	-2.32
19	SUERC-9253	RØ1	0.51	+1.09	802-1051	1.70*	0.20*	-0.61	1.70	0.2	-0.61
22	SUERC-9256	RØ1	0.81	+0.79	1093-1287	1.39	0.13	-0.60	1.10	0.4	-0.31
23	SUERC-9257	RØ1	0.92	+0.68	1351-1518	1.42	0.13	-0.74	1.1	0.4	-0.42
24	SUERC-9259	RØ1	1.68	-0.08	2753-2855	1.40	0.13	-1.48	2.3	0.4	-2.38
25	SUERC-9262	RØ1	1.89	-0.29	3079-3338	1.51	0.13	-1.80	2.30	0.4	-2.59
26	SUERC-9263	RØ1	2.15	-0.55	4162-4424	2.30*	0.40*	-2.85	2.30	0.4	-2.85
27	SUERC-9264	RØ1	2.19	-0.59	4160-419	2.30*	0.40*	-2.89	2.30	0.4	-2.89
28	SUERC-9265	RØ1	2.22	-0.62	4253-4515	2.30*	0.40*	-2.92	2.30	0.4	-2.92
29	SUERC-9266	RØ1	0.55	+1.05	791-936	1.57	0.13	-0.52	1.70	0.2	-0.65
30	SUERC-9267	RØ1	0.60	+1.00	1005-1236	1.50	0.13	-0.50	1.70	0.2	-0.70
31	SUERC-9268	OEA	1.24	+0.38	1698-1868	2.01	0.14	-1.63	2.30	0.4	-1.92
32	SUERC-9269	OEA	1.52	+0.10	2758-2868	2.30*	0.40*	-2.20	2.30	0.4	-2.20
34	SUERC-9274	OEB5	0.82	+0.97	658-730	1.37	0.13	-0.40	1.5	0.2	-0.53
35	SUERC-9275	OEB5	1.01	+0.78	1178-1298	1.39	0.13	-0.61	1.70	0.2	-0.92
36	SUERC-9276	KE1	4.16	-2.59	2748-2849	1.55	0.13	-4.14	1.50	0.4	-4.09
37	SUERC-9277	KE1	5.15	-3.58	3890-4091	1.73	0.17	-5.31	2.30	0.4	-5.88
38	SUERC-9278	KE1	5.98	-4.41	5470-5643	1.69	0.15	-6.10	2.30	0.4	-6.71
39	SUERC-9279	KE1	6.54	-4.97	6208-6408	2.00	0.14	-6.97	2.30	0.4	-7.27
40	SUERC-9282	KE1	6.84	-5.27	6860-7157	1.75	0.15	-7.02	2.30	0.4	-7.57
41	SUERC-9283	KE12	2.35	-0.83	2493-2751	1.62	0.13	-2.45	2.30	0.4	3.13
42	SUERC-9285	KE12	3.80	-2.28	3480-3686	2.17	0.14	-4.45	2.30	0.4	-4.58
43	SUERC-9286	KE13	3.34	-1.75	2470-2736	1.83	0.13	-3.58	2.30	0.4	-4.05
44	SUERC-9287	KE13	5.08	-3.49	5746-5922	1.77	0.13	-5.26	2.30	0.4	-5.79
45	Risø 052803	RØ1	0.23	1.37	366-426 (OSL)	1.72	0.19	-0.35	1.72**	0.19**	-0.35**
46	Risø 052804	RØ1	0.33	1.27	446-526 (OSL)	1.86	0.12	-0.59	1.86**	0.12**	-0.59**
47	Risø 052805	OEB5	0.33	1.46	406-466 (OSL)	1.74	0.13	-0.28	1.74**	0.13**	-0.28**

Table. 9.2. The ^{14}C and OSL samples that are used to document the millennial-scale relative sea-level history of the Ho Bugt embayment. Numbers in red are WA-PLS, diatom-inferred valves, except for samples marked by an asterisk (*), which have been estimated from surveyed heights of present day marsh environments (Table 8.7) because no diatom data are available. Numbers in blue are inferred from lithofacies and lithostratigraphical contacts based on surveyed heights of present day marsh environments (Table 8.7), except for the samples marked by a double asterisk (**), which are diatom inferred because the samples cannot be related to a modern environment (Table 8.7). The information in these columns in used in Section 9.4. Five dated samples (nos. 13, 16, 20, 21, 33 and 48) have been previously excluded (Table 9.1).

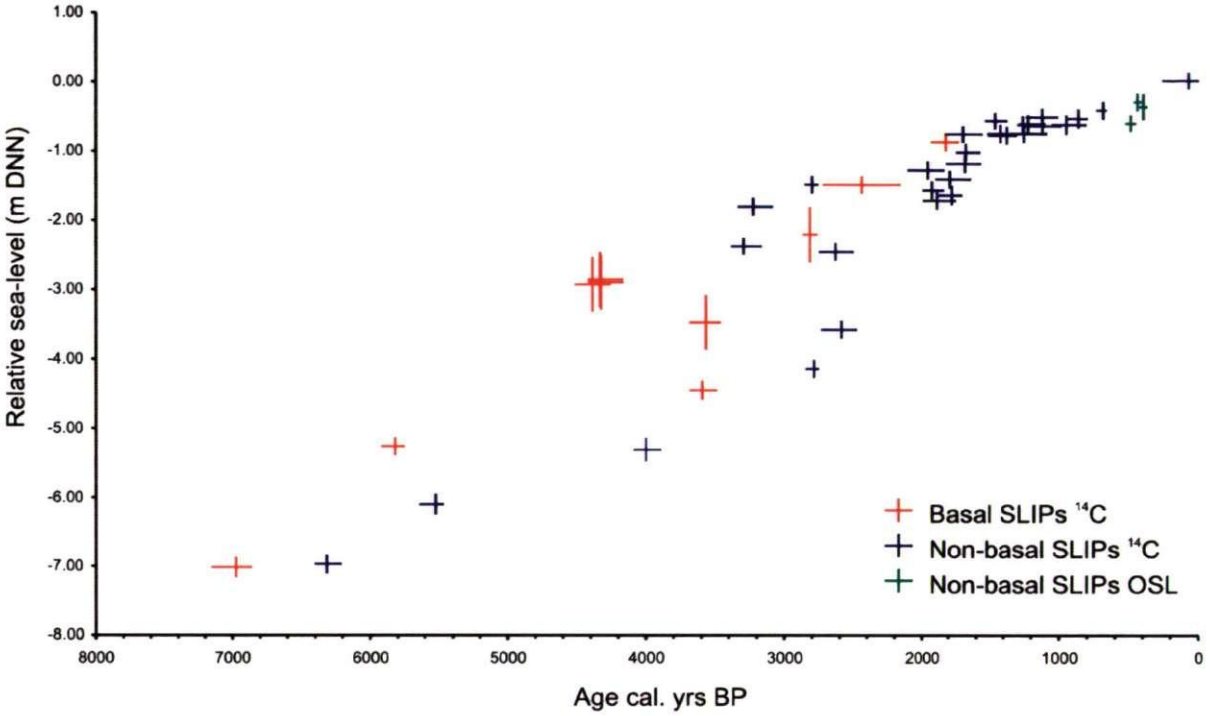

Figure 9.1. Millennial-scale sea-level history of the Ho Bugt embayment based on all available basal and non-basal SLIPs (Table 9.2). The median age of the 2σ calibrated radiocarbon age ranges are plotted, and the full 2σ range is shown by the x-axis error bars. Vertical (height) error bars represent the indicative meaning.

The millennial-scale relative sea-level curve presented in Figure 9.1 has established 42 new sea-level index points for the Ho Bugt embayment. Sixteen of these have been already published in Gehrels et al. (2006a) but are revised in this study on the basis of new quantitative relative sea-level predictions obtained by use of the WA-PLS, diatom-based transfer function. In the previous chapter concerns were highlighted regarding the statistical reliability of many of the diatom-inferred reconstructions presented in this study however, reasonable agreement between the Esbjerg tide gauge data and sea-level reconstructions from Bredmose and Røgel for the past two centuries (Figures 8.15 and 8.18) suggest that the SLIPs presented in this study are perhaps more reliable than the goodness of fit and MAT statistics (Sections 8.2 – 8.5) initially suggest. The limitations of the millennial-scale relative sea-level history are discussed in Section 9.4 where this curve is compared with one established using a qualitative interpretation of lithology, to provide further assessment on the reliability of the diatom-inferred reconstructions.

9.2 Comparison of local water-level curves

In Chapter 8, local water-level histories were presented for cores KE2 (Figures 8.13 and 8.14) and RØ1 (Figures 8.16 and 8.17). These two water-level curves are compared in Figure 9.2. Both curves demonstrate the same general trend in water level and show around 3.5 m of rise in the last 3500 – 4500 yr. Both curves demonstrate that the rate of rise has been slower in the last 1500 yr than in the preceding 3000 yr, as evidenced by the steepness of the two curves prior to 1500 cal. yr BP. This supports the findings of the millennial-scale sea-level record (Figure 9.1), which suggests a slower rate of rise during the last 2000 yr.

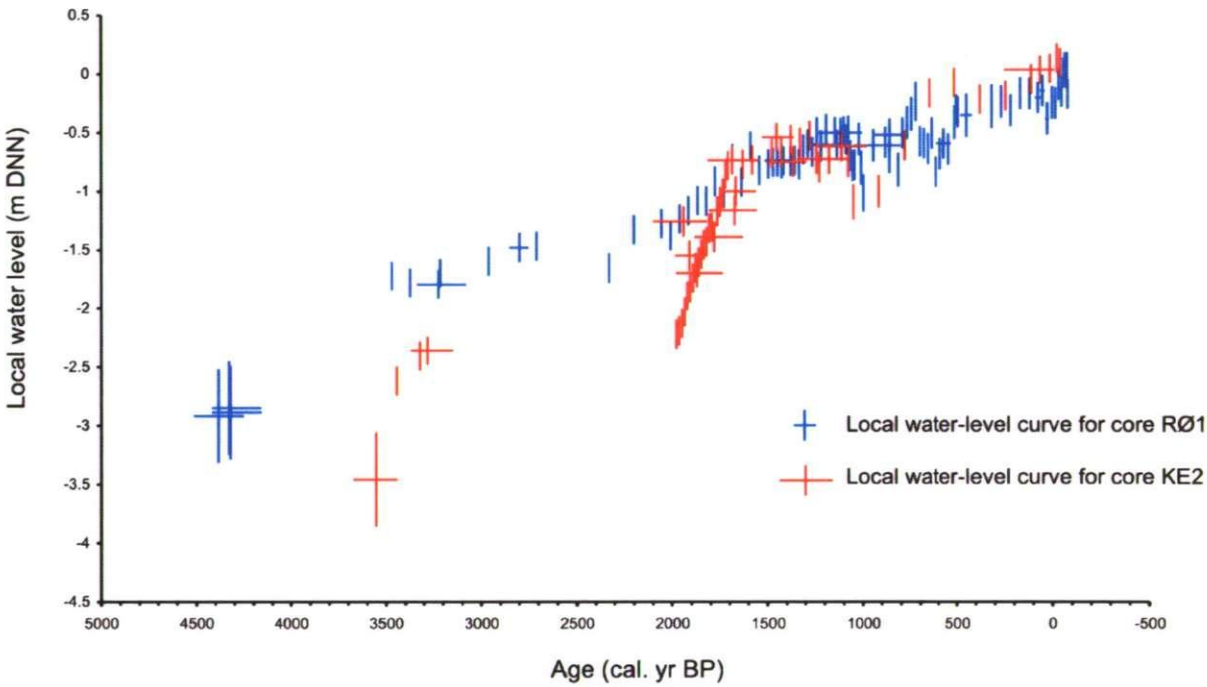

Figure 9.2. Comparison of the diatom-inferred local water-level curves from Kjelst Enge core KE2 and Røgel core RØ1. For SLIPs, the median age of the 2σ calibrated radiocarbon age range is plotted and the full 2σ range is shown by the x-axis error bars. Ages for all other reconstructed points are inferred from the age-depth models (Figures 8.9 and 8.12). Age-errors for interpolated ages are not shown. These errors are at least as large as those from adjacent calibrated ^{14}C ages. Vertical (height) error bars represent the indicative meaning.

Although the two curves from cores KE2 and RØ1 show the same general trend in relative sea-level, the two records appear to be offset prior to 1500 cal. yr BP. In particular, a rapid period of rise is noted in the KE2 record between 2000 and 1500 cal. yr BP which is not identified in the RØ1 record. Here the KE2 record shows around 1.5 m of rise in only a few hundred years. In both cores, the age-depth models for this time period are considered less reliable. In core RØ1, no dates are available for the period between 1420 and 2800 cal.

yr BP. Here inferred ages are estimated by extrapolating the accumulation rate from the upper part of the profile. In core KE2, a series of radiocarbon ages in the lower clay unit with overlapping calibrated ages has resulted in a very high accumulation rate for this particular section for the core. Between 1880 and 3290 cal. yr BP no dates are available and again inferred ages are estimated by extrapolating the accumulation rate from the upper part of the profile. For both cores, the water-level record between approximately 1500 and 3000 cal. yr BP is therefore considered less reliable, primarily because of the uncertainty associated with the interpolated ages.

For the most recent part of the record (post 1500 cal. yr BP) cores KE2 and RØ1 show better agreement. Both curves demonstrate a small fall in relative sea-level around 900 cal. yr BP. A second fall is identified at 500 cal. yr BP in the RØ1 record but not in the KE2 record. Here the lack of data points between approximately 1000 and 200 cal. yr BP in the KE2 record is probably insufficient to infer sub-millennial scale fluctuations in this particular section of the curve.

In Chapter 8, local water-level histories for the past two centuries were presented for cores BR9 (Figure 8.15) and RØ1 (Figure 8.18). These two water-level curves are compared in Figure 9.3. Both records show reasonable agreement with the observed tide gauge data from Esbjerg, although both records tend to under-estimate relative sea level in the earlier parts of the record (before 1955). For the most recent 20 years, the RØ1 record shows better agreement with the observational data than the record from Bredmose. Although the two reconstructed records show the same general trend as the tide gauge data, the diatom-inferred water-level records show a greater amount of change during the past 130 years than is observed in the tide-gauge data. Between AD 1855 and AD 2005 the diatom-inferred records show approximately 0.40 m of rise. However, the Esbjerg tide-gauge record only shows around 0.20 m of rise during the same time period. The reasons for this are unclear but may be related to under-represented and missing taxa in the modern training set.

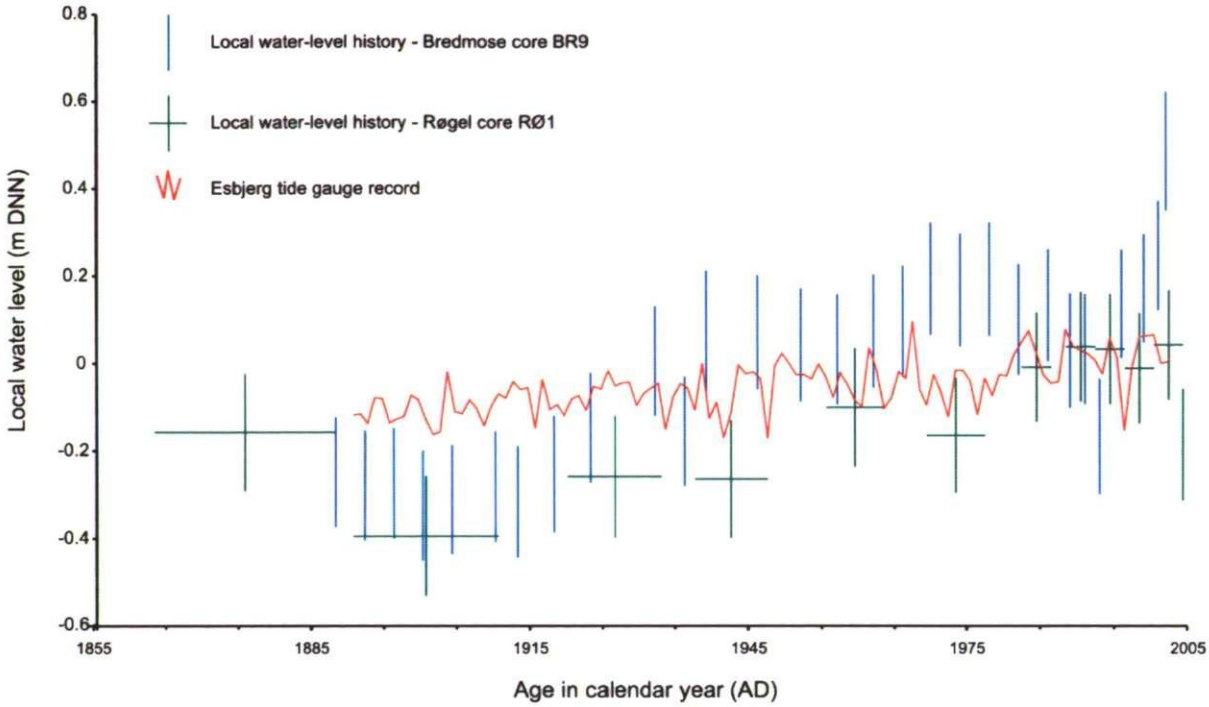

Figure 9.3. Comparison of the most recent part of the diatom-inferred water-level records from Bredmose core BR9 and Røgel core RØ1, alongside observational data for the past two centuries from the Esbjerg tide-gauge record. Age error bars are not available for the Bredmose ^{210}Pb ages, as the laboratory did not provide this information.

9.3. Comparisons with published data

It is difficult to compare the sea-level and local water-level records from Ho Bugt with previously published sea-level curves from other locations in Denmark and along the German North Coast, mainly because the resolution and age-control on these older records is poor (Figures 2.1 and 2.5). Although poorly constrained, sea-level records for the German North Sea region for example, Menke (1976) for the Eider-Miele region, Ludwig et al. (1979, 1981) for the southern North Sea, and Müller (1962) for the German North Sea region (Figure 2.5), all appear to document around 7 m of rise during the last 7000 yr, which is in general agreement with the Ho Bugt records. A number of these curves show evidence to suggest above present day sea levels around 2000 cal. yr BP. The Ho Bugt sea-level histories do not support this.

The sea-level records from Ho Bugt agree less well with the published sea-level curves from other locations in Denmark (Figure 2.1) however, this is in part due to differing isostatic settings (Figure 1.1). Again, it is difficult to make comparisons because the resolution and age-control on many of these older records is very poor. Importantly, the

sea-level records established by this current study disagree with previously published data on sea-level changes along the southern Danish North Sea Coast. Most significantly, the Ho Bugt relative sea-level histories do not provide evidence for a sea-level highstand at any time during the last 7000 yr. The 2500 – 3000 cal. yr BP highstand is an important feature of Mörner's widely cited Kattegat sea-level curve (Figure 2.3 inset) (Mörner, 1969a; 1969b; 1976) and is used by several authors (e.g., Aagaard et al., 1995; Davis et al., 1997; 2001) to speculate that sea level in south west Denmark was at least 1.5 m above present c. 2500 – 3000 cal. yr BP (Section 2.1.2). However, this study does not support such findings. The 'marine deposits' found at a level of +1.5 m DNN west and south of the Grærup cliff (Figure 2.4) by Clemmensen et al. (1996) are likely to represent a recent salt-marsh surface, rather than an old tidal flat as suggested by previous authors, who relate this surface to a sea-level highstand (Gehrels et al., 2006a). This interpretation is consistent with the level of salt-marsh deposition in the modern environment (Table 8.7).

Additionally evidence for refuting the 3000 cal. yr BP highstand is provided by ^{14}C ages obtained from basal peat sections in this study. ^{14}C ages obtained from cores at Røgel (RØ1) and Kjelst Enge (KE2) (Figure 5.1 and 5.2, respectively) clearly indicate that around 3000 cal. yr BP basal peat formation was taking place in the Ho Bugt embayment. In the Ho Bugt embayment basal peat formation occurs above + 1.9 m DNN and forms under fresh water conditions. The suggestion that a sea-level highstand occurred around this time is therefore erroneous. On the basis of the evidence present in this current study, the 3000 cal. yr BP shoreline suggested by Aagaard et al. (1995) and Clemmensen et al. (1996) for the Ho Bugt embayment (Figure 2.3) is incorrect.

9.4 Limitations of the relative sea-level histories

One important limitation of the water-level curves and the millennial-scale relative sea-level history presented in this study is that the indicative meanings for many of the fresh water samples may be under-estimated. This issue was previously highlighted in Chapter 8. Here, several dominant fresh water taxa were identified as being absent or under-represented (< 10% occurrence) in the modern training set. This presented problems in the reconstruction of samples where these taxa are dominant. This is especially true of many of the fresh water basal peat samples (Section 8.5.1). The modern training set extends to a height of 2.53 m DNN and although it does include samples from the high salt marsh and fresh water marshes, the highest elevation is still probably lower than the height at which

much of the basal peat unit formed. In the modern salt-marsh environment, the fresh water marsh is estimated from surveyed heights to have formed around 2.30 ± 0.40 m. The modern training set does not extend to the upper limits of this range, and may therefore be missing a number of fresh water taxa which occupy this part of the marsh environment. Failure to cover the likely palaeo-range of the environmental variable of interest is one of the major limitations of the use of modern training sets and transfer functions (Birks, 1995, 1998).

In Chapter 8 it was argued that given 'better' fresh water analogues and by improving the representation of taxa in the modern training set, the overall trends demonstrated by the palaeomarsh-surface record would remain the same. In some cases these trends would be amplified i.e. high palaeomarsh-surface elevations are likely to become 'higher.' This again is especially true of the fresh water basal peat samples. For samples where the palaeomarsh-surface elevation is under-estimated, resulting relative sea-level predictions are likely to be over-estimated (i.e. too 'high') (Equation 9.1). To provide some assessment on the degree to which relative sea-level predictions may be over-estimated by the transfer function, Figure 9.4 compares the millennial-scale relative sea-level history of the Ho Bugt embayment established using two methods. The first method uses a quantitative approach, whereby the indicative meaning of samples is inferred by use of the WA-PLS transfer function (as previously presented in Figure 9.1). The second method uses a qualitative approach whereby the indicative meaning of samples is inferred from surveyed heights of modern salt-marsh environments (Table 8.7). For this method the indicative meaning is based on an assessment of lithofacies and lithostratigraphical contacts and compared with those established for the modern environment (Tables 8.7 and 9.2). It is important to note that although the qualitative method employed here provides some assessment of the degree to which the relative sea-level predictions may be over-estimated by the transfer function, it does not necessarily provide more 'accurate' predictions.

Figure 9.4 shows that both methods demonstrate the same overall trend in relative sea-level for the Ho Bugt embayment over the last 7000 yr. However, in the majority of cases the SLIPs inferred by use of the WA-PLS transfer function plot slightly above those SLIPs for which the indicative meaning is based on surveyed heights of modern salt-marsh environments. This is especially true for the older part of the record (before 2500 cal. yr BP). In this part of the record, the difference (height) in relative sea-level predictions

between the two reconstruction methods used is around 0.5 m. Here, many of the older fresh water basal peat samples are lacking modern fresh water analogues. For these samples especially, the transfer function significantly under-predicts palaeomarsh-surface elevation, resulting in a higher relative sea-level prediction.

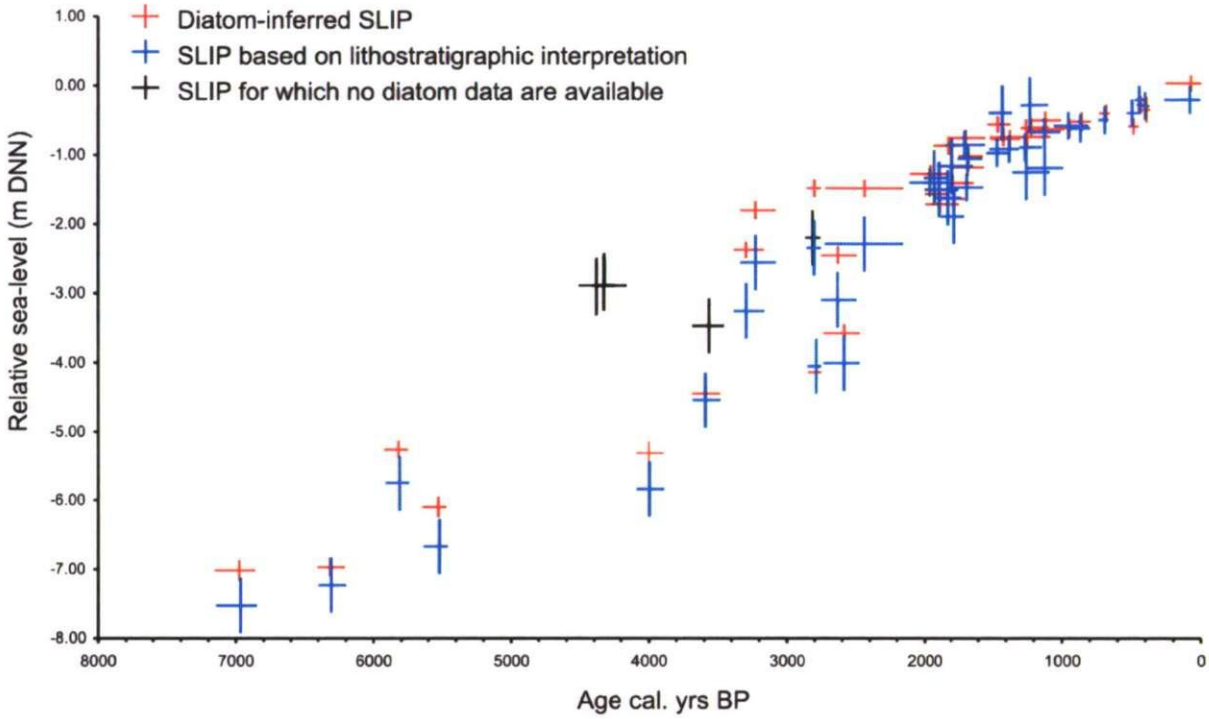

Figure 9.4. Comparison of millennial-scale relative sea-level histories for the Ho Bugt embayment showing SLIPs for which the indicative meaning is diatom-inferred, using the WA-PLS transfer function, and SLIPs for which the indicative meaning is based solely on lithostratigraphical interpretation (Tables 8.7 and 9.2). The position of five SLIPs (shown in black) remains the same between both methods because no diatom data are available for these samples (Table 9.2) and their indicative meanings are based solely on lithostratigraphical interpretation.

In the latter parts of the record (post 2000 cal. yr BP), the SLIPs from both methods are in better agreement. This is because many of the SLIPs in this section of the record are from the clay units. Goodness of fit statistics for these samples suggest that the samples here are more similar to those sampled in the modern environment. For these samples, the majority of fossil taxa have analogues in the modern training set which are well represented. As a result the relative sea-level predictions for both methods are in good agreement. Some exceptions to this are noted. The younger fresh water basal peat SLIPs suffer from the same problems as the older fresh water basal SLIPs. For these samples the transfer function again under-predicts palaeomarsh-surface elevation, resulting in a slightly higher relative sea-level prediction.

In addition, the two reconstruction methods provide very different vertical (height) error bars. Height errors for the WA-PLS inferred SLIPs are much smaller than those inferred from lithostratigraphy (Table 9.2 and Figure 9.4). This is an important point to note and one which has lead many authors to argue that transfer functions are able to provide highly precise reconstructions of relative sea-level (e.g., Horton et al., 2006; Edwards and Horton, 2006; Horton et al., 2003). The drive to reconstruct increasingly precise records of relative sea-level change has been a key theme in sea-level research in recent years, highlighted at international meetings of the IGCP 495 working group[1]. It has also been a major factor behind the growing popularity of the use of transfer functions in relative sea-level studies. Diatom-inferred SLIPs presented in this study reconstruct relative to level with a precision of between 0.12 and 0.15 m. However, the absence of several key fresh water taxa from the modern training set means that the diatom-inferred SLIPs from many of the fresh water samples may over-predict relative sea-level by up to 0.5 m (Figure 9.4). Such potential inaccuracies outweigh any gains in precision. This study has demonstrated the need for a thorough understanding of both the modern and fossil species data, and how these relate to one another, alongside the use of statistical techniques.

A second important limitation of the relative sea-level changes presented in this study is that these reconstructions do not take into account palaeotidal changes. An accurate analysis of tidal changes resulting from, for example, changes in the configuration of spits and tidal inlets would require an extensive modelling approach (e.g., Gehrels et al., 1995) and is beyond the scope of this study. Lithostratigraphical evidence suggests that the connection between the Ho Bugt embayment and the sea was maintained throughout the time period of this study. Stratigraphical cross-sections presented (Section 6.1) suggest a phase of uninterrupted salt-marsh deposition between at least 2000 and 1200 cal. yr BP. The continuous presence of marine allochthonous diatoms such as *Cymatosira belgica*, *Grammatophora oceanica* and *Paralia sulcata* throughout many of the core sections investigated (Figures 6.1, 6.3, 6.4 and 6.5) suggests that a connection to the sea has been maintained throughout the time period of this study.

[1] http://www.geography.dur.ac.uk/research/IGCP_495/Project_Outline/index.html

9.5 The mid- to late Holocene evolution of the Ho Bugt salt marshes

In the next section of this chapter, the relative sea-level histories previously presented and discussed are integrated with the results of litho- and biostratigraphical investigations to explore the evolution of the Ho Bugt embayment. On the basis of the relative sea-level histories established (Chapters 8 and 9), stratigraphical cross-sections (Chapter 5), lithological and sedimentological analyses (Chapter 5) and diatom analyses (Chapter 6), the evolution of the Ho Bugt salt marshes can be divided into four main phases:

Stage 1 – Basal peat formation: 7000 – 2000 cal. yr BP

Between 7000 and 2000 cal. yr BP extensive *Phragmites* marshes were present in Ho Bugt, expanding laterally and vertically under the influence of a rising water table. In the majority of core sections investigated, diatom preservation in the basal peat was found to be extremely poor. In the upper part of the basal peat, polyhalobous diatom valves dominate and are indicative of marine conditions. Many of these polyhalobous taxa are also allochthonous, and are hypothesised to result from the gradual flooding and re-working of the upper part of the basal peat unit. Abundant plant macrofossil remains, found in the majority of basal peat sections, suggests a reed swamp environment commonly found in many Holocene stratigraphic sequences around the North Sea (e.g., Behre, 2004).

Stage 2 – Salt-marsh formation: 2000 – 1200 cal. yr BP

The transgression of the basal peat is characterised by rapid salt-marsh expansion between approximately 2000 and 1200 cal. yr BP. In many locations, this process eroded the upper part of the basal peat, demonstrated by the sharp transition between the basal peat and clay units in many cores investigated. In this period, between one and two metres of clay were deposited in only a few hundred years. Sedimentological results from core RØ1 (Chapter 5) indicate that this clay deposit is characterised by low LOI values and a high silt fraction (> 80%). The presence of many brackish and marine diatom taxa such as *Achnanthes delicatula, Denticula subtilis, Navicula cincta, Navicula mutica* and *Navicula pusilla* are indicative of a low salt-marsh environment. Towards the end of this phase, high salt-marsh conditions dominate with an increase in the abundance of several oligohalobous – indifferent diatom taxa. Taxa such as *Navicula variostriata, Pinnularia major* and *Pinnularia viridis* are indicative of more fresh water conditions.

Stage 3 – Fresh water phase: 1200 - 350 cal. yr BP

With the rapid infill of accommodation space, salt-marsh formation outstripped relative sea-level rise to permit a return to fresh water conditions. It is possible that the infilling of tidal creeks and channels led to a reduction in tidal range and contributed to this process. However, a definite fall in relative sea level is observed in the relative sea-level reconstructions established by this study around this time (Figures 8.14 and 8.17). Along the western side of the Ho Bugt embayment, the salt marshes appear to have dried out resulting in the widespread formation of a humified black layer. A series of ^{14}C dates constrain the formation of this layer to between 1200 and 650 cal. yr BP. Archaeological evidence from the German North Sea coast suggests a period of settlement of the Wadden Sea salt marshes around this time (Behre, 2004). It is possible that this period of settlement was related to the small fall in relative sea-level c. 900 cal. yr BP identified in the Røgel water-level record.

Sedimentological and geochemical investigations of the black layer show that it is characterised by high LOI (> 60%) and TOC (> 20%) values, high calcium content and a microscopic charcoal concentration six times greater than samples from the neighbouring clay and peaty clay units. It seems highly likely that at some point during this fresh water stage the salt marshes along the western side of the Ho Bugt embayment were subjected to a period of burning. The results of geochemical analyses undertaken in this study seem to support this theory. High calcium values have been observed in sediments after burning in contemporary studies (e.g., Neff et al., 2005). The microscopic nature of the charcoal fragments in this layer indicates that it is likely to have been a localised event (Patterson et al., 1987; Whitlock and Millspaugh, 1996). It is unclear whether this event was natural or possibly the result of anthropogenic land clearance. A number of studies have investigated changes in the cultural landscape of Denmark (e.g., Odgaard, 1994; Odgaard and Rasmussen, 2000; Bradshaw et al., 2005; Rasmussen, 2005), but none of these provide evidence to link with data produced in this study.

Diatom preservation in the black layer is extremely poor (Section 6.4). However, samples from Bredmose, Røgel and Oksby Enge indicate that the black layer is associated with a poorly preserved fresh water diatom assemblage. High abundances of allochthonous and polyhalobous taxa also suggest that the black layer may have been reflooded at some point in time. Some of the characteristics of the black layer (high organic content, high relative

abundances of *Pinnularia* diatoms and a sharp upper contact) are very similar to black layers found in the coastal stratigraphy of the German Baltic Sea where they have been hypothesised to relate to sea-level regressions (Lampe and Janke, 2004). The formation of the black layer in this study around the time of a lower relative sea level appears to support such a theory. In this study, much of the black colouration is largely the result of a high microscopic charcoal concentration. Studies in the Baltic by Lampe and Janke (2004) and Lampe (*unpublished data*), did not investigate microscopic charcoal in these layers. In the Tønder salt marsh, along the North Sea coast of southernmost Denmark, a distinct black horizon is associated with the building of embankments in 394 cal. yr BP (Jacobsen, 1964). However, there is no evidence to suggest that the marshes in Ho Bugt were ever diked. Toward the northern end of Ho Bugt at Kjelst Enge, the black layer shows a transition into an organic *Phragmites* peat unit. Here it is hypothesised that the marshes did not dry out completely due to freshwater supply from the surrounding glacial upland. Freshwater drainage is observed in the modern salt marsh at Kjelst Enge today where sedges and oligohalobous-indifferent diatom taxa are found in a low salt marsh habitat near the mouth of drainage channels (Figure 4.5).

The final part of this fresh water phase coincides with the deposition of a widespread sand unit. OSL ages from this unit indicate that it was formed between 450 and 400 cal yr BP, around the time of the Little Ice Age (Lamb, 1982). The geometry of the sand sheet (Figure 5.3) and grain size analyses (Section 5.2.2) strongly suggest an aeolian origin. Within the sand unit, grain size is fairly uniform and the sand is well sorted, suggesting rapid aeolian deposition. Although no diatom data are available from the sand layer itself, biostratigraphical analyses from cores at Røgel and Oksby Enge show that samples close to this sand unit are associated with a predominately fresh water diatom flora, dominated by taxa such as *Fragilaria pinnata* and *Pinnularia viridis*. The local water-level curve from Røgel in particular (Figure 8.17) suggests a lower water level around this time.

Links between coastal dune movement and causal factors, such as relative sea-level change, are poorly understood. Sea-level change is acknowledged as a factor in influencing dune movement, but opinions are divided as to the direction and magnitude of the necessary sea-level change (Pye, 1984; Christiansen and Bowman, 1986). Pye (1984) suggested two main models for coastal dune development (Figure 9.5), whereby dune movement occurs when sea level is either (a) rising or 'high' or (b) falling or 'low'. More

recently, several authors have speculated about the control of low relative sea-level positions on coastal sand movements (e.g., Christiansen et al., 1990; Orford et al., 2000). The bio- and lithostratigraphical evidence presented in this study strongly suggest that aeolian sand invasion of the Ho Bugt marshes took place during a time of low relative sea level. This study is therefore the first to confirm a direct link between low relative sea level and aeolian sand movement by documenting evidence for both processes in the same stratigraphic section.

a) Model 1. Rising and high relative sea level.

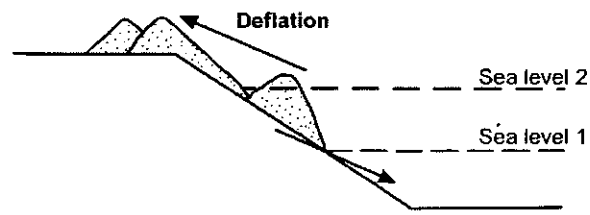

b) Model 2. Falling and low relative sea level.

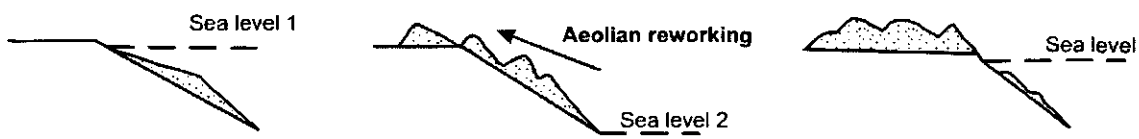

Figure 9.5. Two models of coastal dune formation related to sea-level change a) Model 1 – rising and high relative sea level and b) Model 2 – falling and low relative sea level. Adapted from Pye (1984), Christiansen and Bowman (1986) and Christiansen et al. (1990).

The suggestion that sand invasion of the Ho Bugt salt marshes took place during the early part of the Little Ice Age is consistent with many historical records which document the problems caused by drifting sands in western Denmark during the 15th and 16th centuries (Lamb, 1991). Such records document the burial of houses, farms and even whole villages by sand (Skarregaard, 1989). In West Jutland, approximately 55,000 hectares of land had been destroyed by sand drifting by the end of the 18th century (Jepsen, 1996). Other studies also document increased aeolian sand movement and dune building during the Little Ice Age. For example, Dawson et al. (2004) and Gilbertson et al. (1999) from the Outer Hebrides, NW Scotland and Clarke et al. (2002) along the Aquitaine coast, SW France.

Stage 4 – Renewed salt-marsh deposition: 350 cal. yr BP to present

Some time after the deposition of the sand unit, the Ho Bugt embayment returned to a high salt-marsh environment. Brackish diatom taxa such *Navicula phyllepta, Navicula pygmaea, Navicula cincta* and *Nitzschia debilis* are dominant in the most recent sediments investigated. These high salt marshes are still in existence in the embayment at the present day.

9.6 The glacial isostatic adjustment of Ho Bugt

The study site of Ho Bugt was originally selected because of its proximity to the zone of relative isostatic stability (Figure 1.1). However, relative sea-level records obtained from this study for the mid- to late Holocene, suggest that isostatic processes may have played a more important role in the evolution of the embayment than originally thought. A relative sea-level history which shows around 7 m of rise is 7000 yr cannot be explained entirely by eustatic contribution. To provide insights into the role of glacial isostatic adjustment (GIA) on the Ho Bugt embayment, the millennial-scale relative sea-level history established in this study is compared with a series of relative sea-level curves predicted by models which stimulate the GIA of the Ho Bugt embayment (Figure 9.6). These models include the ice-sheet history of Tushingham and Peltier (1991), except for the British Ice Sheet, which is based on Shennan et al. (2002). Full details on these models can be found in Milne et al. (2006) and references therein. These models are employed in this study on an exploratory basis and cover the time period from approximately 4500 cal. yr BP to the present. Relative sea-level predictions from these models cover the range from -4 to +1 m. Four SLIPs fall outside of the time frame of the GIA model predictions (nos. 38, 39, 40 and 44 Table 9.2), and three fall outside of the relative sea-level range covered by these models (nos. 36, 37 and 42, Table 9.2). These SLIPs are therefore not discussed in the context of these models. Future work (Section 10.9) aims to extend these GIA model predictions for Ho Bugt to incorporate these additional SLIPs.

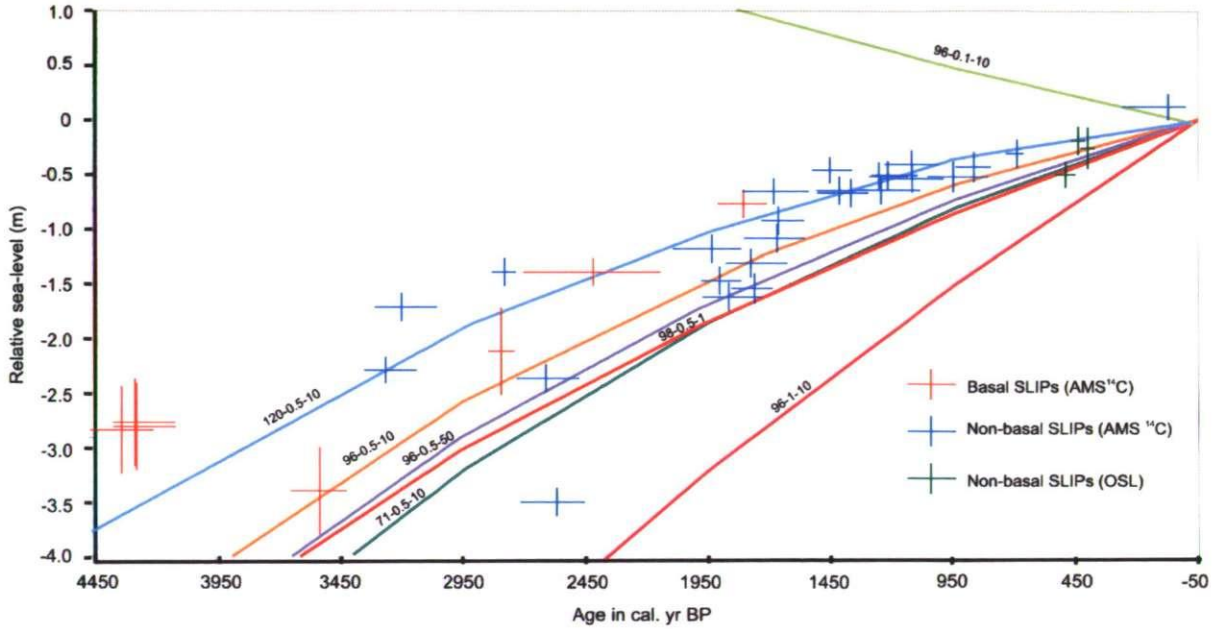

Figure 9.6. SLIPs from Ho Bugt, where the indicative meaning is inferred from the WA-PLS transfer function, compared with relative sea-level curves predicted by the glacial isostatic adjustment (GIA) model of Milne et al. (2006). The curves are labelled by the various rheological parameters as *x*–*y*–*z*, where *x* is the lithospheric thickness (71, 96 and 120 km), *y* is the upper mantle viscosity (0.1, 0.5 and 1 × 10^{21} Pa s) and *z* is the lower mantle viscosity (1, 10 and 50 × 10^{21} Pa s).

Figure 9.6 shows that the WA-PLS diatom-inferred SLIPs established in this study are in best agreement with two of the GIA predicted curves (shown by the light blue and orange lines). The first of these models (shown by the light blue line and hereafter referred to as GIA Model 1) contains a lithosphere thickness of 120 km, an upper mantle viscosity of 0.5 × 10^{21} Pa s and a lower mantle viscosity of 10^{22} Pa s. The second model (shown by the orange line and hereafter referred to as GIA Model 2) contains a lithosphere thickness of 96 km, an upper mantle viscosity of 0.5 × 10^{21} Pa s and a lower mantle viscosity of 10^{22} Pa s. Importantly, in GIA Model 1 the increased lithosphere thickness allows for ~ 0.9 m of melt water contribution in the last 4000 yr. In GIA Model 2 the eustatic function does not include any water addition to the world's oceans after 5000 cal. yr BP.

In the early part of the record (before 2500 cal. yr BP), SLIPs show best agreement with the predictions of GIA Model 1. In the most recent 1000 yrs, SLIPs show better agreement with GIA Model 2. These findings link in with previous arguments in this chapter which highlighted the fact that the diatom-inferred palaeomarsh-surface elevations for many of the older, fresh water samples may be under-estimated, resulting in relative sea-level predictions that are over-estimated. Given better fresh water analogues it is likely that relative sea-level predictions for these samples would be lowered, resulting in a better fit

between these samples and GIA Model 2. Three basal SLIPs which plot at c. -3 m at approximately 4450 cal. yr BP are not in good agreement with either of the two GIA models discussed. The reasons for this are unclear but will be further explored with future GIA modelling (Section 10.9).

Figure 9.7 plots the same SLIPs as Figure 9.6 however, in this diagram the indicative meaning for the samples are inferred from lithostratigraphy and based on surveyed heights of modern salt-marsh environments (Table 8.7) and are not inferred using the WA-PLS transfer function. Figure 9.7 shows that the SLIPs here are in best agreement with GIA Model 2 (lithosphere thickness of 96 km, upper mantle viscosity 0.5×10^{21} Pa s and lower mantle viscosity 10×10^{21} Pa s). This confirms the arguments above in Section 9.4, and suggests that with better fresh water analogues, relative sea-level predictions for older, fresh water basal peat samples would be lower, resulting in best agreement with GIA Model 2. The parameters of this model are consistent with the models employed by Lambeck et al., (1998b). Using sea- and lake-level records from Denmark, Lambeck et al. (1998b) constrain the upper mantle rheology of the region and found the records to be consistent with a lithosphere thickness of 80–100 km and an upper-mantle viscosity of 0.4 –0.5 $\times 10^{21}$ Pa s. GIA Model 2 in this study has very similar parameters to the model employed by Lambeck et al., (1998b). Post-glacial sea-level data from around the British Isles (e.g., Shennan et al., 2002) also show best fit with GIA Model 2. For these data GIA Model 1 is considered implausible because it shows considerable misfit with the British Isles sea-level data (Shennan et al., 2002).

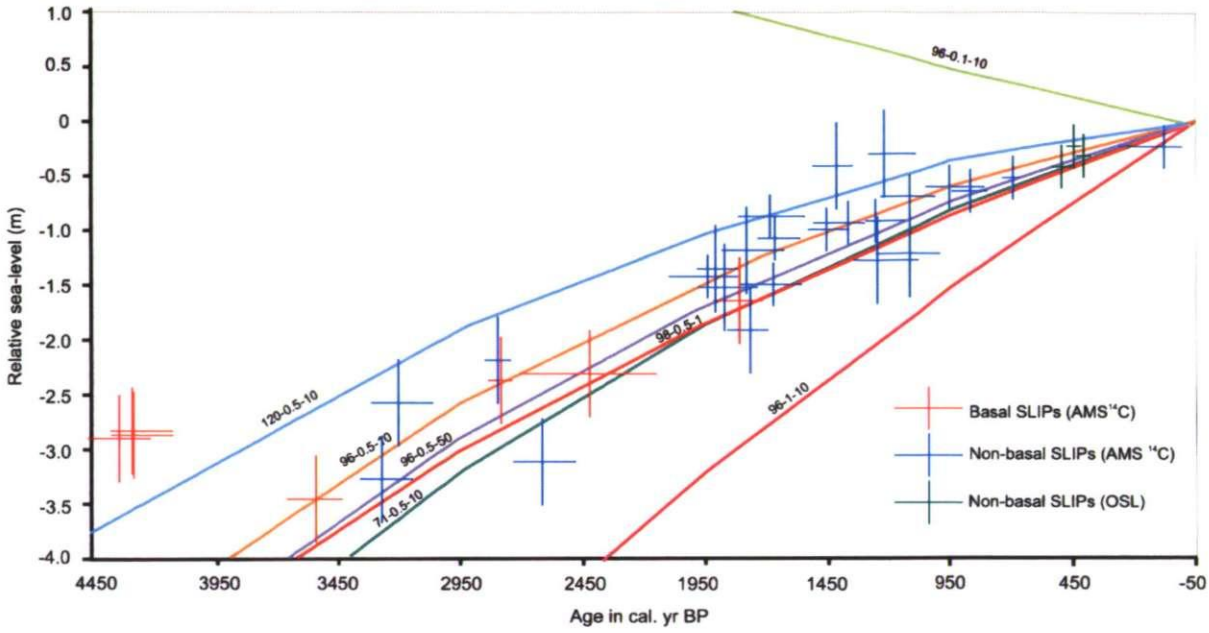

Figure 9.7. SLIPs from Ho Bugt, where the indicative meaning is inferred from surveyed heights of modern salt-marsh environments, compared with relative sea-level curves predicted by the glacial isostatic adjustment (GIA) model of Milne et al. (2006). The curves are labelled by the various rheological parameters as *x*–*y*–*z*, where *x* is the lithospheric thickness (71, 96 and 120 km), *y* is the upper mantle viscosity (0.1, 0.5 and 1 × 10^{21} Pa s) and *z* is the lower mantle viscosity (1, 10 and 50 × 10^{21} Pa s).

9.7 Controls on relative sea-level change in the Ho Bugt embayment

Having established a reasonable fit between the Ho Bugt sea-level data and GIA Model 2, based on the arguments above, this model gives some insight into the dominant process controlling relative sea-level change in the Ho Bugt embayment. The eustatic function of GIA Model 2 does not include any water addition to the world's oceans after 5000 cal. yr BP. This is significant and indicates that the dominant process controlling relative sea-level change in the Ho Bugt embayment during the last 5000 yr is glacio-isostatic rebound, following decay of the Fennoscandian Ice Sheet. In Figure 9.8, GIA Model 2 is used to calculate rates of relative sea-level change for all of Denmark at 5000 cal yr BP and for the present day. For both maps the eustatic function is zero and the relative sea-level movements are produced largely by glacial isostatic movements. At 5000 cal. yr BP, the maps demonstrate that all of Denmark was located in a zone of isostatic subsidence. The modelled rate of relative sea-level rise is 2 mm/yr for Ho Bugt. For the present day, this figure is modelled as 0.5 mm/yr.

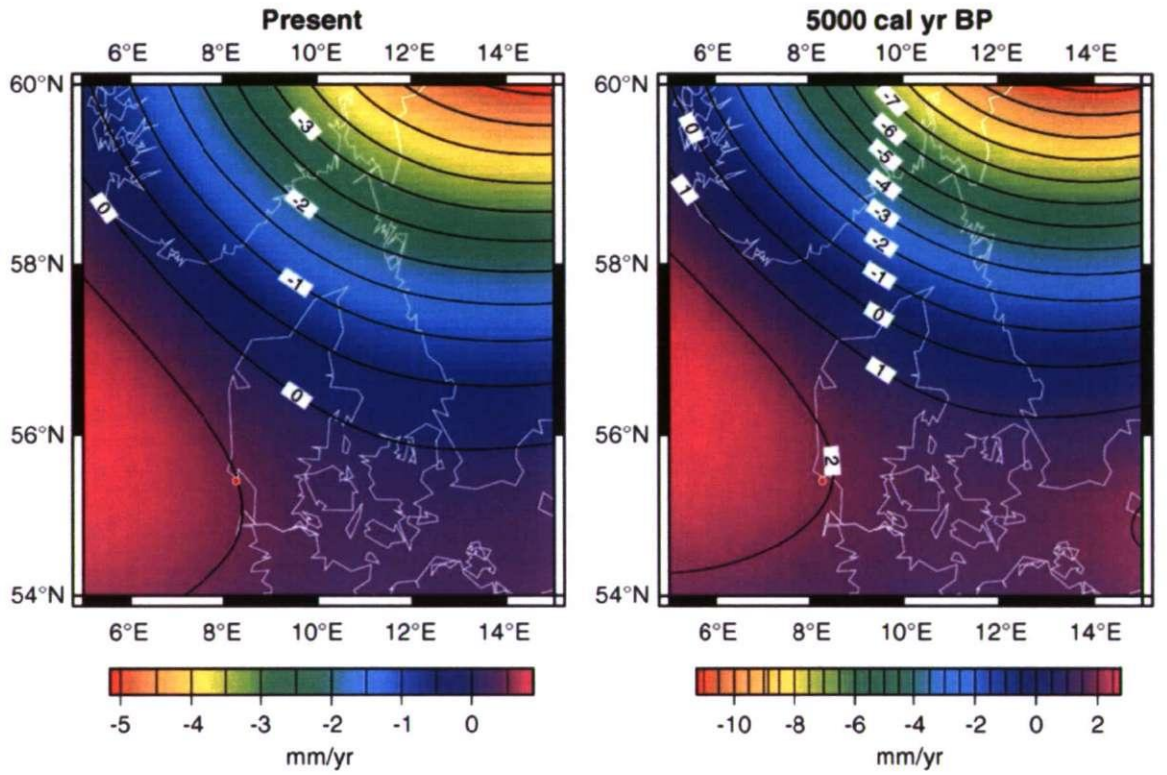

Figure 9.8. Rates of relative sea-level rise in mm/yr predicted by GIA model 2 (Milne et al., 2006) for the present day and for 5000 cal yr BP. The location of Ho Bugt is indicated by the red dot. Published in Gehrels et al. (2006a).

These maps suggest that the rate of isostatic adjustment has not remained constant through time and that the zone of relative isostatic stability has migrated southwards. These findings have important implications for the concept of 'regional eustasy'. Mörner's (1969a; 1969b; 1976) widely cited Kattegat sea-level curve has been argued to provide a record of eustatic sea-level change for the entire North West European region. This curve has been used as a baseline to evaluate crustal movements, tidal variations and local sediment consolidation around the North Sea region (Shennan, 1987). In particular it has been used by Shennan (1989) and Shennan and Horton (2002) to estimate vertical crustal motion around the UK coastline. Maps showing this vertical crustal motion have subsequently been used by government agencies to estimate future flood risk. Exploratory GIA modelling employed in this study and published in Gehrels et al. (2006a) suggests that there is no single locality in which a 'regional' eustatic sea-level curve can be established.

9.8 Implications for estimates of global eustatic sea-level change

The relative sea-level history of Ho Bugt, and conclusions drawn from exploratory GIA modelling, have wider implications for estimates of global eustatic sea-level change in the mid- to late Holocene. The eustatic contribution to global sea-level change during this time has been the subject of great debate in the literature. For example, Peltier (2002) maintains that there has not been any ice melt after 4000 cal. yr BP. Pirazzoli (2005) presents sea-level data from a number of Mediterranean sites (France, Sardinia, Tunisia, Greece, Turkey, Syria and Lebanon) which are consistent with nearly stable global eustasy since 6000 BP. Sea-level data from shorelines in Tunisia, in particular, do not support any water addition to the world's oceans after 6000 cal. yr BP (Morhange and Pirazzoli, 2005). However, from analysis of sea-level data along the French Atlantic and Channel coasts, Lambeck (1997) suggests that there may have been a small (~ 3 m) increase in eustatic sea-level during the last 6000 years. Following evaluation of a variety of data along the Italian coastline, including bivalves, gastropods, speleotherms and submerged archaeological remains, Lambeck et al. (2004) argue that significant melting continued until at least 7000 yr BP and that ocean volumes continued to increase until at least 3000 yr BP. Along the French Mediterranean coast, Lambeck and Bard (2000) use evidence in the form of shells, vermetids and estuarine, fluvial and beach deposits, to argue for less than 0.5 m of ice equivalent sea-level rise during the last 4000 ^{14}C years. Fleming et al. (1998) review observational evidence in the form of corals and shells from Barbados, Papua New Guinea, Tahiti, Australia, Jamaica and Malaysia, to suggest that 3-5 m of water has been added to the world's oceans in the last 7000 ^{14}C yr. Based on a comprehensive review of all available evidence, The Intergovernmental Panel for Climate Change (IPCC) estimates that long-term melting of land-based ice is responsible for 0.25 ± 0.25 mm/yr of global sea-level rise (Church et al., 2001), equivalent to 1.0 ± 1.0 m in the last 4000 yr.

Exploratory GIA modelling employed here indicates that the Ho Bugt sea-level data are best matched by a GIA model that also includes a zero eustatic function in the late Holocene. However, this conclusion must be viewed as tentative, given the uncertainties associated with some of the SLIPs described above. Extension of the GIA modelling predictions to c. 7000 cal. yr BP will enable the additional SLIPs that are outside the time frame of the models presented here, to be included. This will provide further assessment on the controls on relative sea-level change in the Ho Bugt embayment. Additional

modelling will also provide insights into the possible complications arising from effects of glacial forebulge movement (Section 10.9).

In the next part of this chapter, the implications of the results of this study for a number of broader themes are discussed. These include the use of diatoms in the coastal environment, the implications from this study for regional diatom training sets and issues surrounding the development and application of diatom-based transfer functions. A number of these issues have been acknowledged in previous sections of this thesis but are further discussed here as they have important implications for the conclusions of this study.

9.9 The use of diatoms in the coastal environment

This study has relied heavily on the interpretation of diatom data. The use of diatoms in the coastal environment does however, present several problems. In such environments the transportation of diatom valves is an important issue (Sherrod, 1999; Vos and De Wolf, 1993; Brockmann, 1940) and the presence of, and issues associated with, a high abundance of allochthonous values has been acknowledged throughout this study. Attempts were made to develop a diatom-based transfer function which excluded allochthonous taxa (Section 7.6.3). However, the exclusion of such taxa increased the number of fossil taxa without a modern analogue (Sections 8.2.1, 8.3.1 and 8.4.1) and the development of such a transfer function was not further pursued. Consideration was also given to the removal of allochthonous taxa from the fossil samples. However, in many cases this lead to counts in these samples falling below 200 valves and making them statistically less reliable.

Zong (1997) argues that since a mixture of both allochthonous and autochthonous valves occurs in sediments that accumulated in the palaeoenvironment, their presence in modern samples can be considered less significant. Many similar coastal studies therefore give little consideration to the presence and abundance of allochthonous diatom valves. However, results obtained in this study suggest that the presence of allochthonous valves in both modern and fossil samples can have significant implications. This is illustrated in the record from core RØ1. Here a number of polyhalobous and allochthonous taxa have analogues in the modern environment. However, many of these taxa are found in several samples, across a range of elevations. This has resulted in fossil taxa with so-called 'multiple analogues' (Birks, 1998). With hindsight, one way forward would have been to separate out the allochthonous and autochthonous valves during counting in this study

(e.g., Sawai, 2001; Sawai et al., 2004) to enable statistically reliable counts to be obtained, whilst excluding allochthonous valves. However, it was not envisaged that allochthonous valves would present such a problem in this study.

This study has highlighted both advantages and disadvantages in using diatoms as quantitative sea-level indicators. Diatoms span the entire range of salinities, from highly saline marine conditions (> 30 g/l^{-1}) to entirely fresh water environments (Kolbe, 1927; Hustedt, 1957; Simonsen, 1962; Palmer and Abbott, 1986; Juggins, 1992). They are therefore found in all types of salt marsh environment ranging from tidal mudflats to high and fresh water marshes (Section 4.3). This makes them particularly suitable for use as quantitative sea-level indicators. Provided suitable modern analogues are available, the entire range of past environments, from tidal flats to high and fresh water marshes, can be reconstructed. In this sense, diatoms outperform other microfossils used as sea-level indicators such as foraminifera and testate amoebae. Foraminifera are rarely found above MHWSTs and testate amoebae are found only around MHWST (Gehrels et al., 2001). The distribution of such microfossils within the tidal frame restricts the range of past environments that can be reconstructed using transfer functions based only on these microfossils. For example, if a former fresh water environment existed with a particular core section, palaeomarsh-surface elevations and relative sea level in this part of the core cannot usually be reconstructed by use of a foraminifera-based transfer function. Foraminifera do not occur in the modern fresh water marshes and are unlikely to be found in such fossil deposits. This is demonstrated by the absence of foraminifera in many core sections investigated as part of previous work in the Ho Bugt embayment (Gehrels et al., 2006a). Foraminifera are not well preserved in these core sections because the former marsh environment was too 'fresh.'

9.10 Multiproxy training sets

This study has highlighted a number of issues surrounding the use of diatoms in the coastal environment. However, the section above has illustrated the advantages of using diatoms compared to a number of other microfossils commonly used as sea-level indicators. A potential resolution of these conflicting arguments is through the use of multiproxy training sets. The most reliable, precise and accurate sea-level reconstructions are likely to be obtained through the integration of several of these proxies. Although the use of multiproxy training sets in the coastal environment has previously been investigated (e.g.,

Gehrels et al., 2001), such training sets have never been applied to interpret changes in fossil cores. In this study, the initial transfer function developed performs very well (Chapter 7) and out performs many similar training sets published in the literature (Table 7.4). Only when applied to the fossil cores (Sections 8.2 – 8.5) did problems with missing and under-represented taxa become apparent. In order to assess the true predictive abilities of such multiproxy training sets it is essential that they are also applied to interpret changes in fossil cores. It is highly likely that in these situations they will outperform training sets based on single proxies.

9.11 Implications of this study for regional diatom training sets

In Chapter 4 a number of issues were highlighted which have implications for the development of regional diatom training sets for reconstructing changes in relative sea level. Unconstrained cluster analysis on the entire data set (Figures 4.18 and 4.19) demonstrated that samples from the same elevation range are associated with different dominant diatom taxa. These observations have interesting implications with regard to the spatial variability of diatom assemblages within salt marshes, and the subsequent development of modern training sets, and in particular regional training sets. In this study, the decision was made to exclude samples from one of these transects (Kjelst Enge) from the modern training set (Section 7.2). Unconstrained cluster analysis and DCA of the entire diatom data set were important tools in making this decision. However, in many sea-level based studies which develop training sets for reconstructing relative sea level, such a thorough exploration of the modern species data is not considered. Several studies examine these issues on an individual transect basis, using unconstrained cluster analysis and sometimes DCA (e.g., Horton et al., 2006; Horton and Edwards, 2005), but very rarely are such thorough investigations of the modern species data conducted. In developing regional diatom training sets for reconstructing changes in relative sea-level, data from individual transects are often 'lumped' together with little or no further analysis (e.g., Zong and Horton, 1999; Horton et al., 2006). Often with such data sets, specific focus is given to examining the species-environment relationships for the data set as a whole, but spatial variation within the diatom data is not further explored. In this study diatom data from within the same embayment were shown to display very different relationships with elevation. Within regional diatom training sets it is highly likely that these relationships are even more complex. This study has therefore demonstrated the need for a thorough

exploration of both species and environmental at different spatial scales before developing transfer functions.

9.12 Development and application of a diatom-based transfer function for elevation

This investigation has relied heavily on the assumption that the transfer function developed and applied in this study provides a suitable tool for assessing changes in palaeomarsh-surface elevation. In this study problems with under-represented taxa, a lack of modern analogues and multiple analogues, highlighted in Chapter 8, have all affected the reliability of the results obtained. Although the use of a unimodal transfer function model such as WA-PLS was deemed most suitable in this study (Chapter 7), such a model is also likely to over generalise the ecological responses of many of the individual diatom taxa. In reality, species response curves are more complex (e.g., Austin, 1992; Austin et al., 1994; Austin and Gaywood, 1994). Many of the issues surrounding transfer function development and application encountered in this study, such as under-representation of taxa, fossil taxa with no modern analogue and fossil taxa with multiple analogues, are common problems and are widely acknowledged in the literature (Birks, 1995; 1998).

One issue in particular, which is likely to have affected the reliability of the reconstructions in this study, is the fact that elevation is, in reality, a 'compound' or 'composite' variable (Birks, 1998). Across a salt marsh, it is not elevation *per se* which controls diatom distributions. Tidal inundation and associated hydrology and salinity are the main ecological controls on diatom distributions however, the level of tidal inundation is itself controlled by elevation (Gehrels, 2000). Such arguments are commonly used to justify the use of elevation as an environmental variable in the majority of quantitative sea-level reconstructions, and is the case in this study (e.g. Gehrels, 2000; Hamilton and Shennan, 2005a, 2005b; Horton and Edwards, 2005; Boomer and Horton, 2006 and Edwards and Horton, 2000, 2006). This concept however, violates one of the major assumptions of quantitative reconstructions (Juggins, *pers. comm*). In using transfer functions in particular, it is assumed that the environmental variable to be reconstructed is of 'ecological' importance (Birks, 1995; Korsman and Birks, 1996). Elevation is not a 'true' ecological variable (Juggins, *pers. comm*). It is highly likely that the poor reconstructions obtained in this study reflect the fact that the diatoms are responding to some ecological factor other than elevation, but which itself is influenced by elevation.

Another issue that may further have affected the reliability of the transfer function applied here is the issue of spatial autocorrelation. Spatial autocorrelation describes the tendency of sites located close to one another to resemble each other ecologically (Legendre and Fortin, 1989; Legendre, 1993; Telford and Birks, 2005). Recent studies have highlighted the likely over-optimistic estimates of RMSEP and inappropriate model choice when spatial autocorrelation is present in the data set (Telford and Birks, 2005). Chapter 7 explored the development of a series of transfer functions for the Ho Bugt training set. One of the best performing transfer functions was the MAT (Table 7.2). However, the MAT transfer function was not further developed in this study primarily because of concerns regarding the issue of spatial autocorrelation. Telford and Birks (2005) and Telford (2006) argue that MAT is particularly sensitive to spatial autocorrelation and that models based on unimodal methods, such as the ML and WA-PLS transfer functions developed in this study (Chapter 7), are more robust.

Spatial autocorrelation is likely to be a particular problem for sea-level studies, where sampling often takes place along line transects. In this study, as in other similar investigations (e.g., Zong and Horton, 1998; 1999; Gehrels and Newman, 2004; Horton et al., 2006) samples were taken along a series of individual line transects (Chapter 3). It is highly likely that a considerable degree of spatial autocorrelation is therefore present in the data set. This is an issue which has not thus far been considered by the sea-level research community. Future use of random sampling methods and statistical techniques to 'partial out' the degree of spatial autocorrelation provide useful avenues for future research.

9.13 Chapter summary

This chapter has presented a millennial-scale relative sea-level reconstruction for the Ho Bugt embayment using all available SLIPs. This curve documents around 7 m of rise since 7000 cal. yr BP. The local water-level curves established in Chapter 8 were compared and discussed. From these comparisons several key points can be noted:

- Water-level reconstructions from cores RØ1 and KE2 show the same general trend in relative sea level but the curves are offset prior to 1500 cal. yr BP.
- A rapid period of rise is noted in the KE2 record between 2000 and 1500 cal. yr BP which is not identified in the RØ1 record. Here the KE2 record demonstrates around 1.5 m of rise in only a few hundred years.

- In both cores, the age-depth models for this time period are considered less reliable. The water-level records for these two cores between approximately 1500 and 3000 cal. yr BP must therefore be interpreted with caution, primarily because of the uncertainty associated with the interpolated ages.

The millennial-scale relative sea-level record for the Ho Bugt embayment is in broad agreement with the rise established by published sea-level curves for the German North Sea coast. However, the sea-level records for Ho Bugt do not support the concept of a sea-level highstand (or series of highstands) at any time during the last 7000 yr. The sea-level records established in this study agree less well with previously published sea-level records from other locations in Denmark, although this is in part due to differing isostatic settings. Importantly, the Ho Bugt sea-level curves disagree with previously published data on sea-level changes along the southern Danish North Sea coast, many of which provide evidence for a sea-level highstand around 3000 cal. yr BP.

A number of limitations to the relative sea-level records established here have been discussed. Two major issues have arisen which affect the reliability of the sea-level records established:

1. The WA-PLS transfer function under-predicts palaeomarsh-surface elevation, and therefore over-predicts relative sea-level and local water level for many samples. This is especially true of the fresh water basal peat samples.

2. Uncertainly in the age-depth models established for cores KE2 and RØ1 (Figures 8.9 and 8.12, respectively), means that the local water-level histories between approximately 1500 and 3000 cal. yr BP in both these cores are considered less reliable.

Integration of the local water-level curves with the results of litho- and biostratigraphical investigations has enabled the evolution of the Ho Bugt salt marshes to be summarised in four stages:

- Stage 1 – Basal peat formation from 7000 – 2000 cal. yr BP
- Stage 2 – Salt-marsh formation from 2000 – 1200 cal. yr BP
- Stage 3 – Fresh water phase from 1200 – 350 cal. yr BP
- Stage 4 – Renewed salt-marsh deposition from 350 cal. yr BP to present

Comparison of the relative sea-level histories established by this study with relative sea-level predictions from a series of GIA models has provided insights into the role of isostatic adjustment on the Ho Bugt embayment. The Ho Bugt relative sea-level data are best matched by a GIA model that does not include any eustatic function for the last 5000 cal. yr BP. GIA modelling results also suggest that the role of isostatic processes has not remained constant through time and that the zone of relative isostatic subsidence has migrated southwards. Such findings have implications for the concept of 'regional eustasy.'

In the final part of this chapter problems in the use of diatoms in coastal environments were acknowledged. The problems associated with a large abundance of allochthonous taxa have been acknowledged throughout this study. The advantages and disadvantages of using diatoms as quantitative sea-level indicators were highlighted with the suggestion that a potential way to resolve many of these issues is through the increased use of multiproxy training sets. The next chapter presents the conclusions from this study and discusses avenues for possible future research.

Chapter 10

Conclusions

This chapter provides a summary of the results obtained throughout this investigation. The first part of this chapter restates the original aims of this thesis. The second part presents the main conclusions of this study, and relates these to the original aims of the thesis. In the final section of this chapter, recommendations are made for possible avenues for future research.

10.1 Thesis aims

This thesis aimed to reconstruct the relative sea-level history of the Ho Bugt embayment by:

- Documenting the modern diatom assemblages and their controlling environmental variables across the salt marshes in the Ho Bugt embayment
- Recording the detailed stratigraphy of the Ho Bugt embayment to gain an understanding of the major lithostratigraphical and environmental changes occurring
- Establishing the dominant control on diatom assemblages in this embayment through the use of several ordination techniques
- Developing a diatom-based transfer function for reconstructing changes in palaeomarsh-surface elevation
- Applying this transfer function to a series of fossil cores to interpret changes in palaeomarsh-surface history and assessing the reliability of these reconstructions
- Combining these palaeomarsh-surface records with age depth-models to produce a series of local water-level curves and comparing these curves with the local tide-gauge record
- Documenting the millennial-scale relative sea-level history of the Ho Bugt embayment through reconstruction of samples from a number of different cores
- Comparing this transfer-function predicted relative sea-level curve with those established using a qualitative interpretation of lithology
- Comparing the sea-level curves established in this study with predictions based on a series of glacial isostatic adjustment models, to explore the controls on relative sea-level change in the Ho Bugt embayment.

10.2 Modern diatom assemblages

- Modern diatom assemblages and associated environmental variables were investigated from six transects in the Ho Bugt embayment. These transects spanned a range of salt-marsh environments from the fresh water marsh down to the tidal flat. At some individual transect locations diatom assemblages displayed a strong vertical zonation with respect to the tidal frame. At other locations, and for the data set as a whole, they did not.
- Multivariate statistical analysis demonstrated that the diatom assemblages in the Ho Bugt embayment are strongly controlled by elevation.

10.3 Mid to late Holocene salt-marsh stratigraphy

The mid to late Holocene salt-marsh stratigraphy of the Ho Bugt embayment developed over the last 7000 cal. yr BP and shows a sequence of (from bottom to top):

- fresh water basal peat
- low salt-marsh clay
- fresh water clayey peat
- a distinct black organic layer
- an aeolian sand unit
- a high salt marsh clay

10.4 Development and application of diatom-based transfer functions

- A series of diatom-based transfer functions were developed based on the strong relationship established between diatom assemblages and elevation. WA, WA-PLS, ML and MAT transfer function methods were all explored in this study. The ML and WA-PLS transfer functions were found to perform the best when $RMSEP_{jack}$ and max $bias_{jack}$ results were compared. The WA-PLS (2 component) transfer function ($RMSEP_{jack}$ = 0.122, r^2 = 0.934 and max $bias_{jack}$ = 0.109) was found to perform best at the extremes of the environmental gradient and was subsequently applied to a series of cores (KE2, RØ1 and BR) to interpret changes in palaeomarsh-surface history.
- The reliability of these diatom-inferred predictions was assessed via the use of goodness of fit and analogue statistics. In all reconstructions, these statistics indicated that the reconstructions should be interpreted with caution. The majority of samples showed a 'poor fit' with the modern data and had 'no good' modern

analogue. Lack of modern analogues, under representation of taxa and multiple analogues, all contributed to reducing the reliability of the reconstructed palaeomarsh-surface elevations. However, for many of the core sections investigated, under representation of taxa, rather than a complete lack of analogues, was the biggest problem.

- The absence and under-representation of a few fresh water taxa has resulted in the transfer function under-predicting palaeomarsh-surface elevations for many of the fresh water basal peat samples. For these samples relative sea-level predictions are over-predicted.

10.5 Local water-level changes

- The diatom-inferred palaeomarsh-surface records were subsequently combined with age-depth models for cores KE2, RØ1 and BR9 to reconstruct local-water level changes.
- The local water-level curves for cores KE2 and RØ1 show around 3.5 m of rise in approximatley 4500 years.
- The two curves show the same general trend in local water-level but are offset prior to 1500 cal. yr BP.
- Given the lack of dates and the age reversals in the lower part of the clay unit in both cores KE2 (Figure 8.9) and RØ1 (Figure 8.12), inferred ages in these units are much less certain. For both cores, the water-level record between approximately 1500 and 3000 cal. yr BP is considered less reliable.

10.6 The millenial-scale relative sea-level history of the Ho Bugt embayment

- The millennial-scale relative sea-level history of the Ho Bugt embayment documents around 7 m of rise in 7000 cal. yr BP
- The Ho Bugt relative sea-level histories do not provide evidence for a sea-level highstand at any time during the last 7000 cal. yr BP. This refutes older published data on sea-level changes along the southern Danish North Sea coast
- Comparison of the transfer function predicted millenial-scale relative sea-level curve with one produced using a lithology-based approach, confirmed the fact that palaeomarsh-surface elevations for many of the fresh water basal peat samples are under-estimated, and that relative sea-level predictions for these smaples are over-estimated.

10.7 The mid to late Holocene evolution of the Ho Bugt salt marshes

- Integration of the relative sea-level histories with the results of litho- and biostratigraphical analyses enabled the evolution of the Ho Bugt salt marshes to be summarised in four key stages:
  - Basal peat formation from 7000 – 2000 cal. yr BP
  - Salt-marsh formation from 2000 – 1200 cal. yr BP
  - A fresh water phase from 1200 - 350 cal. yr BP with formation of an organic black layer (between approximately 1200 and 650 cal. yr BP) and deposition of an aeolian sand unit (between 450 and 400 cal. yr BP)
  - Renewed salt-marsh deposition from 350 cal. yr BP to present.

10.8 Controls on relative sea-level change in the Ho Bugt embayment

- Exploratory GIA modelling suggests that the dominant control on relative sea-level change in the Ho Bugt embayment during the last 5000 cal. yr BP is glacial isostatic adjustment, following decay of the Fennoscandian Ice Sheet
- Isostatic adjustment rates have not remained consistent through time and the zone of relative isostatic stability has migrated southwards
- These findings have important implications for the concept of 'regional eustasy'
- The Ho Bugt relative sea-level data are best matched by a model that includes a zero eustatic function for the last 5000 cal. yr BP.

10.9 Future work

- The absence and under-representation of several key fresh water taxa has been a major limiting factor in the use of diatom-based transfer functions in this study. Extension of the modern training set to include samples from higher elevations (above 2.3 m DNN) is one way of providing 'better' fresh water analogues and may further refine the diatom-inferred relative sea-level predictions. However, such environments are no longer present in the Ho Bugt embayment
- It has been demonstrated that there are both advantages and disadvantages to the use of diatoms as quantitative sea-level indicators. One possible resolution of these conflicting arguments is via the use of multiproxy training sets. Development and application of such training sets for the Ho Bugt embayment is likely to reduce the problems associated with a lack of modern analogues and under-representation of taxa, and increase the reliability of the reconstructions. For the fresh water basal

peat samples, where these problems are most significant, the use of testate amoebae may provide a potential way forward.

- The uncertainty associated with the age-depth models used in this study has been a major limitation of the local water-level histories established. The development of mixed effect models and weighted-average probability density functions, such as those employed by Heegard et al. (2005) and Gehrels et al. (2005) respectively, were considered beyond the scope of this present study but are potential areas to explore in future work. Such models may enable more robust age-depth models to be developed, further refining the chronology of the cores investigated.
- Additional GIA modelling experiments will provide further insights into the controls on relative sea-level change in the Ho Bugt embayment. In particular, extension of the GIA modelling predictions further back in time will enable an additional number of SLIPs to be compared to the model predictions. Future modelling also aims to explore the possible effects arising from glacial forbulge movement, something which is not considered in the current study. Such effects may greatly affect the pattern of glacial isostatic adjustment of the Ho Bugt embayment.

References

Aagaard, T., Nielsen, N. and Nielsen, J., 1995. Skallingen - Origin and evolution of a barrier spit. *Meddelelser fra Skalling-Laboratoriet*, 35: 1–85.

Admiralty Tide Tables, 2004. Volume 1, 2004, United Kingdom and Ireland. Hydrographer of the Navy.

Altman, D.G. and Bland, J.M., 1983. Measurement in medicine: the analysis of method comparison studies. *The Statistician*, 32: 307-317.

Andersen, T.J., Mikkelsen, O.A., Møller, A.L., and Pejrup, M., 2000. Deposition and mixing depths on some European intertidal mudflats based on 210Pb and 137Cs activities. *Journal of Continental Shelf Research*, 20: 1569-1591.

Appleby P. G., 2001. Chronostratigraphic techniques in recent sediments. In: W.M. Last and J.P. Smol (Eds.). Tracking Environmental Change Using Lake Sediments Volume 1: Basin Analysis, Coring, and Chronological Techniques. Kluwer Academic: 171-203.

Appleby, P.G. and Piliposian, G.T., 2006. Age-depth report for Røgel core RØ1. Environmental Radioactivity Research Centre, University of Liverpool. 6pp.

Appleby P. G., Nolan, P.J., Gifford, D.W., Godfrey, M.J., Oldfield, F., Anderson, N.J. and Battarbee, R.W. 1986. ^{210}Pb dating by low background gamma counting. *Hydrobiologia*, 141: 21-27.

Appleby, P.G., Richardson, N. and Nolan, P.J. 1992. Self-absorption corrections for well type germanium detectors. *Nuclear Instruments and Methods B*, 71: 228-233.

Austin, M.P., 1992. Modelling the environmental niche of plants: implications from plant community response to elevated CO_2 levels. *Australian Journal of Botany*, 40: 615-630.

Austin, M.P. and Gaywood, M.J., 1994. Current problems of environmental gradients and species response curves in relation to continuum theory. *Journal of Vegetation Science*, 5: 473-482.

Austin, M.P., Nicholls, A.O., Doherty, M.D. and Meyers, J.A., 1994. Determining species response functions to an environmental gradient by means of a β-function. *Journal of Vegetation Science*, 5: 214-228.

Baeteman, C., 2006. Sediment variations supported by radiocarbon dates as fingerprints for processes of coastal changes in the late Holocene deposits of a tide-dominated coastal lowland. Abstract volume. IGCP 495 meeting, Quaternary land-ocean interaction: Natural and human forcings on coastal evolution. Santa Catarina, Brazil, 17-22 September 2006: 14-16.

Ball, D.F., 1964. Loss on ignition as an estimate of organic matter and organic carbon in non-calcareous soil. *Journal of Soil Science*, 15: 84 – 92.

Barber, H.G., and Haworth, E.Y., 1994. A guide to the morphology of the diatom frustule. Freshwater Biological Association Scientific Publication 44. 112pp.

Bard. E., Arnold, M., Fairbanks, R.G. and Hemelin, B., 1993. Th-234U and 14C ages obtained by mass spectronomy on corals. *Radiocarbon*, 35: 191 – 199.

Barrows, T.T. and Juggins, S., 2005. Sea-surface temperatures around the Australian margin and Indian Ocean during the last glacial maximum. *Quaternary Science Reviews*, 24 (7-9): 1017-1047.

Bartholdy, J., 1984. Transport of suspended matter in a bar-built Danish estuary. *Estuarine, Coastal and Shelf Science,* 18: 527–541.

Bartholdy, J. and Folving, S., 1986. Sediment classification and surface type mapping in the Danish Wadden Sea by remote sensing. *Netherlands Journal of Sea Research*, 20: 337–345.

Bartholdy, J. and Madsen, P.P., 1985. Accumulation of fine-grained material in a Danish tidal area. *Marine Geology,* 67: 121–137.

Bartholdy, J. and Pejrup, M., 1994. Holocene evolution of the Danish Wadden Sea. *Senckenbergiana Maritima*, 24 (1): 187 – 209.

Bartholdy, J., Christiansen, C. and Kunzendorf, H., 2004. Long term variations in back barrier salt-marsh deposition on the Skallingen peninsula – the Danish Wadden Sea. *Marine Geology*, 203 (1-2): 1-21.

Bartlein, P.J., and Whitlock, C., 1993. Paleoclimatic interpretation of the Elk Lake pollen record. In J.P. Bradbury and W.E. Dean (eds.) Elk Lake, Minnesota: Evidence for rapid climate change in the North-Central United States. Geological Society of America Special Paper, 276: 275-293.

Bartlein, P.J., Edwards, M.D., Shafer, S.L., and Barker, E.D., 1995. Calibration of radiocarbon ages and the interpolation of palaeoenvironmental records. *Quaternary Research*, 44: 417-424.

Battarbee, R.W., 1986. Diatom analysis. In: B.E. Berglund (Ed.). Handbook of Holocene palaeoecology and palaeohydrology. Wiley, Chichester: 527 – 570.

Battarbee, R.W., Carvalho, L., Jones, V.J., Flower, R.J., Cameron, N.G., Bennion, H. and Juggins, S., 2001. *Diatoms.* In: J.P.Smol, H.J.B. Birks and W.M. Last (Eds.). Tracking environmental change using lake sediments. Volume 3: Terrestrial, algal and siliceous indicators. Kluwer Academic Publishers, Dordrecht, Netherlands: 155-202.

Battarbee, R.W., Mackay, A.W., Jewson, D.H., Ryves, D.B. and Sturm, M., 2005. Differential dissolution of Lake Baikal diatoms: correction factors and implications for palaeoclimatic reconstruction. *Global and Planetary Change*, 46 (1-4): 75-86.

Bayens, L., and Denys, L., 1982. Problems in diatom analysis of deposits: allochthonous valves and fragmentation. *Geologie en Mijnebou*, 61: 159-162.

Behre, K.E., 2004. Coastal development, sea-level change and settlement history during the later Holocene in the Clay district of Lower Saxony (Niedersachsen), northern Germany. *Quaternary International,* 112 (1): 37-53.

Behre, K.E., and Menke, B., 1969. Pollenanalytische untersuchungen an einem Bohrkern der südlichen Doggerbank. *Beiträge zur Meereskunde* 24/25: 123-129.

Behre, K.E., Menke, B. and Streif, H., 1979. The Quaternary development of the German part of the North Sea. In: E. Oele, R.T.E. Schuttenhelm and A.J. Wiggers, (Eds). The Quaternary history of the North Sea. Acta University Uppsala Symposium, University of Uppsala Anum Quingentesimum Celebrantis, Uppsala: 85-113.

Bennett, K.D., 1994. Confidence intervals for age estimates and deposition times in late Quaternary sedimentary sequences. *The Holocene*, 4: 337-348.

Bennion, H., 1994. A diatom-phosphorus transfer function for shallow, eutrophic ponds in southeast England. *Hydrobiologia*, 275/276: 391 – 410.

Bennion, H., Juggins, S. and Andersen, N.J., 1996. Predicting epilimnetic phosphorus concentrations using an improved diatom-based transfer function and its application to lake eutrophication management. *Environment, Science and Technology*, 30: 2004-2007.

Berglund, B., 1971. Littoral transgressions at Blekinge, south Sweden. A preliminary report. *Geologiska Foreningens I Stockholm Forhandlingar*, 93: 625 – 652.

Birks, H.J.B., 1995. Quantitative palaeoenvironmental reconstructions. In : D. Maddy and J.S. Brew (Eds.). Statistical Modelling of Quaternary Science Data. Technical guide number 5. Quaternary Research Association, Cambridge: 161 – 236.

Birks, H.J.B., 1998. Numerical tools in palaeolimnology – Progress, potentialities and problems. *Journal of Paleolimnology*, 20: 307 – 332.

Birks, H.J.B., 2001. Maximum likelihood environmental calibration and the computer program WACALIB, a correction. *Journal of Palaeolimnology*, 25(1): 111-115.

Birks, H.H and Birks, H.J.B., 2006. Multiproxy studies in palaeolimnology. *Vegetation and Archaeobotany*, 15 (4): 235-251.

Birks, H.J.B., Juggins, S and Line, J.M 1990a. Lake-surface water chemistry reconstructions from palaeolimnological data. In: B.J. Madson (Ed.). The Surface Waters Acidification Programme. Cambridge University Press, Cambridge: 301 – 311.

Birks, H.J.B., Line, J.M., Juggins, S., Stevenson, A.C., and ter Braak, C.J.F., 1990b. Diatoms and pH reconstructions. *Philosophical Transactions of the Royal Society of London Series B*, 327: 263-278.

Blackford, J.J. and Chambers, F.M., 1993. Determining the degree of peat decomposition for peat-based palaeoclimatic studies. *International Peat Journal* 5: 7-24.

Boomer, I. and Horton, B.P., 2006. Holocene relative sea-level movements along the North Norfolk coast, UK. *Palaeogeography, Palaeoclimatology and Palaeoecology,* 230 (1-2): 32-51.

Borcard, D., Legendre, P. and Drapeau, P., 1992. Partialling out the spatial component of ecological variation. *Ecology*, 73: 1045-1055.

Bowman, S.G.E. and Lees, M.N., 1995. Radiocarbon calibration: current issues. American *Journal of Archaeology*, 99: 102-105.

Bradshaw, E.G., Rasmussen, P., and Odgaard, B.V., 2005. Mid- to late Holocene land-use change and lake development at Dallund So, Denmark: synthesis of multiproxy data, linking land and lake. *The Holocene*, 15 (8): 1152 – 1162.

Brockmann, C., 1940. Diatomeen als leitfossilien in Küstenablagerungen. *Westküste*, 2: 150-181.

Brooks, S.J., 2006. Fossil midges (*Diptera : Chironomidae*) as palaeoclimatic indicators for the Eurasian region. *Quaternary Science Reviews*, 25 (15-16): 1894-1910.

Brooks, S.J. and Birks, H.J.B., 1999. Chironomid-inferred late-glacial and early Holocene mean July air temperature for Kråkenes lake, western Norway. *Journal of Paleolimnology* 23 (1): 73-89.

Burgess, A., 2004. The development of diatom-nutrient palaeolimnological inference models for UK lowland reservoirs. Unpublished PhD thesis, University of Plymouth. 425pp.

Chapman, V.J., 1941. Studies in salt-marsh ecology. *Journal of Ecology*, 20 (8): 69-82.

Charlesworth, J.K., 1966. The Quaternary Era, with special reference to its glaciation. Volume II, Part III. Edward Arnold LTD, London. 595-1700.

Charman, D.J., Roe, H.M. and Gehrels, W.R., 2002. Modern distribution of saltmarsh testate amoebae: regional variability of zonation and response to environmental variables. *Journal of Quaternary Science*, 17, 387-409.

Christiansen, C., 1995. The Littorina Transgressions in Denmark. In: Fischer, A. (ed.), man and sea in the Mesolithic. Proceedings of the international symposium, Kalundborg, Denmark. 1993. Oxbow Books, Oxford, UK.

Christiansen, C. and Bowman, D., 1986. Sea-level changes, coastal dune building and sand drift, north western Jutland, Denmark. *Geografisk Tiddskrift*, 86: 28-31.

Christiansen, C., Dalsgaard, K., Møller, J.T., Bowman D. and Sheva, B., 1990. Coastal dunes in Denmark. Chronology in relation to sea level. *Catena Supplement*, 18: 61-70.

Christiansen, C., Vølund, G., Lund-Hansen, L.C. and Bartholdy, J., 2004. Tidal flat sediment dynamics, Ho Bugt, Denmark, In: J.B. Bartholdy and J.B.T. Pedersen (Eds.). Tidalites 2004, abstract volume. 6th International Conference on Tidal Sedimentology. Institute of Geography, University of Copenhagen, Denmark, pp. 32–35.

Church, J.A., Gregory, J.M., Huybrechts, P., Kuhn, M., Lambeck, K., Nhuan, M. T., Qin, D.,Woodworth, P.L., 2001. Changes in sea level. In: J.T., Houghton, Y. Ding, D.J., Griggs, M., Noguer, P.J., van der Linden, X., Dai, K., Maskell and C.A., Johnson (Eds.). Climate Change 2001: The Scientific Basis. Contribution of Working Group I to the Third Assessment Report of the Intergovernmental Panel on Climate Change. Cambridge University Press, Cambridge: 639–693.

Clarke, M., Rendall, H., Tastet, J.P., Clave, B. and Masse, L., 2002. Late-Holocene sand invasion and North Atlantic storminess along the Aquitaine coast, southwest France. *The Holocene*, 12 (2): 231-238.

Clemmensen, L.B. Richardt, N. and Andersen, C., 2001. Holocene sea-level variation and spit development: data from Skagen Odde, Denmark. *The Holocene,* 11 (3): 323-331.

Clemmensen, L.B., Andreassen, F., Nielsen, S.T. and Sten, E., 1996. The late Holocene coastal dunefield at Vejers, Denmark: characteristics, sand budget and depositional dynamics. *Geomorphology*, 17: 79-98.

Crawley, M.J., 1993. GLIM for ecologists. Blackwell Scientific Publications, Oxford, 379pp.

Dargie, T.C.D., 1986. Species richness and distortion in reciprocal averaging and detrended correspondence analysis. *Vegetatio*, 65: 95 – 98.

Davies, R.A., Bartholdy, J., Pejrup, M. and Nielsen, N., 1997. Stratigraphy of Skallingen – A Holocene barrier in the Danish Wadden Sea. *Aarhus Geoscience*, 7: 9-19.

Davis, R.A., Bartholdy, J., Lykke-Andersen, H., 2001. Sedimentary depositional environments and Holocene geologic evolution of the northern Danish Wadden Sea. Korean Society of Oceanography Special Publication. Proceedings of Tidalites 2000, 63–75.

Davis, R.B. and Anderson, D.S., 1985. Methods of pH calibration of sedimentary diatom remains for reconstructing pH in lakes. *Hydrobiologia*, 120: 69-87.

Davies, S.J., Metcalfe, S.E. and Caballero, M.E., 2002. Developing diatom-based transfer functions for Central Mexican lakes. *Hydrobiologia*, 467 (1-3): 199-213.

Dawson, S. and Smith, D.E., 1997. Holocene relative sea-level changes on the margin of a glacio-isostatically uplifted area: An example from northern Caithness, Scotland. *The Holocene,* 7 (1): 59-77.

Dawson, S., Smith, D.E., Jordan, J. and Dawson, A.G., 2004. Late Holocene coastal sand movements in the Outer Hebrides, NW Scotland. *Marine Geology*, 210 (1-4): 281-306.

Denys, L., 1994. Diatom assemblages along a former intertidal gradient: A palaeoecological study of a suboreal clay layer (western coastal plain, Belgium). *Netherlands Journal of Aquatic Ecology*, 28 (1): 85-96.

Digerfeldt, G., 1971. Investigations of Littorina Transgressions in the ancient lagoon Barsebäckmossen, western Skåne. University of Lund, Department of Quaternary Geology.

Edwards, R.J. and Horton, B.P., 2000. Reconstructing relative sea-level change using UK salt-marsh foraminifera. *Marine Geology,* 169 (1-2): 41-56.

Edwards, R.J. and Horton, B.P., 2006. Developing detailed records of relative sea-level change using a foraminiferal transfer function: an example from North Norfolk, UK. *Philosophical Transactions of the Royal Society A - Mathematical Physical and Enginnering Sciences*, 364 (1841): 973-991.

Ehlers, J., Nagorny, K., Schmidt, P., Stieve, B. and Zietlow, K., 1993. Storm surge deposits in North Sea salt marshes dated by 134Cs and 137Cs determination. *Journal of Coastal Research*, 9; 698 – 701.

Erasto, P. and Holmstrom, L., 2006. Selection of prior distributions and multiscale analysis in Bayesian temperature reconstructions based on fossil assemblages. *Journal of Paleolimnology*, 36 (1): 69-80.

Fairbridge, R.W., 1961. Eustatic changes in sea-level. In: L.H., Athrens (Ed.). Physics and chemistry of the Earth. Pergamon Press, London: 98-185.

Finsinger, W. and Tinner, W., 2005. Minimum count sums for charcoal concentration estimates in pollen slides: accuracy and potential errors. *The Holocene*, 15 (2): 293-297.

Fishbein, E. and Patterson, R.T., 1993. "Error weighted maximum likelihood (EWML)" a new statistically valid method to cluster quantitative micropaleontological data. *Journal of Paleontology*, 67: 475-486.

Fleming, K., Johnston, P., Zwartz, D., Yokoyama, Y., Lambeck, K., Chappell, J., 1998. Refining the eustatic sea-level curve since the Last Glacial Maximum using far- and intermediate-field sites. *Earth and Planetary Science Letters*, 163: 327–342.

Florin, M. –B. 1970. Late-glacial diatoms of Kirchner Marsh, southeast Minnesota. *Nova Hedwigia*, 31: 667 – 756.

Folk, R.L., 1965. Petrology of sedimentary rocks. Hemphill, Austin, Texas. 159pp.

Foster, I.D.L., Mighall, T.M., Proffitt, H., Walling, D.E. and Owens, P.N., 2006. Post-depositional 137Cs mobility in sediments of three shallow coastal lagoons, SW England. *Journal of Paleolimnology*, 35: 881-895.

Freund, H. and Streif, H., 2000. Natüurliche pegelmarken für Meeresspiegelschwankungen der letzen 2000 jahre im bereich der insel Juist. *Petermanns Geographische Mitteilungen*, 143: 20-25.

Freund, H., Gerdes, G., Streif, H., Dellwig, O. and Watermann, F., 2004. The indicative meaning of diatoms, pollen, and botanical macro fossils for the reconstruction of palaeoenvironments and sea-level fluctuations along the coast of Lower Saxony, Germany. *Quaternary International*, 112: 71-87.

Fritz, S.C., 1990. Twentieth-century salinity and water-level fluctuation in Devils Lake, North Dakota: Test of a diatom-based transfer function. *Limnology and Oceanography*, 35 (8): 1771 – 1781.

Fritz, S.C., Juggins, S., Battarbee, R.W. and Engstrom, D.R., 1991. Reconstruction of past changes in salinity and climate using a diatom-based transfer function. *Nature* 353: 706-709.

Gaiser, E.E., Philippi, T.E. and Taylor, B.E. 1998. Distribution of diatoms amoung intermittent ponds on the Atlantic Coastal Plain: development of a model to predict drought periodicity from surface-sediment assemblages. *Journal of Paleolimnology*, 20: 71 – 90.

Gaiser, E.E., Taylor, B.E. and Brooks, M.J. 2001. Establishment of wetlands on the southeastern Atlantic Coastal Plain: paleolimnological evidence of a mid-Holocene hydrologic threashold from a South Carolina pond. *Journal of Paleolimnology*, 26: 373 – 391.

Gasse, F., Juggins, S. and Khelifa, L.B., 1995. Diatom-based transfer functions for inferring past hydrological characteristics of African lakes. *Palaeogeography, Palaeoclimatology and Palaeoecology*, 117: 31-54.

Gauch, H.G., Whittaker, R.H. and Wentworth, T.R., 1977. A comparative study of reciprocal averaging. *Journal of Ecology*, 63: 157 – 174.

Gehrels, W.R., 1999. Middle and late Holocene sea-level changes in eastern Maine reconstructed from foraminiferal salt-marsh stratigraphy and AMS 14-C ages on basal peat. *Quaternary Research* 52: 350 – 359.

Gehrels, W.R., 2000. Using foraminiferal transfer functions to produce high-resolution sea-level records from salt-marsh deposits, Maine, USA. *The Holocene*, 10: 367-376.

Gehrels, W.R. and Newman, S.W.G., 2004. Salt-marsh foraminifera in Ho Bugt, western Denmark, and their use as sea-level indicators. *Geografisk Tidsskrift*, 104, 97-106.

Gehrels, W.R., Belknap, D.F., Pearce, B.R. and Gong, B., 1995. Modelling the contribution of M2 tidal amplification to the Holocene rise of mean high water in the Gulf of Maine and the Bay of Fundy. *Marine Geology*, 124: 71–85.

Gehrels, W. R., Belknap, D. F. and Kelley, J. T., 1996. Integrated high-precision analyses of Holocene relative sea- level changes: Lessons from the coast of Maine. *Geological Society of America Bulletin* 108: 1073-1088.

Gehrels, W.R., Roe, H.M. and Charman, D.J., 2001. Foraminifera, testate amoebae and diatoms as sea-level indicators in UK salt marshes: a quantitative multiproxy approach. *Journal of Quaternary Science*, 16 (3): 201 – 220.

Gehrels, W. R., Belknap, D. F., Black, S. and Newnham, R. M., 2002. Rapid sea-level rise in the Gulf of Maine, USA, since AD 1800. *The Holocene*, 12: 383-389.

Gehrels, W.R., Kirby, J., Prokoph, A., Newnham, R.M., Acterberg, E.P., Evans, H., Black, S. and Scott, D.B. 2005. Onset of rapid sea-level rise in the western Atlantic Ocean. *Quaternary Science Reviews*, 24 (18 – 19): 2083 – 2100.

Gehrels, W.R., Szkornik, K., Bartholdy, J., Kirby, J.R., Bradley, S.L., Heinemeier, J., Pedersen, J.B.T. and Marshall, W.A., 2006a. Late Holocene sea-level changes and isostasy in western Denmark. *Quaternary Research*, 66 (2): 288-302.

Gehrels, W.R., Hendon, D. and Charman, D.J., 2006b. Distribution of testate amoebae in salt marshes along the North American East Coast. *Journal of Foraminiferal Research*, 36 (3): 201-214.

Gehrels, W.R., Marshall, W.A., Gehrels, M.J., Larsen, G., Kirby, J.R., Eiriksson, J., Heinemeier, J. and Shimmield, T., 2006c. Rapid sea-level rise in the Noth Atlantic Ocean since the first half of the 19th century. *The Holocene*, 16: 948-694.

Gilbertson, D.D., Schwenninger, J.L., Kemp, R.A. and Rhodes, E.J., 1999. Sand-drift and soil formation along an exposed North Atlantic coastline: 14,000 years of diverse geomorphological, climatic and human impacts. *Journal of Archaeological Science* 26: 439–469.

Grimm, E.C., 1987. CONISS: A FORTRAN 77 program for stratigraphically constrained cluster analysis by the method of incremental sum of squares. *Computers and Geosciences*, 13: 13-55.

Grimm, E.C., 2004. TILIA Version 2.0.2: A pollen program for analysis and display. Illinois State Museum, Springfield, IL, USA.

Griffith, D.A., 1987. Spatial autocorrelation: a primer. Resource Publications in Geography. Washington DC: Association of American Geographers. 86pp.

Griffith, D.A., 1992. What is spatial autocorrelation? Reflections on the past 25 years of spatial statistics. *L'espace Géographique*, 3: 265 – 280.

Gripp, K., 1964. Erdgeschichte von Schleswig-Holstein. Karl Wachholtz Verlag, Neumünster.

Hall, R.I. and Smol, J.P., 1992. A weighted-averaging regression and calibration model fro inferring total phosphorus concentration from diatoms in British Columbia (Canada) lakes. *Freshwater Biology*, 27: 417 – 434.

Hamilton, S. and Shennan I., 2005a. Late Holocene relative sea-level changes and the earthquake deformation cycle around upper Cook Inlet, Alaska. *Quaternary Science Reviews*, 24: 1479 – 1498.

Hamilton, S. and Shennan, I., 2005b. Late Holocene great earthquakes and relative sea-level change at Kenai, southern Alaska. *Journal of Quaternary Science*, 20 (2): 95-111.

Harman, M., 2006. Mid- to late Holocene relative sea-level changes in the north of Ireland. *Quaternary Newsletter*, 110: 57.

Hartley, B., 1996. An atlas of British diatoms based on illustrations by H.G. Barber and J.R. Carter and edited by P.A. Simms. Biopress LTD, Bristol. 601pp.

Haslett, J., Whiley, M., Bhattacharya, S., Salter-Townshend, M., Wilson, S.P., Allen, J.R.M., Huntley, B. and Mitchell, F.J.G., 2006. Bayesian palaeoclimate reconstruction. *Journal of the Royal Statistical Society Series A-Statistics in Society*, 169: 395-430.

Hazell, Z.J., 2004. Holocene palaeoclimate reconstruction from New Zealand peatlands. Unpublished PhD thesis, University of Plymouth.

Heegard, E., 2003. Age-depth routine for R. http://www.bio.uu.nl/~palaeo/Congressen/Holivar/Literature_Holivar2003.htm#Age-Depth%20routine%20for%20R. Accessed 26/11/2006.

Heegaard, E., Birks, H.J.B. and Telford, R.J., 2005. Relationships between calibrated ages and depth in stratigraphic sequences: an estimation procedure by mixed-effect regression. *The Holocene*, 15 (4): 612-618.

Hemphill-Haley, E., 1996. Diatoms as an aid in identifying late Holocene tsunami deposits. *The Holocene,* 6: 439 – 448.

Hill, M.O., 1979. DECORANA – a FORTRAN Program for Detrended Correspondence Analysis and Reciprocal Averaging. Cornell University, Department of Ecology and Systematics, Ithaca, New York.

Hill, M.O. and Gauch, H.G., 1980. Detrended correspondence analysis: an improved ordination technique. *Vegetatio*, 83: 187 – 194.

Horton, B.P., 1997. Quantification of the indicative meaning of a range of Holocene sea-level index points from the western North Sea. Unpublished PhD thesis, University of Durham.

Horton, B.P., 1999. Development and application of diatom-based transfer functions for palaeo-tide level and palaeoenvironmental reconstructions. In D.R. Bridgeland, B.P. Horton and J.B. Innes (Eds). Late Quaternary of northeast England. Field Guide, Quaternary Research Association, University of Durham: 81-85.

Horton, B.P. and Edwards, R.J., 2005. The application of local and regional transfer functions to the reconstruction of Holocene sea levels, north Norfolk, England. *The Holocene*, 15 (2): 216-228.

Horton, B.P., Larcombe, P., Woodroffe, S.J., Whitaker, J.E., Wight, M.R. and Wynn, C., 2003. Contemporary foraminiferal distributions of a mangrove environment, Great Barrier Reef coastline Australia: implications for sea-level reconstructions. *Marine Geology*, 198 (3-4): 225-243.

Horton, B.P., Corbett, R., Culver, S.J., Edwards, R.J. and Hillier, C., 2006. Modern salt marsh diatom distributions and the development of a transfer function for high resolution reconstructions of sea level. *Estuarine, Coastal and Shelf Science*, 69 (3-4): 381-394.

Hustedt, F., 1953. Die systematik der diatomeen in ihren beziehungen zur geologie und ökologie nebst einer revision des halobien-systems. *Svensk Botanisk Tidskrift*, 47: 509-519.

Hustedt, F., 1957. Die diatomeenflora des fluss-systems der weser im Gebiet der Hansestadt Breman. *Abhandlungen Herausgegeben vom Naturwissenschafflichen Vereine zu Bremen,* 34: 181-440.

International Geological Correlation Programme Project 495. "Quaternary Land-Ocean Interactions: Driving mechanisms and coastal responses." http://www.geography.dur.ac.uk/research/IGCP_495/Project_Outline/index.html Accessed 11th November 2006.

Imbrie J. and Kipp, N.G., 1971. A new micropaleontological method for quantitative palaeoclimatology: application to a late Pleistocene Caribbean core. In: K.K. Turekian (Ed.). The late Cenozoic glacial ages. New Haven and London, Yale University Press: 71-181.

Iversen, J. 1937. Undersøgelser over Littorinatransgressioner i Danmark. *Meddelelser fra Dansk Geologisk Forening*, 9: 223 – 232.

Jacobsen, N.K., 1964. Træk af Tøndermarskens naturgeografi med særligt henblik på morfogenesen (summary in English). *Folia Geographica Danica* 7: 299–350.

Jelgersma, S., 1961. Holocene sea-level changes in the Netherlands. Thesis Leiden, Mededelingen Geologische Stichting, C-VI-7.

Jelgersma, S., 1979. Sea-level changes in the North Sea basin. In: E. Oele, R.T.E. Schuttenhelm and A.J. Wiggers (Eds.). The Quaternary history of the North Sea. Acta University of Uppsala Symposium. University of Upsala Annum Quingentesimum Celebrantis 2, Uppsala: 233 – 248.

Jepsen, P. U., 1996. Images of West Jutland – from Skallingen to Nymindegab. Varde Town and Regional Museum. Translated by Michael Cain. 131pp.

Jessen, A., 1920. Stenalderhavets Udbredelse I det nordlige Jylland. Danmarks Geologiske Undersøgelse II, 35, København, C.A. Reitzel.

Jessen, K., 1937. Litorinasækningen ved Klintesö I pollenfloristisk Belysning. *Meddelelser fra Dansk Geologisk Forening,* 9: 232 – 236.

Jonassen, H., 1957. Bidrag til Filsøegrens naturhistorie. *Meddelelser fra Dansk Geologisk Forening* 13: 192 – 205.

Jones, V.J. and Juggins, S., 1995. The construction of a diatom-based chlorophyll *a* transfer function and its application at three lakes on Signy Island (maritime Antarctic) subject to differing degrees of nutrient enrichment. *Freshwater biology*, 34: 433 – 445.

Jones, V.J., Juggins, S. and Ellis-Evans, J.C., 1993. The relationship between water chemistry and surface sediment diatom assemblages in maritime Antarctic lakes. *Antarctic Science*, 5 (4): 339 – 348.

Jongman, R.H.G., ter Braak, C.J.F. and Van Tongeren, O.F.R., 2002. Data analysis in community and landscape ecology. Cambridge University Press, 299pp.

Juggins, S., 1992. Diatoms in the Thames Estuary, England: Ecology, palaeoecology and salinity transfer function. Bibliotheca Diatomologica Band 25. J. Cramer Berlin, Stuttgart. 216pp.

Juggins, S., 2003-2006. C2 User Guide. Software for Ecological and Palaeoecological Data Analysis and Visualisation. University of Newcastle, Newcastle-upon-Tyne, UK. 69pp.

Juggins, S., Battarbee, R.W. and Fritz, S.C., 1994. Diatom/salinity transfer functions and climate change: an assessment of methods and application to two Holocene sequences from the northern Great Plains, North America. In: B.M. Funnell and R.L.F. Kay (Eds.). Palaeoclimate of the Last Glacial/Interglacial cycle, Special Publication 94/2, NERC Earth Science Directorate, Swindon: 37-41.

Kendall, D.G., 1971. Seriation from abundance matrices. In: F.R. Hodson, D.G. Kendall amd P. Tautu (Eds.). Mathematics in archaeological and historical sciences, Edinburgh University Press: 215 – 252.

Kent, M. and Coker, P., 1992. Vegetation description and analysis. A practical approach. John Wiley and Sons, 363pp.

Kidson, C., 1982. Sea-level changes in the Holocene. *Quaternary Science Reviews*, 1: 121-151.

Kidson, C. and Heyworth, A., 1973. The Flandrian sea-level rise in the Bristol Channel. *Proceedings of the Usher Society*, 2: 565-584.

Knox, R.G., 1989. Effects of detrending and rescaling on correspondence analysis: solution, stability and accuracy. *Vegetatio*, 83: 129 – 136.

Kolbe, R.W., 1927. Zur ökologie, morphologie und systematik der brackwasser-diatomeen. *Pflanzenforschung*, 7: 1-146.

Konradi, P.B., 1976. Foraminifera in Eemian deposits at Stensigmose, southern Jutland. Danmarks Geologiske Undersøgelse II Række 105, 55pp.

Konradi, P.B., Larsen, B. and Sørensen, A.B. 2005. Marine Eemian in the Danish eastern North Sea. *Quaternary International*, 133-134: 21-31.

Korhola, A. and Weckström J., 2000. A quantitative Holocene climate record from diatoms in Northern Fennoscandia. *Quaternary Research,* 54: 284-294.

Korsman, T. and Birks, H.J.B., 1996. Diatom-based water chemistry reconstructions from northern Sweden: a comparison of reconstruction techniques. *Journal of Paleolimnology*, 15: 65-77.

Kosack, B. and Lange, W., 1985. Das Eem-Vorkommen von Offenbüttel/Schnittlohe und die Ausbreitung des Eem-Meeres zwischen Nordund Ostsee. *Geologisches Jahrbuch* A, 86: 3 – 17.

Koster, D., Racca, J.M.J. and Pienitz, R., 2004. Diatom-based inference models and reconstructions revisited: methods and transformations. *Journal of Paleolimnology*, 32 (3): 233-245.

Krammer, K. and Lange-Bertalot H., 1991a. Bacillariophyceae, 3.Teil, Centrales, Fragilariaceae, Eunotiaceae. In: H. Ettl, J. Gerloff, H. Heynig, and D. Mollenhauer (Eds.). Süsswasserflora von Mitteleuropa. Band 2/3. Gustav Fischer Verlag, Stuttgart.

Krammer, K. and Lange-Bertalot H., 1991b. Bacillariophyceae 4.Teil, Achnantaceae. Kritische Ergänzungen zu Navicula (Lineolatae) und Gomphonema. In: H. Ettl, G. Gärtner, J. Gerloff, H. Heynig and D. Mollenhauer (Eds.). Süsswasserflora von Mitteleuropa. Band 2/4. Gustav Fischer Verlag, Stuttgart.

Krammer, K. and Lange-Bertalot H., 1997a. Bacillariophyceae, 1.Teil, Naviculaceae. In: H. Ettl, H. J. Gerloff, H. Heynig and D. Mollenhauer (Eds.). Süsswasserflora von Mitteleuropa, Band 2/1. Gustav Fischer, Jena.

Krammer, K. and Lange-Bertalot H., 1997b. Bacillariophyceae, 2.Teil Bacillariaceae, Epithemiaceae, Surirellaceae. In: H. Ettl, J. Gerloff, H. Heynig and D. Mollenhauer (Eds.). Süsswasserflora von Mitteleuropa, Band 2/2. Gustav Fischer, Jena.

Krog, H. 1960. Post-glacial submergence of the Great Belt (Store Bælt) dated by pollen analysis and radiocarbon. International Geological Congress session XXI, Norden, part IV: 127 – 133.

Krog, H., 1973. The early post-glacial development of the Store Bælt as reflected in a former fresh water basin. Danmarks Geologiske Undersøgelse, Arbog 1972: 37 – 47.

Krog, H., 1979a. Late Pleistocene and Holocene shorelines in western Denmark. In: E. Oele, R.T.E. Schuttenhelm and A.J. Wiggers (Eds.). The Quaternary history of the North Sea. Acta University of Uppsala Symposium. University of Upsala Annum Quingentesimum Celebrantis 2, Uppsala: 75 – 83.

Krog, H., 1979b. The Quaternary history of the Baltic, Denmark. In: V. Gudelis and L.K. Konigsson (Eds.). The Quaternary history of the Baltic. Acta Universitatis Upsaliensis, Uppsala: 207-217.

Kucera, M., Weinelt, Kiefer, T., Pfaumann, U., Hayes, A., Weinelt, M., Chen, M.T., Mix, A.C., Barrows, T.T., Cortijo, E., Duprat, J., Juggins, S. and Waelbroeck, C., 2005. Reconstruction of sea-surface temperatures from assemblages of planktonic foraminifera: a multi-technique approach based on geographically constrained calibration data sets and its application to glacial Atlantic and Pacific Oceans. *Quaternary Science Reviews*, 24 (7-9): 951-998.

Laird, K.R., Fritz, S.C., Grimm, E.C. and Mueller, P.G., 1996. Century-scale paleoclimatic reconstruction from Moon Lake, a closed basin in the northern Great Plains. *Limnology and Oceanography*, 41: 890-902.

Lamb, H., 1982. Climate, history and the modern world. Mutheun. 433pp.

Lamb, H., 1991. Historic storms of the North Sea, British Isles and Northwest Europe. Cambridge University Press. 204pp.

Lambeck, K., 1990. Late Pleistocene, Holocene and present sea-levels: constraints on future change. *Palaeogeography, Palaeoclimatology and Palaeoecology*, 89: 205-217.

Lambeck, K., 1995. Late Devensian and Holocene shorelines of the British Isles and North Sea from models of glacio-hydro-isostatic rebound. *Journal of the Geological Society of London*, 152: 437 – 448.

Lambeck, K., 1996. Limits on the aerial extent of the Barents Sea ice sheet in Late Weichselian time. *Global and Planetary Change*, 12 (1-4): 41 – 51.

Lambeck, K., 1997. Sea-level change along the French Atlantic and Channel coasts since the time of the Last Glacial Maximum. *Palaeogeography, Palaeoclimatology, Palaeoecology*, 129: 1–22.

Lambeck, K. and Bard, E., 2000. Sea-level change along the French Mediterranean coast for the past 30,000 years. *Earth and Planetary Science Letters,* 175: 203–222.

Lambeck, K., Smither, C. and Johnston, P., 1998a. Sea-level change, glacial rebound and mantle viscosity for northern Europe, *Geophysical Journal International,* 134: 102-144.

Lambeck, K., Smither, C. and Elkman, M., 1998b. Tests of glacial rebound models for Fennoscandinavia based on instrumented sea- and lake-level records. *Geophysical Journal International*, 135, 275–387.

Lambeck, K., Antonionli, F., Purcell, A. and Silenzi, S., 2004. Sea-level change along the Italian coast for the past 10, 000 yr. *Quaternary Science Reviews,* 23: 1567-1598.

Lampe, R., 2005. Late glacial and Holocene water-level variations along the NE German Baltic coast: review and new results. *Quaternary International* 133-134: 121-136.

Lampe, R. and Janke, W., 2004. The Holocene sea level rise in the southern Baltic as reflected in coastal peat sequences. *Polish Geological Institute Special Papers,* 11: 19–30.

Larsen, J., Jones, V.J. and Eide, W., 2006. Climatically driven pH changes in two Norwegian alpine lakes. *Journal of Paleolimnology*, 36 (2): 175 – 187.

Latychev, K., Mitrovica, J.X., Tamisiea, M.E., Tromp, J., Christara, C.C. and Moucha, R., 2005a. GIA-induced secular variations in the Earth's long wavelength gravity field: Influence of 3-D viscosity variations. *Earth and Planetary Science Letters*, 240 (2): 322 – 327.

Latychev, K., Mitrovica, J.X., Tromp, J., Tamisiea, M.E., Komatitsch, D. and Christara, C.C., 2005b. Glacial isostatic adjustment on 3-D Earth models: a finite-volume formulation. *Geophysical Journal International*, 161 (2): 421 – 444.

Latychev, K., Mitrovica, J.X., Tamisiea, M.E., Tromp, J. and Moucha, R., 2005c. Influence of lithospheric thickness variations on 3-D crustal velocities due to glacial isostatic adjustment. *Geophysical Research Letters*, 32 (1): Article number L01304, January 7th 2005.

Legendre, P., 1993. Spatial autocorrelation: trouble or new paradigm? *Ecology*, 74: 1659 – 1673.

Lengendre, P. and Fortin, M-J., 1989. Spatial pattern and ecological analysis. *Vegetatio*, 80: 107 – 138.

Lepš, J. and Šmilauer, P., 2003. Multivariate analysis of ecological data using CANOCO. Cambridge University Press. 269pp.

Line, J.M., ter Braak, C.J.F. and Birks, H.J.B., 1994. WACALIB version 3.3 – a computer programme to reconstruct environmental variables from fossil assemblages by weighted averaging and to derive sample-specific errors of prediction. *Journal of Paleolimnology*, 10: 147-152.

Long, A.J., Waller, M.P. and Stupples, P., 2006. Driving mechanisms of coastal change: Peat compaction and the destruction of late Holocene coastal wetlands. *Marine Geology,* 225: 63-84.

Lotter, A.F., 1998. The recent eutrophication of Baldeggersee (Switzerland) as assessed by fossil diatom assemblages. *The Holocene*, 8: 395-405.

Lowe, J.J. and Walker, M.J.C., 1997. Reconstructing Quaternary Environments. Second edition, Addison Wesley Longman Limited, Hong Kong. 446pp.

Ludwig, G., Müller, H. and Streif, H., 1979. Neuere daten zum Holozänen Meeresspiegelansteig im bereich der Deutschen Bucht. *Geologisches Jahrbuch*: 3-22.

Ludwig, G., Muller, H. and Streif, H., 1981. New dates on Holocene sea-level changes in the German Blight. In: S.D. Nio, R.T.E. Schuttenhelm and T.C.E. Weering (Eds.). Holocene marine sedimentation in the North Sea basin. Special publication of the International Association of Sedimentology: 211-219.

Lund, J.W.G., 1946. Observations on soil alage. I. The ecology, size and taxonomy of British soil diatoms. *New Phytologist*, 44: 196 – 219.

Mackay, A.W., Vivienne, J.J. and Battarbee, R.W., 2003. Approaches to Holocene climate reconstructions using diatoms: In A. Mackay, R.W. Battarbee, H.J.B. Birks and F. Oldfield (Eds.). Global changes in the Holocene. Arnold, London: 294-309.

Madsen, A.T., Murray, A.S., Andersen, T.J., Pejrup, M. and Breuning-Madsen, H., 2005. Optically stimulated luminescence dating of young estuarine sediments: a comparison with Pb-210 and Cs-137 dating. *Marine Geology*, 214 (1 – 3): 251 – 268.

Madsen, A.T., Murray, A.S. and Andersen, T.J. 2006. *In press*. Optical dating of dune ridges on Rømø, a barrier island in the Wadden Sea, Denmark. *Journal of Coastal Science*, article in press.

Malmgren, B.A., Kucera, M., Nyberg, J. and Waelbroeck, C., 2001. Comparison of statistical and artificial neural network techniques for estimating past sea surface temperatures from planktonic foraminifer census data. *Paleoceanography*, 16 (5): 520-530.

Martens, H. and Nates, T., 1989. Multivariate calibration. John Wiley, Chichester. 419pp.

Menke, B., 1976. Befunde und Überlegungen zum nacheiszeitlichen Meeresspiegelandstieg. (Dithmarschen und Eiderstedt, Schleswig-Holstein). *Eiszeitalter und Gegenwart*, 21: 145-161.

Mertz, E.L., 1924. Oversigt over de sen- og postglaciale niveauforandringer I Danmark. *Danmarks Geologiske Undersøgelser II Række*, 41: 1 – 50.

Mikkelsen, V.M., 1949. Præsto Fjord – The development of the post-glacial vegetation and a contribution to the history of the Baltic Sea. *Dansk Botanisk Arkiv*, 13 (5): 1 – 171pp.

Milne, G.A., David, J.L., Mitrovica, J.X., Scherneck, H. –G. Johansson, J.M., Vermeer, M. and Koivula, H., 2001. Space-geodetic constraints on glacial isostatic adjustment in Fennoscandia. *Science*, 291: 2381–2385. (doi: 10.1126/science.1057022).

Milne, G.A., Mitrovica, J.X. and Schrag, D.P., 2002. Estimating past continental ice volume from sea-level data. *Quaternary Science Reviews*, 21 (1-3): 361 – 376.

Milne, G.A., Shennan, I., Youngs, B.A.R., Waugh, A.I., Teferle, F.N., Bingley, R.M., Bassett, S.E., Cuthbert-Brown, C. and Bradley, S.L., 2006. Modelling the glacial isostatic adjustment of the UK region. *Philosophical Transactions of the Royal Society A*, 364: 931 – 948.

MINITAB® 2004. Statistical Software, Release 14.20. LEAD Technologies, Inc.

Montgomery, D.C. and Peck, E.A., 1982. Introduction to linear regression analysis. J. Wiley and Sons, New York, 504pp.

Morhange, C. and Pirazzoli, P.A., 2005. Mid-Holocene emergence of southern Tunisian coasts. *Marine Geology,* 220: 205–213.

Murray, A.S. and Olley, J.M., 2002. Precision and accuracy in the optically stimulated luminescence dating of sedimentary quartz: A status review. *Geochronometria*, 21: 1-16.

Mörner, N.A., 1969a. Eustatic and climate changes during the last 15, 000 yrs. *Geologie en Mijnbouw,* 48: 399pp.

Mörner, N.A., 1969b. The late Quaternary history of the Kattegat Sea and the Swedish west coast: Deglaciation, shoreline displacement, isostasy and eustasy. *Sveriges Geologisk Undersökning* C-640: 1-487.

Mörner, N.A., 1976. Eustatic changes during the last 8000 years in view of radiocarbon calibration and new information from the Kattegat region and other northwestern European coastal areas. *Palaeogeography, Palaeoclimatology, Palaeoecology*, 19: 63 – 85pp.

Mörner, N.A., 1979. The northwest European "sea-level laboratory" and regional eustasy. *Palaeogeography, Palaeoclimatology, Palaeoecology*, 29: 281-300.

Müller, W., 1962. Der ablauf de Holozänen Meerestransgression an der südlichen Nordseeküste und folgerungen in bezug auf eine geochronologische Holozängliederung. *Eiszeitalter und Gegenwart*, 13: 197-226.

Neff, J.C., Harden, J.W. and Gleixner, G., 2005. Fire effects on soil organic matter, content, composition and nutrients in boreal interior Alaska. *Canadian Journal of Forest Research*, 35 (9): 2178 – 2187.

Nielsen, S.T., Clemmensen, L.B. and Andreassen, F., 1995. The middle and late Holocene barrier spit system at Vejers, Denmark: Structure and development. *Bulletin of the Geological Society of Denmark,* 42: 105-119.

Nelson, A.R. and Kashima, K., 1993. Diatom zonation in Southern Oregon, tidal marshes relative to vascular plants, foraminifera and sea-level. *Journal of Coastal Research*, 9: 673–697.

Ng, S.L. and King, R.H., 1999. Development of a diatom-based specific conductivity model for the glacio-isostatic lakes of Truelove Lowland: implications for palaeoconductivity and palaeoenvironmental reconstructions in Devon Island lakes, NWT, Canada. *Journal of Paleolimnology*, 22(4): 367-382.

Ng, S.L. and Sin, F.S., 2003. A diatom model for inferring sea-level change in the coastal waters of Hong Kong. *Journal of Paleolimnology,* 30: 427 – 440.

Odgaard, B.V., 1994. The Holocene vegetation history of northern West Jutland, Denmark. *Opera Botanica*, 123: 1-171.

Odgaard, B.V. and Rasmussen, P., 2000. Origin and temporal development of macro-scale vegetation patterns in the cultural landscape of Denmark. *Journal of Ecology,* 88: 733-748.

Oksanen, J., Läärä, E., Huttunen, P. and Meriläinen, J., 1990. Maximum likelihood prediction of lake acidity based on sedimented diatoms. *Journal of Vegetation Science*, 1: 49-56.

Orford, J.D., Wilson, P., Wintle, A.G., Knight, J. and Bradley, S., 2000. Holocene dune initiation in Northumberland and Norfolk, eastern UK: Climate and sea-level changes as possible forcing agents for dune initiation. In: I. Shennan and J. Andrews (Eds.). Land-ocean interaction and environmental change around the North Sea. Geological Society of London, Special Publication, 166: 197-217.

Orlóci, I., 1966. Geometric models in ecology. I. Theory and application of some ordination methods. *Journal of Ecology*, 54: 193-215.

Overpeck, J.T., Webb, T. and Prentice, I.C., 1985. Quantitative interpretation of fossil pollen spectra: dissimilarity coefficients and the method of modern analogues. *Quaternary Research*, 23: 87-108.

Palmer, A.J.M. and Abbott, W.H., 1986. Diatoms as indicators of sea-level change. In: O. Van de Plassche (Ed.). Sea-level research, a manual for the collection and evaluation of data. Geo Books, Norwich: 457 – 473.

Patrick, R. and Reimer, C.W., 1966. The diatoms of the United States exclusive of Alaska and Hawaii I. The Academy of Natural Sciences of Philadelphia, Monograph 13.

Patterson, W.A., Edwards, K.J. and Maguire, D.J., 1987. Microscopic charcoal as a fossil indicator of fire. *Quaternary Science Reviews,* 6: 3-23.

Patterson, R.T. and Fishbein, E., 1989. Re-examination of the statistical methods used to determine the number of point counts needed for micropaleontological quantitative research. *Journal of Paleontology*: 63: 245-248.

Patterson, R.T., Hutchinson, I., Guilbault, J. –P. and Clague, J.J., 2000. A comparison of the vertical zonation of diatom, foraminifera and macrophyte assemblages in a coastal marsh: Implications for greater paleo-sea level reconstruction. *Micropaleontology*, 46 (3): 229 – 244.

Patterson, R.T., Dalby, A.P. and Roe, H.M., 2005. Relative utility of foraminifera, diatoms and macrophytes as high resolution indicators of paleo-sea level in coastal British Columbia, Canada. *Quaternary Science Reviews*, 24 (18-19): 2002-2014. Special Issue 2005.

Pedersen, A., 1974. Granineernes udbredelse i Danmark. Spontane og naturaliserede arter. *Botanisk Tidsskrift*, 68: 177-343.

Pedersen, J.B., 1935. Studies on the biology and taxonomy of soil alage. *Dansk Botanisk*, 8: 1-171.

Pedersen, J.B.T., 2004. Fine-grained sediment budgets for the Grådyb, Knudedyb and Juvredyb tidal areas, the Danish Wadden Sea. Unpublished prize dissertation, University of Copenhagen, 233pp.

Pejrup, M., 1986. Parameters affecting fine-grained suspended sediment concentrations in a shallow micro-tidal estuary, Ho Bugt, Denmark. *Estuarine Coastal and Shelf Science*, 22: 241 – 254.

Peltier, W.R., 1994. Ice age palaeotopography. *Science*, 265: 195-201.

Peltier, W.R., 2002. On eustatic sea level history: last glacial maximum to Holocene. *Quaternary Science Reviews*, 21: 377–396.

Peltier, W.R., 2004. Global glacial isostasy and the surface of the ice-age Earth: The ICE-5G (VM2) model and GRACE. *Annual Review of Earth and Planetary Sciences*, 32: 111 – 149.

Petersen, K.S., 1981. The Holocene marine transgression and its' molluscan fauna in the Skagerrak-Limfjord region, Denmark. In: Nio, S.D., Schuttenhelm, R.T.E and Weering, T.C.E (eds). Holocene marine sedimentation in the North Sea basin. Special publication of the International Association of Sedimentology: 497 – 503.

Petersen, K.S., 1985. The late Quaternary history of Denmark, the Weichselian ice sheets and land/sea configuration in the later Pleistocene. *Journal of Danish Archaeology*, 4: 7-22.

Petersen, K.S., 1994. Limfjordstangerne. Holocæne marine miljøudvikling. DGU Customer's Report 85.

Petersen, K.S. and Rasmussen, K.L. 1995. Late Weichselian and Holocene changes in the marine environment – with examples from North West Denmark. In: A. Fischer (Ed.). Man and sea in the Mesolithic. Oxbow books, Oxford, UK: 35 – 38.

Pirazzoli, P.A., 1991. World atlas of Holocene sea-level changes: 62pp.

Pirazzoli, P.A., 2005. A review of possible eustatic, isostatic and tectonic contributions in eight late-Holocene relative sea-level histories from the Mediterranen area. *Quaternary Science Reviews*, 24 (18-19): 1989-2001.

Prell, W.L., 1985. The stability of low-latitude sea surface temperatures: an evaluation of the CLIMAP reconstruction with emphasis on the positive SST anomalies. Technical Report TR025, US Department of Energy, Washington, DC

Prentice, I.C., 1980. Multidimensional-scaling as a research tool in Quaternary palynology – A review of theory and methods. *Review of Palaeobotany and Palynology*, 31: 71 – 104.

Preuss, H., 1979. Progress in computer evaluation of sea-level data within IGCP Project No. 61.

Pye, K., 1984. Models of transgressive coastal dune building episodes and their relationship to Quaternary sea-level change: a discussion with evidence from eastern Australia. In: M.W. Clark (Ed.), Coastal research, UK perspectives. Geobooks, Norwich: 81-104.

Racca, J.M.J., Philibert, A., Racca, R. and Prairie., Y.T., 2001. A comparison between diatom-based pH inference models using artificial neural networks (ANN), weighted averaging (WA) and weighted averaging partial least squares regression. *Journal of Paleolimnology*, 26 (4): 411-422.

Rasmussen, P., 2005. Mid- to late Holocene land-use change and lake development at Dallund So, Denmark: vegetation and land-use history inferred from pollen data. *The Holocene*, 8: 1116-1129.

Reimer, P.J., Baillie, M.G.L., Bard, E., Bayliss, A., Beck, J.W., Bertrand, C.J.H., Blackwell, P.G., Buck, C.E., Burr, G.S., Cutler, K.B., Damon, P.E., Edwards, R.L., Fairbanks, R.G., Friedrich, M., Guilderson, T.P., Hogg, A.G., Hughen, K.A., Kromer, B., McCormac, F.G., Manning, S.W., Ramsey, C.B., Reimer, R.W., Remmele, S., Southon, J.R., Stuiver, M., Talamo, S., Taylor, F.W., van der Plicht, J. and Weyhenmeyer, C.E., 2004. IntCal04 Terrestrial radiocarbon age calibration, 26 - 0 ka BP. *Radiocarbon*, 46: 1029-1058.

Round, F.E., Crawford, R.M. and Mann, D.G., 1990. The diatoms, biology and morphology of the genera. Cambridge University Press, Cambridge. 747pp.

Ryves, D.B., Juggins, S., Fritz, S.C. and Battarbee, R.W., 2001. Experimental diatom dissolution and the quantification of microfossil preservation in sediments. *Palaeogeography, Palaeoclimatology and Palaeoecology*, 172 (1-2): 99-113.

Ryves, D.B., Battarbee, R.W., Juggins, S., Fritz, S.C. and Anderson, N.J., 2006. Physical and chemical predictors of diatom dissolution in freshwater and saline lake sediments in North America and West Greenland. *Limnology and Oceanography*, 51 (3): 1355-1368.

Sawai, Y., 2001. Distribution of living and dead diatoms in tidal wetlands of northern Japan: relation to taphonomy. *Palaeogeography, Palaeoclimatology, Palaeoecology*, 173: 125 – 141.

Sawai, Y., Horton, B.P. and Nagumo, T., 2004. The development of a diatom-based transfer function along the Pacific coast of eastern Hokkaido, northern Japan – an aid in paleoseismic studies of the Kuril subduction zone. *Quaternary Science Reviews*, 23: 2467 – 2483.

Schulz, H., Emis, K. -C., Winn, K. and Erlenkeuser, H., 2001. Oberflächentemperaturen dea Eem-Meeres in Schleswig-Holstein – die UK '37 – Indizien. *Meyniana*, 53: 163 – 181.

Schütte, H., 1933. Der geologische Aufbau des Jever-und Harlingerlandes und die erste Marschbesiedlung. *Oldenburger Jahrbuch*, 37: 1-39.

Schütte, H., 1939. Sinkendes land an der Nordsee? Öhringen/Württ.

Scouse, J. and HOLSMEER Partners., 2004. Late HOLocene Shallow Marine Environments of EuRope. Final report, June 2004. Section 5-6, executive summary and detailed report: 63pp. http://www.bangor.ac.uk/os/holsmeer/FWV%20section%205-6.pdf

Seierstad, J., Nesje, A., Dahl, S.O. and Simonsen, J.R., 2002. Holocene glacier fluctuations of Grovabreen and Holocene snow-avalanche activity reconstructed from lake sediments in Grøningstølsvatnet, western Norway. *The Holocene*, 12:211-222.

Sejrup, H.P., Larsen, E., Landvik, J., King, E.L., Haflidason, H. and Nesje, A., 2000. Quaternary glaciations in southern Fennoscandia: evidence from southwestern Norway and the northern North Sea region. *Quaternary Science Reviews,* 19 (7): 667-685.

Shennan, I., 1982. Interpretation of Flandrian sea-level data from the Fenland, England. *Proceedings of the Geologists Association,* 83 (1): 53-63.

Shennan, I., 1986a. Flandrian changes in the Fenland I: The geographical setting and evidence of relative sea-level changes. *Journal of Quaternary Science*, 1(2): 119-154.

Shennan, I., 1986b. Flandrian changes in the Fenland II: Tendencies of sea-level movement, altitudinal changes and local and regional factors. *Journal of Quaternary Science*, 1(2): 155-179.

Shennan, I., 1987. Holocene sea-level changes in the North Sea region. In: M.J. Tooley and I. Shennan (Eds.). Sea-level changes. Oxford: Basil Blackwell: 109 – 151.

Shennan, I., 1989. Holocene crustal movements and sea-level changes in Great Britain. *Journal of Quaternary Science*, 4, 77–89.

Shennan I. and Horton B., 2002. Holocene land- and sea-level changes in Great Britain. *Journal of Quaternary Science*, 17 (5-6): 511-526.

Shennan, I., Tooley, M.J., Davis, M.J. and Haggart, B.A., 1983. Analysis and interpretation of Holocene sea-level data. *Nature,* 302 (March, 1983): 404-406.

Shennan, I., Innes, J.B., Long, A.J. and Zong, Y., 1995. Holocene relative sea-level changes and coastal vegetation history at Kentra Moss, Argyll, NW Scotland. *Marine Geology*, 124: 43–59.

Shennan, I., Long, A.J., Rutherford, M.M., Green, F.M., Innes, J.B., Lloyd, J.M., Zong, Y. and Walker, K.J., 1996. Tidal marsh stratigraphy, sea-level change and large earthquakes – II Submergence events during the last 3500 years at Netarts Bay, Oregon, USA. *Quaternary Science Reviews*, 17 (4-5): 365-393.

Shennan, I., Lambeck, K., Horton, B., Innes, J., Lloyd, J., McArthur, J., Purcell, T. and Rutherford, M., 2000a. Late Devensian and Holocene records of relative sea-level changes in northwest Scotland and their implications for glacio-hydro-isostatic modelling. *Quaternary Science Reviews*, 19: 1103 – 1135.

Shennan, I., Horton, B.P., Innes, J.B., Gehrels, W.R. Lloyd, J.M., McArthur, J. and Rutherford, M.M., 2000b. Late Quaternary sea-level changes, crustal movements and coastal evolution in Northumberland, UK. *Journal of Quaternary Science* 15: 215-237.

Shennan, I., Peltier, W.R., Drummond, R. and Horton, B.P., 2002. Global to local scale parameters determining relative sea-level changes and the post-glacial isostatic adjustment of Great Britain. *Quaternary Science Reviews*, 21: 397–408.

Shepard, F.P., 1963. Thirty-five thousand years of sea-level. In: T. Clements (Ed.). Essays in marine geology in honour of K.O. Emery. University of South California Press, Los Angeles: 1-10.

Sherrod, B.L., 1999. Gradient analysis of diatom assemblages in a Puget Sound salt marsh: can such assemblages be used for quantitative palaeoecological reconstructions? *Palaeogeography, Palaeoclimatology, Palaeoecology* 149 (1-4): 213:226.

Sherrod, B.L., Rollins, H.B. and Kennedy, S.K., 1989. Sub recent intertidal diatoms from St Catherine's Island, Georgia: Taphonomic implications. *Journal of Coastal Research*, 5 (4): 665-677.

Simonsen, R., 1962. Untersuchungen zur systematik und ökologie der bodensiatomeen der Wesrlichen Ostsee. *Int. Rev. Hydrobiol. Syst. Beih*, 1: 1-144.

Simonsen, R., 1969. Diatoms as indicators in estuarine environments. Veröffentl. Inst. Meeresforch. *Bremerhaven*, 11: 287-291.

Skarregaard, P., 1989. The history of dune management. In: Perspectives in coastal dune management. F. Van der Meulen, P.D. Jungeriusc and J.H. Visser (Eds.). SPB Academic Publishing by The Hague, The Netherlands: 151 – 161.

Šmilauer, P., 1999-2003. Canodraw for Windows, Version 4.1.

Stevenson, A.C., Juggins, S., Birks, H.J.B., Anderson, D.S., Anderson, N.J., Battarbee, R.B., Berge, F., Davis, R.B., Flower, R.J., Haworth, E.Y., Jones, V.J., Kingson, J.C., Kreiser, A.M., Line, J.M., Munro, M.A.R. and Renberg, I., 1991. The Surface Waters Acidification Project Palaeolimnology Programme: Modern Diatom/Lake-water Chemistry Data-set. ENSIS Publishing, London, England.

Stockmarr, J., 1971. Tablets with spores used in absolute pollen analysis. *Pollen et Spores,* 13: 615-621.

Streif, H., 1990. Das ostfriesische Küstengebiet – Nordsee, Inseln, Watten und Marschen. Sammlung Geologischer Führer 57. Gebrüder Borntraeger, Berlin. 376pp.

Streif, H., 2004. Sedimentary record of Pleistocene and Holocene marine inundations along the North Sea coast of Lower Saxony, Germany. *Quaternary International*, 112 (1): 3-28.

Stuvier, M. and Reimer, P.J., 1993. Extended 14C data base and revised CALIB 3.0 14C age calibration programme. *Radiocarbon*, 35: 215-230.

Stuiver, M., Reimer, P. J. and Reimer, R. W., 2005. CALIB 5.0. [WWW program and documentation]. http://calib.qub.ac.uk/calib/ Accessed 03/12/2006.

Szkornik, K., Kirby, J. and Gehrels, W.R., 2005. The use of salt-marsh diatoms as sea-level indicators in Ho Bugt, western Denmark. "Late Quaternary Coastal Changes: Sea Level, Sediment Forcing and anthropogenic Impacts". Abstract Volume, INQUA and IGCP-496 Joint Meeting, Dunkerque, France. 28th June – 2nd July 2005: 53.

Szkornik, K., Gehrels, W.R., and Kirby, J., 2006. Salt-marsh diatom distributions in Ho Bugt (western Denmark) and the development of a diatom-based transfer function for reconstructing relative sea-level change. *Marine Geology*, 235 (1-4): 137-150.

Telford, R.J., 2006. Limitations of dinoflagellate cyst transfer functions. *Quaternary Science Reviews*, 25: 1375-1382.

Telford, R.J. and Birks, H.J.B., 2005. The secret assumption of transfer functions: problems with spatial autocorrelation in evaluating model performance. *Quaternary Science Reviews*, 24: 2173 – 2179.

Telford, R.J., Heegard, E. and Birks, H.J.B., 2004a. The intercept is a poor estimate of calibrated radiocarbon age. *The Holocene*, 14 (2): 296-298.

Telford, R.J., Heegaard, E. and Birks, H.J.B., 2004b. All age-depth models are wrong: but how badly? *Quaternary Science Reviews*, 23: 1-5

Temmler, H., 1995. Neue Ergebnisse zum Aufbau des Eem-Interglazials in Nordfriesland. *Meyniana*, 47: 83 – 100.

ter Braak, C.J.F., 1985. Correspondence analysis of incidence and abundance data properties in terms of a unimodal response. *Biometrics* 41: 859 – 873.

ter Braak, C.J.F., 1986. Canonical correspondence analysis: a new eigenvector technique for multivariate direct gradient analysis. *Ecology*, 67: 1167 – 1179.

ter Braak, C.J.F., 1987a. Calibration. In: Data analysis in community landscape ecology. R.H.G. Jongman, C.J.F. ter Braak and O.F.R. van Tongeren (Eds.). Pudoc, Wageningen: 78 – 90.

ter Braak, C.J.F., 1987b. Unimodal models to relate species to environment. Doctoral thesis. University of Wageningen. 152pp.

ter Braak, C.J.F., 1987c. CANOCO – a FORTRAN program for *canon*ical *c*ommunity *o*rdination by [partial] [detrended] [canonical] correspondence analysis, principal components analysis and redundancy analysis (version 2.1). TWO Institute of Applied Computer Science, 6700 AC Wageningen, The Netherlands, 95pp.

ter Braak, C.J.F., 1995. Non-linear methods for multivariate calibration and their use in paleoecology: a compariosn of inverse (K-nearest neighbours, PLS and WA-PLS) and classical approaches. *Chemometrics and Intelligent Laboratory Systems*, 28 (1): 165-180.

ter Braak, C.J.F. and Juggins, S., 1993. Weighted-averaging partial least squares regression (WA-PLS): an improved method for reconstructing environmental variables from species assemblages. *Hydrobiologia*, 269/270: 485 – 502.

ter Braak, C.J.F. and Looman, C.W.N., 1986. Weighted averaging logistic regression and the Gaussian response model. *Vegetatio*, 65: 3-11.

ter Braak, C.J.F. and Šmilauer, P., 2002. CANOCO reference manual and CanoDraw for Windows user's guide. Software for Canonical Community Ordination, version 4.5. Microcomputer Power (Ithaca, NY, USA), 500pp.

ter Braak., C.J.F. and Šmilauer, P., 2003. CANOCO for Windows version 4.51. Biometris-Plant Research International Wageningen, The Netherlands.

ter Braak, C.J.F. and van Dam, H., 1989. Inferring pH from diatoms: a comparison of old and new calibration methods. *Hydrobiologia*, 178: 209-223.

Tooley, M.J., 1974. Sea-level changes during the last 9000 years in North West England. *The Geographical Journal*, 140: 18-42.

Tooley, M.J., 1982. Introduction to IGCP Project 61. *Proceedings of the Geologists Association*, 93: 3-6.

Tooley, M.J., 1985. Sea-levels. *Progress in Physical Geography*, 9: 113-120.

Trites, M., Kaczmarska, I., Ehrman, J.M., Hicklin, P.W. and Ollerhead, J., 2005. Diatoms from two macro-tidal mudflats in Chignecto Bay, Upper Bay of Fundy, New Brunswick, Canada. *Hydrobiologia*, 544: 299 – 319.

Troels-Smith, J., 1937. Datering of Ertebollebopladser ved Hjealp af Litorina-Transgressioner og pollenanalyse. *Meddelelser fra Dansk Geologisk Forening*, 9: 253 – 255.

Troels-Smith, J., 1942. Ecologisk datering af Dyrholm-Fundet. In: T. Mathiassen, M. Degerbøl and J. Troels-Smith (Eds.). Dyrholmen Det kgl. Danske Videnskab. Selskab, Arkæol – kunsthist. Skl, No. 1.

Turner, R., Kelly, A., and Roberts, N., 2006: *In press*. A critical assessment and experimental comparison of microscopic charcoal extraction methods. In: G. Fiorentino and D. Magri (Eds.). Charcoals from the past: cultural and palaeoenvironmental implications. Proceedings of the Third International Meeting of Anthracology, Cavallino (Lecce), June 2004. BAR International Series, Archaeopress, Oxford, UK.

Turner, R., 2007. Late Quaternary fire histories in the Eastern Mediterranean region from lake sedimentary microchracoals. Unpublished PhD thesis, University of Plymouth.

Tushingham, A.M. and Peltier, W.R., 1991. ICE-3G: a new global model of late Pleistocene deglaciation based on geophysical predictions of postglacial relative sea level change. *Journal of Geophysical Research*, 96: 4497-4523.

Törnquist, T.E., Van Ree, M.H.M., Van 't Veer, R. and Van Geel, B., 1998. Improving methodology for high-resolution reconstruction of sea-level rise and neotectonics by palaeoecological analysis and AMS 14C dating of basal peats. *Quaternary Research* 49: 72-85.

Van de Plassche, O., 1986. Sea-level research: A manual for the collection and evaluation of data. Geobooks, Norwich: 617pp.

Van der Werff, A., Huls, H., 1957-1974. Diatomeeënflora van Nederland. Reprint. Otte Koeltz science Publishers, Koenigstein.

Van den Wollenberg, A.L., 1977. Redundancy analysis. An alternative for canonical correlation analysis. *Psychometrika*. 42, 207-219.

Varekamp, J.C., 1992. Relative sea-level rise and climate change over the last 1500 years. *Terra Nova*, 4: 293-304.

Vos, P.C. and de Wolf, H., 1993. Diatoms as a tool for reconstructing sedimentary environments in coastal wetlands – methodological aspects. *Hydrobiologia*, 269: 285 – 296.

Vos, P.C., and de Wolf, H., 1998. Methodological aspects of palaeoecological diatom research in coastal areas of the Netherlands. *Geologie en Mijnbouw*, 67: 31-40.

Wartenberg, D., Ferson, S. and Rohlf, F.J., 1987. Putting things in order: a critique of detrended correspondence analysis. *American Naturalist*, 129: 434 – 448.

Whitehorse, P., Latychev, K., Milne, G.A., Mitrovica, J.X. and Kendall, R., 2006. Impact of 3-D Earth structure on Fennoscandian glacial isostatic adjustment: Implications for space-geodetic estimates of present-day crustal deformations. *Geophysical Research Letters*, 33 (13). Art. No. L13502 July 7 2006.

Whiting, M.C. and McIntire, C.D., 1985. An investigation of distributional patterns in diatom flora of Netarts Bay, Oregon, USA by correspondence analysis. *Phycology*, 21: 655-661.

Whitlock, C. and Millspaugh, S.H., 1996. Testing the assumptions of fire history studies: an extension of modern charcoal accumulation in Yellowstone National Park. *The Holocene*, 6, 7-15.

Wold, S., Ruhe, A., Wold, H. and Dunn, W.J., 1984. The collinearity problem sin linear regression: the partial least squares (PLS) approach to generalised inverses. Society for Industrial and Applied Mathematics Journal of Scientific Statistical Computing, 5: 735-743.

Zong, Y.Q., 1997. Mid-and late-Holocene sea-level changes in Roudsea Marsh, northwest England: a diatom biostratigraphical investigation. *The Holocene*, 7 (3): 311-323.

Zong, Y.Q., 1998. Diatom and sedimentary responses to sea-level change during the last 8000 years in Roudsea Wood, northwest England. *The Holocene*, 8 (2): 219-228.

Zong, Y.Q. and Horton, B.P., 1998. Diatom zones across intertidal flats and coastal salt marshes in Britain. *Diatom Research*, 13: 375–394.

Zong, Y.Q. and Horton, B.P., 1999. Diatom-based tidal-level transfer functions as an aid in reconstructing Quaternary history of sea-level movements in the UK. *Journal Quaternary Science*, 14: 153-167.

APPENDIX 4

Inventory of all available datable material (^{14}C). Numbered samples correspond to those samples dated (Table 5.2). A total of twenty-six samples were selected for analysis based on sample weights and the degree to which they met the objectives detailed in Section 3.6.1.

Sample number	Sample depth (m)	Elevation (m DNN)	Sample weight (mg)	Sample description	Stratigraphic context
Røgel core RØ1					
1	0.51	+1.09	4.5	Unidentified plant remains	Bottom of black layer
2	0.68	+0.92	10.9	*Phragmites*	*Phragmites* clay
3	0.72	+0.88	15.7	*Phrgamites*	*Phragmites* clay
	0.74	+0.86	5	*Phragmites*	*Phragmites* clay
	0.78	+0.82	5.6	*Phragmites*	*Phragmites* clay
	0.80	+0.8	5.8	*Phragmites*	*Phragmites* clay
4	0.81	+0.79	8.9	*Phragmites*	*Phragmites* clay
	0.91	+0.69	21.7	*Phragmites*	*Phragmites* clay
5	0.92	+0.68	11.2	Unidentified plant remains	*Phragmites* clay
6	1.68	-0.008	22.1	Unidentified plant remains	Top of basal peat
	1.70	-0.1	31.3	Wood	Top of basal peat
	1.73	-0.13	4.8	Unidentified plant remains	Top of basal peat
	1.83	-0.23	4.2	Unidentified plant remains	Top of basal peat
	1.87	-0.27	7.1	*Phragmites*	Top of basal peat
7	1.89	-0.29	17.6	Reed stem (*Juncus*)?	Top of basal peat
	2.14a	-0.54	10.7	Reed stem (*Juncus*)?	Top of basal peat
	2.14b	-0.54	33	Reed stem (*Juncus*)?	Top of basal peat
	2.14c	-0.54	8.6	Unidentified plant remains	Top of basal peat
8	2.15	-0.55	14.3	*Phragmites*	Top of basal peat
	2.16	-0.56	8.7	Unidentified plant remains	Top of basal peat
	2.17	-0.57	60	*Phragmites*	Top of basal peat
	2.18	-0.58	15.4	Unidentified plant remains	Top of basal peat
	2.19	-0.59	25.6	Reed fragments	Top of basal peat
	2.20	-0.60	4.3	Grass fragment	Top of basal peat
10	2.22	-0.62	4.4	Grass fragment	Top of basal peat
	2.24	-0.64	4.4	*Phgramites*	Top of basal peat
Røgel Monolith					
11	0.55	+1.05	8.7	*Phgramites*	Bottom of black layer
12	0.60	+1.00	15.9	*Phragmites*	Clay
	0.61	+0.99	5.6	*Phragmites*	Clay
	0.66	+0.94	2.1	Grass	Clay
Oksby Enge Monolith OEA					
	0.17	+1.45	514.97	Wood	Peaty clay
	1.00	+0.62	3	*Phragmites*	Clay
	1.09	+0.53	24.3	*Phragmites*	Clay
	1.17	+0.45	15.15	*Phragmites*	Clay
13	1.24	+0.38	77.48	*Phragmites*	Top of basal peat
	1.42	+0.20	228.66	*Phragmites*	Basal peat
	1.43a	+0.19	125.36	*Phragmites*	Basal peat
	1.43b	+0.19	82.08	*Phrgamites*	Basal peat
	1.52a	+0.10	1070.55	Wood	Basal peat
14	1.52b	+0.10	38.24	Reed stem?	Basal peat
Oksby Enge OEB5					
	0.15	+1.64	131.6	*Phragmites*	Top of sand layer
	0.17	+1.62	26	*Phragmites*	Top of sand layer
15	0.18	+1.61	78.6	*Phragmites*	Top of sand layer
16	0.82	+0.97	20.5	*Phragmites*	Clay
	0.84	+0.95	3.5	*Phragmites*	Clay
	0.92	+0.87	49	*Phragmites*	Clay
	0.93	+0.86	15.7	*Phragmites*	Clay
	0.94	+0.85	6.3	*Phragmites*	Clay
	0.96	0.83	34.7	*Phragmites*	Clay
17	1.01	+0.78	27.8	*Phragmites*	Clay
	1.02	+0.77	16.9	*Phragmites*	Clay
	1.04	+0.75	11.4	*Phragmites*	Clay

Sample number	Sample depth (m)	Elevation (m DNN)	Sample weight (mg)	Sample description	Stratigraphic context
Kjelst Enge core KE1					
18	4.16	-2.59	25.9	Unidentified plant fragment	*Phragmites* clay
	4.19	-2.62	29.9	*Phragmites*	*Phragmites* clay
	4.21	-2.64	54.4	*Phragmites*	*Phragmites* clay
	4.25	-2.68	34.6	*Phragmites*	*Phragmites* clay
	4.41	-2.84	50.1	*Phragmites*	*Phragmites* clay
	4.57	-3.00	38.9	*Phragmites*	*Phragmites* clay
	4.81	-3.24	12.8	*Phragmites*	*Phragmites* clay
	4.82	-3.25	24.2	*Phragmites*	*Phragmites* clay
	4.86	-3.29	12.8	*Phragmites*	*Phragmites* clay
	4.89	-3.32	36.3	*Phragmites*	*Phragmites* clay
	4.92	-3.35	16	*Phragmites*	*Phragmites* clay
	4.96	-3.39	39	Grass steams	*Phragmites* clay
	4.97	-3.40	9.5	Grass stem?	*Phragmites* clay
	5.00	-3.43	42.8	Reed stem (*Juncus?*)	*Phragmites* clay
	5.09	-3.52	3.9	Grass stem	Basal peat
	5.12	-3.55	61.5	Wood	Basal peat
	5.14	-3.57	5.1	Unidentified plant remains	Basal peat
19	5.15	-3.58	10.6	Reed stem (*Juncus?*)	Basal peat
	5.165	-3.595	7.7	Rees stem (*Juncus?*)	Basal peat
	5.17	-3.6	0.9	Reed stem (*Juncus?*)	Basal peat
	5.23	-3.66	2.8	Unidentified plant remains	Basal peat
20	5.98	-4.41	59.3	*Phragmites*	Basal peat
	6.185	-4.615	16.9	*Phragmites*	Basal peat
	6.205	-4.635	40.2	*Phragmites*	Basal peat
	6.22	-4.65	18	*Phragmites*	Basal peat
	6.235	-4.665	29.5	*Phragmites*	Basal peat
	6.245	-4.675	33.5	*Phragmites*	Basal peat
	625	-4.68	26.5	*Phragmites*	Basal peat
	6.275	-4.705	75	*Phragmites*	Basal peat
	6.375	-4.805	38.4	*Phragmites*	Basal peat
	639	-4.82	31.8	*Phragmites*	Basal peat
	6.43	-4.86	11.4	*Phragmites*	Basal peat
21	6.54	-4.97	19.8	*Phragmites*	Basal peat
	6.62	-5.05	14.3	*Phragmites*	Basal peat
	6.655	-5.085	23.2	*Phragmites*	Basal peat
	6.68	-5.11	18.6	Unidentified plant remains	Basal peat
	6.71	-5.14	21.1	Unidentified plant remains	Basal peat
	6.73	-5.16	17.2	*Phragmites*	Basal peat
	6.77	-5.2	43.4	*Phragmites*	Basal peat
	6.80	-5.23	13.3	Unidentified black fragments	Basal peat
22	683.5	-5.265	13.6	Unidentified black fragments	Basal peat
Kjelst Enge core KE12					
23	2.35	-0.83	26.3	*Phragmites*	Top of basal peat
	2.38	-0.86	17.2	*Phragmites*	Top of basal peat
	3.80	-2.28	33.9	*Phragmites*	Bottom of basal peat
	3.81	-2.29	19.8	*Phragmites*	Bottom of basal peat
Kjelst Enge core KE13					
25	3.335	-1.745	19.3	*Phragmites*	Top of basal peat
	4.86	-3.27	40.1	*Phragmites*	Top of basal peat
	4.995	-3.405	18.8	*Phragmites*	Bottom of basal peat
26	5.08	-3.49	36	*Phragmites*	Bottom of basal peat

APPENDIX 5

Unidentified Diatom Taxa

This appendix presents and describes unidentified diatom taxa encountered during this study. Only unidentified taxa with ≥ 1% relative abundance are described. The remaining unidentified taxa are excluded from all analysis and interpretation and are therefore not described. Of the unidentified taxa described, only SpeciesC and SpeciesG1 occur with a maximum relative abundance of > 3%. The image analysis system, AnalySIS®, was used to aid taxonomic work. However, images presented here were taken with an Olympus camera attached to an Olympus BX-50 microscope, as this method was found to produce clearer illustrations. Morphological descriptions follow Barber and Haworth (1994).

SpeciesC (Figure 1)

Valve clavate, heterpolar and asymmetrical. Valve length c. 18 µm, valve width c. 3 µm. Striae not visible through light microscope. Found in the palaeoenvironment and associated with taxa such as *Achnanthes delicatula, Cymatosira belgica, Navicula cincta* and *Navicula pusilla.*

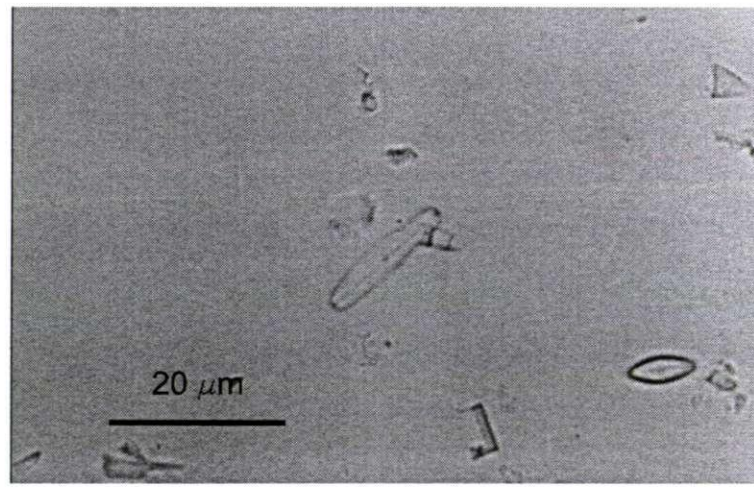

Figure 1. SpeciesC.

SpeciesG (Figure 2)

Valve elliptic. Valve length c. 8 μm, valve width 3-5 μm. Striae not clearly visible through light microscope but appear dense. Found alongside occurrences of SpeciesC.

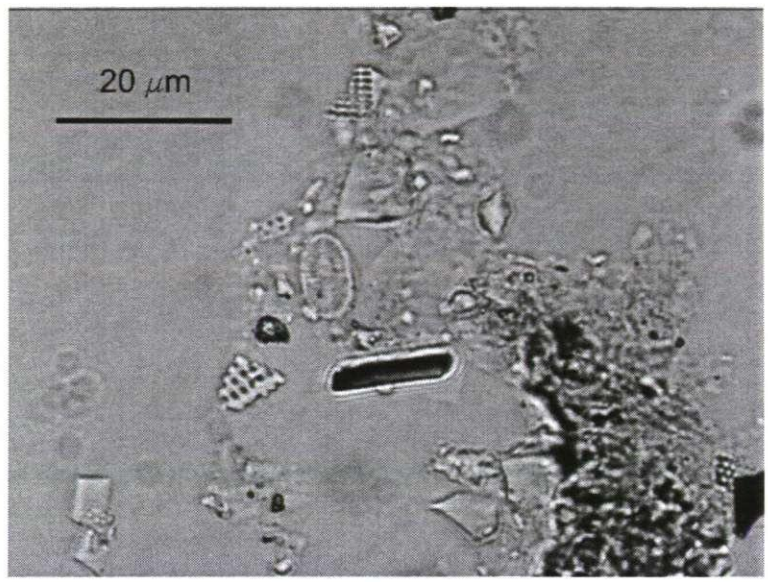

Figure 2. Species G.

SpeciesX (Figure 3)

Valve elliptic. Valve length typically c. 12μm, valve width c.2 μm. Striae radiate throughout, striae count c. 12/10 μm. Found in low relative abundances (< 2%) in the black layer in core BR9 alongside occurrences of several *Pinnularia* species.

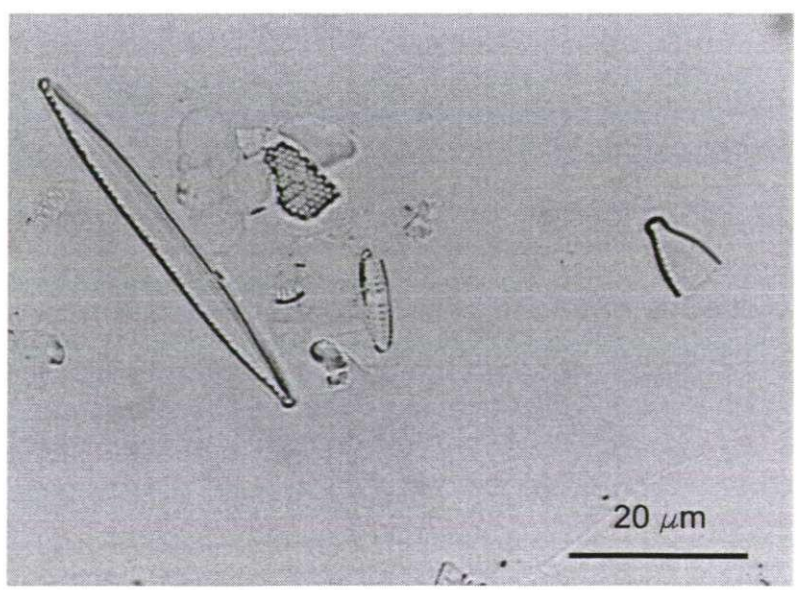

Figure 3. SpeciesX.

SpeciesA1 (Figure 4)

Valve elliptic. Valve length c. 4 μm, valve width 3-5 μm. Possibly a P-valve of Achnanthes sp? Found sporadically throughout the master core sequence in association with *Pinnularia* species.

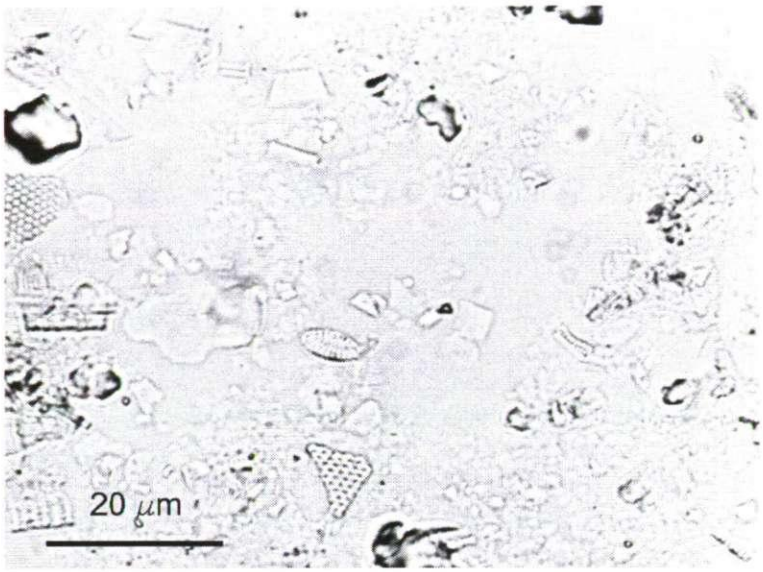

Figure 4. SpeciesA1.

SpeciesB1 (Figure 5)

Valve triangular, ends rounded and slides slightly convex. Found alongside occurrences of *Achnanthes delicatula, Cyclotella striata* and *Navicula cincta.*

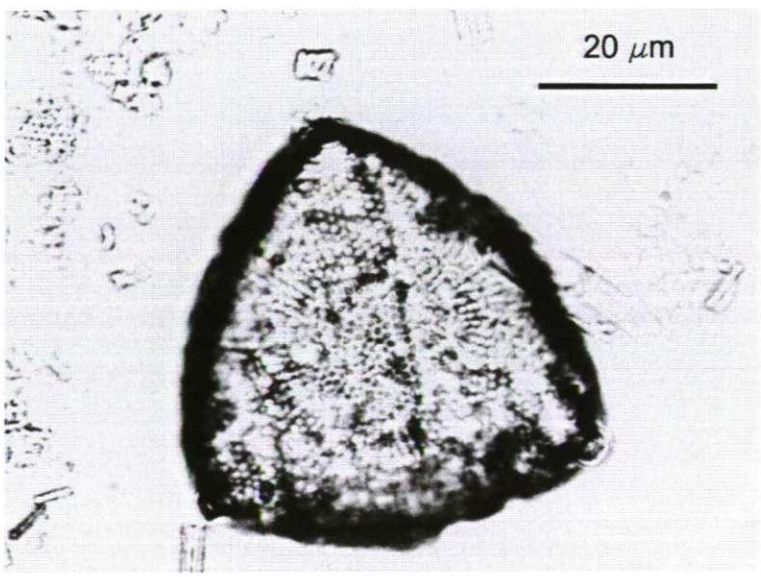

Figure 5. SpeciesB1.

SpeciesC1

Photo not shown, valve too small to be seen clearly on photo. Valve elliptic, valve length c. 3-5 μ, valve width c. 2-3 μm. Possibly a very small Fragilaria spp. Occurs sporadically in core RØ1 in very low abundances. Maximum relative abundance 1.6%. Found alongside occurrences of *Navicula cincta*.

SpeciesN1 (Figure 6)

Valve ovate and slightly heteropolar? Valve length c. 8-10 μm, valve width 4-5 μm. Striae unclear and difficult to differentiate. Most probably *Fragilaria exigua*? Only present in one sample (RØ1 0.88 m core depth).

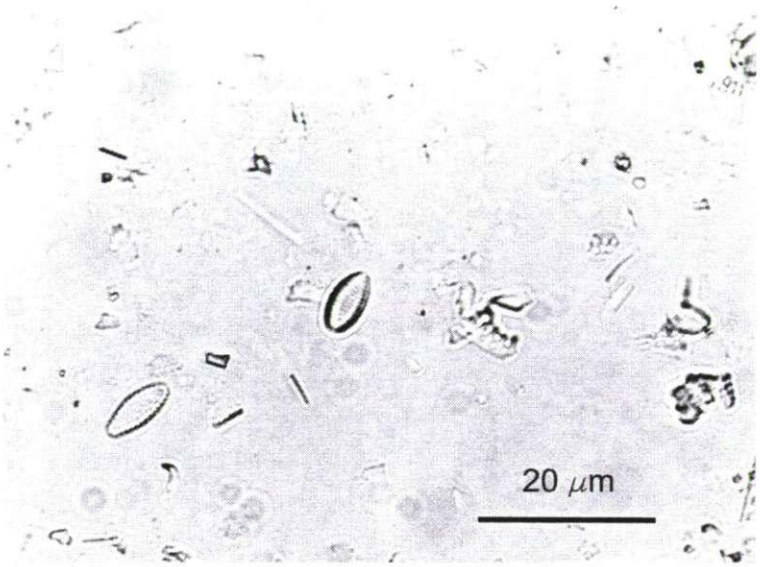

Figure 6. SpeciesN1

SpeciesG1 (Figure 7)

Valve elliptic, with subcapitate ends. Valve length c. 20 µm, valve width c. 7 µm, striae sigmoid, c. 10/10 µm. Central raphe terminals appear to be bent unilaterally. Associated with *Pinnularia* taxa (Figures 4.9 and 4.11).

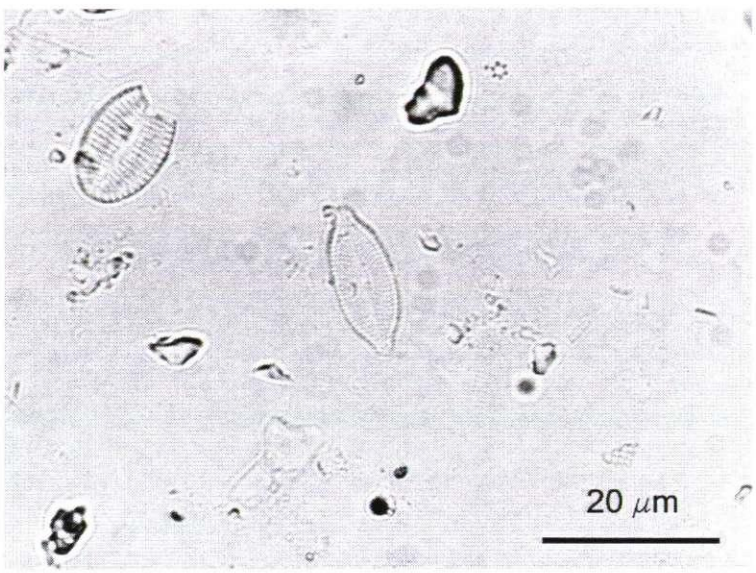

Figure 7. SpeciesG1

SpeciesS1 (Figure 8)

Valve lanceolate with rostrate ends. Valve length c. 65 µm, valve width, c. 20 µm, striae radiate throughout, striae count 17/10 µm. Found in the palaeoenvironment in association with taxa such as *Navicula phyllepta* and *Navicula pygmaea*.

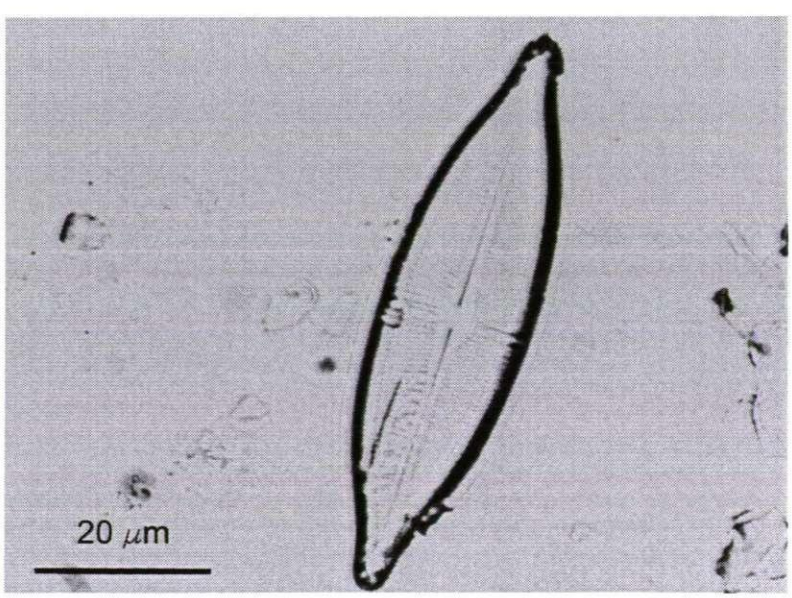

Figure 8. SpeciesS1

SpeciesX1 (Figure 9)

Valve lanceolate with rostrate ends. Valve length 19-22 μm, valve width c. 3 μm. Striae slightly convergent at the ends and radiate towards the centre, striae count at least 25/10 μm. Possibly *N. cryptocephala*? Found in the modern environment on the high salt marsh alongside occurrences of *Achnanthes minutissima*, *Navicula cincta, Nitzschia terrestris* and *Pinnularia ignobilis*.

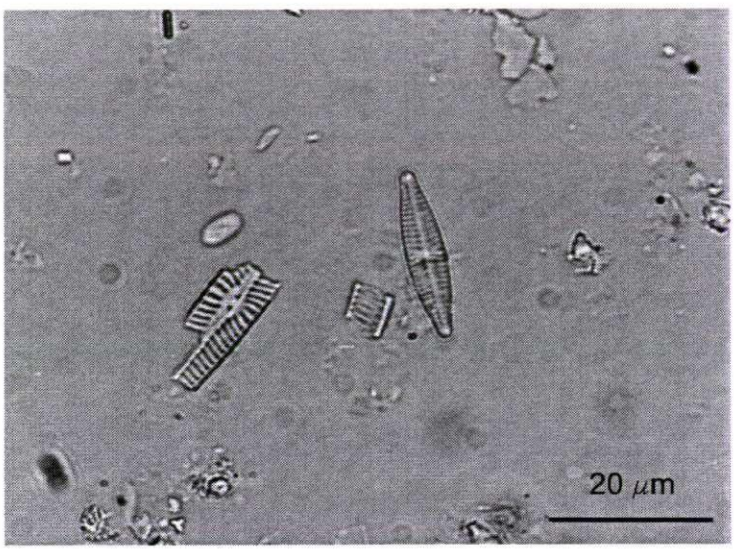

Figure 9. SpeciesX1. Possibly *N. cryptocephala*?

SpeciesC2 (Figure 10)

Valve linear with slightly panduriform centre. Valve length c. 20 μm, valve width c. 5 μm, striae parallel, striae count 8/10 μm. Found in the modern environment on the low salt marsh in association with polyhalobous and mesohalobous taxa.

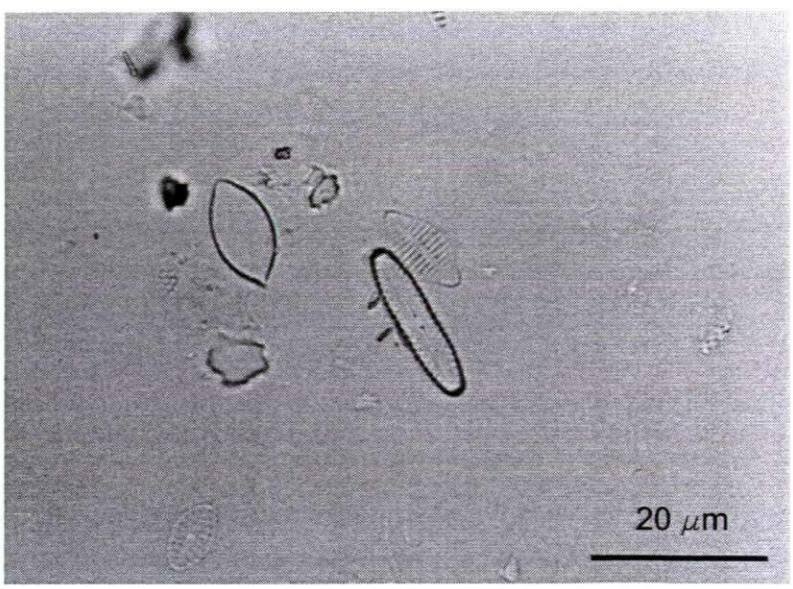

Figure 10. SpeciesC2.

SpeciesD2 (Figure 11)

Valve narrow elliptic, valve length 12-15 μm, valve width c. 3-4 μm, striae appear slightly radiate but difficult to differentiate. Central area appears circular. Found in the low salt marsh on Langli Island in association with polyhalobous and mesohalobous taxa such as *Diploneis didyma* and *Achnanthes delicatula*.

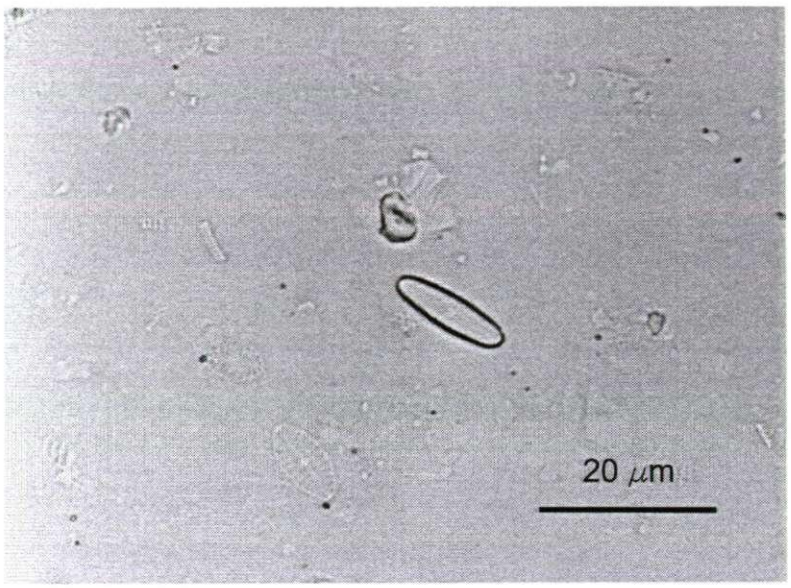

Figure 11. SpeciesD2.

SpeciesE2 (Figure 12)

Valve shape lanceolate, cuneate ends. Valve length c. 24 μm, valve width c. 5 μm, striae slightly radiate, striae count 13/10 μm. Found in the modern environment on the low salt marsh, in association with *Diploneis didyma* and high abundances of *Achnanthes delicatula* (58%).

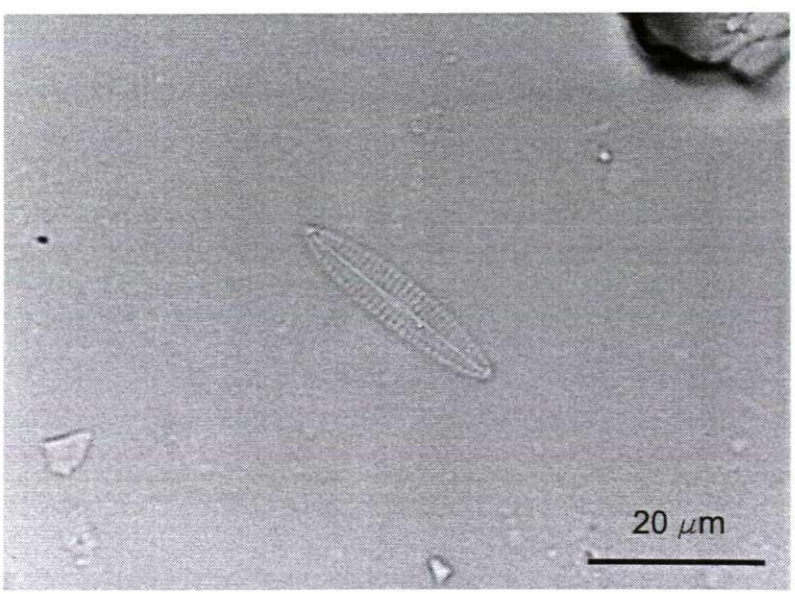

Figure 12. SpeciesE2.

SpeciesG2 (Figure 13)

Valve elliptic, slightly narrowed, valve length 16-18 μm, valve width 4-5 μm. Striae parallel at the ends and radiate towards the centre, striae count c. 17/10 μm. Found alongside occurrences of species C2, D2 and E2 on the low salt marsh and in association with polyhalobous and mesohalobous taxa.

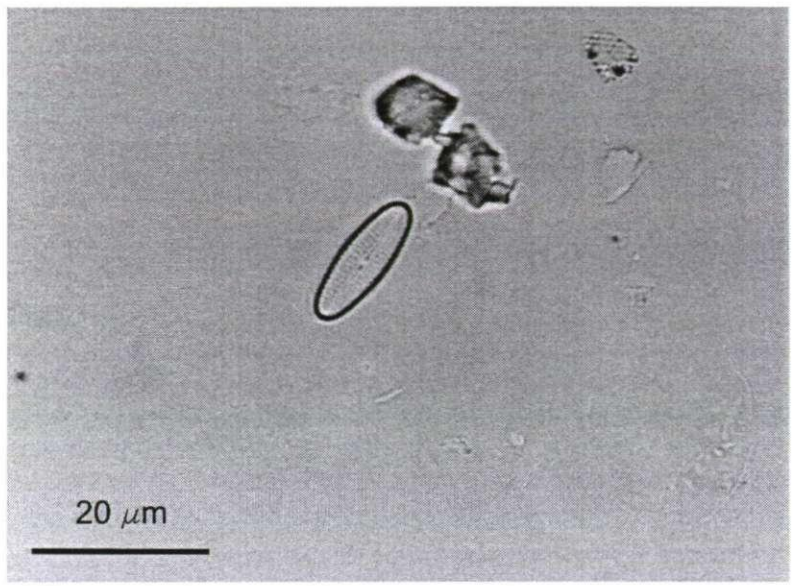

Figure 13. SpeciesG2.

Species I2 (Figure 14)

Valve narrow elliptic with rostrate ends. Valve length c. 45 μm, valve width c. 5-7 μm. Striae strongly radiate towards the centre and parallel at the ends. Striae count c. 10/10 μm. Found in the modern environment in the low salt marsh.

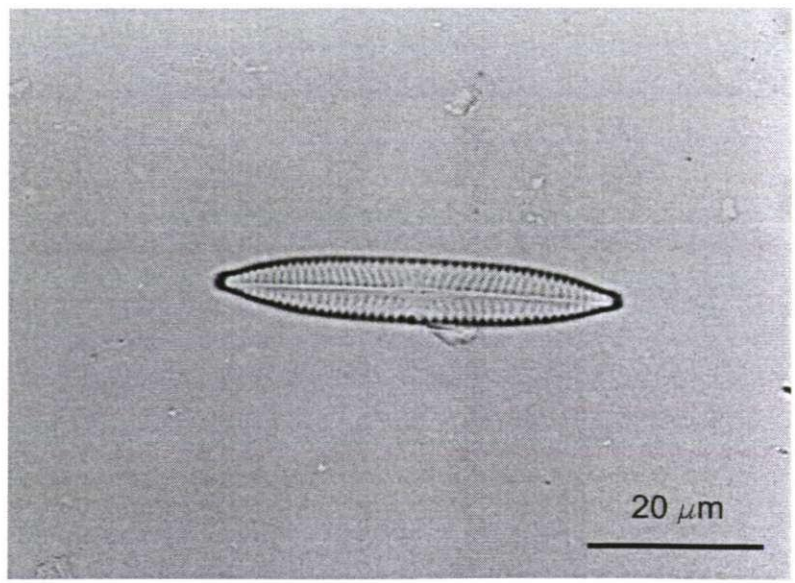

Figure 14. SpeciesI2.

SpeciesJ2 (Figure 15)

Valve panduriform. Valve length c.20 μm, valve width c. 4 μm, striae parallel throughout, slightly radial in the centre, striae count 11/10μ. Found in the modern environment on the low salt marsh in association with polyhalobous and mesohalobous taxa.

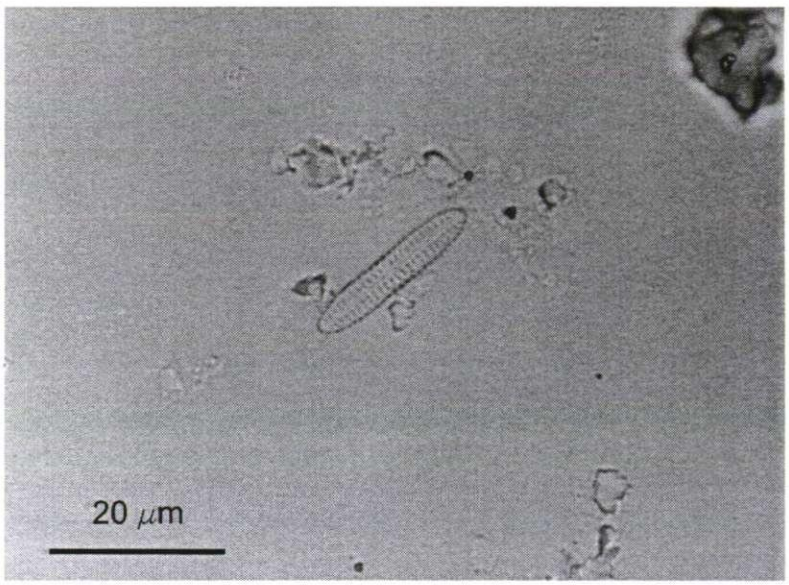

Figure 15. SpeciesJ2.

Species M2 (Figure 16)

Valve narrow elliptic with slightly rostrate ends. Valve length c. 38 μm, valve width c. 5 μm. Striae parallel throughout, slightly convergent towards the ends? Striae count c. 11/10 μm. Central area a wide transverse fascia.

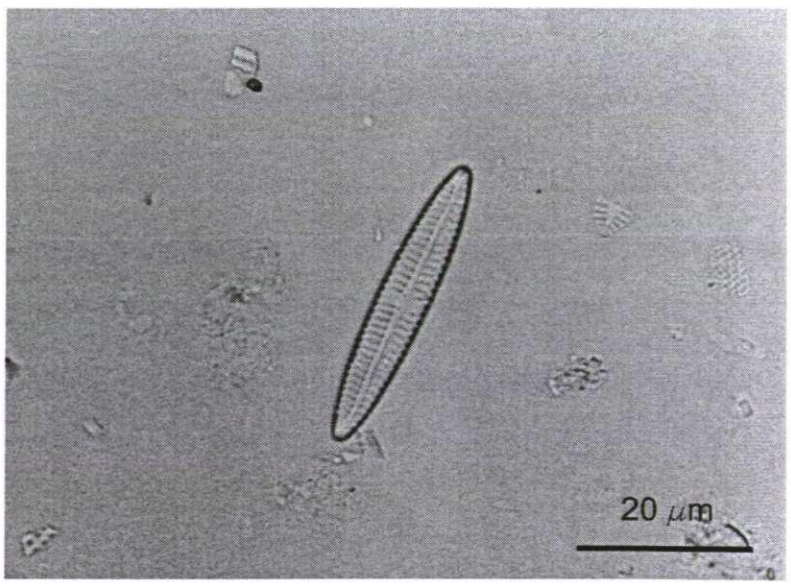

Figure 16. SpeciesM2.

SpeciesN2 (Figure 17)

Valve lanceolate. Valve length c. 11 μm, valve width c. 3 μm. Striae difficult to differentiate but appear parallel? Possibly *Achnanthes minutissima*? Found towards the top of core BR9 in association with polyhalobous and mesohalobous taxa.

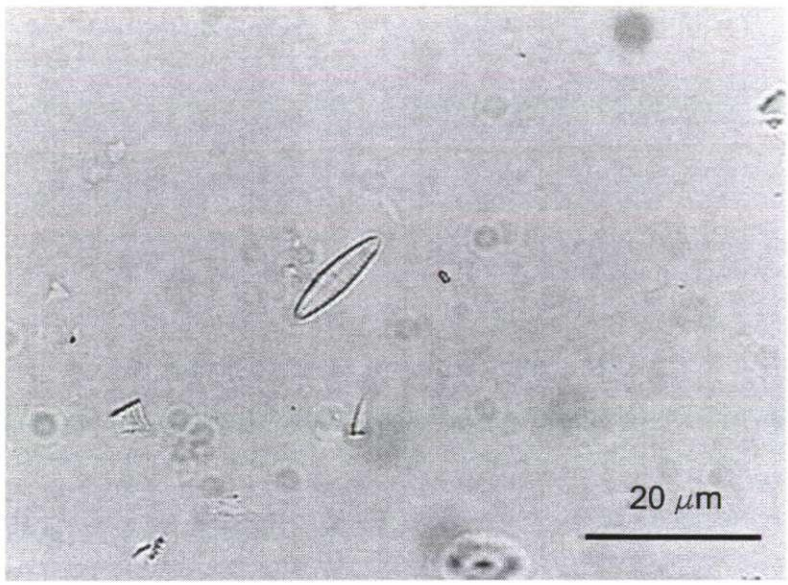

Figure 17. SpeciesN2.

SpeciesP2 (Figure 18)

Valve narrow, elliptical. Valve length c.38 μm, valve width c. 10 μm, striae radiate and composed of very fine puncta, central area not differentiated. Striae count 15/10 μm. Presence of a pseudo-septum? Found in the palaeoenvironment in association with taxa such as *Mastagloia smithii*, *Nitzschia obtusa*, and *Caloneis bacillum*.

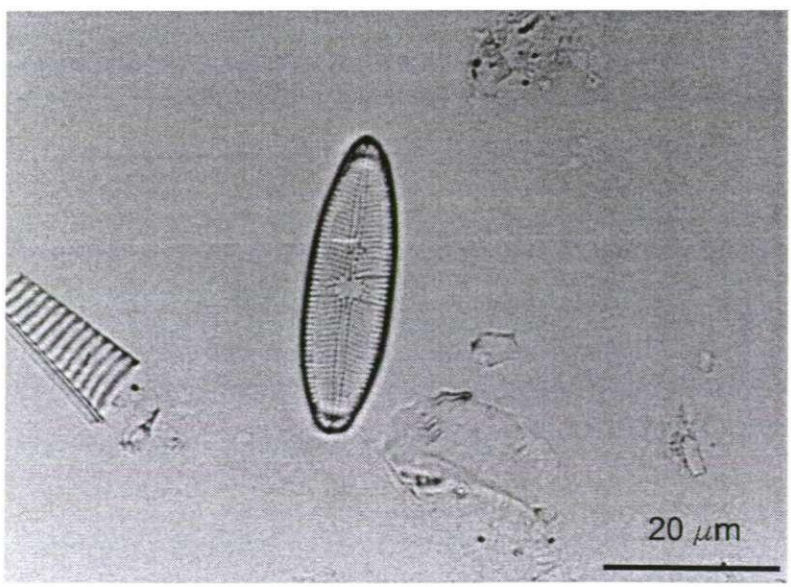

Figure 18. SpeciesP2.

SpeciesQ2 (Figure 19)

Valve elliptic, slightly narrowed, valve length 24-26 μm, valve width 4-6 μm. Striae radial throughout, striae count typically c.10/10 μm. Striae are denser towards the valve ends. Found in the palaeoenvironment in core RØ1 (c. 0.30 m core depth) in association with several *Pinnularia* species and *Caloneis bacillum*.

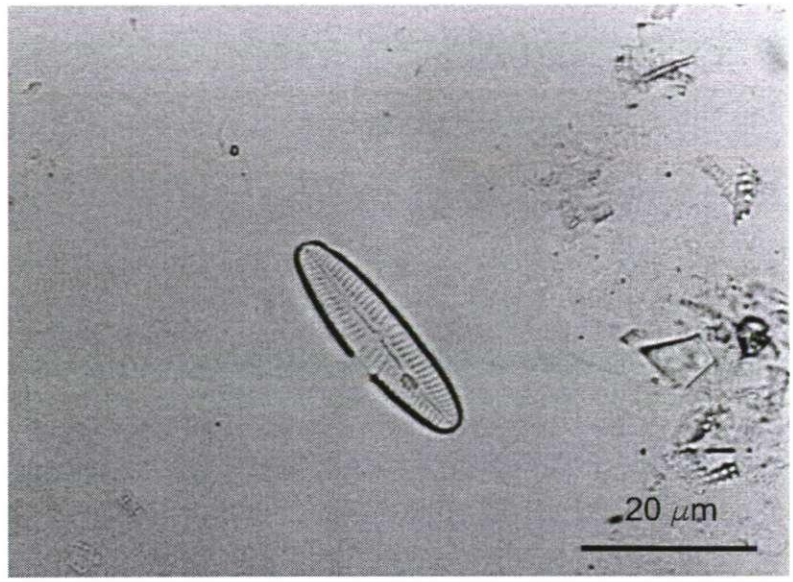

Figure 19. SpeciesQ2.

APPENDIX 6

Descriptive statistics for each environmental variable at individual transects. Statistics were calculated using MINITAB® Release 14. Descriptive statistics for each environmental variable for the data set as a whole are summarised in Table 4.3.

Environmental Variable	Minimum	Maximum	Mean	Median	Standard Deviation
Elevation (m DNN)	0.74	1.86	1.50	1.63	0.32
pH	4.09	7.85	6.02	5.94	0.88
Salinity (g/l^{-1})	0.93	1.64	1.15	1.12	0.16

Table 1. Descriptive statistics for each environmental variable measured from Kjelst Enge.

Environmental Variable	Minimum	Maximum	Mean	Median	Standard Deviation
Elevation (m DNN)	1.88	2.66	2.18	2.15	0.25
pH	4.45	6.83	6.070	6.29	0.65
Salinity (g/l^{-1})	0.02	0.51	0.20	0.14	0.16
LOI (%)	15.29	65.13	49.95	56.76	15.93
$CaCO_3$ (%)	0.3	2.23	1.430	1.58	0.58
Sand (%)	11.07	94.15	29.85	21.47	22.42
Silt (%)	5.85	82.72	64.92	71.31	20.40
Clay (%)	< 0.001	7.98	5.23	5.95	2.47

Table 2. Descriptive statistics for each environmental variable measured from Moservå.

Environmental Variable	Minimum	Maximum	Mean	Median	Standard Deviation
Elevation (m DNN)	1.34	1.455	1.40	1.41	0.03
pH	5.54	7.1	6.37	6.47	0.46
Salinity (g/l^{-1})	0.26	3.07	0.93	0.73	0.76
LOI (%)	24.85	39.17	32.25	32.88	4.60
$CaCO_3$ (%)	2.02	3.53	2.83	2.89	0.43
Sand (%)	4.23	20.43	13.78	13.86	5.24
Silt (%)	70.06	91.02	76.65	75.53	6.13
Clay (%)	4.75	11.78	9.56	9.56	1.66

Table 3. Descriptive statistics for each environmental variable measured from Storbæk.

Environmental Variable	Minimum	Maximum	Mean	Median	Standard Deviation
Elevation (m DNN)	1.50	2.34	1.88	1.83	0.27
pH	4.90	6.98	5.66	5.64	0.43
Salinity (g/l^{-1})	0.04	2.75	1.08	0.79	0.96
LOI (%)	22.4	65.46	48.91	49.34	11.97
$CaCO_3$ (%)	2.57	5.27	3.44	3.19	0.74
Sand (%)	4.26	25.76	10.30	8.93	5.57
Silt (%)	71.09	90.95	82.46	83.09	5.12
Clay (%)	0.95	12.17	7.24	7.24	3.89

Table 4. Descriptive statistics for each environmental variable measured from Oksby Enge.

Environmental Variable	Minimum	Maximum	Mean	Median	Standard Deviation
Elevation (m DNN)	0.23	1.74	1.06	1.09	0.433
pH	6.84	8.51	7.51	7.37	0.457
Salinity (g/l^{-1})	0.49	3.36	2.34	2.48	0.57
LOI (%)	1.16	44.10	16.84	1.16	13.61
$CaCO_3$ (%)	0.66	5.29	2.48	2.70	1.13
Sand (%)	14.06	93.38	40.39	35.78	21.58
Silt (%)	6.62	75.32	52.37	57.14	19.11
Clay (%)	< 0.001	10.62	7.23	7.055	2.55

Table 5. Descriptive statistics for each environmental variable measured from Langli North.

Environmental Variable	Minimum	Maximum	Mean	Median	Standard Deviation
Elevation (m DNN)	0.66	1.53	1.16	1.20	0.22
pH	7.04	8.75	1.71	7.70	0.47
Salinity (g/l^{-1})	1.04	2.47	1.66	1.69	0.30
LOI (%)	2.98	17.77	19.14	17.77	11.88
$CaCO_3$ (%)	1.09	8.41	2.58	2.16	1.62
Sand (%)	22.32	65.79	45.04	47.23	12.08
Silt (%)	29.39	68.78	48.01	45.56	10.92
Clay (%)	4.82	9.15	6.95	6.98	1.25

Table 6. Descriptive statistics for each environmental variable measured from Langli South.

APPENDIX 7

Abbreviations for taxa with ≥ 1% relative abundance in both modern and fossil samples, including full taxon name and authority. Unidentified taxa with ≥ 1% relative abundance are described in Appendix 5.

Taxon code	Full taxon name	Authority
Achnbrev	*Achnanthes brevipes*	Agardh 1824
Achncera	*Achnanthes ceramii*	Hendy 1977
Achndeli	*Achnanthes delicatula*	(Kützing) Grunow 1880
Achnhols	*Achnanthes holsatica*	Hustedt in A. Schmidt et al., 1936
Achnlanc	*Achnanthes lanceolata*	(Brébisson) Grunow in Cleve and Grunow 1880
Achnlate	*Achnanthes laterostrata*	Hustedt 1933
Achnlong	*Achnanthes longipes*	Agardh 1824
Achnminu	*Achnanthes minutissima* – type	Kützing 1833
Achnoblo	*Achnanthes oblongella*	Oestrup 1902
Achnrupe	*Achnanthes rupestoides*	Hohn 1961
Actisena	*Actinoptychus senarius*	(Ehrenberg) Ehrenberg 1843
Actinorm	*Actinocyclus normanii*	(Gregory ex. Greville) Hustedt 1957
Ardicrys	*Ardissoni crystallina*	Unknown
Amphexig	*Amphora exigua*	Gregory 1857
Amphcoff	*Amphora coffeaeformis*	(Agarth) Kützing 1844
Amphline	*Amphora lineolata*	Ehrenberg (1838) 1843
Amphlybi	*Amphora lybica*	Ehrenberg 1840
Amphprot	*Amphora proteus*	Gregory 1857
Amphturg	*Amphora turgida*	Gregory 1857
Auliscul	*Auliscus sculptus*	(W. Smith) Ralfs in Pritchard, 1861
Actisena	*Actinoptychus senarius*	(Ehrenberg) Ehrenberg 1843
Caloamph	*Caloneis amphisbeana*	Bory (Cleve) 1894
Calobaci	*Caloneis bacillum*	(Grunow) Cleve 1894
Calosili	*Caloneis silicula*	(Ehrenberg) Cleve 1894
Calowest	*Caloneis westii*	(W.Smith) Hendey 1964
Campeche	*Campylodiscus echeneis*	(Ehrenberg) Kützing, 1844
Campcymb	*Campylosira cymbelliformis*	(Schmidt) Grunow in H. Van Heurck 1885
Coccpedi	*Cocconeis pediculus*	Ehrenberg 1838
Coccpelt	*Cocconeis peltoides*	Hustedt 1939
Coccplac	*Cocconeis placentula*	Ehrenberg 1838
Coccscpa	*Cocconeis scutellum var parva*	(Grunow in Van Heurck 1880) Cleve 1895
Coccscut	*Cocconeis scutellum var scutellum*	Ehrenberg 1838
Coccstau	*Cocconeis stauroneiformis*	(W. Smith) Okuno 1957
Coscradi	*Coscinodiscus radiatus*	Ehrenberg 1841
Cyclstri	*Cyclotella striata*	(Kützing) Grunow (1880) in Cleve and Grunow
Cymbaspe	*Cymbella aspera*	(Ehrenberg) Peragallo 1849
Cymbnavi	*Cymbella naviculformis*	(Auerswald) Cleve 1894
Cymbsile	*Cymbella silesiaca*	Bleisch in Rabenhorst 1864
Cymabelg	*Cymatosira belgica*	Grunow in Van Heurck 1880-1885
Delpsuri	*Delphineis surirella*	(Ehrenberg) G. Andrews 1981
Dentsubt	*Denticula subtilis*	Grunow 1862
Diattenu	*Diatoma tenuis*	Agardh 1812
Dimemino	*Dimeregramma minor*	(Gregory) Ralfs in Pritchard 1861
Diplbomb	*Diploneis bombus*	(Ehrenberg) Cleve 1894
Dipldidy	*Diploneis didyma*	(Ehrenberg) Ehrenberg 1854
Diplelli	*Diploneis elliptica*	(Kützing) Cleve 1891
Diplinte	*Diploneis interrupta*	(Kützing) Cleve 1894
Diploblo	*Diploneis oblongella*	(Naegeli) Cleve-Euler 1922
Diploval	*Diploneis ovalis*	(Hilse) Cleve 1891
Diplsmit	*Diploneis smithii*	(Brébisson) Cleve 1894
Diplsubo	*Diploneis suborbicularis*	Gregory (Cleve)

Epitadna	*Epithemia adnata*	(Kützing) Rabenhorst 1853
Eunoarcu	*Eunotia arcus*	Ehrenberg 1837
Eunobilu	*Eunotia bilunaris*	(Ehrenberg) Mills 1934
Eunoexig	*Eunotia exigua*	(Brébisson ex Kützing) Rabenhorst 1853
Eunofall	*Eunotia fallax*	Cleve 1895
Eunomino	*Eunotia minor*	(Kützing) Rabenhorst 1864
Eunopect	*Eunotia pectinalis*	(Kützing) Rabenhorst 1864
Epitadna	*Epithemia adnata*	(Kützing) Brébisson 1838
Epitturg	*Epithemia turgida*	(Ehrenberg) Kützing 1844
Fragbrev	*Fragilaria brevistriata* – type	Grunow in Van Heurck 1885
Fragcape	*Fragilaria capensis*	Grunow 1862
Fragcapu	*Fragilaria capucina*	Desmazieres 1825
Fragcons	*Fragilaria construens* - type	(Ehrenberg) Grunow 1862
Fragpinn	*Fragilaria pinnata*	Ehrenberg 1843
Fragelli	*Fragilaria elliptica*	Schumann 1867
Fragexig	*Fragilaria exigua*	Grunow in Cleve & Möller 1878
Fragfasc	*Fragilaria fasciculata*	(Agardh) Lange-Bertalot 1980 sensu lato.
Fragneop	*Fragilaria neoproducta*	Lange-Bertalot, 1991
Fragnitz	*Fragilaria nitzschoides*	Grunow in Van Heurck 1881
Fragschu	*Fragilaria schulzii*	Brockmann 1950
Fragtene	*Fragilaria tenera*	(W. Smith) Lange-Bertalot 1980
Fragvire	*Fragilaria virescens*	Ralfs 1843
Frusrhom	*Frustulia rhomboides*	(Ehrenberg) De Toni 1891
Gompacum	*Gomphonema acuminatum*	Ehrenberg 1832
Gompangu	*Gomphonema angustatum*	(Kützing) Rabenhorst 1864
Gompparv	*Gomphonema parvulum*	(Kützing) Kützing 1849
Gramocea	*Grammatophora oceanica*	Ehrenberg 1854
Gyroacum	*Gyrosigma acuminatum*	(Kützing) Rabenhorst 1853
Gyrobalt	*Gyrosigma balticum*	(Ehrenberg) Rabenhorst 1853
Gyrofasi	*Gyrosigma fasciola*	(Ehrenberg) Griffith & Henrey 1856
Hyalradi	*Hyalodiscus radiatus*	(O' Meara) Grunow 1862
Hantamph	*Hantzschia amphioxys*	(Ehrenberg) Grunow in Cleve and Grunow 1880
Mastsmit	*Mastagloia smithii*	Thwaites in W. Smith 1856
Naviabru	*Navicula abrupta*	(Gregory) Donkin, Asmus 1982
Naviamph	*Navicula amphibola*	Cleve 1891
Naviatla	*Navicula atlantica*	(A.W.F.Schmidt) H.Perag. & Perag
Navicari	*Navicula cari*	Ehrenberg 1843
Navicinc	*Navicula cincta* – type	(Ehrenberg) Ralfs in Pritchard 1861
Navicryp	*Navicula cryptocephala*	Kützing 1844
Navicusp	*Navicula cuspidata*	(Kützing) Kützing 1844
Navidigi	*Navicula digitoradiata*	Gregory) Ralfs in Pritchard 1861
Navielgi	*Navicula elginensis*	(Gregory) Ralfs in Pritchard 1861
Naviforc	*Navicula forcipata*	Greville 1859
Navigreg	*Navicula gregaria*	Donkin 1861
Navihalo	*Navicula halophila*	(Grunow) Cleve 1894
Navihume	*Navicula humerosa*	Brébisson in W. Smith 1856
Navimari	*Navicula marina*	Ralfs in Prichard 1861
Navimeni	*Navicula menisculus*	Schumman 1867
Navimuti	*Navicula mutica*	Kützing 1844
Navipere	*Navicula peregrina*	(Ehrenberg) Kützing 1844
Naviphyl	*Navicula phyllepta*	Kützing 1844
Navipupu	*Navicula pupula*	Kützing 1844
Navipusi	*Navicula pusilla*	W. Smith 1853
Navipygm	*Navicula pygmaea*	Kützing 1849
Naviradi	*Navicula radiosa*	Kützing 1844
Navirhyn	*Navicula rhynchocephala*	Kützing 1844
Navitrip	*Navicula tripunctata*	(O.F. Müller) Bory 1822
Navisali	*Navicula salinarum*	(Grunow) in Cleve and Grunow 1880
Navivari	*Navicula variostriata*	Krasske 1923
Nitzacum	*Nitzschia acuminata*	(W. Smith) Grunow 1878
Nitzbilo	*Nitzschia bilobata*	W. Smith 1853
Nitzbrem	*Nitzschia bremensis*	Hustedt 1930
Nitzbrev	*Nitzschia brevissima*	Grunow in Van Heurck

Nitzcoar	*Nitzschia coarctata*	Grunow in Cleve & Grunow 1880
Nitzcomp	*Nitzschia compressa*	(Bailey) Boyer 1916
Nitzcomv	*Nitzschia compressa var compressa*	(Bailey) Boyer 1916
Nitzcons	*Nitzschia constricta*	(Kützing) in Ralfs Prichard 1861
Nitzdebi	*Nitzschia debilis*	(Arnott) Grunow in Cleve & Grunow non Pantocsek 1902
Nitzdiss	*Nitzschia dissipata*	(Kützing) Grunow 1862
Nitzdubi	*Nitzschia dubia*	W. Smith 1853
Nitzfili	*Nitzschia filiformis*	(W. Smith) Van Heurck 1896
Nitzfont	*Nitzschia fonticola*	Grunow in Van Heurck 1881
Nitzfoss	*Nitzschia fossilis*	Grunow in Van Heurck 1881
Nitzfrus	*Nitzschia frustulum*	(Kützing) Grunow in Cleve & Grunow 1880
Nitzgran	*Nitzschia granulata*	Grunow 1862
Nitzhung	*Nitzschia hungarica*	Grunow 1862
Nitzlevi	*Nitzschia levidensis*	Grunow 1862
Nitzline	*Nitzschia linearis*	W. Smith 1853
Nitzlitt	*Nitzschia littoralis*	Grunow in Cleve and Grunow 1880
Nitzmarg	*Nitzschia marginulata*	Grunow in Cleve and Möller 1878
Nitznana	*Nitzschia nana*	Grunow in Van Heurck 1881
Nitznavi	*Nitzschia navicularis*	(Brébisson) Grunow in Cleve and Grunow 1880
Nitznorm	*Nitzschia normannii*	Grunow in Van Heurck 1880-1885
Nitzobtu	*Nitzschia obtusa*	W.Smith 1853
Nitzpale	*Nitzschia palea*	(Kützing) W.Smith 1856
Nitzpell	*Nitzschia pellucida*	Grunow in Cleve & Grunow 1880
Naviplac	*Navicula placentula*	(Ehrenberg) Kützing 1844
Nitzplan	*Nitzschia plana*	W. Smith 1853
Nitzscal	*Nitzschia scalaris*	(Ehrenberg) W. Smith 1853
Nitzsgma	*Nitzschia sigma*	(Kützing) W. Smith 1853
Nitzsgmd	*Nitzschia sigma var diminuta*	Grunow 1862
Nitzsgmo	*Nitzschia sigmoidea*	(Nitzsch) W. Smith 1853
Nitzterr	*Nitzschia terrestris*	(Petersen) Hustedt 1934
Nitzvitr	*Nitzschia vitrea*	Norman 1861
Odonauri	*Odontella aurita*	(Lyngbye) Agardh 1832
Odonrhom	*Odontella rhombus*	(Ehrenberg) Kützing 1844
Opeppaci	*Opephora pacifica*	(Grunow) Petit 1888
Opepparv	*Opephora parva*	(Van Heurck) Krasske 1939
Parasulc	*Paralia sulcata*	(Ehrenberg) Cleve 1873
Pinnbore	*Pinnularia borealis*	Ehrenberg 1843
Pinngibb	*Pinnularia gibba*	Ehrenberg 1841
Pinnigno	*Pinnularia ignobilis*	(Krasske) Cleve-Euler 1955
Pinninte	*Pinnularia intermedia*	(Lagerstedt) Cleve 1895
Pinnlage	*Pinnularia lagerstedtii*	(Cleve) Cleve-Euler 1934
Pinnlund	*Pinnularia lundii*	Hustedt 1954
Pinnmajo	*Pinnularia major*	(Kützing) Rabenhorst 1853
Pinnmicr	*Pinnularia microstauron*	(Ehrenberg) Cleve 1891
Pinnsimi	*Pinnularia similis*	Hustedt 1954
Pinnsubc	*Pinnularia subcapitata*	Gregory 1856
Pinnsuco	*Pinnularia subconstricta*	Ehrenberg 1843
Pinnviri	*Pinnularia viridis*	(Nitzsch) Ehrenberg 1843
Plagstau	*Plagiogramma staurophorum*	(Gregory) Heiberg 1863
Plagvanh	*Plagiogramma vanheurckii*	Grunow 1862
Podostel	*Podosira stelligera*	(Bailey) A. Mann
Pseuwest	*Pseudopodosira westii*	(W. Smith)
Rhabadri	*Rhabdonema adriaticum*	Kützing 1844
Rhabarcu	*Rhabdonema arcuatum*	(Lyngbye in Hornemann) Kützing 1844
Rhabminu	*Rhabdonema minutum*	Kützing 1844
Rhapamph	*Rhaphoneis amphiceros*	(Ehrenberg) Ehrenberg 1854
Rhopacum	*Rhopalodia acuminata*	Krammer in Lange-Bertalot and Krammer 1987
Rhopgibb	*Rhopalodia gibba*	(Ehrenberg) O Müller 1895
Rhopmusc	*Rhopalodia musculus*	(Kützing) O. Müller 1899
Rhopoper	*Rhopalodia operculata*	(Agardh) Håkansson, 1979
Stauphon	*Stauroneis phoenicenteron*	(Nitzsch) Ehrenberg 1843
Stauprod	*Stauroneis producta*	Grunow 1880
Stauprom	*Stauroneis prominula*	(Grunow) Hustedt 1959

Suribreb	*Surirella brebissonii*	Krammer & Lange-Bertalot 1987
Suribrig	*Surirella brightwellii*	W. Smith, 1853
Surioval	*Surirella ovalis*	Brébisson 1838
Synearcu	*Synedra arcus*	Kützing 1844
Synefasi	*Synedra fasciculata*	(Agardh) Kützing 1844
Syneulna	*Synedra ulna*	(Nitzsch) Ehrenberg 1836
Tabefloc	*Tabellaria flocculosa*	(Roth) Kützing 1844
Thalnitz	*Thalassionema nitzschioides*	(Grunow) Grunow ex Hustedt
Thalecce	*Thalassiosira eccentrica*	(Ehrenberg) Cleve 1904
Tracaspe	*Trachyneis aspera*	(Ehrenberg) Cleve 1894
Tricbale	*Triceratium balearicum*	Cleve & Grunow